

REPORT ON THE DEVELOPMENT OF
THE MANNED ORBITAL RESEARCH LABORATORY (MORL)
SYSTEM UTILIZATION POTENTIAL

TASK AREA IV
MORL SYSTEM IMPROVEMENT STUDY

FACILITY FORM 602

(ACCESSION NUMBER)

(PAGES)

(NASA CR OR TMX OR AD NUMBER)

(THRU)

(CODE)

(CATEGORY)



BOOK 5

FACILITY FORM 602

N67 20166
(ACCESSION NUMBER)
307
(PAGES)
CR-66292
(NASA CR OR TMX OR AD NUMBER)

(THRU)
1
(CODE)
31
(CATEGORY)

SM-48819A
JANUARY 1966

MISSILE & SPACE SYSTEMS DIVISION
DOUGLAS AIRCRAFT COMPANY, INC.
SANTA MONICA/CALIFORNIA

[REDACTED]



AG-43193

REPORT ON THE DEVELOPMENT OF
THE MANNED ORBITAL RESEARCH LABORATORY (MORL)
SYSTEM UTILIZATION POTENTIAL

Task Area IV
MORL System Improvement Study

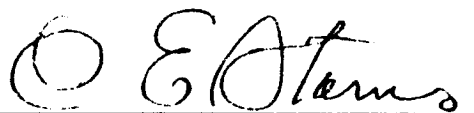
"Available to U.S. Government Agencies and
U. S. Government Contractors Only."

BOOK 5

SM-48819A
JANUARY 1966

PREPARED BY A. PISCIOTTA
BRANCH CHIEF
PROPULSION

APPROVED BY



C. E. STARNES
PROGRAM MANAGER

SUBMITTED BY
DOUGLAS AIRCRAFT COMPANY, INC.

PRESENTED TO
NATIONAL AERONAUTICS AND SPACE ADMINISTRATION
LANGLEY RESEARCH CENTER
CONTRACT NO. NAS1-3612

APPROVED BY



J. GUNKEL
DIRECTOR, ADVANCED MANNED SPACECRAFT SYSTEMS

DOUGLAS MISSILE & SPACE SYSTEMS DIVISION

The Manned Orbital Research Laboratory (MORL) is a versatile facility for experimental research which provides for:

- Simultaneous development of space flight technology and man's capability to function effectively under the combined stresses of the space environment for long periods of time.
- Intelligent selectivity in the mode of acquisition, collation, and transmission of data for subsequent detailed scientific analyses.
- Continual celestial and terrestrial observations.

Future application potential includes use of the MORL as a basic, independent module, which, in combination with the Saturn Launch Vehicles currently planned for the NASA inventory, is responsive to a broad range of advanced mission requirements.

The laboratory module includes two independently pressurized compartments connected by an airlock. The larger compartment comprises the following functional spaces:

- A Control Deck from which laboratory operations and a major portion of the experiment program will be conducted.
- An Internal Centrifuge in which members of the flight crew will perform re-entry simulation, undergo physical condition testing, and which may be useful for therapy, if required.
- The Flight Crew Quarters, which include sleeping, eating, recreation, hygiene, and liquids laboratory facilities.

The smaller compartment is a Hangar/Test Area which is used for logistics spacecraft maintenance, cargo transfer, experimentation, satellite check-out, and flight crew habitation in a deferred-emergency mode of operation.

The logistics vehicle is composed of the following elements:

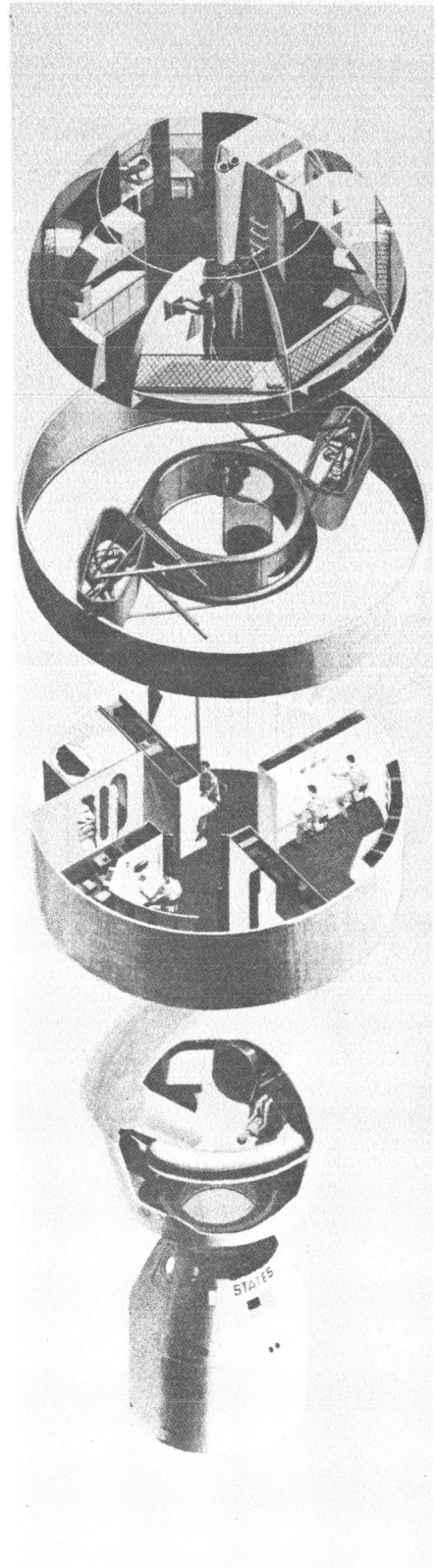
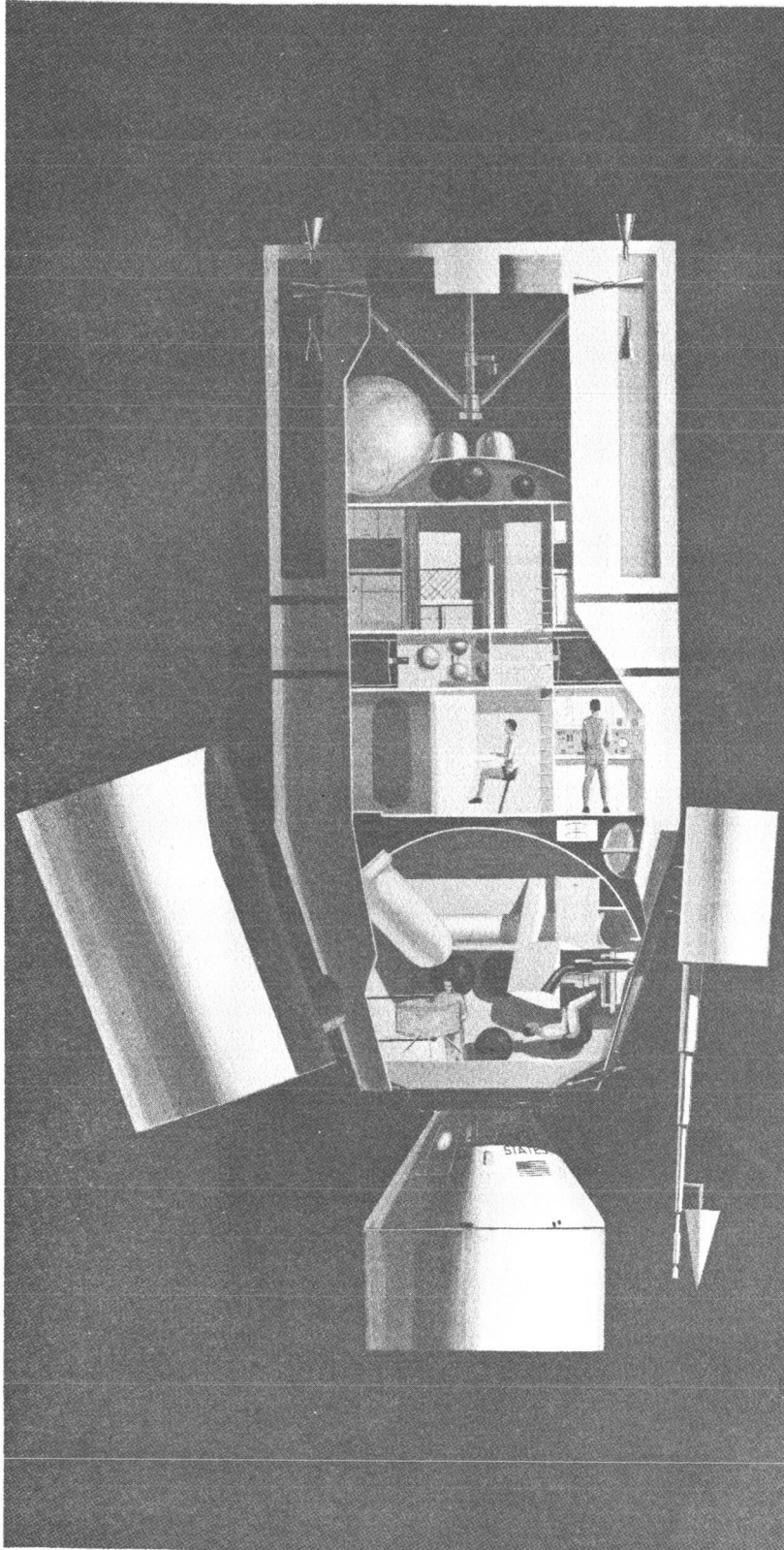
- A Logistics Spacecraft which generally corresponds to the geometric envelope of the Apollo Command and Service Modules and which includes an Apollo Spacecraft with launch escape system and a service pack for rendezvous and re-entry maneuver propulsion; and a Multi-Mission Module for either cargo, experiments, laboratory facility modifications, or a spacecraft excursion propulsion system.
- A Saturn IB Launch Vehicle.

Integration of this Logistics System with MORL ensures the flexibility and growth potential required for continued utility of the laboratory during a dynamic experiment program.

In addition to the requirements imposed by the experiment program, system design parameters must reflect operational requirements for each phase of the mission to ensure:

- Functional adequacy of the laboratory.
- Maximum utilization of available facilities.
- Identification of important parameters for consideration in future planning of operations support.

For this reason, a concept of operations was developed simultaneously with development of the MORL system.



The length of Book 5, Task Area IV, has made it necessary to divide the document into two volumes. The first volume, SM-48819A, contains Sections 1 through 4 of the report. Sections 5 through 7, as well as Appendixes A through E, are included in the second volume, SM-48819B.

PREFACE

This report is submitted by the Douglas Aircraft Company, Inc., to the National Aeronautics and Space Administration's Langley Research Center. It has been prepared under Contract No. NAS1-3612 and describes the analytical and experimental results of a preliminary assessment of the MORL's utilization potential.

Documentation of study results are contained in two types of reports: A final report consisting of a Technical Summary and a 20-page Summary Report, and five Task Area reports, each relating to one of the five major task assignments. The final report will be completed at the end of the study, while the Task Area reports are generated incrementally after each major task assignment is completed.

The five Task Area reports consist of the following: Task Area I, Analysis of Space Related Objectives; Task Area II, Integrated Mission Development Plan; Task Area III, MORL Concept Responsiveness Analysis; Task Area IV, MORL System Improvement Study; and Task Area V, Program Planning and Economic Analysis.

This document contains 1 of the 5 parts of the Task Area IV report, MORL System Improvement Study. The study evaluates potential improvements to the MORL, necessitated by the limitations identified in Task Area III, and evaluates those improvements stemming from investigations aimed at increasing the effectiveness of the MORL through the addition of new system elements.

The contents and identification of the five parts of this report are as follows: Book 1, Douglas Report SM-48815, presents the summary of the Task Area effort and the results of the configuration, structure, electrical power, logistics system and performance analyses; Book 2, Douglas Report SM-48816, presents the results of the analyses performed on the Environmental Control/Life Support subsystem; Book 3, Douglas Report SM-48817, presents the results of the analyses performed on the Stabilization and Control subsystem; Book 4, Douglas Report SM-48818, presents the results of the analyses performed on the Communications and Telemetry subsystem; Book 5, Douglas Report SM-48819, presents the results of the analyses performed on the Propulsion subsystem.

Requests for further information concerning this report will be welcomed by R.J. Gunkel, Director, Advance Manned Spacecraft Systems, Advance Systems and Technology, Missile & Space Systems Division, Douglas Aircraft Company, Inc.

PRECEDING PAGE BLANK NOT FILMED.

CONTENTS

VOLUME 1--SM-48819A

	LIST OF ILLUSTRATIONS	ix
	LIST OF FIGURES	xxi
Section 1	INTRODUCTION AND SUMMARY	1
Section 2	SYSTEMS DESCRIPTION	9
	2.1 MORL System	9
	2.2 Phase IIb P/RCS	20
Section 3	LOW THRUST SYSTEMS	59
	3.1 Systems Concept Evaluation	59
	3.2 Preliminary Design Considerations	100
	3.3 Resistojet Parametric Study	114
	3.4 Radioisotope Thrustor	171
Section 4	BASELINE SYSTEM EVALUATION STUDY	239
	4.1 Performance Requirements	239
	4.2 Component Evaluation	241
	4.3 Preliminary Design	265
	ABBREVIATIONS	277
	NOMENCLATURE	279
	REFERENCES	281

VOLUME 2--SM-48819B

Section 5	SYSTEMS INTEGRATION	1
	5.1 Stabilization and Control/Flight Mechanics	1
	5.2 EC/LS	73
	5.3 Power System	83
	5.4 MORL Configuration	97
	5.5 Logistics Resupply	169
	5.6 Crew and Mission Operations	185

Section 6	DEVELOPMENT PLANS	201
	6.1 Updated Bipropellant System	201
	6.2 Resistojet System	214
	6.3 Radioisotope Thrustor System	230
Section 7	SYSTEMS COMPARISON	241
	7.1 Data Summary	241
	7.2 Evaluation Criteria	249
	7.3 Systems Evaluation	250
	7.4 Conclusion and Recommendations	257
	ABBREVIATIONS	267
	NOMENCLATURE	269
Appendix A	P/RCS MODEL SPECIFICATION	271
Appendix B	EXHAUST PLUME ANALYSIS	315
Appendix C	RELIABILITY ANALYSIS	333
Appendix D	RADIOISOTOPE THRUSTOR SHIELDING CURVES	365
Appendix E	PRESSURE SPIKES ASSOCIATED WITH VACUUM IGNITION	369

FIGURES

VOLUME 1--SM-48819A

1-1	MORL Summary Schedule	2
1-2	Task Plan	3
2-1	Manned Orbital Research Laboratory	10
2-2	Propellant RCS Engine Location	13
2-3	MORL Configuration	14
2-4	Brayton Cycle System	17
2-5	Precession and Drag Control Thrust MORL in Spin Mode	25
2-6	P/RCS Bipropellant Schematic	26
2-7	Typical Radiation-Cooled Engine	27
2-8	Resistojet Thrustor	33
2-9	Resistojet Module	36
2-10	Resistojet Hydrogen System	37
2-11	Resistojet Ammonia System	38
2-12	Electric Power Profile	41
2-13	Schematic of Resistojet Power System	42
2-14	Radioisotope Thrustor	44
2-15	Radioisotope Hydrogen System	46
2-16	Radioisotope Ammonia System	47
2-17	Logistics Vehicle	51
2-18	Logistics Vehicle Propellant Transfer System (Bipropellant) (B)	53
2-19	Logistics Vehicle Propellant Transfer System (Advanced Thrustors) (B)	54
2-20	Bipropellant Advanced Orbit Injection System	57
3-1	Marquardt 3kW Concentric Tube Resistojet	62
3-2	Frozen Flow Efficiency as a Function of Specific Impulse	65

3-3	Radioisotope Thrustor for MORL Mission	66
3-4	Ion Engine	69
3-5	Engine Efficiency as a Function of Specific Impulse	70
3-6	Catalytic Monopropellant Engine	70
3-7	AVCO Radiation-Cooled Arc Jet	72
3-8	General Electric Resistance Jet	75
3-9	AVCO 3kW Resistojet	77
3-10	Ion Engine Space Station Control Systems	80
3-11	Linear Strip Ion Engine	81
3-12	Cesium Ion Engine Block Diagram	82
3-13	Typical Pu-238 Fueled Thrustors	83
3-14	Dimensions of Pu-238 Heat Sources	85
3-15	Temperature Distribution for 0.030-lb Thrust Engine	86
3-16	Sublimation Rate for Commercially Pure Tungsten	86
3-17	Vacuum Hot Pulse Performance for Catalytic Monopropellant Engine	87
3-18	Pressure Fed Monopropellant Propulsion Thrustor Schematic	90
3-19	Power as a Function of Thrust	93
3-20	System Weight as a Function of Impulse--Brayton Isotope Configuration	95
3-21	System Weight as a Function of Total Impulse--Solar Panel Configuration	96
3-22	Thrust Effectiveness ϵ	103
3-23	Thrust Allocation	106
3-24	Resistojet Thrustor Allocations	106
3-25	Propellant Weight as a Function of Mission Impulse	108
3-26	Specific Impulse as a Function of Temperature for Several Propellants	109
3-27	Estimated Liquid Hydrogen Storage Tank Weight for Low Thrust Missions	110
3-28	Total Hydrogen Tank Weight as a Function of Propellant Weight Using 100 Layers of HPI.	125
3-29	Tank Weight as a Function of Propellant Weight--Ammonia Propellant	125

3-30	Marquardt 3kW Concentric Tube Resistojet	115
3-31	Resistojet Specific Impulse (as Influenced by Power Level)	116
3-32	Electric Power to Thrust Ratio as a Function of I_{sp}	117
3-33	Tank to Propellant Weight Ratio Comparison	118
3-34	Resistojet Thrustor Locations	121
3-35	Thrust Allocation Zero G Solar Power	121
3-36	Thrust Allocation Zero G Brayton Cycle Power	123
3-37	Laboratory Orbit Relationships, Spin Mode	124
3-38	Resistojet Thrustor Locations, Spin Mode	125
3-39	Thrust Allocation Sequence	125
3-40	Viscous Effects on Low Thrust Nozzle Performance	130
3-41	Estimated Resistojet Performance Specific Impulse as a Function of Thrust	132
3-42	Estimated Resistojet Performance Overall Efficiency as a Function of Thrust	134
3-43	Resistojet Thrust and Propellant Flow Rate as a Function of Design Electric Power Level--Hydrogen	135
3-44	Resistojet Thrust and Propellant Flow Rate as a Function of Design Electric Power Level--Ammonia	136
3-45	Resistojet Thrust and Propellant Flow Rate as a Function of Design Electric Power Level--Hydrazine	137
3-46	Resistojet Thrust and Propellant Flow Rate as a Function of Design Electric Power Level--Water	138
3-47	Resistojet Thrust and Propellant Flow Rate as a Function of Design Electric Power Level--Carbon Dioxide	139
3-48	Resistojet Thrust and Propellant Flow Rate as a Function of Design Electric Power Level--Carbon Dioxide and Water	140
3-49	Total Engine Weight as a Function of Design Electric Power Level	141
3-50	Engine Diameter as a Function of Design Electric Power Level	142

3-51	10-MLB Thrustor Layout	143
3-52	High Response Resistojet Concept	144
3-53	Resistojet Performance for Constant Specific Impulse	146
3-54	Resistojet Performance for Constant Thrust	147
3-55	Resistojet Performance for Cold Flow	147
3-56	3kW Resistojet Discharge Coefficient	151
3-57	High Response Resistojet Chamber Pressure Time Response	152
3-58	Steady-State Resistojet Chamber Pressure Time Response	153
3-59	Hydrogen Resistojet Specific Impulse	154
3-60	Resistojet Thrust Response	155
3-61	Estimated Transient Performance of High Response Resistojet 3kW	156
3-62	Estimated Transient Performance of Steady-State Resistojet 3kW	156
3-63	Typical RCS Thrust Response	159
3-64	RCS Schematic	161
3-65	Biowaste RCS Schematic	162
3-66	Resupply Launch Weight 90 Days	166
3-67	Power Supply Weight	167
3-68	Total Initial Launch Weight	168
3-69	Grand Total Launch Weight (Initial and Resupply)--5-Years	169
3-70	MORL in the Zero G Mode	173
3-71	MORL RCS in the Zero G Mode	173
3-72	MORL in the Spin Mode	178
3-73	MORL Spin Mode Configuration	179
3-74	Specific Impulse as a Function of Temperature	182
3-75	Radioisotope Thrustor for MORL Mission	185
3-76	Radiation Dose Rate--RBP Function	189
3-77	Po-210 Thrustor Weight as a Function of Specific Impulse, RBP Configuration, Ammonia Propellant	195
3-78	Po-210 Thrustor Weight as a Function of Specific Impulse, RBP Configuration, Hydrogen Propellant	196

3-79	Po-210 Thrustor Weight as a Function of Specific Impulse, Solar Powered Configuration, Ammonia Propellant	197
3-80	Po-210 Thrustor Weight as a Function of Specific Impulse, Solar Powered Configuration, Hydrogen Propellant	198
3-81	Pm-147 Thrustor Weight as a Function of Specific Impulse, RBP Configuration, Ammonia Propellant	202
3-82	Pm-147 Thrustor Weight as a Function of Specific Impulse (Hydrogen Propellant RBP Configuration)	202
3-83	Pm-147 Thrustor Weight as a Function of Specific Impulse, Solar Power Configuration, Ammonia Propellant	203
3-84	Pm-147 Thrustor Weight as Function of Specific Impulse, Solar Power Configuration, Hydrogen Propellant	203
3-85	Pm-147 Thrustor Weight as a Function of Specific Impulse, RBP Configuration, Ammonia Propellant	205
3-86	Pm-147 Thrustor Weight as a Function of Specific Impulse, RBP Configuration, Hydrogen Propellant	205
3-87	Pm-147 Thrustor Weight as a Function of Specific Impulse, Solar Power Configuration, Ammonia Propellant	206
3-88	Pm-147 Thrustor Weight as a Function of Specific Impulse, Solar Power Configuration, Hydrogen Propellant	206
3-89	Temperature Profiles, Ammonia Thrustor, 125°F Gas Inlet	214
3-90	Temperature Profiles, Hydrogen Thrustor, -420°F Gas Inlet	215
3-91	Temperature Profiles, Hydrogen Thrustor, 125°F Gas Inlet	215
3-92	Thrustor Thermal Efficiency as a Function of Exit Gas Temperature	217
3-93	Pu-238 Isotope Power as a Function of Thrust Level	218
3-94	Unshielded Pu-238 Thrustor Weight as a Function of Thrust Level	218
3-95	Pu-238 Thrustor Weights as a Function of Specific Impulse, RBP Configuration, Ammonia Propellant	220

3-96	Pu-238 Thrustor Weight as a Function of Specific Impulse, RBP Configuration, Hydrogen Propellant	220
3-97	Pu-238 Thrustor Weights as a Function of Specific Impulse, Solar Power Configuration, Ammonia Propellant	221
3-98	Pu-238 Thrustor Weights as a Function of Specific Impulse, Solar Power Configuration, Hydrogen Propellant	221
3-99	Structure Factor, Initial Launch as a Function of I_{sp} Zero G RBP Configuration, Ammonia Propellant	224
3-100	Structure Factor of Initial Launch as a Function of I_{sp} Zero G, RBP Configuration, Hydrogen Propellant	225
3-101	Structure Factor of Initial Launch as a Function for I_{sp} Zero G, Solar Power, Ammonia Propellant	226
3-102	Structure Factor of Initial Launch as a Function of I_{sp} Zero G, Solar Power, Hydrogen Propellant	227
3-103	Structure Factor, 90-Day Resupply Mission as a Function of I_{sp} Zero G, RBP Configuration, Ammonia Propellant	228
3-104	Structure Factor, 90-Day Resupply Mission as a Function of I_{sp} Zero G, RBP Configuration, Hydrogen Propellant	229
3-105	Structure Factor, 90-Day Resupply Mission as a Function of I_{sp} Zero G, Solar Power, Ammonia Propellant	230
3-106	Structure Factor, 90-Day Resupply Mission as a Function of I_{sp} Zero G, Solar Power Hydrogen Propellant	231
3-107	Structure Factor, 5-Year Mission as a Function of I_{sp} Zero G, RBP Configuration, Ammonia Propellant	232
3-108	Structure Factor, 5-Year Mission as a Function of I_{sp} Zero G, RBP Configuration, Hydrogen Propellant	233
3-109	Structure Factor, 5-Year Mission as a Function of I_{sp} Zero G, Solar Power, Ammonia Propellant	234
3-110	Structure Weight Factor, 5-Year Mission as a Function of I_{sp} Zero G, Solar Power, Hydrogen Propellant	235

3-111	Nozzle Efficiency as a Function of Throat Reynolds Number, 20° Half Angle	237
4-1	Radiation Engine Concept	243
4-2	Radiation/Regeneration Engine Concept (Radiamic)	245
4-3	Radiation/Conduction Engine Concept	247
4-4	Radiation Cooled Engine Maximum Soakback Temperature (Fuel Valve Standoff)	249
4-5	Radiation Cooled Engine Maximum Soakback Temperature (Oxidizer Valve Standoff)	250
4-6	Candidate Propellant Storage Requirements	251
4-7	P/RCS Engine Performance (N ₂ O ₄ /MMH, $\epsilon = 40:1$)	255
4-8	P/RCS Engine Performance (N ₂ O ₄ /50-50, $\epsilon = 40:1$)	256
4-9	P/RCS Engine Performance (I _{SP} DEL = 0.92 I _{SP} F102)	257
4-10	Propellant Equal Volume Tank Mixture Ratio	257
4-11	P/RCS Bipropellant Engine Thrust Level Efficiency	258
4-12	P/RCS Engine Performance (Test-Data)	258
4-13	P/RCS Bipropellant Engine Duty Cycle Efficiency	259
4-14	Predicted Coating Life as a Function of Maximum Wall Temperature Steady-State	260
4-15	P/RCS Engine Maximum Metal Temperature as a Function of Time	261
4-16	P/RCS Engine Cooling Cycle	262
4-17	Propulsion/Reaction Control System Schematic	264
4-18	P/RCS Bipropellant System Performance, Zero G--Solar Panel	266
4-19	P/RCS Bipropellant System Performance, Zero G--Brayton Cycle	268
4-20	P/RCS Bipropellant Artificial G, Engine Efficiency	269
4-21	P/RCS Bipropellant System Performance Artificial G--Solar Panel	270
4-22	P/RCS Bipropellant System Performance Artificial G-Brayton System	272

VOLUME 2--SM-48819B

5-1	MORL Orientations	6
5-2	Effect of Orbit Injection Thrust on Attitude Control Thrust Requirements	9
5-3	Configuration X	12
5-4	Impulse History--Belly-Down Orientation	13
5-5	Impulse History--Inertial Orientation	15
5-6	Yaw and Roll Orientation for Belly-Down Orientation	18
5-7	Simplified Model for Artificial G Spin Mode	23
5-8	Drag Thrust Schedule Over Spin Sector 1, Orbit Sector B	25
5-9	Drag Thrust Over Spin Sector 1, Orbit Sector B	25
5-10	Location of Drag Thrusters	26
5-11	Thrust Level Required to Control Longitudinal Docking Disturbance	26
5-12	Yaw Phase Plane with Low-Thrust RCS	33
5-13	Pitch Phase Plane with Low-Thrust RCS	34
5-14	Engine Locations	39
5-15	Desaturation Thrust Schedule Inertial Orientation	42
5-16	Desaturation Thrust Schedule Inertial Orientation Constant Power	43
5-17	Desaturation Thrust Schedule Belly-Down Orientation	46
5-18	Desaturation Thrust Schedule Belly-Down Constant Power	47
5-19	Thrust Schedule Inertial Drag and Make-up, Attitude Control	47
5-20	Thrust Schedule for Typical Maneuver	49
5-21	P/RCS Bipropellant System Performance, Zero-G Belly-Down	54
5-22	P/RCS Bipropellant System Performance, Zero-G Inertial Mode	56
5-23	P/RCS Bipropellant System Performance, Both Modes	57

5-24	P/RCS Bipropellant Engine Location	58
5-25	P/RCS Bipropellant Belly-Down Duty Cycle	60
5-26	P/RCS Bipropellant Inertial Duty Cycle	61
5-27	P/RCS Bipropellant First Orbit Following Inertial Mode	62
5-28	Resistojet Thrustor Locations	64
5-29	Daily Thrust Allocation	65
5-30	Radioisotope Daily Thrusting Schedule	69
5-31	Engine Out Thrusting, Local Horizon Orientation	71
5-32	Phase IIa EC/LS System	74
5-33	Phase IIb EC/LS System--H ₂ O Electrolysis	76
5-34	Phase IIb EC/LS System--O ₂ Regeneration	78
5-35	Brayton Cycle System Schematic	84
5-36	Dual K _{WE} Reference Block Diagram	85
5-37	Resistojet RCS Block Diagram	86
5-38	Daily Electric Power Profile--H ₂	88
5-39	Resistojet Power Schematic	93
5-40	Heat Exchange Schematic	95
5-41	Radiation Engine Concept	98
5-42	10-mlb Thrustor Layout	102
5-43	Resistojet Thrustor Module	105
5-44	Resistojet H ₂ Schematic	106
5-45	Resistojet NH ₃ Schematic	107
5-46	Radioisotope Module	108
5-47	Exit Gas Temperature as a Function of Total Mass Flow Rate	112
5-48	Thrust Level as a Function of I _{SP} Delivered	112
5-49	Bipropellant Tank and Feed System	114
5-50	Advanced RCS NH ₃ Storage System	118
5-51	NH ₃ Feed System Installation	120
5-52	Hydrogen Feed System Installation	122
5-53	Total H ₂ Weight as a Function of Tank Pressure	123
5-54	Advanced RCS H ₂ Tank Heat Balance	126

5-55	H ₂ Tank Support System	126
5-56	H ₂ Tank Heat Transfer Analysis	128
5-57	Advanced RCS Tank System Characteristics	131
5-58	Advanced RCS H ₂ Storage System	133
5-59	Nuclear Radiation Shield H ₂ Thrustor	137
5-60	Variation of Shield Weight with Gamma Fraction and Power Level	140
5-61	Solid Engine Selection Thrust Level as a Function of Lift/Drag	143
5-62	Advanced RCS Solid Motor Orbit System	144
5-63	Advanced P/RCS Solid Motor Orbit Injection System	146
5-64	Bipropellant Orbit Injection System (A)	148
5-65	Monopropellant Orbit Injection System	151
5-66	Resistojet Reaction Control System Layout	158
5-67	Radioisotope Thrustor Reaction Control System Layout	159
5-68	Bipropellant Reaction Control System Layout	164
5-69	Logistics System Utilization	170
5-70	Propellant Supply Processes	174
5-71	Final Tank Temperature as a Function of Initial Tank Quality	174
5-72	Heating Effects of Aluminum Fill Line	175
5-73	Logistics Vehicle Cargo Module	179
5-74	Logistics Vehicle Propellant Transfer System (Bipropellant) (A)	182
5-75	Logistics Vehicle Propellant Transfer System (Advanced Thrustors) (A)	183
5-76	Stagnation Heat Flux for Tumbling Thrustor (Orbital Decay)	191
5-77	Tumbling Thrustor Temperature Profile (Orbital Decay)	192
5-78	Heat Flux Profile for Spinning Finned Thrustor (Orbital Decay)	193
5-79	Temperature Profiles for Spinning Finned Thrustor (Orbital Decay)	194
5-80	Isodose Curves	197

6-1	Resistojet Development Plan	215
6-2	Radioisotope RCS Development Schedule	231
6-3	Radioisotope RCS Development Test Sequence	232
7-1	Launch Weight as a Function of Specific Impulse	253
7-2	Initial Launch Weight as a Function of Resupply Weight	253

PRECEDING PAGE BLANK NOT FILMED.

TABLES

VOLUME 1--SM-48819A

2-1	MORL System Design Criteria	11
2-2	P/RCS System Summary	22
2-3	Propulsion System Design Data	29
2-4	Propulsion/Reaction Control System Engine Performance	30
2-5	P/RCS Weight Summary	32
2-6	Resistojet P/RCS Design Characteristics	35
2-7	Resistojet P/RCS Engine Performance	39
2-8	Resistojet P/RCS Weight Summary	43
2-9	Propulsion System Design Parameters	48
2-10	RCS Performance	49
2-11	Weight Summary	50
2-12	Advanced P/RCS Storable Bipropellant Orbit Injection System Design Parameters	56
3-1	MORL RCS Preliminary Requirements and Specifications	60
3-2	RCS Duty Cycle	61
3-3	Thruster Concepts and Contractors	62
3-4	Radioisotope Radiation Fields and Availability	68
3-5	Marquardt Resistojet Performance	74
3-6	Giannini Resistojet Performance	74
3-7	General Electric Resistance Jet Performance	76
3-8	AVCO Resistojet Performance (1kW)	76
3-9	Arc-Jet Performance	78
3-10	Contact Ion Engine	79
3-11	Radioisotope Thruster Performance	83
3-12	Catalytic Monopropellant Thruster Performance	88
3-13	Thruster Performance	89
3-14	RCS Duty Cycle (Typical)	92

3-15	System Weight Tabulations (147 Days)	97
3-16	Reaction-Control System Requirements (Preliminary Design Phase)	101
3-17	Reduced Spin Cycle Requirements	105
3-18	Propellant Physical and Thermodynamic Properties	114
3-19	Total Impulse Requirements	119
3-20	Total Impulse Requirements (Combined Thrust Functions)	122
3-21	Total Impulse Requirements (Precession)	123
3-22	Summary of Impulse Requirements	127
3-23	Resultant Thrust Levels	127
3-24	Resistojet Performance Test (25 Hours)	128
3-25	3 kW Resistojet Time Constants	152
3-26	Preliminary Design Summary (Zero-G Mode--Local Horizontal Oriented)	163
3-27	Preliminary Design Summary (Artificial-G Mode--Spin Axis Sun Oriented)	164
3-28	System Weights (Zero-G Mode/Local/ Horizontal Oriented)	169
3-29	System Weights (Artificial-G Mode--Spin Axis Sun Oriented)	170
3-30	Near-Optimum Yaw Thrust Levels and Burn Times for the Solar-Powered MORL in the Zero-G Mode (Pu-238-Fueled Thrustors)	174
3-31	Thrust and Impulse Requirements for the RBP Configuration Zero-G Mode	176
3-32	Thrust and Impulse Requirements for the Solar-Powered Configuration Zero-G Mode	177
3-33	Impulse Requirements for the MORL in the Spin Mode	180
3-34	Potential Performance Capability of Biowaste Propellants	183
3-35	Biowaste Propellant Utilization Zero-G Mode	185
3-36	Radioisotope Radiation Fields and Availability	188
3-37	Typical Capsule Dimensions and Weights Po-210 Isotope--207 Day Capsule Life	194
3-38	Typical Capsule Dimensions and Weights (Pm-147 Isotope--5.17 Yr Capsule Life)	201

3-39	Typical Capsule Dimensions and Weights (Pm-147 Isotope--1,090-Day Capsule Life) F = 0.015 lb	204
3-40	Typical Capsule Dimensions and Weights (Pu-238 Isotope--F = 0.015 lb)	210
3-41	Typical Capsule Dimensions and Weights (Pu-238 Isotope--CO ₂ Propellant)	212
4-1	Propulsion/RCS Engine Requirements (Total Impulse/Orbit or Event) lb-sec	240
4-2	Propellant Environmental Temperature	248
4-3	Propellant Physical and Chemical Properties	252
4-4	Propulsion/Reaction Control System Thrust Levels	273
4-5	Propulsion/Reaction Control System Propellant Quantity Requirements	274
4-6	Zero-G, Brayton-Cycle Propulsion System Design Parameters	275

VOLUME 2--SM-48819B

5-1	Stabilization and Control Performance Requirements	4
5-2	Impulse Requirements for Long-Term Manned Zero-G Stabilization	16
5-3	Impulse Requirements--Inertial Orientation	20
5-4	Impulse Requirements for Artificial-G Spin Mode	22
5-5	Disturbances	29
5-6	Gradient Disturbance Torques	31
5-7	Gradient Disturbance Torques with Solar Panels	31
5-8	Typical Maneuver of MORL Spacecraft	36
5-9	Inertial Orientation	40
5-10	Belly-Down Orientation	45
5-11	Propulsion/RCS Operational Requirements, lb-sec/Orbit	53
5-12	Thruster Assignments	66
5-13	Available Impulse	73
5-14	EC/LS Scheme IIC	79
5-15	Combined EC/LS and Propulsion Logistic Requirements	80
5-16	Load Distribution, Watts	90
5-17	Heated Gas System Performance	96

5-18	Thrustor System Design Parameters	99
5-19	P/RCS Engine Performance	100
5-20	Electrical Parameters Nominal 10 mlb Thrustor	103
5-21	Performance Summary Nominal 10 mlb Thrustor	103
5-22	Thrustor Characteristics	109
5-23	Thrustor Performance Characteristics	110
5-24	P/RCS Tank Volumetric Design Criteria	115
5-25	P/RCS Tank Design Criteria	116
5-26	Advance Thrustor RCS NH ₃ Requirements	119
5-27	Advance Propulsion Tank Design Requirements	124
5-28	Advance RCS H ₂ Tank Support Characteristics	127
5-29	Advance RCS H ₂ Tank Support--Total Heat Transfer	127
5-30	Advance RCS H ₂ Tankage System Characteristics	132
5-31	Tank and Feed System Characteristics Summary	135
5-32	Shielding Requirements	139
5-33	Advance RCS Solid Propellant Injection Motor Design Summary	144
5-34	Advance RCS Solid Motor Orbit Injection System Summary	147
5-35	Advanced RCS Storable Liquid Injection System Design	150
5-36	Advance RCS Monopropellant Injection System Design Parameters	152
5-37	Advance RCS Orbit Injection System Selection	154
5-38	P/RCS Propellant Weight Summary	166
5-39	P/RCS Hardware Weight Summary	166
5-40	P/RCS System Weight	167
5-41	Propellant Resupply	178
5-42	Resupply System Summary	180
5-43	Guidelines for Protracted Radiation Exposures for MORL	196
5-44	Reliability Summary of P/RCS	199
6-1	Resistojet Cost	229

7-1	Updated Bipropellant (MORL Baseline) P/RCS Performance	242
7-2	Advanced Thrustor P/RCS Performance	243
7-3	P/RCS Performance Comparison	244
7-4	Updated Bipropellant (MORL Baseline) Dry System Weight Summary	246
7-5	Advanced Thrustor Dry System Weight Summary	247
7-6	P/RCS Weight Summary Chart (Zero-G Configuration)	248

Section 1

INTRODUCTION AND SUMMARY

The MORL Propulsion/Reaction Control system (P/RCS) study consisted of the following three major study phases: (1) an advance P/RCS study, (2) a baseline system evaluation study, and (3) a systems integration study.

Figure 1-1 is a summary schedule of the 6-month study.

The advance P/RCS study consisted of an evaluation of advanced chemical, electrical, and radioisotope thermal propulsion system concepts for application to the MORL mission. At the conclusion of this evaluation, a selection was made. A Resistojet and a radioisotope thruster system were selected for preliminary design integration into the MORL system. Two propulsion subcontractors were selected: (1) The Marquardt Corporation to perform the preliminary design for the Resistojet thruster; (2) TRW Systems to perform the preliminary design effort on the radioisotope thruster.

The baseline system evaluation study consisted of a review of the components of the P/RCS baseline system established during the MORL Phase IIa study. The purpose of this evaluation was to establish those components of the system requiring updating of the design as a result of advances in technology, related subsystem design changes resulting from the MORL responsiveness analysis, and the change in the anticipated MORL launch date to the 1970 time period.

The systems integration study utilized the results of the two previous studies to integrate the preliminary designs of both the updated liquid bipropellant system and the two advanced systems with the MORL mission and operations. This study was performed during the latter phase of the MORL Phase IIb study and made maximum use of MORL study personnel and information.

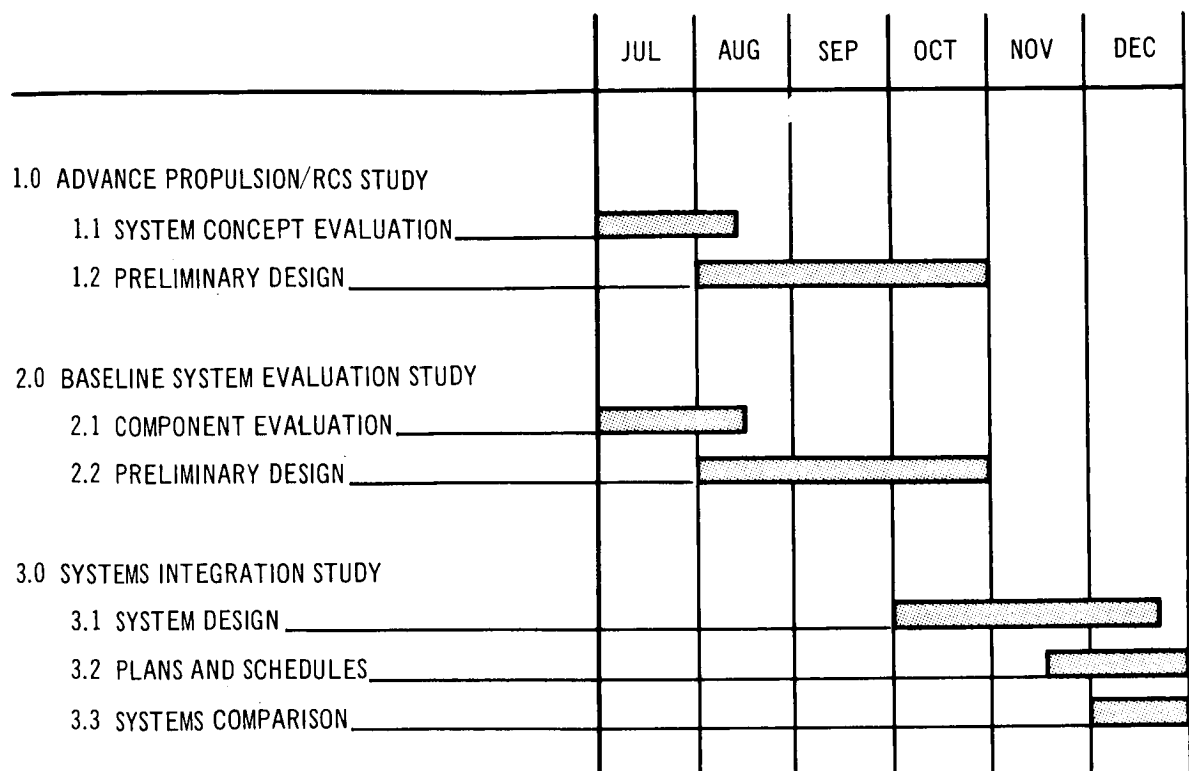


Figure 1-1. MORL Summary Schedule

Subcontractor work statements were revised to extend the scope of Marquardt and TRW contracts to support the effort to integrate both the Resistojet and radioisotope thruster system with the MORL Phase IIb study. The primary objective of this study was to define complete integrated P/RCS systems which satisfied the MORL mission requirements so that a detailed comparison of the systems could be made.

Figure 1-2 is a logic diagram of the task plan utilized for the study. This diagram illustrates the iterative logic which was utilized in performing the study, beginning with an evaluation and parametric design and, finally, an integration of these designs with the MORL system.

Initially, preliminary requirements and design constraints, such as thrust and impulse duty cycles, launch and orbital environment, and detailed operational mission requirements, were established for use in the parametric

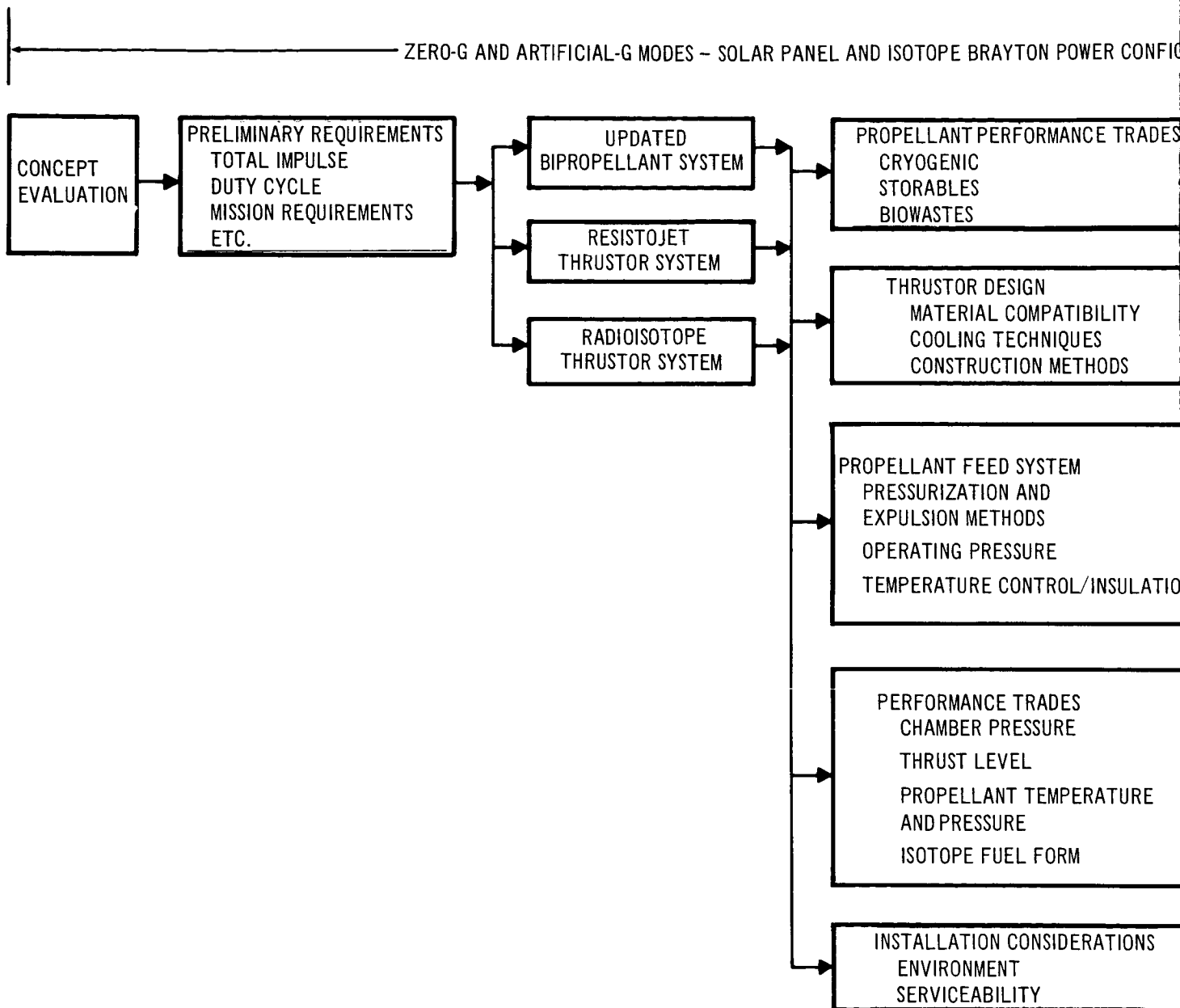
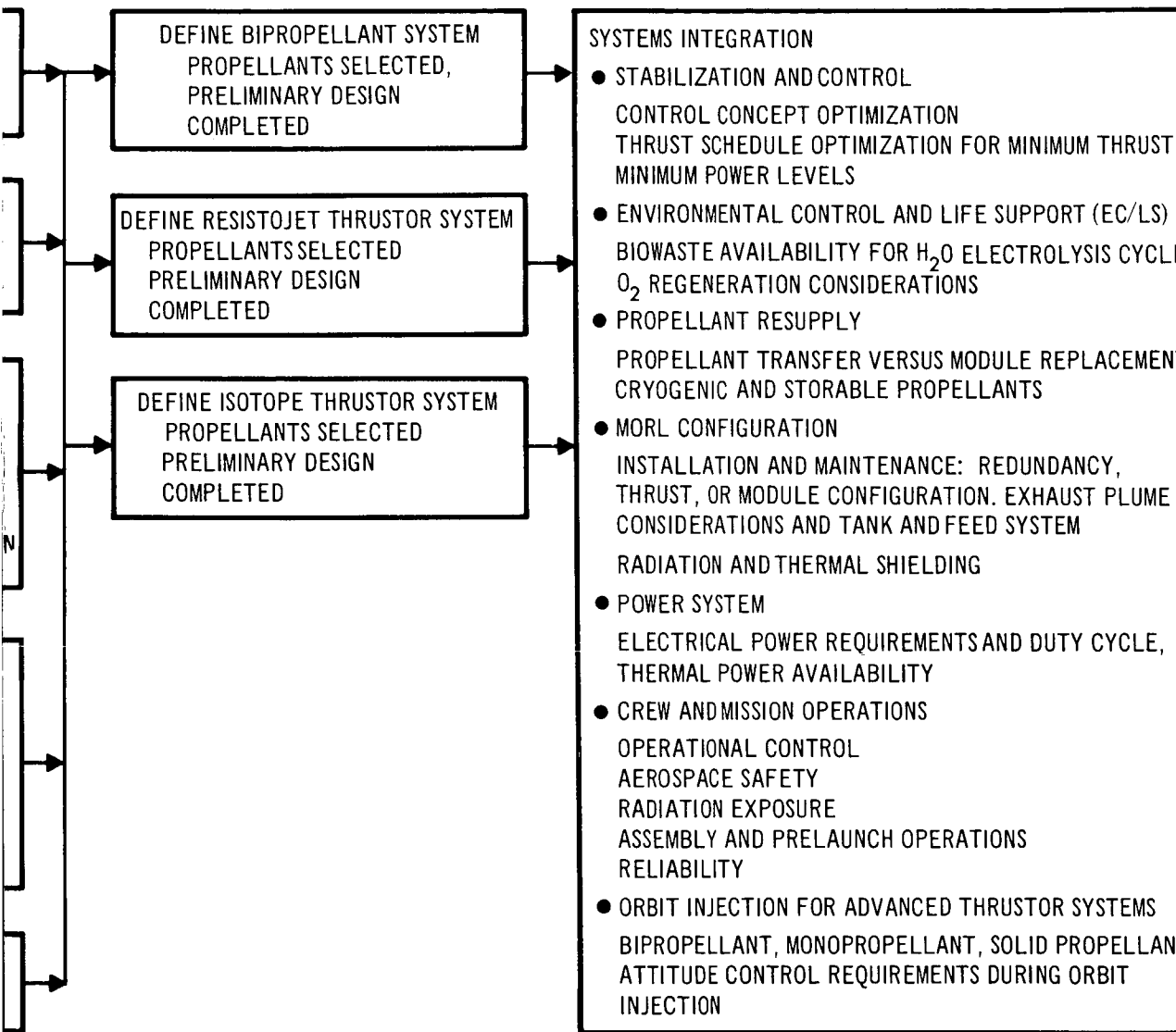
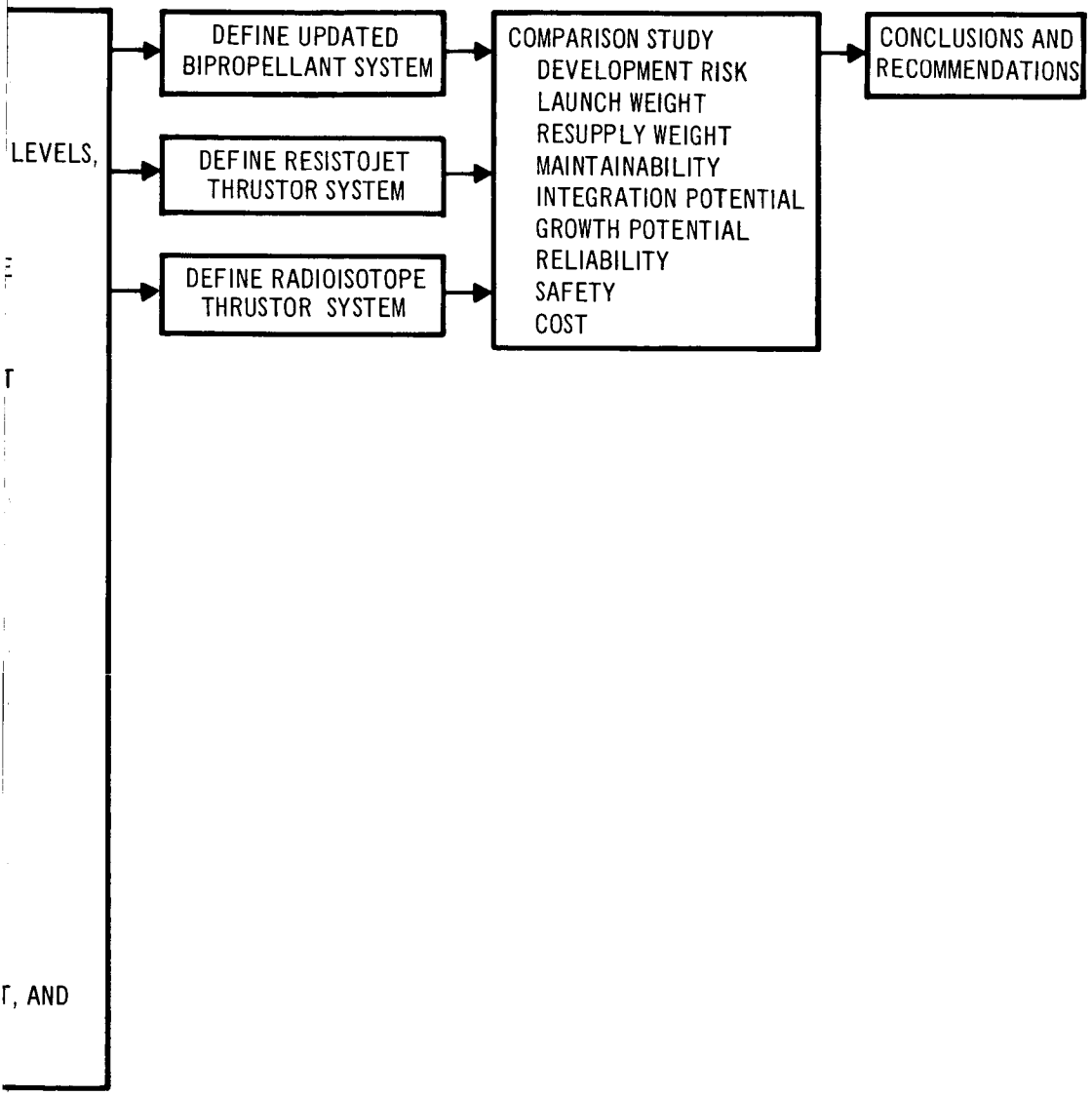


Figure 1-2. Task Plan



RATION (ZERO-G MODE, ISOTOPE BRAYTON POWER SYSTEM)



design of the three thrusters. Both the solar panel and the Brayton Cycle power system laboratory configurations were considered during this phase of the study. These configurations were evaluated for both the zero-g and artificial-g modes. On the basis of this work, the parametric design and analysis was then undertaken for the bipropellant system, the Resistojet system, and the radioisotope system.

The analysis consisted of evaluation and tradeoff studies which led to the solution of problems in the following areas:

1. Propellants.
2. Thrustor materials and cooling techniques.
3. Radioisotope fuel form.
4. Propellant storage, pressurization, and feed techniques compatible with resupply, environmental, and serviceability considerations for potential installation of the systems on the vehicle.

Also, performance tradeoff studies in terms of chamber pressure, thrust levels, and overall efficiencies were performed.

The results of this phase of the study provided a preliminary definition in the form of parametric data for the integration of both the bipropellant and the advanced thrusters with the MORL system.

The systems integration study identified the following significant interfaces with the propulsion systems: (1) stabilization and control/flight mechanics, (2) environmental control/life support (EC / LS), (3) power, (4) laboratory configuration, (5) logistic resupply, (6) orbit injection requirements, and (7) interface with the MORL mission crew operations.

Total impulse and torque requirements were defined for each mission event, function, or disturbance, and the ability of the low-thrust systems to satisfy these requirements was investigated. Thrust schedules and control logic were established for both the high- and low-thrust systems based on the zero-g baseline vehicle which utilizes the belly-down orientation with 4-hour excursions of inertial orientation per day. 100-lb and 50-lb thrust engines were selected for the updated bipropellant system. A thrust level of 9.8 mlb

was selected for the resistojet thrusters and thrust levels of 16.4 and 4.0 mlb were selected for the radioisotope thrusters. 100-lb thrust level engines were selected to perform all high thrust mission requirements for both the updated bipropellant's systems and the advanced systems. Thrust schedules for the advanced low thrust systems were established to provide controls for attitude hold, orbit keeping and CMG desaturation during zero-g operation. In addition, orbit keeping and precession control thrust schedules were established for the alternate spin mode.

The effect of the resistojet load characteristics and power consumption profile on the electrical power system was investigated and the optimum load bus assignment and weight penalties were determined. The maximum power demand for the hydrogen resistojet system is 1.16 kW electrical. This represents approximately 10% of the total PBC capacity. A weight penalty for power consumption of 289 lb is assessed for the hydrogen resistojet and 186 lb for the ammonia system. Waste heat of 4.8 kW at 335°F downstream of the EC/LS heat exchanger is utilized to satisfy the thermal requirements for the cryogenic tank and feed system.

EC/LS biowastes (CO_2 , H_2O , and H_2) were identified during the integration phase and performance of these wastes as potential propellants was evaluated. It was determined that sufficient biowastes are available to satisfy the performance requirements for the MORL baseline mission. The combined MORL logistics resupply weight can be reduced by 985 lb if a P/RCS utilizing biowastes with a water electrolysis life support system is considered. With an oxygen regeneration life support system, although no biowastes are available for propulsion, the lowest combined resupply weight results when combined with a hydrogen advanced P/RCS. However an oxygen regeneration system imposes a high power requirement on the MORL system. A detailed tradeoff study should be performed to evaluate an optimum P/RCS-EC/LS system before a final conclusion is made.

The propellants selected for the updated bipropellant system are NTO/MMH. This selection represents a change from the Phase IIa bipropellant system which utilized IFRNA/MMH and represents an increase in overall system performance and a reduction in total system weight. The thruster logic utilized for the updated bipropellant system results in an additional system weight savings because of the

reduced impulse requirements. Both hydrogen and ammonia propellants are good candidates for the advanced resistojet and radioisotope thrusters. The hydrogen system although providing a higher specific impulse and therefore minimum propellant consumption requires cryogenic storage which results in some increase in total systems weight. Both propellants are expelled from the tanks by their own saturation pressure thus providing a system which does not require a separate pressurization system for propellant feed to the engines. Pu-238 fuel was selected for the radioisotope thruster because its long half life, when utilized with the porous plug technique, results in the lowest total systems weight.

The orbit injection systems selected consist of four 100-lb thrust engines utilizing the same bipropellant combinations NTO/MMH. For the updated bipropellant system, attitude control is provided by the 50-lb RCS thrusters. For the advanced systems, roll control is performed by separate bipropellant thrusters, and pitch and yaw control is accomplished by differential throttling of the 100-lb thrust engines.

Several problem areas were identified in terms of the operation, maintenance and replacement of the thrust systems onboard the MORL. Preliminary studies indicate that in all cases extravehicular activities are required by the crew members for replacement and maintenance of the thrusters. Replacement of a radioisotope thruster requires crew member protection by radiation shielding. Based on a cursory evaluation of crew time considerations, it appears desirable to utilize a boom for thruster replacement in most cases. This would require modification or redesign of the present experimental boom.

A thermodynamic analysis to evaluate the feasibility of transferring cryogenics in zero-g environment indicates that technique is feasible. Although the logistics launch weight is about 75 lb heavier for the propellant transfer technique, it was concluded that propellant transfer is more feasible because of the logistic and accessibility problems associated with tank transfer.

The detailed definition of the three propulsion/RCS systems resulting from the systems integration study is given in Section 2. The comparison of these systems in terms of their capability to satisfy the MORL system requirements is given in Section 7.

The following summarizes the major conclusions and recommendations resulting from this study.

The bipropellant system has the least development risk. It has a limited integration or growth potential because of the low specific impulse and is not easily adaptable to the utilization of biowastes. It has a low launch weight, but requires a high logistics resupply weight as shown in Figure 7.2-2. Resupply operations are more complex for the bipropellant.

The resistojet has fewer maintainability problems and fewer safety hazards in operational use than the bipropellant or radioisotope thruster systems. The radioisotope thruster system has a lower launch weight than the resistojet system, because of the weight assessment for the resistojet power demand. It has a higher development risk at this time because of its early stage of development. The availability of the fuel form is not well defined at the present time.

Both advanced systems provide an essentially continuous thrust, thus minimizing interference with experiments by:

1. Continuous drag cancellation (provides a constant vehicle velocity, orbital altitude, and zero-g field).
2. Elimination of noise disturbances.

Hydrogen propellant offers a logistic weight saving but results in a higher launch weight as shown in Table 7.2-1.

The results of this study indicate that further integration studies should be performed to fully define an advance P/RCS system for application to MORL. In addition, a test vehicle should be defined for space environment systems test and evaluation.

As shown in Section 5.2, a biowaste propulsion system can reduce resupply weight significantly compared to a bipropellant system. Even greater weight savings are possible using an oxygen regeneration life support cycle, however, a tradeoff in terms of cost and complexity exists since higher electrical and

thermal power is required and a propellant (cryogenic hydrogen or NH_3) must be resupplied rather than water. Further study is necessary to establish the optimum biowaste conditioning system and propulsion system combination.

The P/RCS control logic and mechanization schemes should be defined by further optimization. The optimum control logic should consider the combined requirements of the high thrust functions such as orbit injection, and the low thrust attitude control function.

Several techniques for orbit injection should be investigated in order to determine the optimum method of providing the velocity increment and attitude control requirements.

The advanced thruster recommended for early application is the Resistojet because of the greater amount of technology available, and fewer safety and availability problems.

As discussed in Section 8.3, engine life may be influenced by several factors. The determination of engine life by long-duration tests of a Resistojet thruster is recommended. These tests should provide correlation data to support the conclusions resulting from the analysis work performed in a system study. Inputs from the system study, such as thrust level, flow rates, feed system geometry, and duty cycle based on the required control logic will establish a meaningful test plan. In addition, measurements should be made of the exhaust plume characteristics to provide a foundation for data correlation for regions away from the nozzle exit, as discussed in Section 7.3.

Further study of the radioisotope thruster for later application to the MORL is also recommended because of the potential advantages of a long operating life and an independent power source.

Section 2

SYSTEMS DESCRIPTION

The purpose of this section is to present a summary description of the MORL baseline (Phase IIb) system and the three Propulsion/Reaction Control systems (P/RCS) which resulted from the study.

2.1 MORL SYSTEM

The Manned Orbital Research Laboratory (MORL) is a 260 in. diam vehicle designed to perform scientific and engineering experiments in a low Earth orbit for an extended mission life of up to 5 years (Figure 2-1). This section describes the MORL mission, the vehicle, and the design criteria which provided the bases for the design and integration of the P/RCS with the MORL. Table 2-1 presents a summary of design criteria.

2.1.1 Mission

The MORL baseline mission is performed in a 164-nmi circular orbit at an inclination of 50° . Alternate missions will be circular 164-nmi orbits at 30° and 90° inclinations and circular 19,350-nmi (synchronous) orbits at a 28.72° inclination.

The MORL vehicle will be launched by a Saturn IB booster in the period between 1972 and 1975. Initial manning with a crew of three is expected to occur 2 to 5 days after launch. Full manning, with a crew of six men, will occur with the second supporting logistic launch at approximately 50 days. Thereafter, logistic support of the mission will occur at nominal 90-day intervals with a maximum interval of 147 days. Emergency resupply can be obtained in a maximum of 6 days; however, such measures are available only for critical mission problems. Adequate logistic capability is maintained to provide for evacuation of the entire crew aboard the laboratory at any time. Provision is also made for scheduled rotation of crew members.

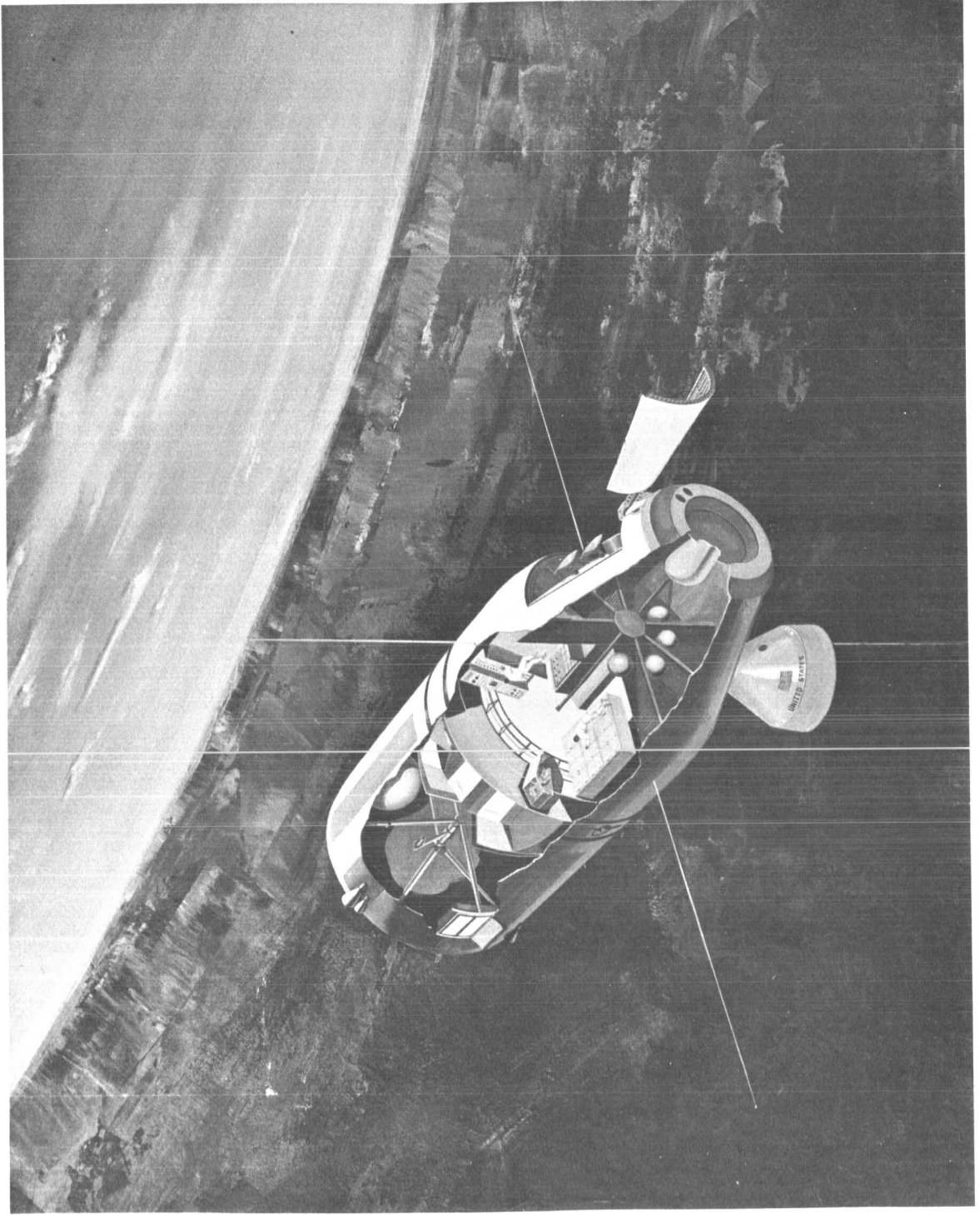


Figure 2-1. Manned Orbital Research Laboratory

Table 2-1
MORL SYSTEM DESIGN CRITERIA

Criteria	Description or Magnitude
Mission duration	5 years
Orbital mode	Zero-g-Local horizontal orientation (belly-down) or inertial orientation for extended periods with return to belly-down for drag makeup Artificial-g Solar orientation (alternate)
Power supply	Isotope Brayton Cycle 11 kW _e ; solar cell (alternate) 6 kW _e
Electrical power available for P/RCS	1-3 kW _e (assess 300 lb/kW _e for Brayton Cycle; 500 lb/kW _e for solar panels)
Thermal power available for P/RCS	
Isotope Brayton Cycle (waste heat)	4.8 kW _{th} , 335°F
Isotope fuel block	4-12 kW _{th} , 1,650°F (assess 41.0 lb/kW _{th})
Critical radiation	225 Rem/man/90 days
Reliability	0.998
MORL weight	
In orbit (max)	100,000 lb
Launch (max)	33,000 lb
Environment	Design criteria in accordance with Specifications SM-48150 and SM-48151
Personnel	6-9 men
Resupply frequency	90-147 days
Propellant supply	
Operational	147 days
Launch	20 days
Biowastes	
CO ₂	14.0 lb/day
H ₂	1.6 lb/day
Temperature conditions	
Interstage skin	40° to 240°F
Aft section internal area	125° ±10°F
Cabin pressure O ₂ (50%), N ₂ (50%)	7 psia at 75°F

The MORL will be placed into orbit without spin-deployment capability to operate solely as a zero-g laboratory. However, if zero g proves to be unacceptable for long-term operations, spin-deployment equipment can be added to a second MORL vehicle for subsequent launch. The spent S-IVB stage is deployed by cables to act as a counterweight and the laboratory and Saturn IVB are rotated about a common axis. The configurations of the laboratory for the zero-g and rotating modes are shown in Figure 2-2.

2.1.2 Vehicle Configuration

The MORL configuration (Figure 2-3) consists of five sections:

- Hangar/Test area.
- Control deck.
- Centrifuge.
- Flight crew quarters.
- Aft section.

There are two access ports, one through the Hangar/Test area and one through the aft airlock. As shown in Figure 2-3 a boom is attached to the external skin of the vehicle. This boom is normally used as an experiment handling boom for a number of experiments that need to be conducted at a distance from the laboratory.

The Hangar/Test area is separated from the forward pressure compartment by a pressure bulkhead. It is an environment-controlled experimental test area and acts as a transfer airlock for personnel moving from the logistic spacecraft into the main portion of the laboratory. It also provides an emergency living area for the crew.

The control deck or operations area is the area from which the MORL is managed. The major portion of the experimental program is conducted and controlled from this area. It is divided into four sections by the consoles and partitions. One console is associated with operations, as well as with

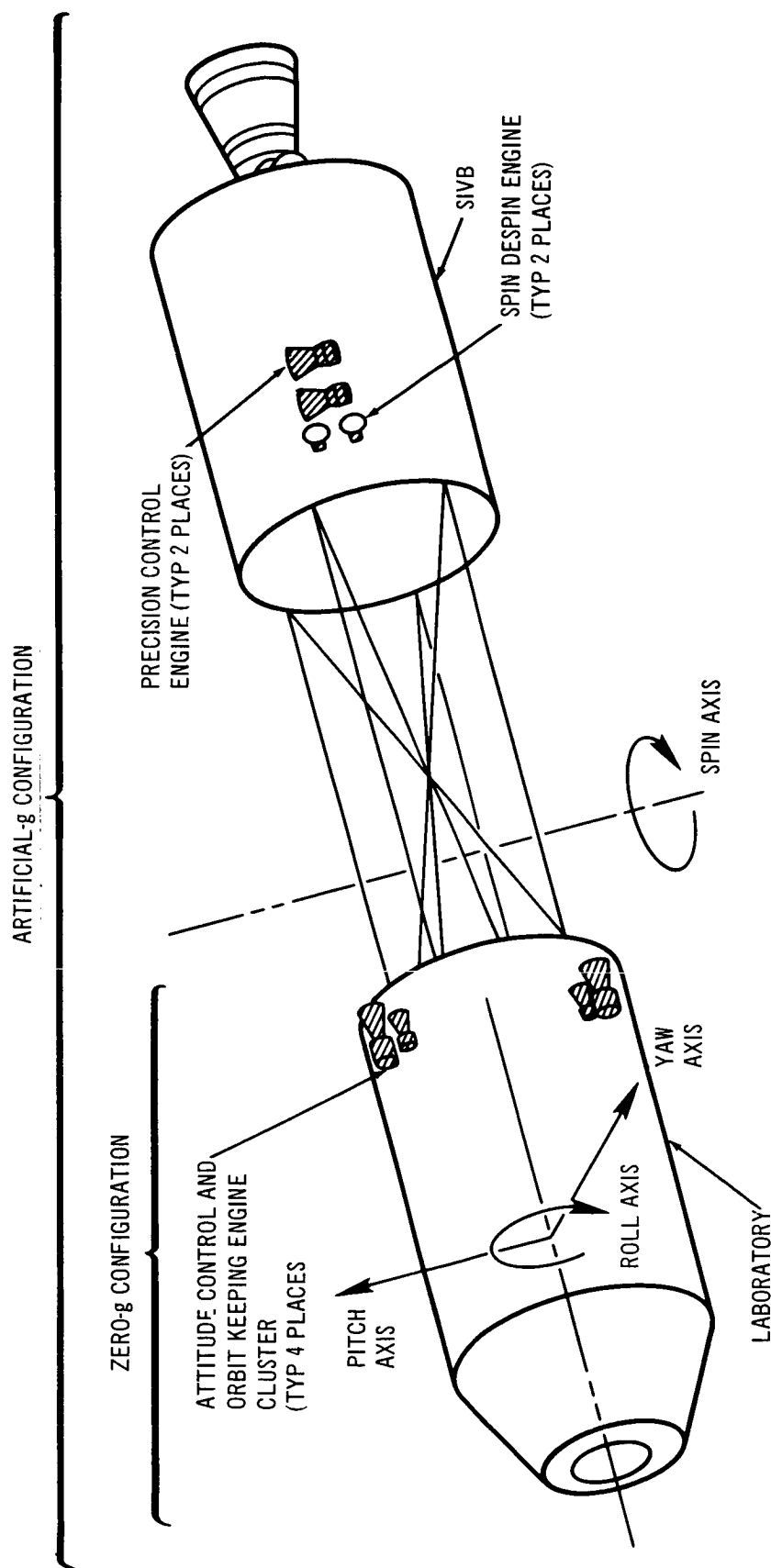


Figure 2-2. Propellant RCS Engine Location

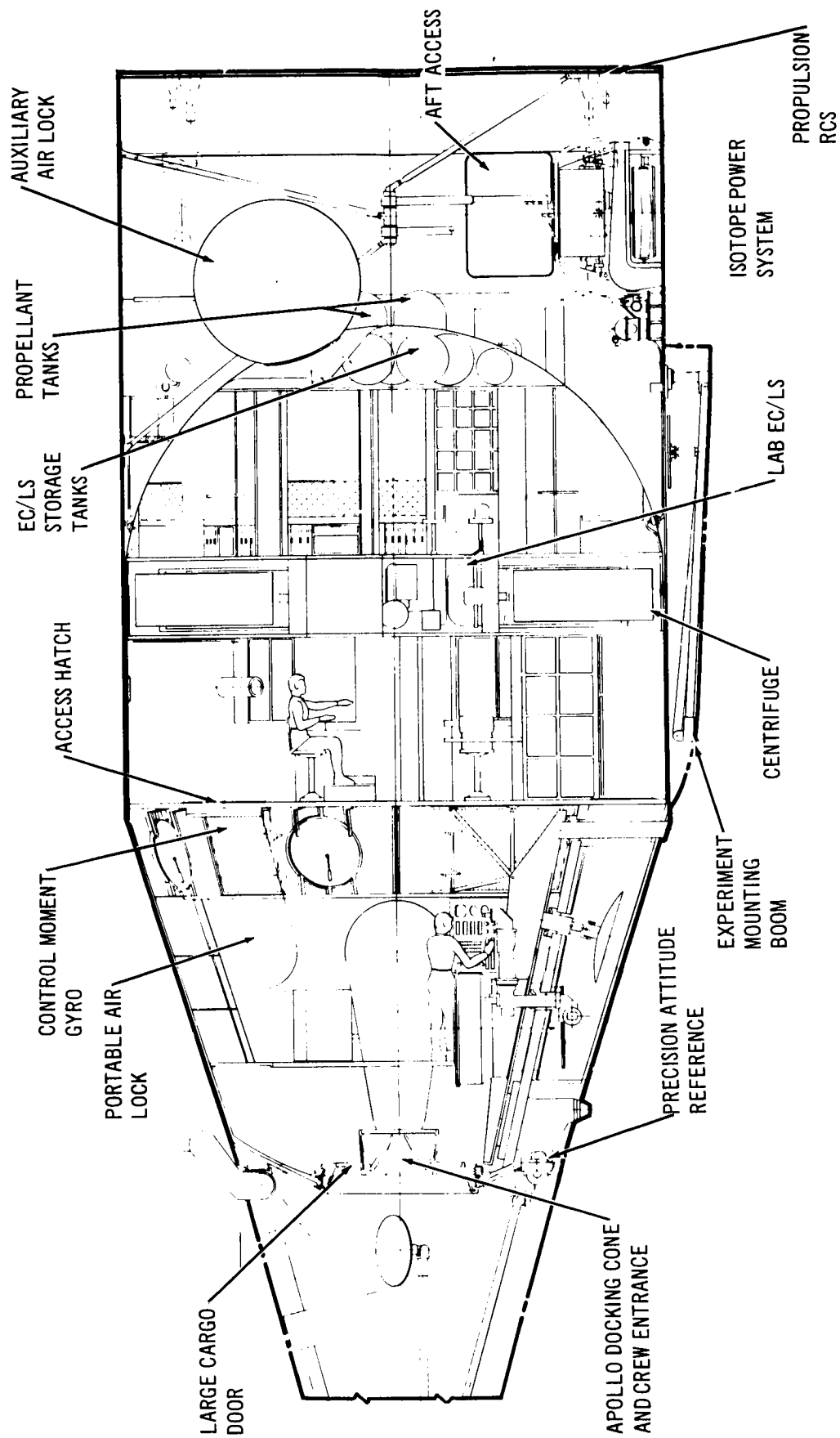


Figure 2-3. MORL Configuration

command and control of the stations; one is associated with experiment control; the last two are devoted to experiment procedures.

The centrifuge is used for personnel conditioning and experimental studies and is located in a cylindrical section between the crew-quarters deck and the operations deck.

The flight crew quarters is designed for normal off-duty living. Six compartments are provided for sleeping and for storage of personal effects. The center area of the flight crew quarters is a recreation and exercise area.

The aft section of the laboratory is an unpressurized area enclosed within the interstage structure. This area contains the PBC system and the P/RCS propellant tanks, and it is used for special space vacuum experiments and installation of special items of equipment.

2.1.3 Subsystems

The major mechanical functions required of the laboratory are provided by the following subsystems.

2.1.3.1 P/RC System

The P/RCS (zero-g mode) comprises four engine modules which are installed outside the laboratory meteoroid-protection structure. Each engine module contains three 50-lb and one 100-lb thrust engines, for a total of 16 engines on the laboratory. Figure 2-2 shows the location of the engines on the MORL.

The P/RCS precession and spin-despin modules (artificial-g mode) are installed on the forward interstage area of the S-IVB stage. There are two independent self-contained modules located 180° apart. Each contains a cluster of four 100-lb thrust chambers, propellant tanks, and appropriate pressurization and feed-system components. A detailed description of the Phase IIb baseline P/RCS is given in Section 2.2.

2.1.3.2 Stabilization and Control System

The stabilization and control system (SCS) is designed to satisfy the orientation and attitude control requirements which arise from both the experimental phase of the mission and the operational events associated with placing and maintaining a laboratory facility in space.

To accommodate the fine attitude hold requirements of some experiments, a precision attitude reference is provided. This system, which can provide attitude reference information in either the belly-down or inertial orientations, consists of a 3-platform gyro package, two 2-axis star trackers, and a special purpose computer. The gyro package differs from the conventional gimbaled platform in that three separate, single gimbal platforms are used. This configuration improves maintainability by permitting replacement of an individual platform.

Control torques, needed to maneuver the laboratory or stabilize it in a selected orientation, are provided by control moment gyros and the P/RCS. The CMG's provide primary actuation because of the efficiency resulting from their momentum storage feature. The P/RCS supplies external torques for desaturating the CMG's and for other events requiring high torque capability.

2.1.3.3 Power Systems

The power systems are discussed in the following sections.

Brayton Power Cycle

The baseline power source consists of a dual Pu-238 Radioisotope Brayton Cycle system. (Figure 2-4). Each loop is capable of generating 5.5 kW_e using a Pu-238 fueled heat source. Argon is heated at the fuel block and expands through a turbine, passes to a recuperator and a radiator heat exchanger, into a compressor, and returns to the fuel block via the recuperator. The radiator heat exchanger loop carries FC-75 organic coolant to the 920 ft^2 main vehicle radiator located on the 17.4 ft cylindrical aft portion of the space station. Thus a total of 11 kW_e average is generated

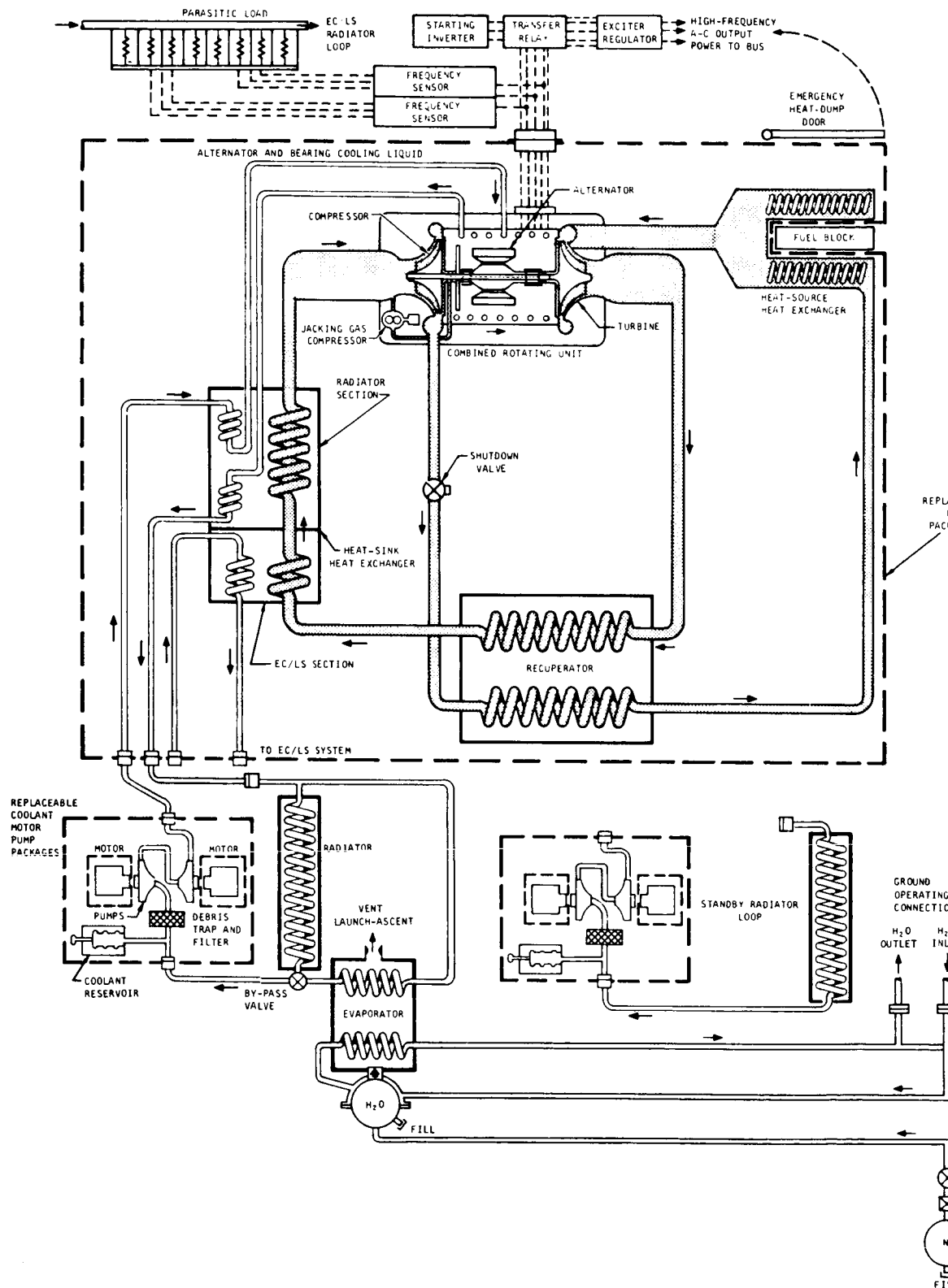
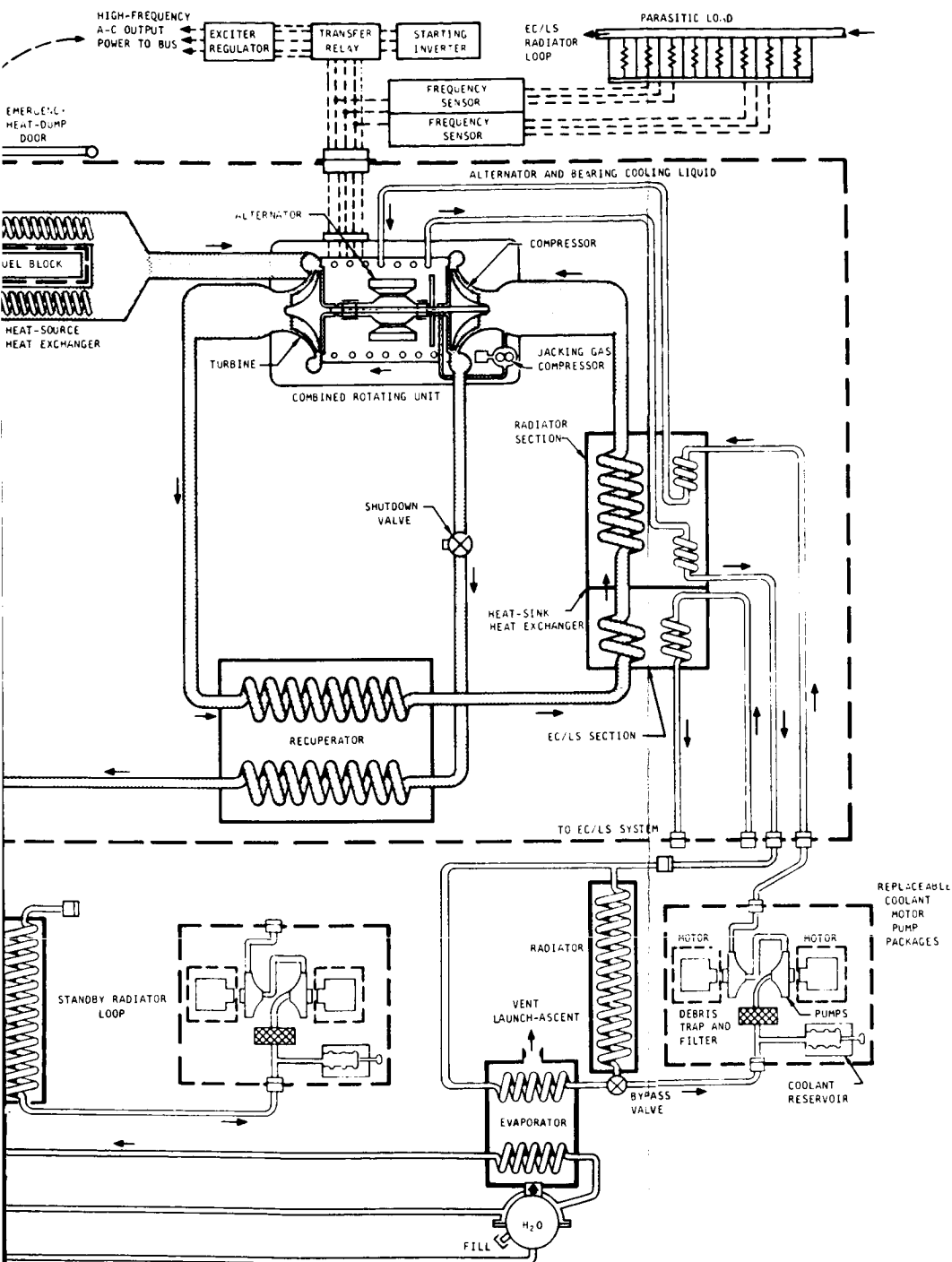


Figure 2-4. Brayton Cycle System



17-2

by the system with overload capacity of approximately 16.5 kW_e for one hour per day in conjunction with batteries. The total system weight is 4,562 lb.

Solar Cell

An alternate power system consists of four 2,676 ft² solar-cell panels with a system rating of 9.6 kW and an overload power capability of 14.4 kW for 1 hour/day. This system is augmented by nickel-cadmium batteries which handle the eclipsed portion of the orbit and overload requirements. The total system weight including batteries is 3,400 lb.

2.1.3.4 EC/LS System

The primary objective of the environmental control/life support system (EC/LS) is to maintain a habitable cabin environment during the MORL mission with a minimum expenditure of consumables and power.

The baseline EC/LS system has the following design characteristics:

1. A 7 psia 50% oxygen 50% nitrogen atmosphere at 75°F.
2. Consumable oxygen is obtained by the electrolysis of water, which is resupplied as required.
3. The water cycle is completely closed, that is, no water resupply is required except that needed to provide oxygen. The excess metabolic water is electrolyzed to reduce resupply requirements.
4. Fecal and other laboratory wastes are collected, dehydrated, and stored for ultimate disposal with resupply module.
5. Laboratory waste heat is rejected to space via a radiator.

Waste materials from the EC/LS system which may be considered as possible propellant candidates are hydrogen, from the electrolysis process, and carbon dioxide.

2.1.4 Logistic Resupply

The logistic vehicle selected for the MORL system uses the Apollo command module and a special service pack in conjunction with a multimission module concept and the Saturn IB launch vehicle system.

The multimission module can be separated from the command module and separately docked to the MORL hangar. An access port is installed in the forward dome of the multimission module pressurized section to permit direct shirtsleeve environment transfer of cargo to the MORL hangar/test area. Prepackage cargo (clothing, food, spares, and small equipment) will be manually transferred to the MORL. Propellants will be transferred through the umbilical panel by means of a positive expulsion transfer system located on the logistic vehicle.

2.1.5 Reliability

A minimum reliability of 0.9985 has been established for operation of the MORL subsystems for a 5-year mission. Reliability is defined for this purpose as the ability of a component or system to support the basic MORL mission without causing serious degradation of that mission. Maintenance and repair activities that do not cause reversion to emergency modes of operation are considered to be part of the normal operations. To meet the reliability goals the system incorporates redundancy, as required; moreover, it is designed to facilitate maintenance and repair both on the ground and in orbit.

2.1.6 MORL Weight

The maximum allowable laboratory launch weight is approximately 33,000 lb, set by the Saturn IB launch vehicle, for a 164-nmi orbit. The weight of the laboratory when operating may approach 100,000 lb dependent upon the number of logistics, ferry craft, and experimental modules stored on it.

2.1.7 Environment

The environmental design criteria for the MORL system is based upon the design criteria levels currently specified for the Saturn IB and Saturn V vehicles. These criteria and conditions are discussed in detail in the MORL specifications documents SM-48150 and SM-48151.

2.2 PHASE IIb P/RCS

Design features of the three P/RCS resulting from the Phase IIb study are described in this section. The updated bipropellant system described herein is redesignated as the Phase IIb baseline P/RCS and a design charge for the MORL has been initiated.

Only the baseline MORL configuration in the zero-g, belly-down, and inertial orientation modes was considered in the integration study. Therefore, the systems described herein do not include the spin-despin capability for the alternate artificial-g mode. However, provisions for attitude control of the laboratory during a spin mode was studied during the preliminary design of the thrusters and is discussed in Sections 3 and 4.

2.2.1 System Functions and Requirements

The purpose of the P/RCS is to provide the necessary impulse to satisfy the following functions for the MORL mission:

1. Orbit injection.
2. Orbit keeping.
3. Attitude control.

These functions establish the performance requirements based on the vehicle orientations necessary to perform the mission events described below. In the control of vehicle attitudes, impulse resulting from cyclic torques (caused primarily by aerodynamic drag and gravity gradient) are stored in the control moment gyros (CMG's). Steady state or bias torque disturbances, which result in a net accumulation of momentum, are handled by the P/RCS by desaturating the CMG's. Velocity change requirements are also handled by the P/RCS.

For long term operation of the laboratory in the zero-g mode, an orientation is selected which aligns the longitudinal axis with the velocity vector and maintains one side of the vehicle facing the Earth. This is referred to as the belly-down orientation. In addition to this basic orientation, the MORL must be capable of maneuvering to any desired inertial orientation for short-term experiment operations. This is referred to as the inertial orientation.

In the artificial-g spin mode (alternate mode) the momentum storage devices are used to control wobble about two axes and the P/RCS system is used for spin control of the laboratory about the third axis. The velocity increments necessary for spin-despin of the laboratory are also handled by the P/RCS.

Table 2-2 lists the functions and requirements which the P/RCS must supply for each of the mission events. All impulse values given represent only impulses which accumulate from the bias term of the gravity gradient and aerodynamic disturbance torques, since cyclical terms of the disturbance torques will be stored in CMG's.

The values given are based on performing each control function completely independent of all others; however, if control functions are combined (Section 5.1) the total impulse requirement is reduced accordingly.

The number of required pulses per orbit for the drag function in the zero-g mode is a variable since MORL is always in the current orientation for applying drag control. However, continuous thrusting (as noted in the table) is desirable in that it minimizes drag engine thrust level requirements. The established number of pulses for the attitude control functions is based on engine efficiencies as discussed in Section 5.1.

2.2.1.1 Orbit Injection

Orbit injection is the first event in the MORL mission requiring the use of the on-board P/RCS. The belly-down orientation is maintained throughout the entire event. The total impulse required for attitude control is 4,950 lb-sec. This requirement results from a disturbance torque produced by thrust misalignment, thrust eccentricity, and thrust variation of the orbit injection engines. The total impulse required for the velocity increment necessary for the injection maneuver is 185,000 lb-sec.

2.2.1.2 Unmanned Orientation

No orientation or attitude hold requirements exist for this mission event. However, it is desirable to maintain the body axis rates below 0.03 deg/sec to ensure satisfactory completion of the docking events. This rate

Table 2-2
P/RCS SYSTEM SUMMARY

Mission Event	Orientation, Power Source and Configuration	Control Function	Impulse per Orbit or Event	*Pulse per Orbit	*Pulse Duration (sec)	*Combined Thrust per Pulse (lb)	*Thrust Time per Orbit (sec)
Orbit injection	Belly-down	Attitude control	4, 950 lb-sec	---	---	---	---
	Either Brayton Cycle or Solar						
	Basic laboratory						
Unmanned orientation	Any	Rate stabilization	250 $\frac{\text{lb-sec}}{\text{orbit}}$	---	---	---	---
	Brayton Cycle						
	Basic laboratory						
Long term manned zero-g stabilization	Belly-down	Drag	150 "	1	5, 500	0. 0273	5, 506
	Solar panel	Pitch desaturation	100 "	2	150-2, 700	0. 333-0. 0185	300-5, 400
	Laboratory with 3 logistic modules (configuration x)	Yaw desaturation	113 "	2	150-2, 700	0. 377-0. 0323	15-900
		Roll desaturation	8 "	4	8-133. 3	0. 25-0. 015	150-2, 500
	Belly-down						
		Drag	90 "	1	5, 500	0. 01635	5, 500
	Laboratory with 3 logistic modules (configuration x)	Pitch desaturation	82 "	2	150-2, 750	0. 273-0. 0152	300-5, 500
		Yaw desaturation	8 "	4	8-133. 3	0. 25-0. 015	32-533
		Roll desaturation	8 "	4	8-133. 3	0. 25-0. 015	32-533
Artificial-g spin mode	Y axis to sun	Drag	500 "	50 2	3. 92 1, 375	0. 141 0. 141	1, 375 2, 750
	Solar panel	Precession	500 "	100	3. 92	0. 202	2, 750
	Laboratory with 4 logistic modules and S-IVB counterweight	Drag**	420 "	50	3. 92	0. 118	1, 375
	Any	Precession	420 "	100	3. 92	0. 17	2, 750
	Brayton Cycle						
	Laboratory with 4 logistic modules and S-IVB counterweight						

*Applies to low thrust systems only

**Drag makeup accomplished when in belly-down orientation

stabilization must be provided by the P/RCS since the CMG's are inactive during this mission event. Gravity gradient and aerodynamic torques are the only significant disturbances which affect impulse requirements. Impulse requirements are difficult to establish without a detailed analysis since impulse consumption is a function of the MORL attitude, which determines the disturbance torques. However, a rough estimate of impulse consumption is 4,000 lb/sec per day or 80,000 lb/sec for a 20-day mission event.

2.2.1.3 Long Term Manned Zero-G Orientation

The belly-down orientation is the basic orientation for this mission phase. Since the impulse requirements for this mission phase vary depending on the specific configuration of the MORL (that is, number and location of docked resupply and experimental modules), the requirements used to establish the P/RCS thrust levels and CMG size are based on a worst case configuration (Section 5.1, Table 5-1).

2.2.1.4 Experiments

Experiments are performed in two different orientations. Earth experiments require a belly-down orientation and the remainder require an inertial orientation. The requirements for the belly-down orientation are the same as those for long term manned zero-g stabilization. Impulse requirements in the inertial orientation are listed in Table 2-2. The total impulse consumption per day is based on a typical experiment which requires the following sequence of events:

1. A 90° maneuver of 15-minute duration.
2. Four hours in an arbitrary inertial orientation.
3. A 90°, 15-minute maneuver to return to a belly-down orientation.

Other than gravity gradient and aerodynamic torques, crew motion will be the only significant disturbance affecting performance during an experiment. Drag control cannot be accomplished while in the inertial orientation as the engine thrust axis is fixed relative to the body axis, and the body axis is misaligned relative to the orbit velocity vector. Therefore, drag impulse

which accumulates while in the inertial orientation will be removed upon return to the belly-down orientation of the long term manned zero-g stabilization phase.

2.2.1.5 Artificial-G Spin Mode

The requirements for the spin mode are shown in Table 2-2. Figure 2-5 describes the manner in which drag and precession control is applied. The orbit plane is divided into four sectors, A, B, C, and D; the spin plane of the MORL is divided into four sectors, 1, 2, 3, and 4. The spin axis is assumed to lie in the orbit plane. At the midpoints of orbit sectors A and C the spin axis and the orbit velocity vector are coincident. At the midpoints of orbit sectors B and D, the spin axis and the orbit velocity vector are normal. The desired control torque vector lies in the orbit plane and is always in the direction shown in orbit Sector A on Figure 2-5.

2.2.2 Updated Baseline (Storable Bipropellant)

The detailed schematic of the P/RCS is shown in Figure 2-6. The system employs 16 fixed mounted radiation-cooled engines contained in four clusters, each of which consist of one 100-lb thrust level engine for orbit injection and inertial drag makeup and three 50-lb thrust level engines for attitude control. The design of the engine is shown in Figure 2-7. The propellants (NTO/MMH) are stored in four tanks of equal volume; two oxidizer tanks and two fuel tanks. This redundancy insures a minimum propellant supply loss in the event of a single tank failure. The tanks have a capacity for 90-day operation in the combined belly-down inertial orientation plus a 57-day reserve supply for operation in the belly-down orientation. Each tank consists of a metal bellows and a nitrogen pressurant bottle to provide the positive expulsion of the propellant from the tanks and feed system to the thrustors. The propellant storage tanks are interconnected by manifolds which provide the system with refilling capability in orbit. In addition, if one fuel or oxidizer tank is depleted for any reason, the system is able to equalize volumes in both tanks, thus ensuring minimum propellant loss if a single tank failure should occur.

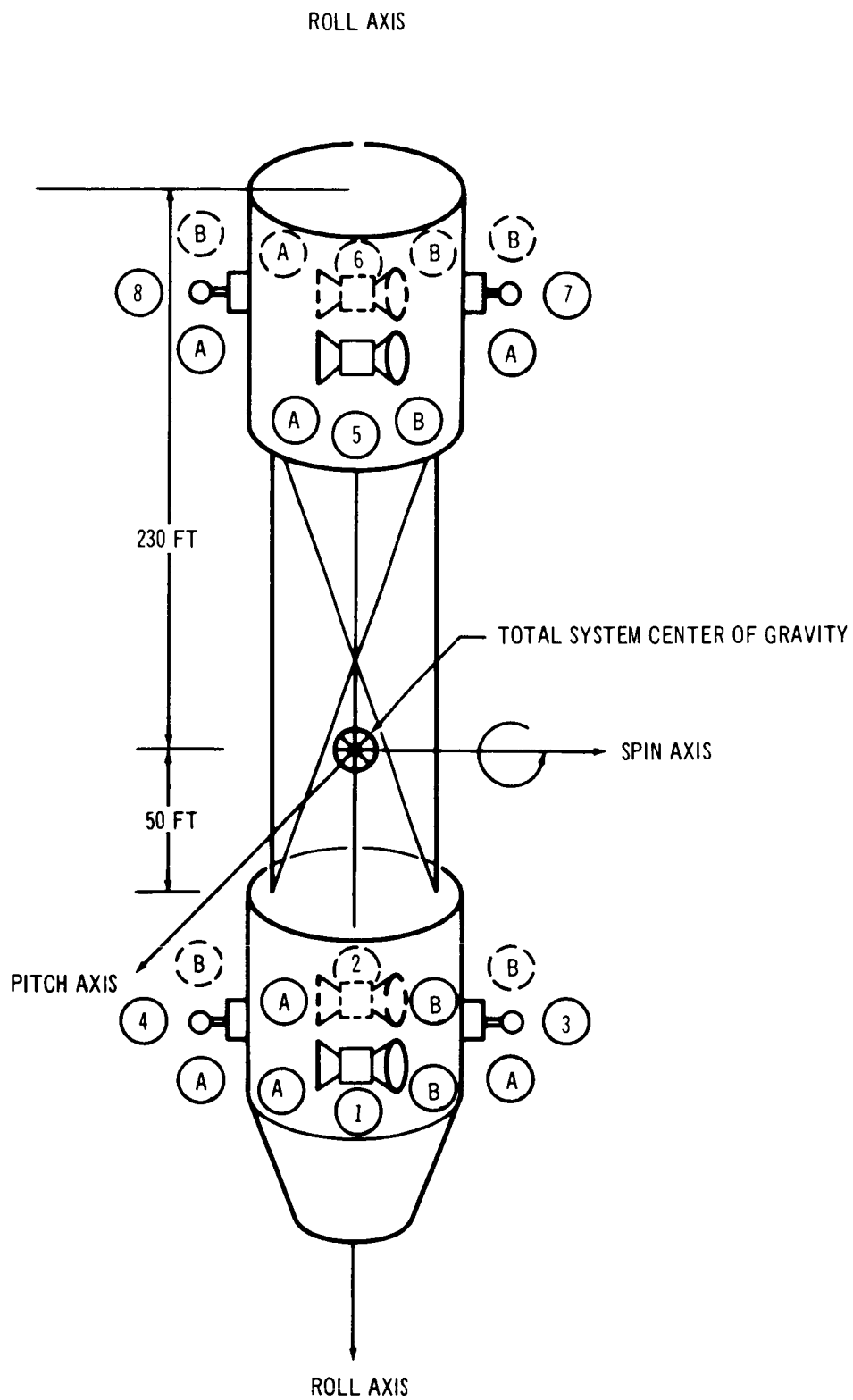


Figure 2-5. Precession and Drag Control Thrust MORL in Spin Mode

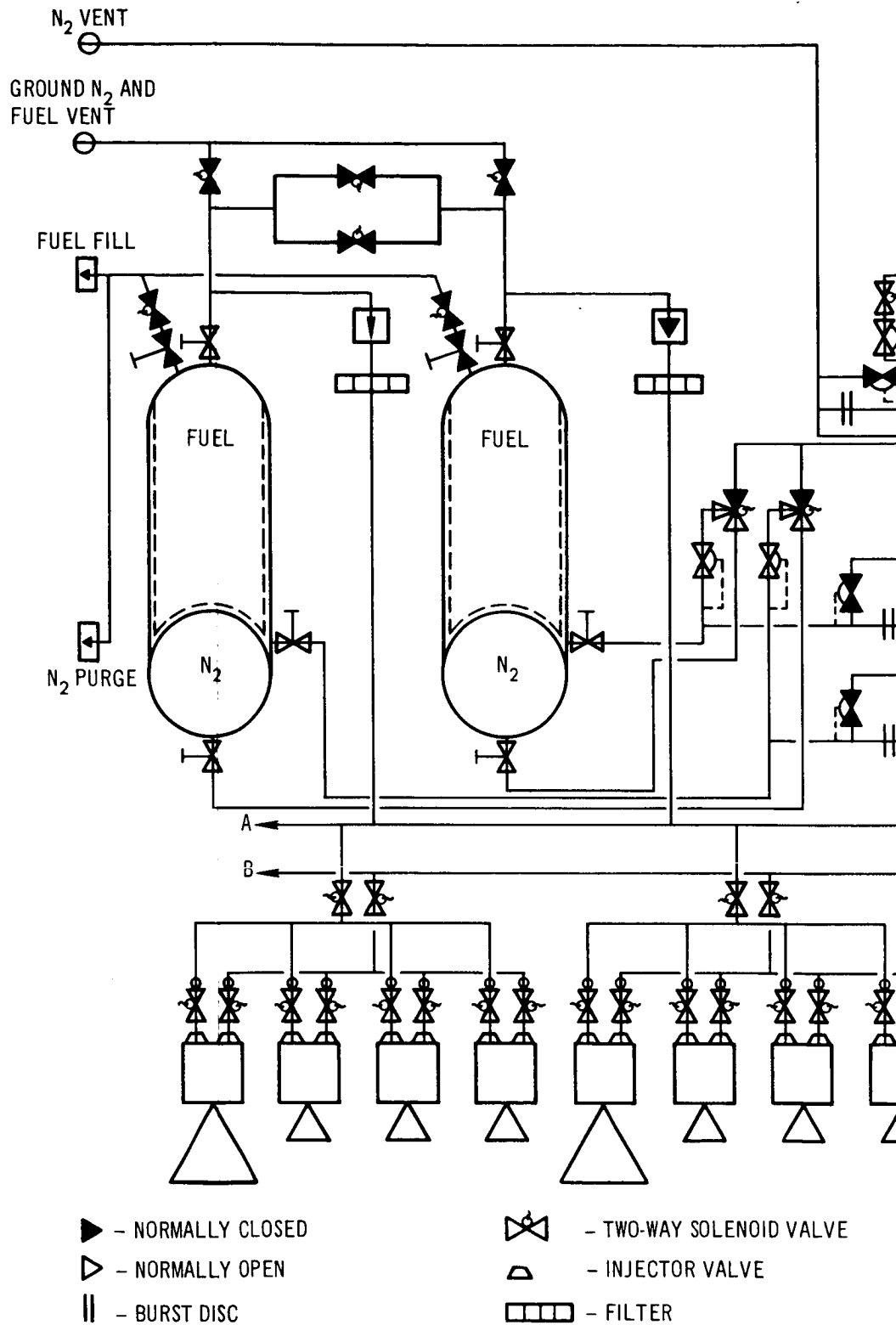
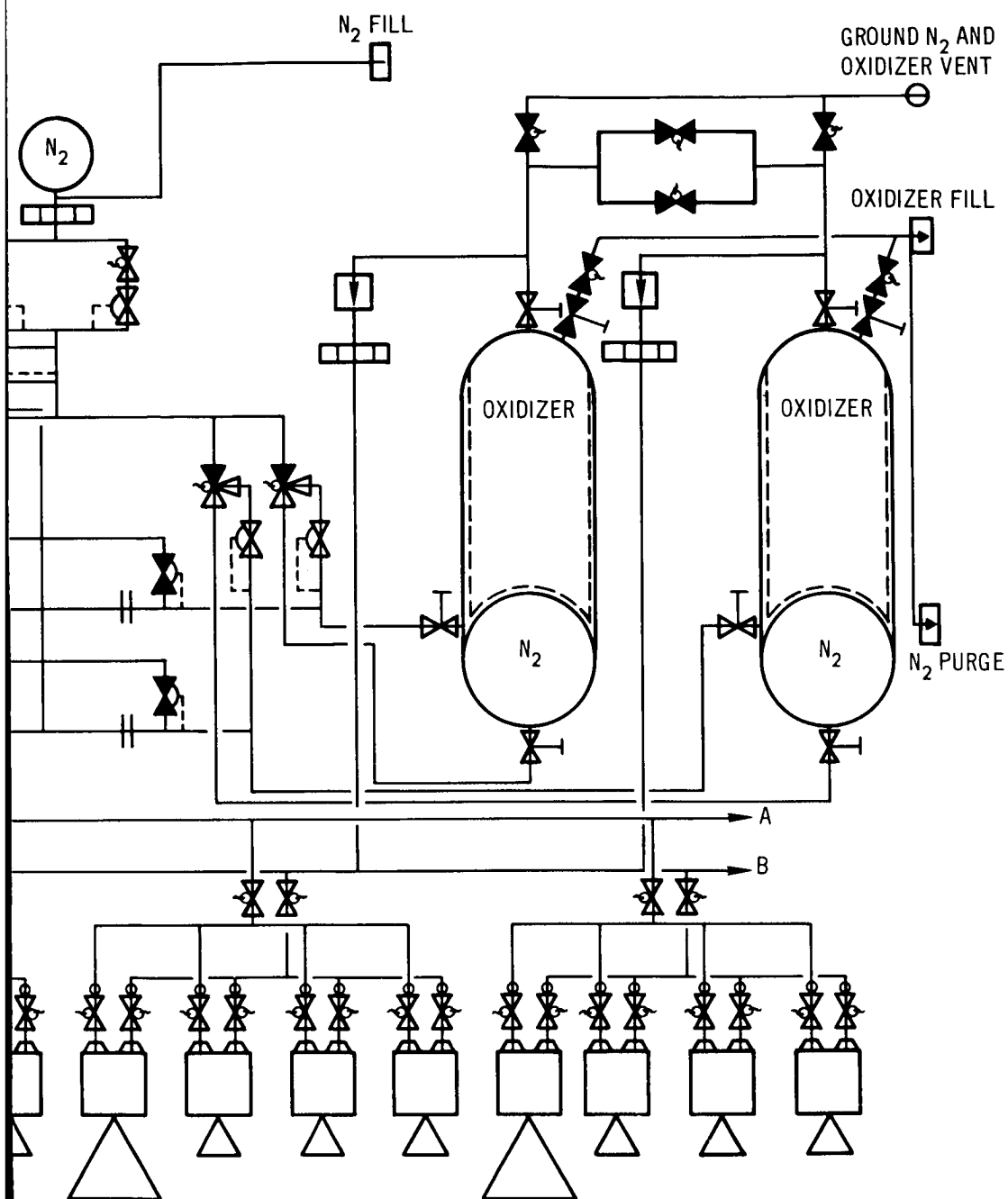








Figure 2-6. P/RCS Bipropellant Schematic



- | | |
|---|--|
|  - THREE-WAY SOLENOID VALVE |  - CHECK VALVE |
|  - SOLENOID VALVE W/LEAK DETECTOR |  - RELIEF VALVE |
|  - HAND VALVE |  - QUICK DISCONNECT |

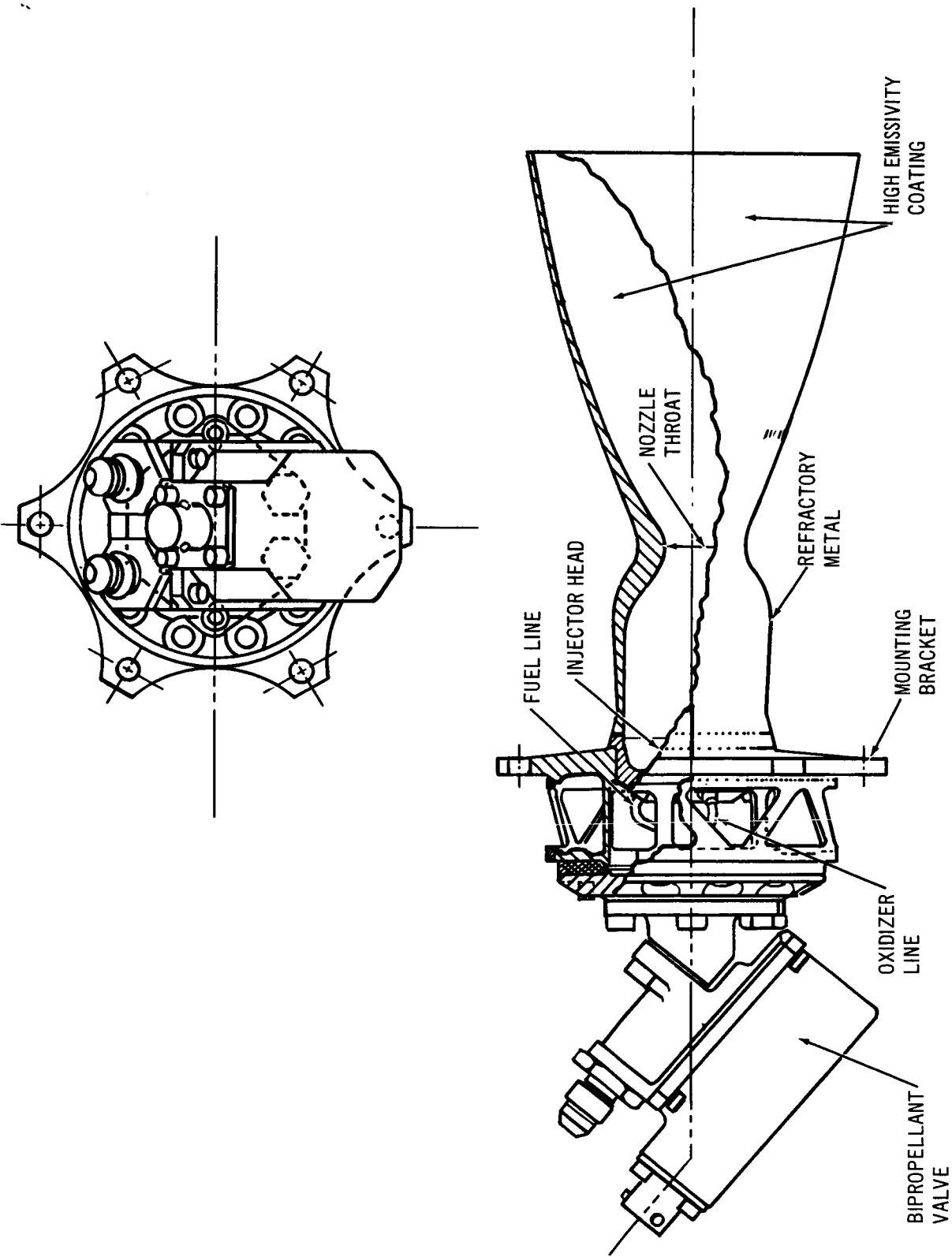


Figure 2-7. Typical Radiation-Cooled Engine

The propellant manifold completely encircles the periphery of the aft interstage compartment to supply the four thrust chamber assemblies. This manifold has sufficient valving to allow isolation of a section between the thrust chamber assemblies if a meteoroid breaks a section of the manifold. This will allow normal operation to be maintained while the section is repaired.

A detailed tabulation of the design characteristics of the system are shown in Table 2-3.

2.2.2.1 Installation and Location

The four engine clusters are positioned externally, 90° apart, on the aft interstage section.

The 100-lb thrust orbit injection engine is positioned on the periphery 12 in. from the aft facing pitch/yaw engine. The roll engine is positioned approximately 12 in. from these engines, toward the front of the vehicle. The forward facing pitch/yaw engine is located approximately 47 in. from the aft facing engine, also toward the front of the vehicle. This cluster arrangement permits a minimum heat input to the engine injector valves from an adjacent chamber.

The propellant tankage system is positioned to take advantage of the Brayton Cycle radiators to maintain a nominal temperature of 125°F, (140°F maximum). The tanks are positioned to allow sufficient clearance between them to permit access for replacement in the event of failure.

The nitrogen low pressure bottles are positioned at the top of each tank reducing tank weight by the use of a common bulkhead design. In addition, this positioning offers a geometry (spherical-convex) which is conducive to optimum bellows operation.

2.2.2.2 System Performance

The system performance of the P/RCS is shown by Table 2-4. In addition to providing pitch/yaw control, the thrustors facing in the aft direction

Table 2-3

PROPULSION SYSTEM DESIGN DATA

System Characteristic	Magnitude or Description
Number of engines	16
Total weight (loaded)*	1, 563. 5 lb
<u>Propellant</u>	
Oxidizer	N_2O_4
Fuel	MMH
Mixture ratio, O/F	1. 6:1 (by weight) 1. 0:1 (by volume)
Total weight**	1, 137. 9 lb
<u>Engines</u>	
Cooling concept	Radiation
Chamber pressure	90 psia
Thrust - Attitude control	50 lb
Orbit injection	100 lb
Nozzle expansion ratio	100:1
Vacuum specific impulse F = 100 lb	303 sec
F = 50 lb	295 sec
<u>Tankage and Pressurization</u>	
Tank pressure (operating)	250 psia
Tank pressure (maximum)	300 psia
Fuel and oxidizer tank diameter	17. 5 in.
Length/diameter (L/D)	2. 0
Positive expulsion device	Metal bellows
Pressurant	Nitrogen
Pressure storage pressure	1, 500 psia

*147-day propellant supply

**Includes weight of N_2 pressurant

Table 2-4

PROPULSION/REACTION CONTROL SYSTEM ENGINE PERFORMANCE

Function	Total Impulse (lb/sec)	Duty Cycle	Thrust/ Engine (lb)
Orbit injection	185, 000	Continuous	100
<u>Belly-Down Mode (20 hours/day)</u>			
Orbit keeping	Accomplished by pitch/yaw control		
Attitude control	98.8/orbit		
Pitch		1.64 sec/orbit*	50
Yaw		0.16 sec/orbit	50
Roll		0.16 sec/orbit	50
<u>Inertial Mode (4 hours/day) (All engines operated in a couple)</u>			
Orbit keeping	Accomplished during the first orbit of the next belly-down orientation		
Attitude control	216/orbit		
Pitch		1.80 sec/orbit*	50
Yaw		0.18 sec/orbit**	50
Roll		0.18 sec/orbit**	50
<u>First Orbit Following Inertial Orientation (Belly-Down)</u>			
Orbit keeping (for inertial makeup)		1.572 sec	100
Orbit keeping (for normal belly-down)	Accomplished by pitch/yaw control		
Attitude control	98.8/orbit		
Pitch		1.64 sec/orbit *	50
Yaw		0.16 sec/orbit	50
Roll		0.16 sec/orbit	50
*Done in two equally spaced pulses			
**Done in two random spaced pulses			

accomplish drag makeup by single thrust translation for the belly-down mode. The same thrusters in the inertial mode are operated in couples with forward facing thrusters, thereby providing attitude control without translation (drag, makeup). The orbit keeping impulse requirement, resulting from the inertial mode, is deferred until the first orbit (belly-down mode) after completion of the inertial mode. This operation is accomplished with the four 100-lb thrust level engines.

In addition to providing orbit injection and drag makeup, these engines provide pitch/yaw control by differential thrusting during orbit injection.

During orbit injection roll control is accomplished by operating the 50-lb thrust attitude roll control engines in a couple.

2.2.2.3 Propellant Resupply and Feed System

The propellant storage tanks are interconnected by manifolds which provide the system with refilling capability in orbit. A schematic of this system is shown in Figure 2-6. In addition, if one fuel or oxidizer tank is depleted by a higher rate of use than the other, the system has the capability to equalize volumes in both tanks thus ensuring minimum propellant loss in the event of a single tank failure.

The propellant manifold completely encircles the periphery of the aft inter-stage compartment to supply the four thrust chamber assemblies. This manifold has sufficient valving to allow isolation of a section between the thrust chamber assemblies if a meteoroid breaks a section of the manifold. This would allow normal operation to be maintained while the section is repaired.

2.2.2.4 Weights

A detailed breakdown of the system weight is shown in Table 2-5.

2.2.3 Resistojet

A detailed design of the Resistojet engine is presented in Figure 2-8. The concentric cylinders shown are connected in series and heated by electric

Table 2-5
P/RCS WEIGHT SUMMARY

Item	Weight (lb)
Propellant*	
Onboard at launch	742.5
First resupply (147-day supply)	1,137.9
Normal resupply (90-day supply)	843.0
Hardware	
High pressure N ₂ module	22.2
Low pressure N ₂ module	24.7
Pressurization system	11.8
Feed system (includes leak detection system)	75.6
Engine system (includes mounting structure)	95.7
Tankage (includes N ₂ bottle and bellows)	195.6
Total	425.6
System	
Total launch weight	1,168.1
Resupply weight ** (90-days propellant)	960.1
<hr/> * Includes weight of nitrogen ** Includes N ₂ and logistic vehicle propulsion hardware.	

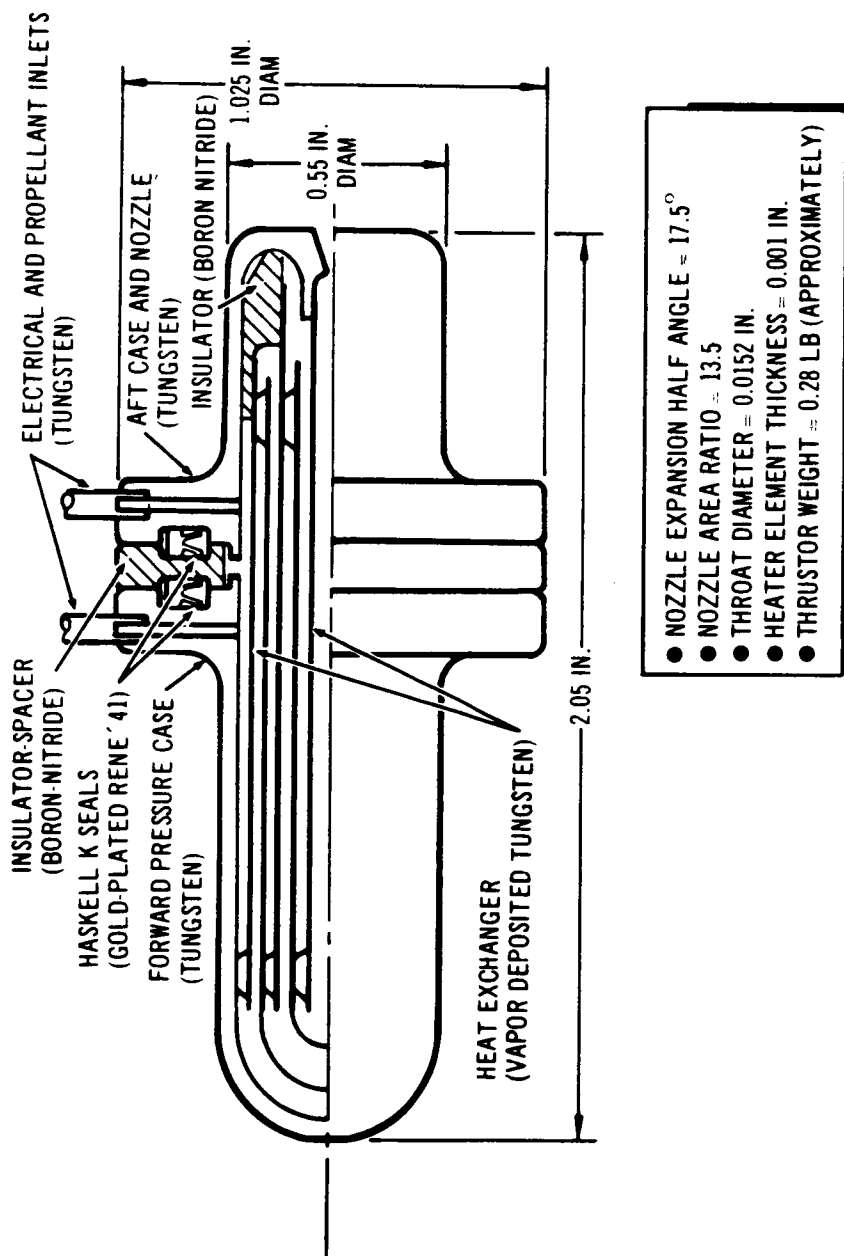


Figure 2-8. Resistojet Thrustor

current. The annular passages formed by the concentric cylinders are also serially connected to permit the propellant to flow in alternate directions from the outside toward the center, continuously receiving heat from the walls. Therefore, the concentric cylinders serve concurrently as heating elements, radiation shields, and regenerative cooling passages, thereby producing a high thermal efficiency. The propellant is discharged through a DeLaval nozzle connected to the high-temperature central element. Vapor deposited tungsten is employed for the electrically energized heat exchanger, and the spacers and electric insulators are machined from boron nitride. The heat exchanger is operated at a constant temperature of approximately 4,400°R. Therefore, the attainable specific impulse depends upon the type of propellant employed. The Resistojet engine design characteristics are presented in Table 2-6 for both the hydrogen and ammonia thrusters.

A total of 24 Resistojet engines are arranged in four modules of six engines each, as shown in Figure 2-9. It will be noted that the engines facing fore and aft in each module are arranged in pairs and therefore offer some redundancy. This redundancy permits all engines to be of identical design, and thereby minimizes the development and production cost, and increases system reliability.

The Resistojet thruster modules are insulated with zirconia foam and a thermal blanket to minimize heat losses. A solenoid valve controls the propellant flow to each engine and a squib-actuated shutoff valve (for each module) precludes large propellant losses if a failure occurs in the module. In the event of such failure the entire module will be replaced.

The design characteristics of the Resistojet thruster systems are given in Table 2-6 for both the H_2 and NH_3 propellant systems. A schematic of the two thruster systems is given in Figures 2-10 and 2-11.

Table 2-7 shows the total impulse required for each vehicle function, the duty cycle, and the number of thrusters employed. These data are shown for the inertial phase, the belly-down phase, and the transition phase. The drag incurred during the inertial phase is made up by drag thruster

Table 2-6
RESISTOJET P/RCS DESIGN CHARACTERISTICS

System Characteristics	Propellant	
	H ₂	NH ₃
Number of engines	24	24
Total weight (loaded)*	1,005 lb	1,230 lb
Propellant		
Total weight	426 lb	851 lb
Engines		
Cooling concept	Regeneration	Regeneration
Chamber temperature	4,356°R	4,356°R
Chamber pressure	35 psia	44.1 psia
Thrust/engine	9.82 mlb	9.82 mlb
Nozzle expansion ratio, A/A*	13.6	22.2
Vacuum specific impulse	754	377
Electric propulsive power/engine	237 watts	150 watts
Overall electric power efficiency	0.68	0.54
Tankage and Pressurization		
Tank pressure (operating)	80 psia	400 psia
Length/diameter (L/D)	1	1
Diameter	6.92 ft	3.73 ft
Expulsion principle	Thermal	Thermal
Propellant (tank) temperature	49.8°R	594°R

*147-Day propellant supply.

Note: Total weight includes the pro rata share weight of the power supply needed for the Resistojet RCS system, or 289 lb and 186 lb for hydrogen and ammonia respectively.

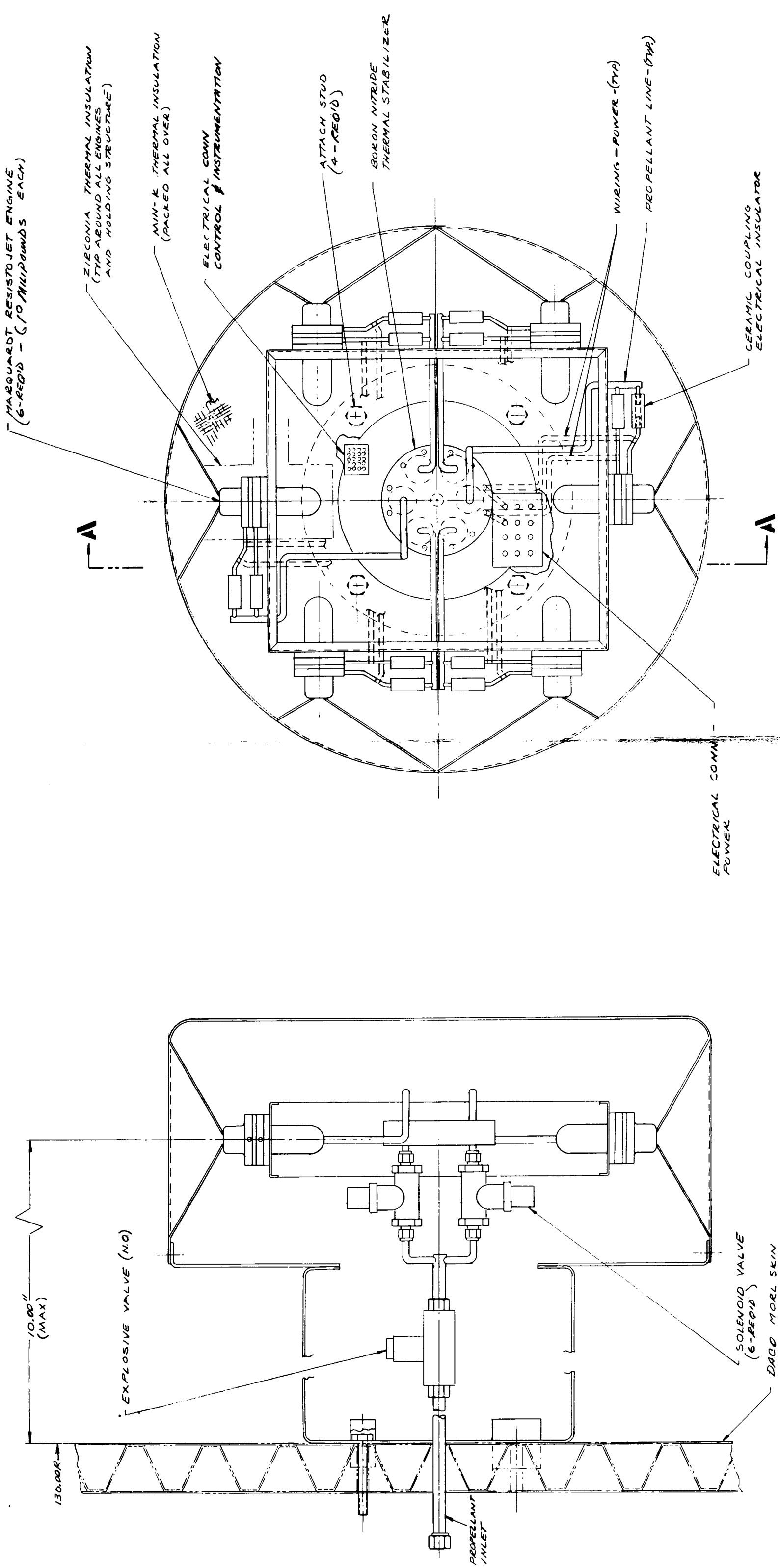


Figure 2-9. Resistojet Module

VIEW A-A

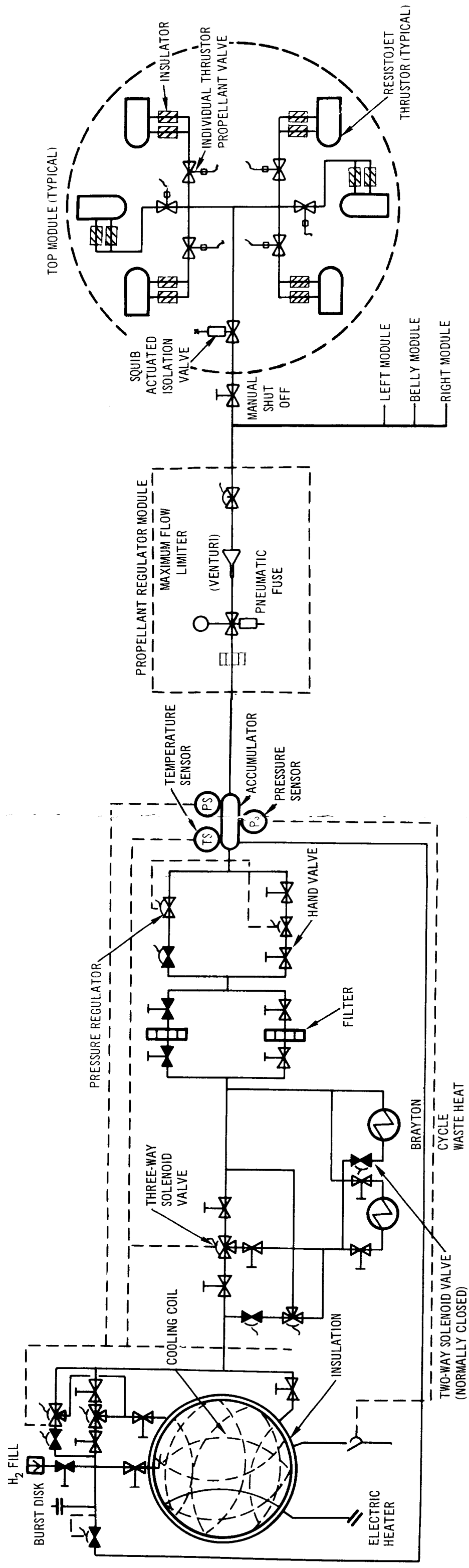


Figure 2-10. Resistojet Hydrogen System

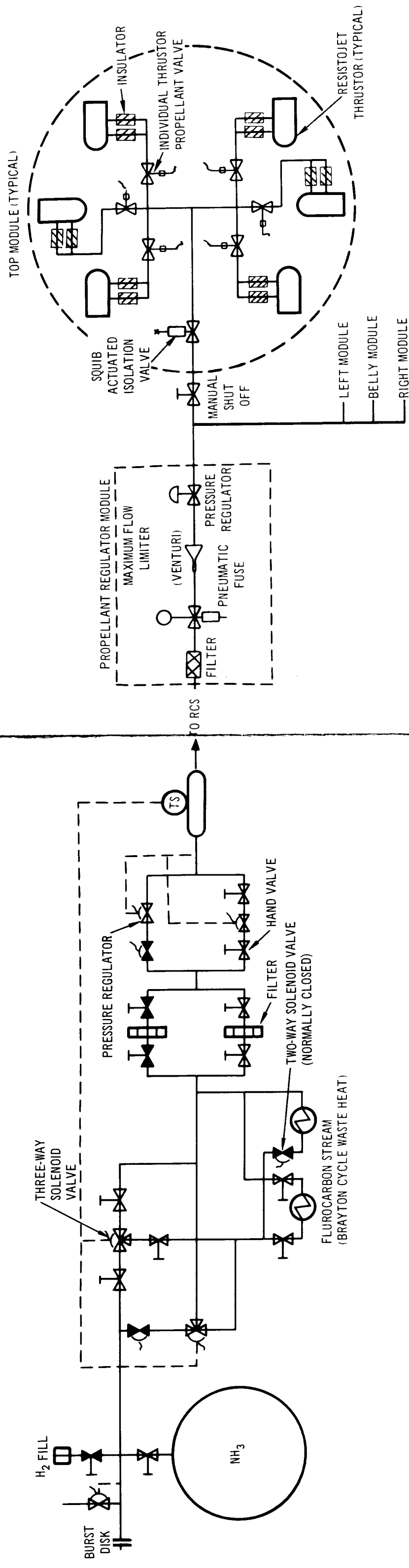


Figure 2-11. Resistojet Ammonia System

Table 2-7
RESISTOJET P/RCS ENGINE PERFORMANCE

Function	Total Impulse ($\frac{\text{lb/sec}}{\text{orbit}}$)	Duty Cycle (sec/orbit)	Number of Thrusters*
Maneuver to/from inertial (1.74%)	59 [†]	1,500 ^{††}	4
Inertial (15.9%)			
Drag**			
Attitude control	216	continuous	4
Pitch	180	458.4	4
Yaw	18	458	4
Roll	18	458	4
Belly-down + deferred drag from inertial (83.33%)			
Drag (deferred from inertial)	52.5	2,670	2
Drag (normal)***	90		
Attitude Control	98	4,990	2
Pitch	82	4,175	2
Yaw	8	407.5	2
Roll	8	407.5	2

*All engines operate at 9.82 mlb thrust level.

**Deferred to belly-down mode.

***Accomplished by pitch-yaw control

[†]This value given in $\frac{\text{lb/sec}}{\text{day}}$.

^{††}This value given in sec/day.

operation during the belly-down phase. Full advantage is taken of each opportunity to operate the pitch and yaw thrusters on a single-sided basis, rather than as a couple, to compensate for drag losses simultaneously.

The system design philosophy for the electric thrusters makes every attempt to lower the peak power requirement, in order to minimize the weight of the portion of the vehicle electric power supply which is chargeable to the reaction control system. This was accomplished by utilizing continuous thrust for the engines. The electric power profile achieved for the hydrogen system is presented in Figure 2-12. The peak power requirement is 1.16 kW and the average power is approximately 75% of this value. The power required for the ammonia system is lower due to the lower specific impulse of that system.

A schematic diagram of the Resistojet electric power system is shown in Figure 2-13. A small amount of power is continuously supplied to each engine to reduce the thermal capacitance of the engine and thereby increase thermal response. Power control is achieved by tapping the secondary winding of a three-phase transformer. Silicon-controlled rectifiers provide dc power to the thrusters and also serve as switches. The propellant solenoid valve actuating circuit is synchronized with the electric power circuit.

The total reaction control system weight and the total propellant weight for a 147-day period is shown in Table 2-6 for hydrogen and ammonia propellants. Table 2-8 shows the detailed hardware weight breakdown of the two Resistojet systems. Although the hydrogen system provides the lowest resupply weight, the hardware weight is higher than that for the ammonia system. This is caused by the insulation required for the cryogenic hydrogen propellant tank and the higher power level associated with the higher specific impulse of hydrogen.

2.2.4 Radioisotope Thruster System

The potential advantages of radioisotope heating for propulsion application have been long recognized. For the past 3 years funded research programs

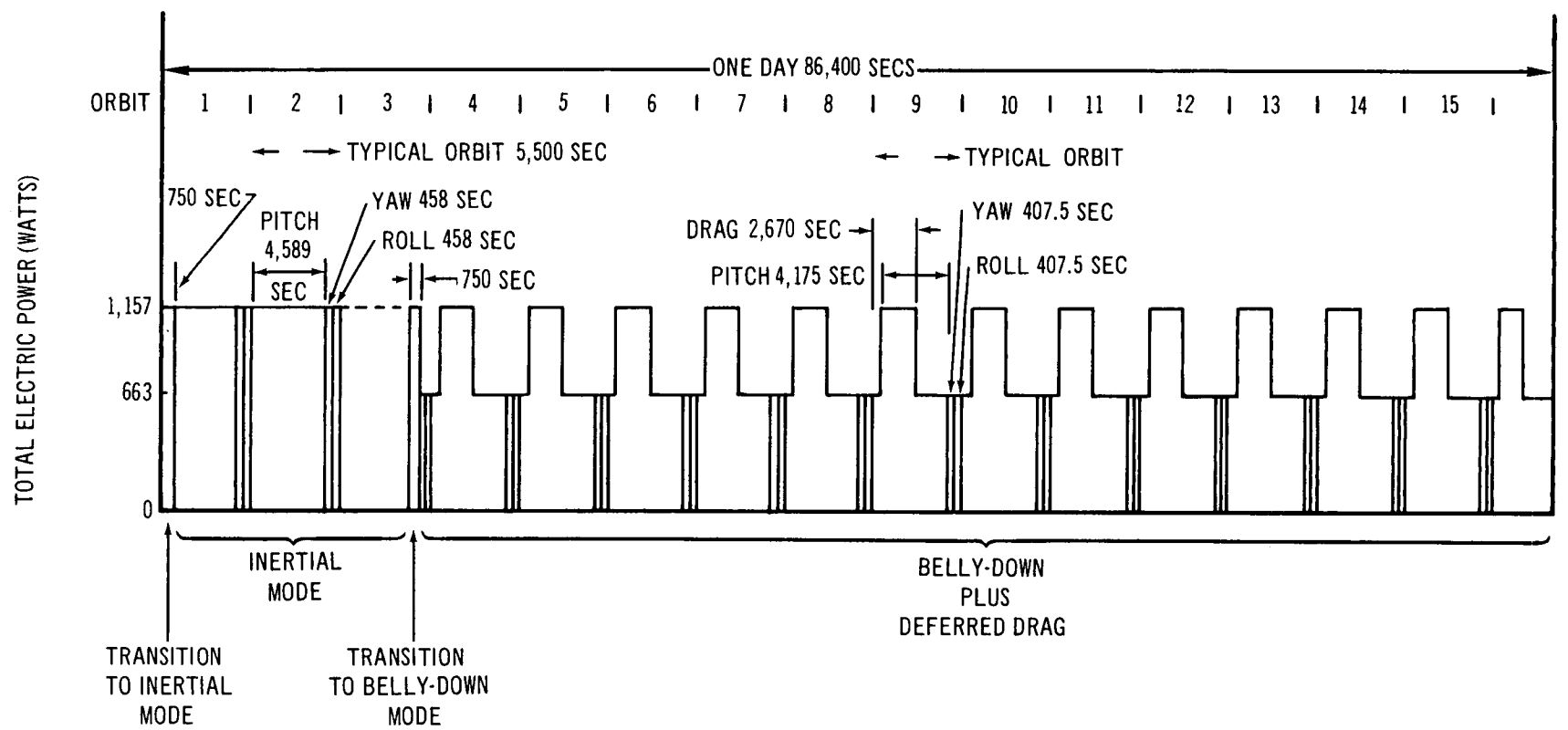


Figure 2-12. Electric Power Profile

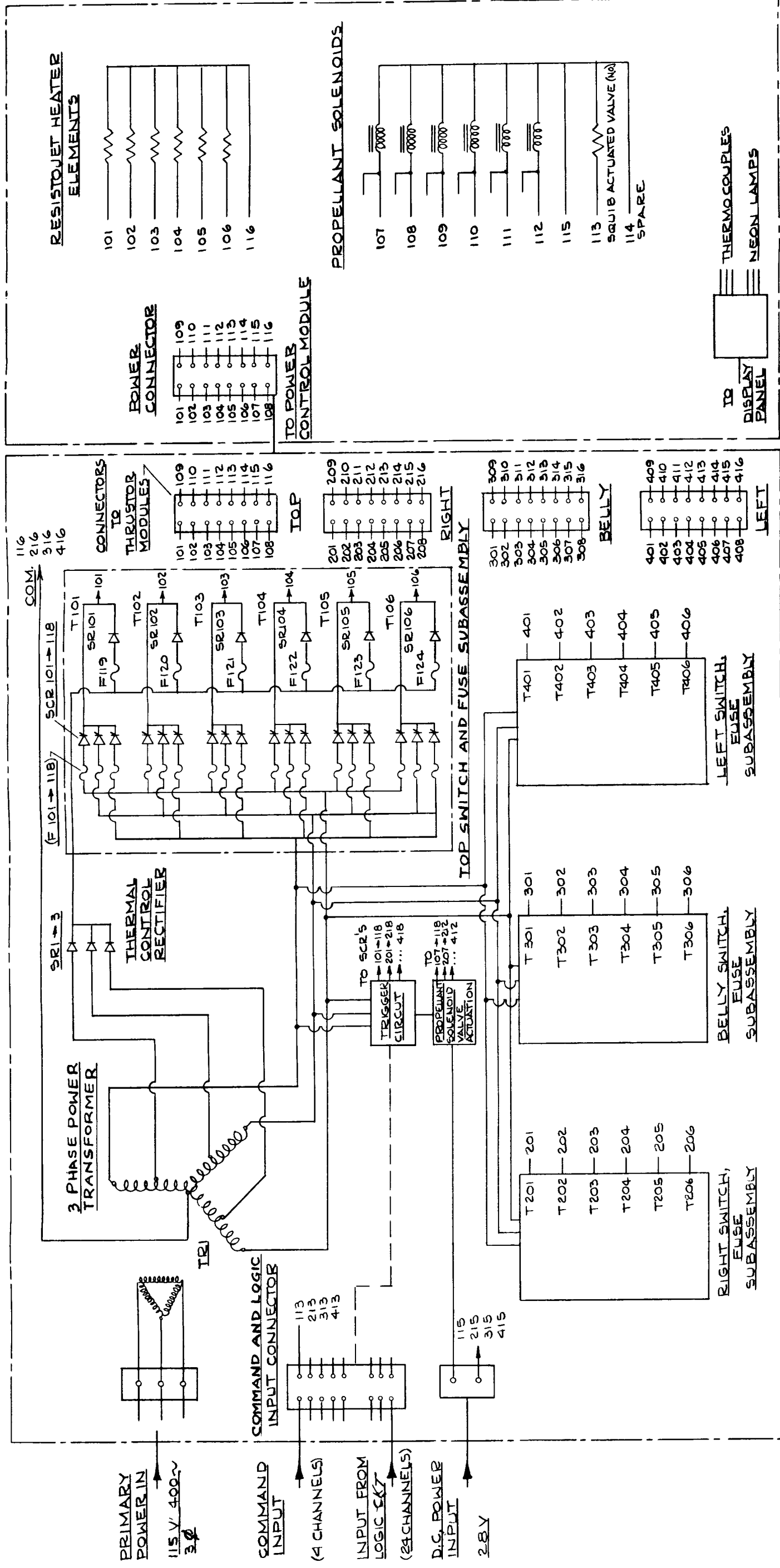


Figure 2-13. Schematic of Resistojet Power System

Table 2-8
RESISTOJET P/RCS WEIGHT SUMMARY

Component	Weight (lb)	
	H ₂ Propellant	NH ₃ Propellant
Propellant tank module	196	92
Propellant regulator module	5	5
Thruster modules (4) including mounts	32	32
Power control module	43	35
Display module	5	5
Electrical cable	26	20
Propellant lines	8	8
P/RCS dry weight	315	197
Weight assessment of power supply*	289	186
Total weight including assessment	604	383

*Based upon peak power demand

have been conducted by TRW Systems under the sponsorship of both the AEC and NASA. This concept uses heat from radioisotope decay to provide thermal energy to a monopropellant such as hydrogen or ammonia.

The detailed design of the radioisotope-fueled thruster module utilizing hydrogen or ammonia propellants is presented in Figure 2-14.

Each thruster module includes four nozzles. A propellant feed line is provided for each of the nozzles. The modules are located at 90° intervals on the periphery of the MORL spacecraft. The thruster module and its radiation shield are supported within a cradle which is bolted to the spacecraft structure. A screen is provided around the top of each installation to

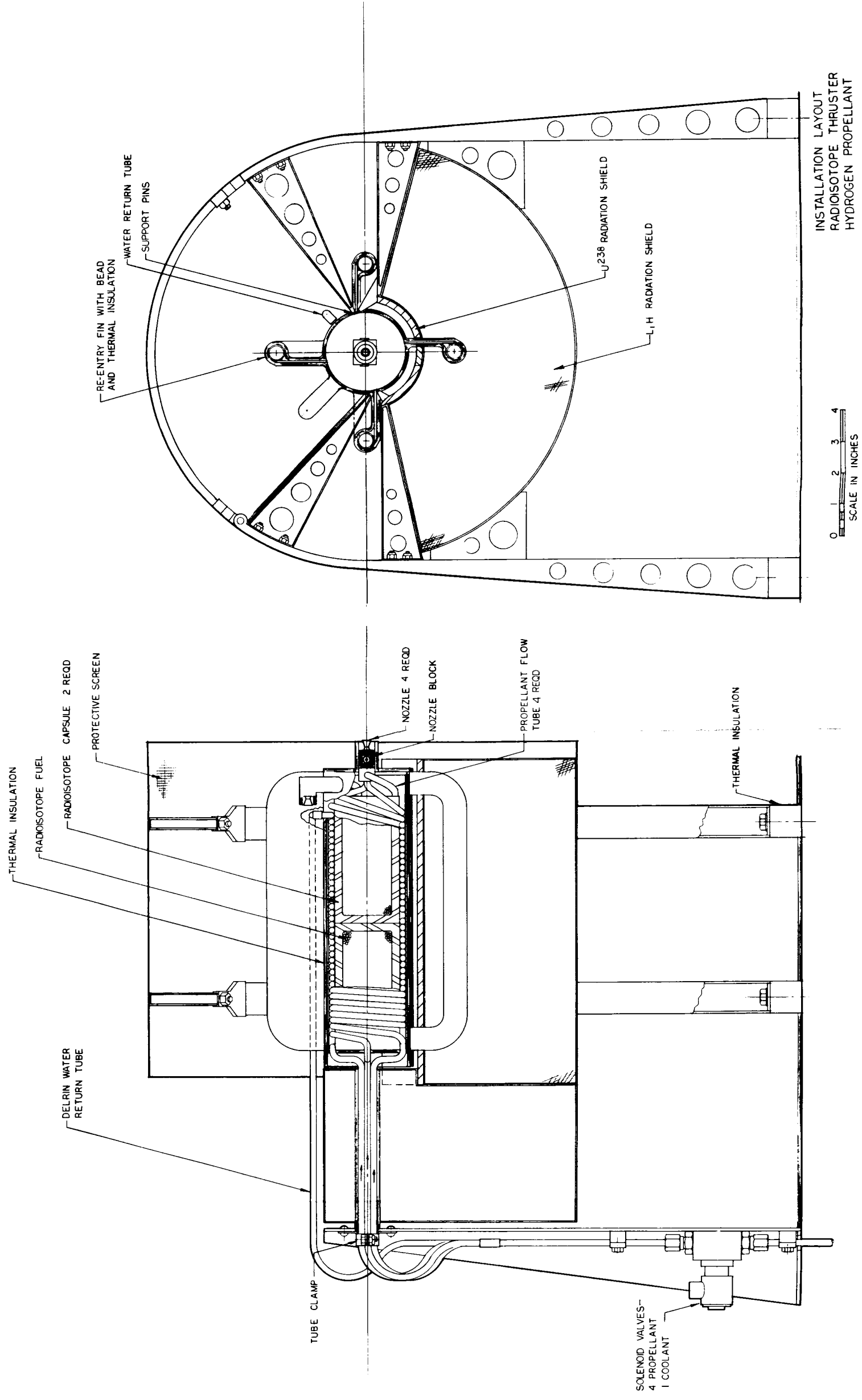


Figure 2-14. Radioisotope Thruster

protect it from any physical damage resulting from extravehicular activities associated with the MORL mission. A water coolant-line, required for pre-launch cooling, is provided as part of thruster installation.

Each thruster module is wrapped in high temperature metal foil insulation to minimize heat losses during mission operation. Additional insulation is used to prevent local overheating of the spacecraft skin.

Figures 2-15 and 2-16 are schematics of the thruster systems. A propellant storage tank, designed to store a 147-day propellant requirement, feeds the pressure regulator through a vaporizer. The vaporizer ensures that the propellant is delivered to the pressure regulator in the gaseous phase. Propellant flow to each nozzle is controlled by a solenoid valve. Pressure regulators maintain a constant supply pressure to each solenoid valve.

A detailed tabulation of design parameters selected for the ammonia and hydrogen reaction control system is presented in Table 2-9.

2.2.4.1 System Performance

The radioisotope-thruster is a high performance system which provides constant thermal power available for propellant heating. The design reflects a constant thrust level requirement for the fore and aft nozzles of 0.0164-lb thrust each with the roll nozzles having a capability of 0.004-lb thrust each. The total of sixteen nozzles provides redundancy for the roll function as well as capability for continued orbit-keeping if any one of the thrusters is inoperative. This subject is treated in more detail in Section 5.2.3.1.

The requirements, consisting of drag makeup, pitch, yaw, and roll functions associated with the four operating modes defined in Section 2.2, are presented in Table 2-10.

2.2.4.2 Weight Characteristics

Table 2-11 summarizes the system hardware and propellant weight characteristics of the radioisotope thruster.

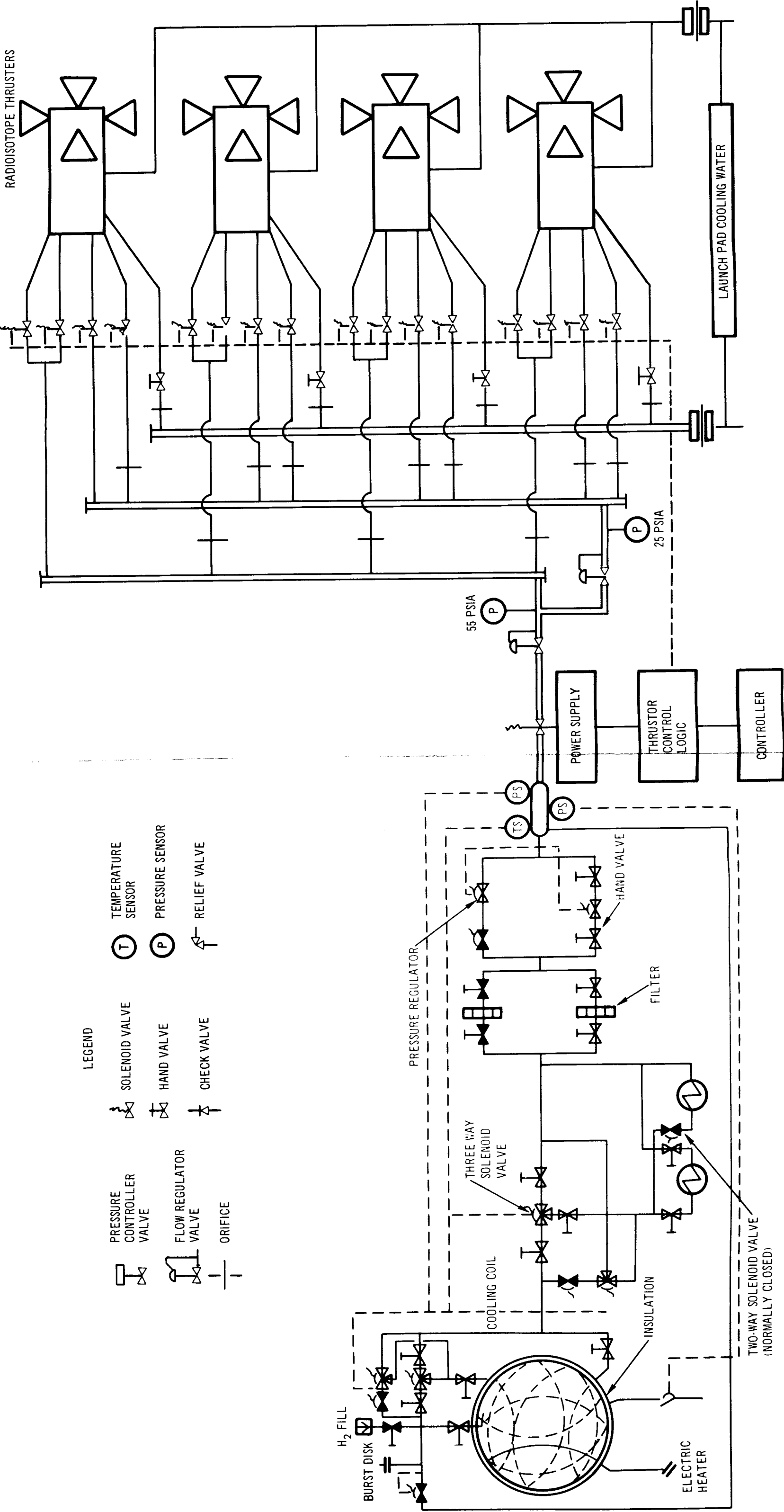


Figure 2-15. Radioisotope Hydrogen System

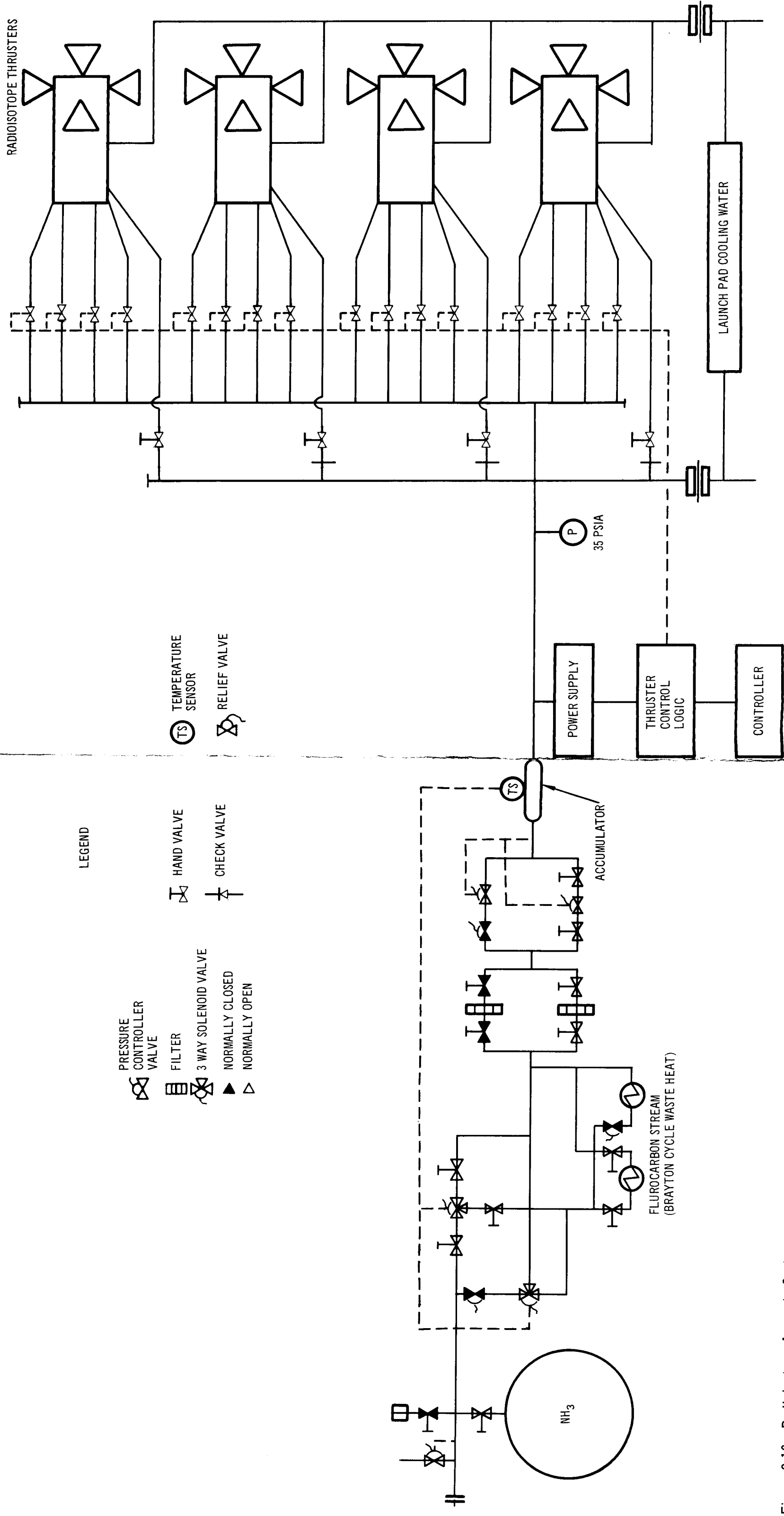


Figure 2-16. Radioisotope Ammonia System

Table 2-9
PROPULSION SYSTEM DESIGN PARAMETERS

Propellant System Parameters	Ammonia	Hydrogen
Storage tank operating pressure (psi)	310	45
Storage tank operating temperature (°F)	135	-415
Maximum flowrate (lb/sec x 10 ⁵)	18.4	9.2
Minimum flowrate (lb/sec x 10 ⁵)	4.6	2.3
Regulator upstream pressure (psia)	100	35
Regulator downstream pressure (psia)		
Resistojet approach	55	25
Radioisotope approach	35	25
Radioisotope thruster fuel	Pu-238	Pu-238
Radioisotope power per thruster (watts)	527	826
Thermal efficiency (%)	50	50
Number of thrusters	4	4
Number of nozzles per thruster	4	4
Maximum thrust (lb)	0.0164	0.0164
Minimum thrust (lb)	0.004	0.004
Nozzle expansion ratio	50	50
Exit gas temperature (°F)	3,500	3,500
Delivered specific impulse (sec)		
0.0164-lb thrust nozzle	360	721
0.004-lb thrust nozzle	345	683
Nozzle efficiency (%)		
0.0164-lb thrust nozzle	94	90
0.004-lb thrust nozzle	90	85
Chamber pressure (psia)		
0.0164-lb thrust nozzle	53	23
0.004-lb thrust nozzle	29	23

Table 2-10

RCS PERFORMANCE

Orientation	Function Impulse Per Orbit (lb-sec)				Function Burntime per Orbit (sec)				Total Thrust (lb)	Number of Nozzles Firing
	Drag	Pitch	Yaw	Roll	Drag	Pitch	Yaw	Roll		
Belly-down	90	82*	8*	8	5,000	5,000*	500*	1,000	0.0164-0.0328	1 - 3
						500				
Inertial	---	180	18	18	---	5,500	550	2,250	0.0328-0.0756	2 - 4
Maneuver	---	29.5	---	---	---	900	---	---	0.0328	2
Belly-down with drag makeup	90 164	82*	8*	8	5,000	5,000*	500*	1,000	0.0164-0.0572	1 - 5
						500				
<u>*Combined drag/pitch and drag/yaw functions</u>										

*Combined drag/pitch and drag/yaw functions

Table 2-11
WEIGHT SUMMARY

Component	Ammonia System	Hydrogen System
Thruster (lb)	13	20
Shield (lb)	8	24
Total thruster and shield (lb)	87	177
Propellant (147 days, lb)	893	445
Propellant tank (lb)	68	125
Total feed system	94	163
Total RCS dry	213	376
Total RCS launch (20-day propellant)*	320	454
90 day resupply (lb)	909	511
Total mission (lb) 5 year (19 resupplied)	18,393	10,997

*Not including orbit injection weight chargeable

2.2.5 Propellant Transfer System

The propellant transfer system on board the logistic vehicle is essentially identical for both the bipropellant system using NTO/MMH and the advanced systems using NH_3 and cryogenic H_2 .

The propellant tanks, pressurant tank, control modules, and electronic equipment are packaged in the aft portion of the cargo module as shown in Figure 2-17.

The propellant tank contains a hemispherical convoluted metal diaphragm for positive expulsion. When the tank is loaded, the diaphragm is folded into a hemispherical position against the tank wall. When pressure is applied between the diaphragm and the tank wall the diaphragm reverses and expels the propellants from the tanks.

Nitrogen gas is the pressurant for expulsion of the NH_3 , NTO, and MMH; nitrogen is stored in spherical tanks at 3,600 psia for NTO as well as MMH,

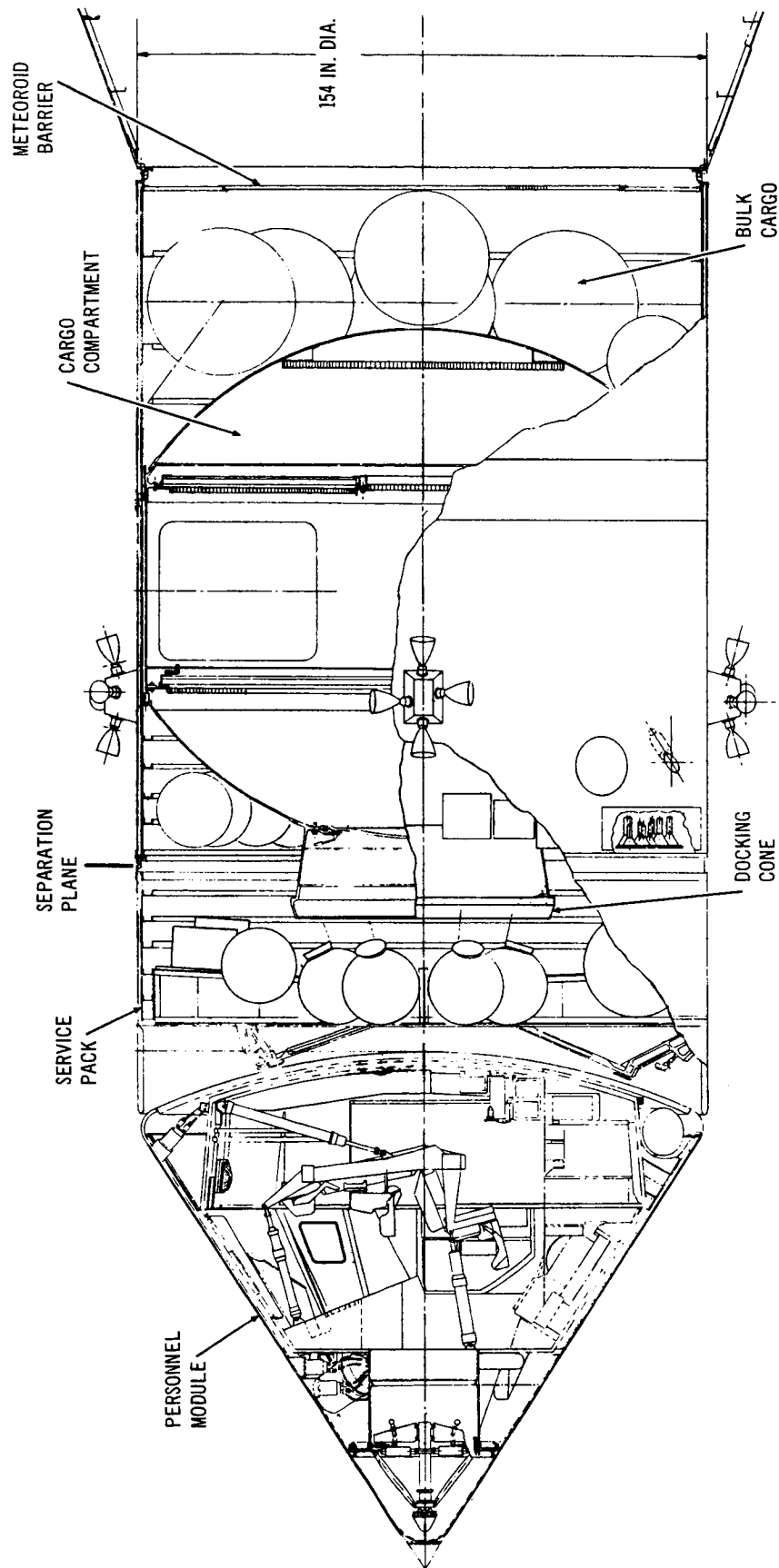


Figure 2-17. Logistics Vehicle

and at 3,000 psia for NH_3 . Hydrogen gas stored in a spherical tank at 3,000 psia is used for expulsion of the H_2 . System components are arranged in single-body multicomponent assemblies to provide automatic checkout and reduce weight and potential leaks. Automatic disconnects are located at the MORL/cargo-module umbilical interface and are engaged during docking operations.

Figure 2-18 is the flow schematic for the bipropellant system aboard the logistic vehicle. The operating sequence is as follows:

1. When the transfer system is activated, the solenoid valve in the pressurant transfer control module is opened and the gas flows to a pressure regulator. The pressure is then reduced from 3,600 psia to 3,100 psia, and this regulated nitrogen gas is transferred to the MORL propulsion system pressurant tanks.
2. Upon completion of the N_2 transfer, the solenoid valve in the propellant transfer control module is opened and the N_2 flows to a pressure regulator. The pressure is reduced to 150 psia and this regulated pressure is imposed on the propellant tanks. The application of this pressure expels the propellant through an umbilical connection at the MORL/cargo-module interface into the MORL propellant tanks.

Figure 2-19 is the flow schematic for the ammonia and the hydrogen systems aboard the logistic vehicle. The operating sequence for these systems is essentially identical to that discussed above except that no pressurant transfer to MORL tanks is necessary since each propellant is expelled by its own vapor pressure.

2.2.6 Orbit Injection System (Advanced Thrusters)

This section discusses the characteristics of the engines and the propellant loading system of the orbit injection thrusters.

2.2.6.1 System Design

The advanced thruster orbit injection system was designed to provide impulsive velocity and pitch/yaw and roll control. Pitch/yaw control is accomplished by modulating the orbit injection engines; roll control is accomplished by separate roll engines.

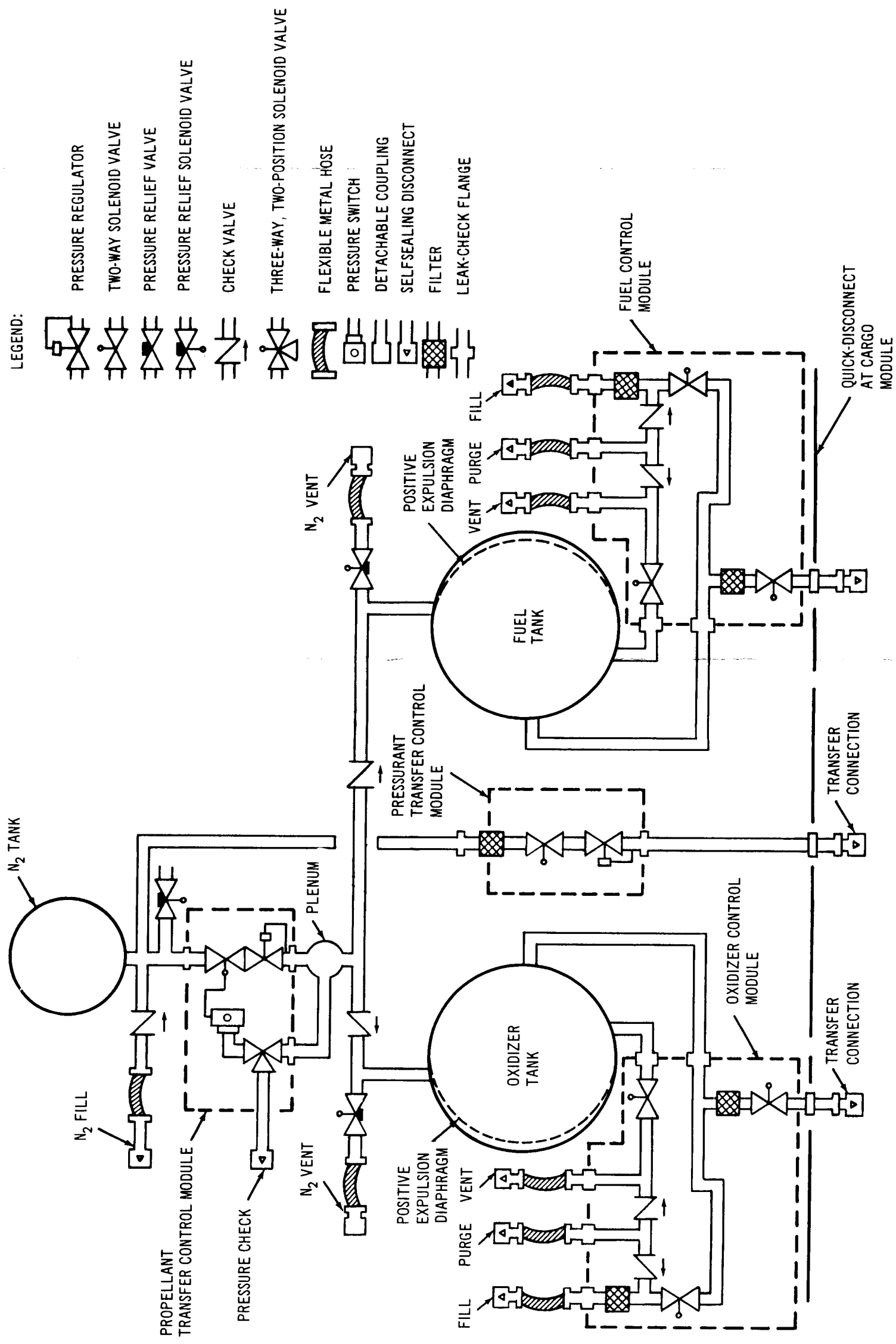
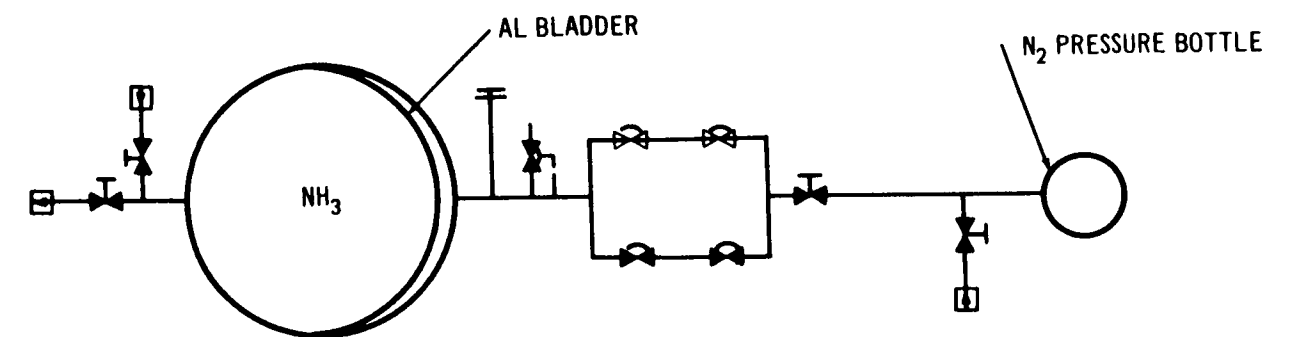


Figure 2-18. Logistics Vehicle Propellant Transfer System (Bipropellant) (B)

H₃ SYSTEM ON BOARD LOGISTICS VEHICLE



H₂ SYSTEM ON BOARD LOGISTICS VEHICLE

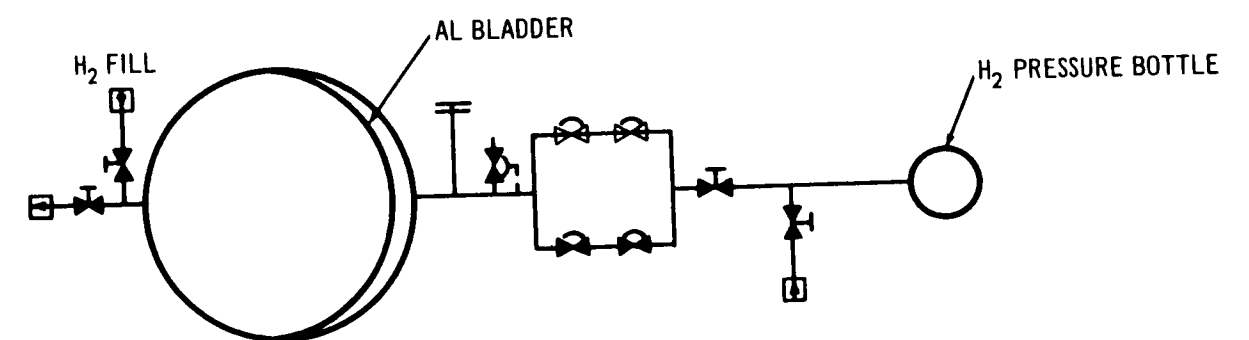


Figure 2-19. Logistics Vehicle Propellant Transfer System (Advanced Thrustors) (B)

The system consists of eight radiation-cooled engines on fixed mountings, contained in four clusters of two engines each. One engine at a 100 lb thrust level is used for pitch/yaw, and orbit injection; one engine at a thrust level of 5 lb is used for roll control. The fuel and oxidizer (NTO, MMH) are stored in two tanks of equal volume, each containing a metal bellows positive expulsion device and a nitrogen pressurant bottle. The nitrogen acts on the bellows which contains the propellants, causing a controlled collapse which forces the propellant from the tanks through the feed system to the thrusters.

The system can be refilled in space by direct transfer of propellant or by switching tanks.

2.2.6.2 Installation and Location

The engines are located 90° apart on the periphery of the aft interstage section. The propellant tankage system is located adjacent to the lower temperature section (outlet) of the Brayton Cycle radiators and adjacent to each other to allow sufficient clearance for switching.

2.2.6.3 System Performance

The system performance is shown by Table 2-12. It has a total loaded weight of 822.5 lb; dry weight is 182.3 lb. The radiation engines operate at a chamber pressure of 90 psi, and, with an expansion ratio of 100:1, deliver a vacuum specific impulse of 303 sec at the 100-lb thrust level and a 270-sec vacuum specific impulse at the 5-lb thrust level. The equal-volume tanks are designed to operate at 250 psi, with a maximum operating pressure of 300 psi. Nitrogen stored at 1,400 psi is used as the pressurant.

2.2.6.4 Propellant Resupply and Feed System

The propellant and nitrogen storage tanks are fitted with sufficient manifolding to provide the system with refilling capability. A schematic diagram of this system is shown in Figure 2-20.

Table 2-12
ADVANCED P/RCS STORABLE BIPROPELLANT ORBIT
INJECTION SYSTEM DESIGN PARAMETERS

	Magnitude or Description
System characteristics	
Number of engines	8
Total weight loaded	822.5 lb
Propellants	
Oxidizer	N_2O_4
Fuel	MMH
Mixture ratio, O/F	1.6:1 (by weight) 1.0:1 (by volume)
Total weight*	640.2 lb
Engines	
Cooling concept	Radiation
Thrust--orbiting	
Pitch/yaw	100 lb
Roll	5 lb
Expansion ratio	100:1
Chamber pressure	90 psi
Vacuum I_{sp} (steady-state)	
F = 100 lb	303 sec
F = 5 lb	270 sec
Tankage and Pressurization	
Tank pressure (operating)	250 psi
Tank pressure (maximum)	300 psi
Fuel and oxidizer tank diameter	18.5 in.
Pressurant	Nitrogen
Pressurant storage pressure	1,400 psi
*Includes weight of N_2 pressurant	

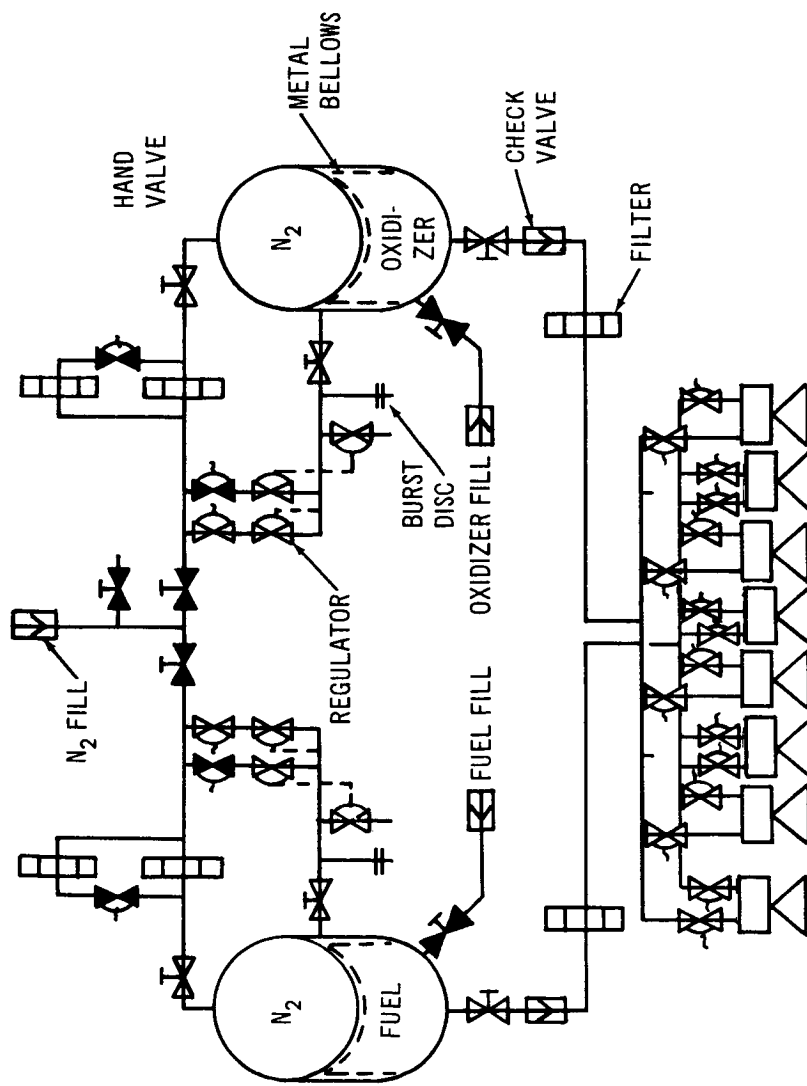


Figure 2-20. Bipropellant Advanced Orbit Injection System

PRECEDING PAGE BLANK NOT FILMED.

Section 3 ADVANCE P/RCS SYSTEMS

This section describes the scope of work and the activities carried out in order to evaluate the various advanced low thrust system concepts. A compilation of MORL specifications and requirements was prepared and is presented in Tables 3-1 and 3-2.

3.1 SYSTEMS CONCEPT EVALUATION

Initially, it was assumed that, for purposes of thruster sizing, two thrusters would be assigned for each control axis and two for drag compensation. Also it was assumed that the pitch, yaw, and roll requirements were in the form of pure couples. Thus, for propellant inventory per orbit, the weight of propellant was given by

$$W_p = \frac{\text{Total Impulse}}{\text{Specific Impulse}}$$

This figure could then be used for tank sizing. Later, a more careful study indicated that the drag compensation could be performed simultaneously with pitch and yaw adjustments, thereby reducing the thruster impulse output requirements per orbit below that specified in the table.

3.1.1 Thruster Concepts

The following thruster concepts were selected for investigation through internal studies conducted by Douglas Aircraft Corporation Inc., or through requests for information obtained from engine manufacturers. Table 3-3 lists the thruster concepts and the engine manufacturers who responded to the RFP.

Table 3-1
MORL RCS PRELIMINARY REQUIREMENTS
AND SPECIFICATIONS

Parameter	Magnitude
Power:	
Solar cell system	1 - 2 kWe
Radioisotope system	1 - 3 kWe
Heat:	
Radioisotope system waste	2 kW-thermal at 1,650°F 4.8 kW-thermal at 335°F
Propellants:	
Compatible with thruster requirements (hydrogen, ammonia, and so forth)	
Baseline open system EC/LS expends:	
Co ₂	14 lb/day
H ₂ O	1.62 lb/day
Mission duration	5 years
Orbit altitude	200 nmi
Resupply period	90 to 147 days
Total vehicle lab weight	100,000 lb

3.1.1.1 Resistojet

The Resistojet is an electrically heated rocket which heats a propellant by forced convection. Electrically heated resistive elements within the rocket body are raised to a very high temperature and the propellant, flowing over the surface, acquires this thermal energy, expands through a nozzle, and is accelerated, thereby developing thrust.

The design of the resistive element takes many forms. It may consist of a tungsten wire heater, a single tube-type heater, or a nested tube-regenerative-type heater. An example of the latter is shown in Figure 3-1.

Table 3-2
RCS DUTY CYCLE

Mode	Vehicle Configuration	Control Function	Impulse Per Orbit (lb-sec)	Impulse Per Year (lb-sec)	Pulses Per Orbit	Duration of One Pulse (sec)	Combined Thrust Per Pulse (lb)	Thrust-Time Per Orbit (sec)	Minimum Number of Engines Per Thrust	Average Thrust Per Engine (lb)
Zero-g	Solar panel	Drag	150	0.862×10^6	1	5,500	0.0273	5,500	2	0.01365
	Local horizontal	Pitch	100	0.573×10^6	2	150-2,700	0.333-0.0185	300-5,500	2	0.1665-0.00925
		Yaw	113	0.648×10^6	2	150-2,700	0.377-0.0323*	300-5,500	2	0.1885-0.01615
		Roll	8	0.0458×10^6	4	8-133.3	0.25-0.015*	32-533	2	0.125-.0075
Isotope Brayton Cycle	Local horizontal	Drag	90	0.516×10^6	1	5,500	0.01635	5,500	2	0.008175
		Pitch	82	0.470×10^6	2	150-2,700	0.273-0.0152	300-5,500	2	0.1365-0.0076
		Yaw	8	0.0458×10^6	4	8-133.3	0.25-0.015*	32-533	2	0.125-0.0075
		Roll	8	0.0458×10^6	4	8-133.3	0.25-0.015*	32-533	2	0.125-0.0075
Artificial g spin mode (0.4 Radians per sec)	Solar panel	Drag	500	2.87×10^6	350	3.92	0.134**	1,370	2	0.067
		Precession	500	2.87×10^6	350	3.92	0.134**	2,740	2	0.067
							0.134**	1,370	2	0.067
	Axis	Drag	420	2.41×10^6	350	3.92	0.114**	1,370	2	0.057
Fixed	Isotope Brayton Cycle	Precession	420	2.41×10^6	350	3.92	0.114**	2,740	2	0.057
							0.114**	1,370	2	0.057

* τ = 2,700 sec., thrust efficiency factor = 0.648

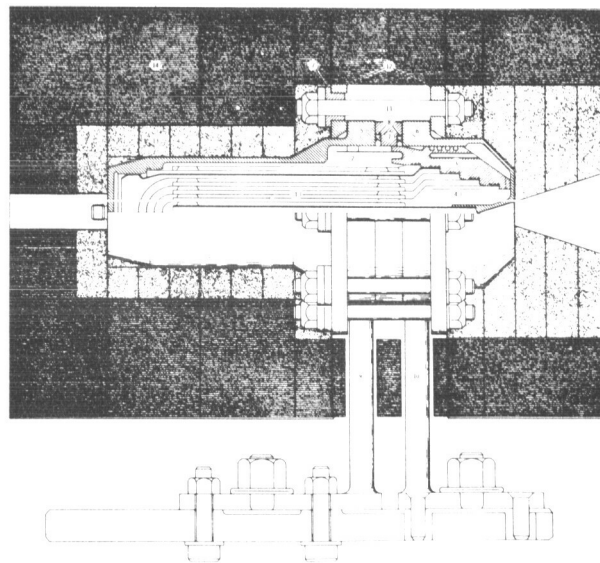
τ = 133.3 sec., thrust efficiency factor = 1.0

** Thrust efficiency factor = 0.9

Table 3-3

THRUSTOR CONCEPTS AND CONTRACTORS

Concept	Contractors
Resistojet	The Marquardt Corporation Giannini Scientific General Electric Company Avco Corporation
Arc Jet	The Marquardt Corporation Giannini Scientific
Ion engine	Hughes Research Laboratory
Radioisotope thruster	TRW Systems General Electric Company
Catalytic monopropellant	Rocket Research Corporation



1. ^{238}Pu HEATED EXCHANGER TUBES (9) - TUNGSTEN
2. REGENERATIVELY COOLED SHIELDS (3) - TUNGSTEN
3. HEAT EXCHANGER SUPPORT (ELECTRICAL INSULATOR) - BORON NITRIDE
4. NOZZLE RADIATION SHIELD - TUNGSTEN
5. FORWARD PRESSURE CASE - MOLYBDENUM - 0.9% TITANIUM
6. AFT PRESSURE CASE - TUNGSTEN - 2% THORIA
7. ELECTRICAL INSULATIONS - BORON NITRIDE
8. METALLIC FACE SEALS (2) - INCOME X - SILVER PLATED
9. ELECTRICAL (+), PROPELLANT FEEDER, THRUSTOR SUPPORT - MOLYBDENUM - 0.3% TITANIUM
10. ELECTRICAL (-), PROPELLANT FEEDER, THRUSTOR SUPPORT - TUNGSTEN - 2% THORIA
11. TIE BOLTS - MOLYBDENUM - 0.9% TITANIUM
12. COLLARS (2) - MOLYBDENUM - 0.9% TITANIUM
13. THERMAL INSULATION - DYNAQUARTZ
14. THERMAL INSULATION - MIN-R-2000
15. CASE - 321 STAINLESS STEEL

Figure 3-1. Marquardt 3-kW Concentric Tube Resistojet

The electric current flows from the outer concentric tube to the inner tube via the electrical connectors. The entering propellant passes over the outermost tube and, after making several passes through the concentric annuli, reaches the center tube, where it is finally expanded through the nozzle.

Temperatures may be developed of the order of 4,000°F, and materials used must be of the refractory type (for example, tungsten or tungsten rhenium alloys) in order to maintain structural integrity at high temperatures as well as good working properties. Details of construction and configuration are discussed in Section 5.

The following simplified equation relates the kinetic energy in the exhaust to the electric power input to the electric terminals.

$$F = \frac{46 \eta_o P}{I_{sp}}$$

where

F = thrust, lb

P = electric power, kW

I_{sp} = specific impulse, sec

η_o = engine overall efficiency

The specific impulse is a function of the propellant species, temperature, and chamber pressure, whereas the overall efficiency is determined by the geometry as well as design, and is primarily a product of three separate efficiencies given by

$$\eta_o = \eta_H \cdot \eta_N \cdot \eta_F$$

where

η_o = overall efficiency

η_H = heater efficiency

η_N = nozzle efficiency

η_F = frozen flow efficiency

Each of the efficiencies will be briefly discussed in the following.

Heater Efficiency, η_H

The heater efficiency, η_H , is a measure of the efficiency that the electric power delivered to the engine terminals is converted into thermal energy in the propellant. The power losses are attributed to the following: (1) heat lost by conduction via the electric power and propellant leads and the engine mounts, (2) heat losses by convection and, primarily, radiation from the outer case of the engine, and (3) heat losses due to poor heater design.

In general, these losses may be minimized by improved design (for example, by the use of regenerative propellant heating and adequate insulation).

Nozzle Efficiency, η_N

The nozzle efficiency, η_N , is a measure of the nozzle's ability to convert the propellant thermal energy to kinetic energy. The nozzle contour, area ratio, and surface condition for these low flow rates each affect the efficiency. Generally, these factors may be controlled by using the design and manufacturing techniques required for the small throat areas and by employing nozzle dimensions appropriate for very low thrust applications.

Frozen Flow Efficiency, η_F

The frozen flow efficiency, η_F , is a measure of the dissociation effects experienced by the propellant as it is heated to the very high temperatures. Molecules may dissociate to atoms and the latter to ions with an increase in energy absorption. As the gas is expanded through the nozzle, a recombination of the dissociated species would result in this energy being imparted to increasing the kinetic energy of the gas. Unfortunately, the residence time in the nozzle is too short, and the recombination does not take place. The stream kinetic energy is thus less than the total energy absorbed by the propellant, and this unrecovered energy or loss is the frozen flow efficiency, that is,

$$\eta_F = \frac{\text{Kinetic Energy}}{\text{Absorbed Energy}}$$

Figure 3-2 (Reference 1) is a plot of frozen flow efficiency as a function of specific impulse, I_{sp} , or, in effect, propellant temperature, for a variety

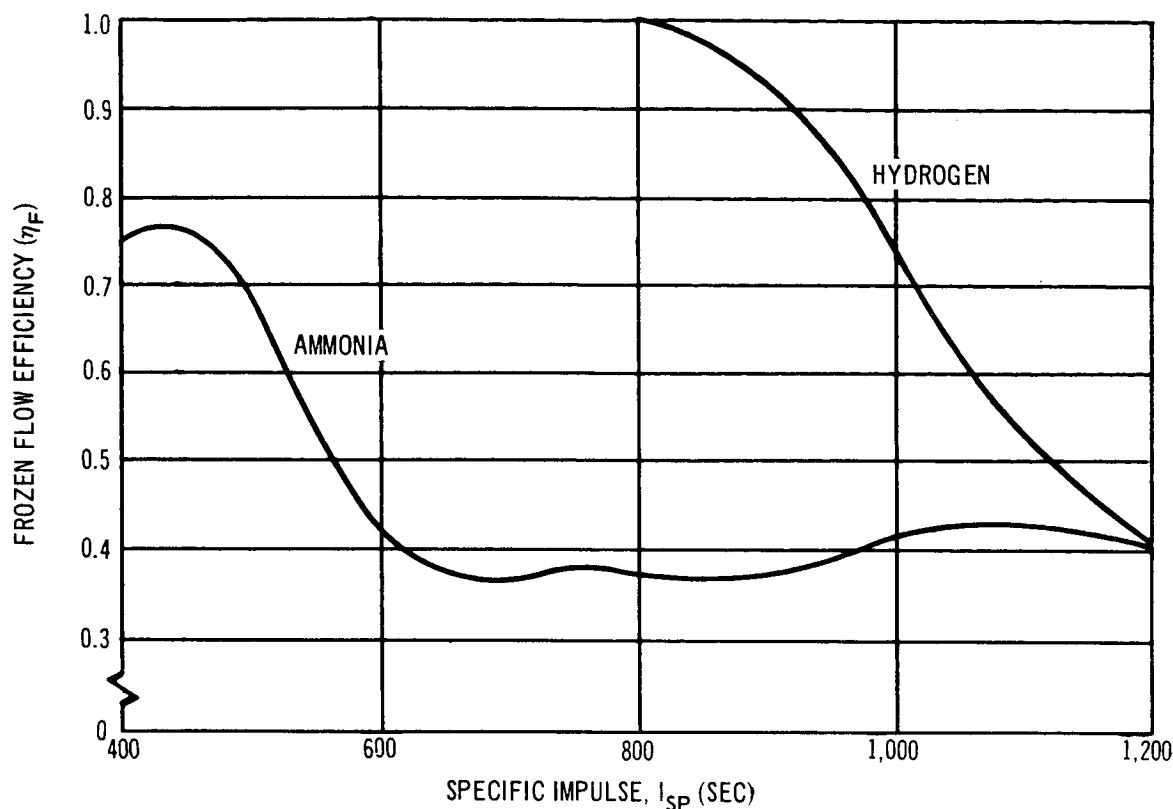


Figure 3-2. Frozen Flow Efficiency as a Function of Specific Impulse

of propellants. Hydrogen has an η_F of unity up to an I_{sp} of 800 sec while ammonia, in the same range if I_{sp} , shows a large decrease in η_F .

In summary, the overall efficiency associated with a given propellant I_{sp} is influenced most by the frozen flow efficiency, since η_H and η_N can be designed for near unity.

3.1.1.2 Radioisotope Thrustors

Recent advances in the development of radioisotope thrustors, such as those developed and tested at Morind Laboratories, prompted consideration of these thrustors for the MORL application. They appeared attractive, because they are inherently low-thrust, high-performance engines that are completely independent of an electric power source for their operation, and their fuel-form requirements could be compatible with that of the Brayton Power Cycle.

A schematic drawing of a typical radioisotope-heated reaction control thrustor is shown in Figure 3-3. The unit consists of a radioisotope fuel form

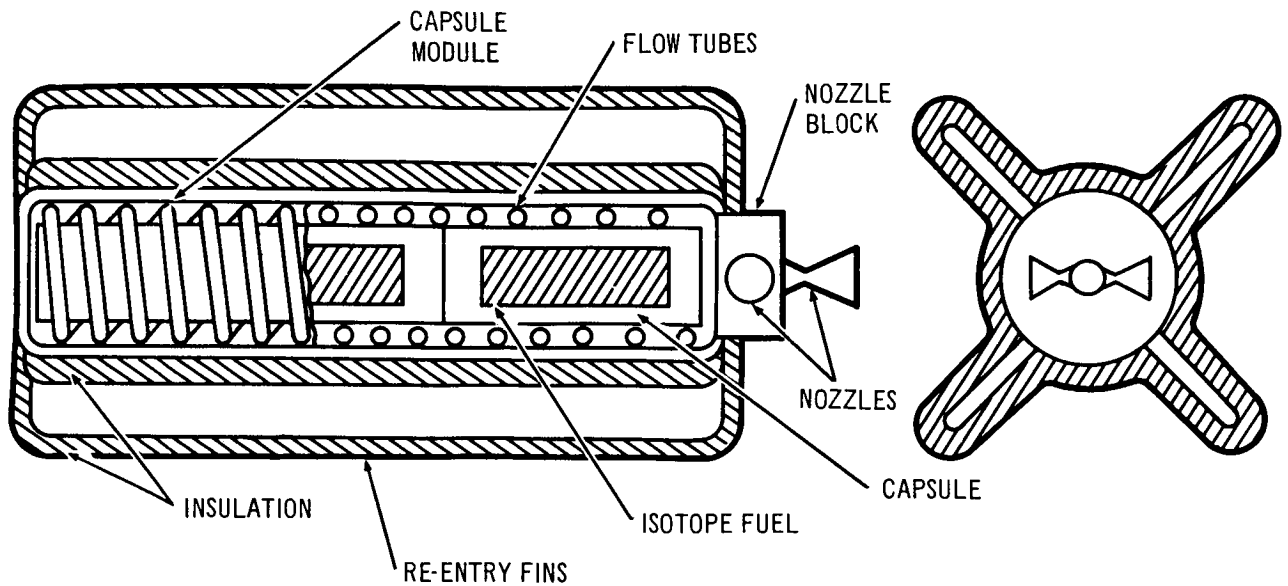


Figure 3-3. Radioisotope Thruster for MORL Mission

encapsulated in a cylindrical metallic container which is coiled with propellant flow tubes. Each tube is connected to a separate exhaust nozzle. The number of nozzles depends upon mission requirements. An additional tube is provided for cooling water on the launch pad. A concentric shell, with thermal insulation attached to its outer surface, encloses the entire assembly. Four longitudinal fins are attached to the thruster and act as re-entry aids in the event of mission abort. A solenoid valve is attached to each propellant tube upstream of the thruster inlet to control propellant flow through each nozzle. The thruster operates by heating the propellant as it flows through the propellant flow tube and then expelling the propellant through a converging-diverging nozzle to create propulsive thrust.

Radioisotope Fuel

The radioisotope fuel must be compatible with mission requirements. Its half life must provide the required design power without frequent replenishment; its nuclear radiation must be easily attenuated so as to keep the module shield weight within reason; and its fuel form must meet AEC safety

requirements in case of catastrophic failure, and it must be available in sufficient quantities to provide a complete thruster system. Table 3-4 shows the radiation characteristics and availability of several candidate isotopes. The first four are alpha emitters, while the latter three are essentially beta emitters. Using depleted uranium and lithium hydride for shielding against the gamma and neutron radiation, it was concluded that Pu-238, Po-210 and Pm-147 are the best candidates for further studies.

Thermal Considerations

The thermal insulation is necessary to ensure that, at steady state operation, the heat generated by the fuel goes primarily into heating the propellant in the tubes. Also, the design requires that, at no-flow conditions, the temperature rise will not result in melting of the fuel or in attainment of too high a wall or tube temperature. By proper design, it is possible to achieve both the proper thermal radiation surface requirements as well as the proper mechanical impact characteristics.

3.1.1.3 Ion Engines

Ion engines are a class of electrostatic thrusters which accelerate ions through an electrostatic field. The increase in the kinetic energy of the charged particles, results in an interchange of momentum with the vehicle. These engines are capable of developing high specific impulse (to 10,000 sec) but, because of electric power limitations, they develop a very low thrust. This is seen from the electric equation:

$$F = \frac{46\eta P}{I_{sp}}$$

where the I_{sp} in the denominator reduces the thrust level by an order of magnitude over that of Resistojets.

Figure 3-4 is a schematic diagram of an ion engine. A suitable propellant such as liquid cesium is heated and its vapor is then passed through a porous tungsten ionizer where the C_s atoms are stripped of their electrons and converted to cesium ions, C_s^+ . The latter forms a beam of ions which is subjected to beam shaping, accelerating, decelerating, and neutralizing

Table 3-4

RADIOISOTOPE RADIATION FIELDS AND AVAILABILITY

Isotope	Half Life	Gamma Radiation/kW Thermal (mrem/hour at 10 ft)* Bare Capsule 0.4 in U	Neutron Radiation/kW Thermal (mrem/hour at 10 ft)* Bare Capsule 8-in. LiH	Estimated Production Per Year in 1970** (kW Thermal)
Po-210	138 days	10	0.3	0.02
Pu-238	89.8 years	0.08	9.0	1.1
Cm-242	163 days	0.8	13	1.4
Cm-244	18.4 years	9	365	50
Pm-147	2.67 years	15.5	-	-
Tm-170	127 days	1.1×10^4	-	-
Tl-204	3.9 years	200	-	-

*Radiation field data taken from ORNL-3576, Handbook of Shielding Requirements and Radiation Characteristics of Isotopic Power Sources for Terrestrial, Marine, and Space Applications by E. D. Arnold.

***Availability data taken from Present and Potential Annual Availability of Isotopic Power Fields by Division of Isotopes Development, USAEC (1963).

*Radiation field data taken from ORNL-3576, Handbook of Shielding Requirements and Radiation Characteristics of Isotopic Power Sources for Terrestrial, Marine, and Space Applications by E. D. Arnold.

**Availability data taken from Present and Potential Annual Availability of Isotopic Power Fields by Division of Isotopes Development, USAEC (1963).

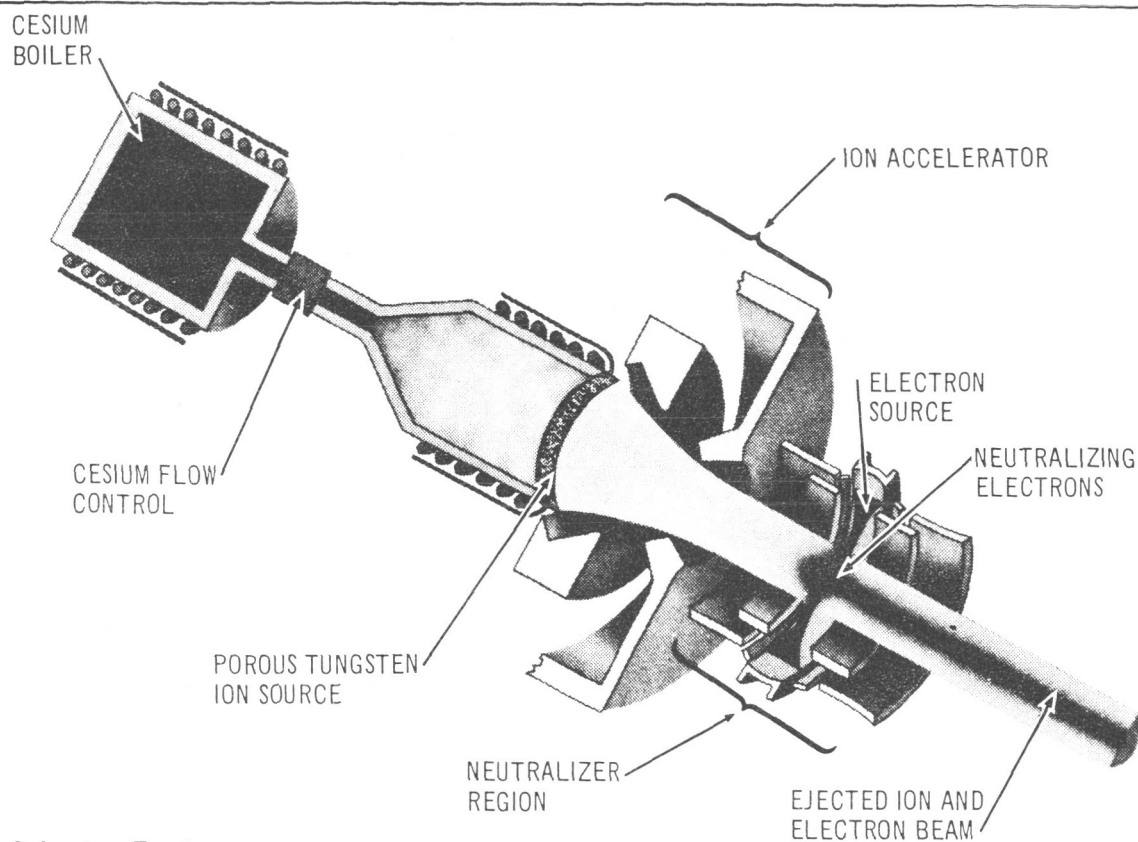


Figure 3-4. Ion Engine

electrodes. The latter adds the stripped electrons back to the beam, so that the emerging stream is electrically neutral.

The ion engine described is a contact type. A more efficient type is the bombardment engine which achieves ionization of the propellant by electron bombardment prior to accelerating the propellant through the electrostatic field. It is a more efficient engine particularly in the lowered I_{sp} range (4,000 sec) which appeared to be more practical for the MORL application.

Figure 3-5 shows the performance of the engines where efficiency is plotted against I_{sp} .

3.1.1.4 Monopropellant Catalyst Engine

A hydrazine monopropellant catalytic engine was considered for application to the MORL for the reason that hydrazine forms the basis for the fuel in the high thrust functions of the baseline system, and thereby provides a compatibility in tankage and feed system. Figure 3-6 shows a typical

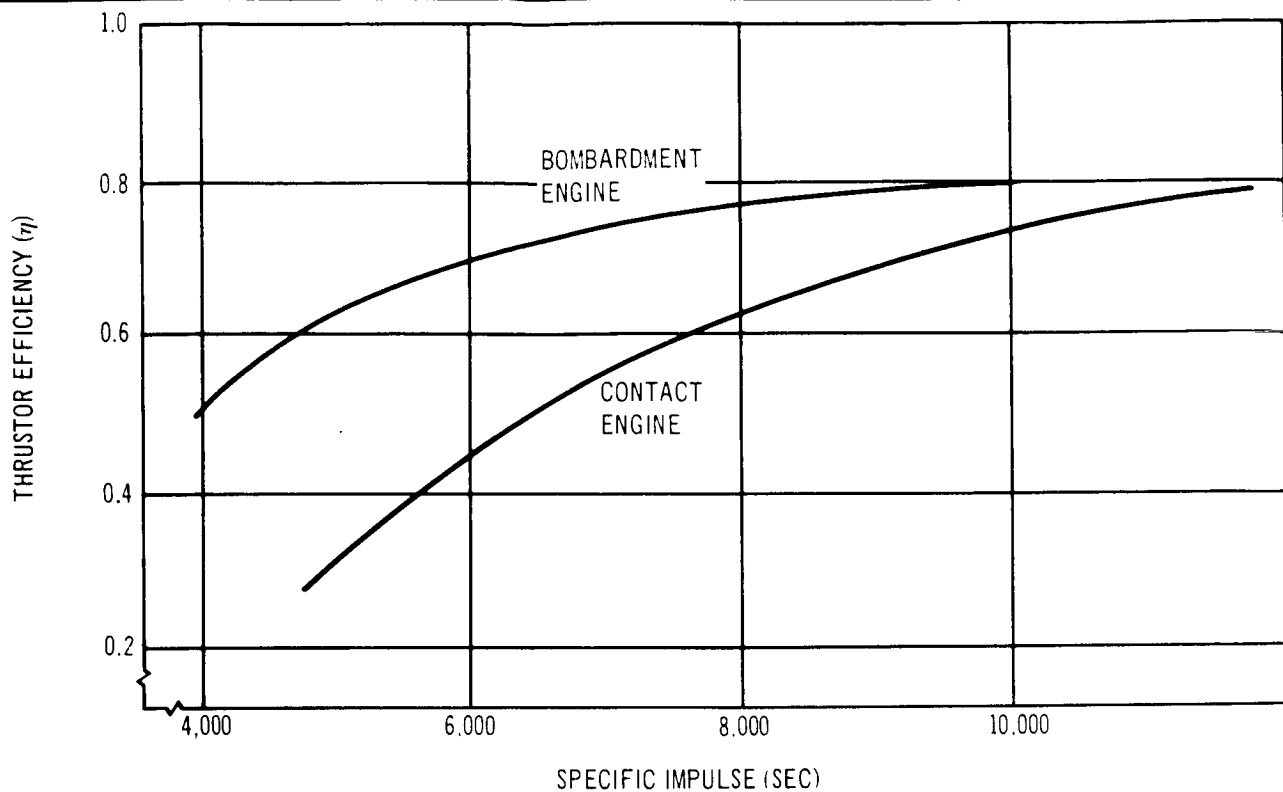


Figure 3-5. Engine Efficiency as a Function of Specific Impulse

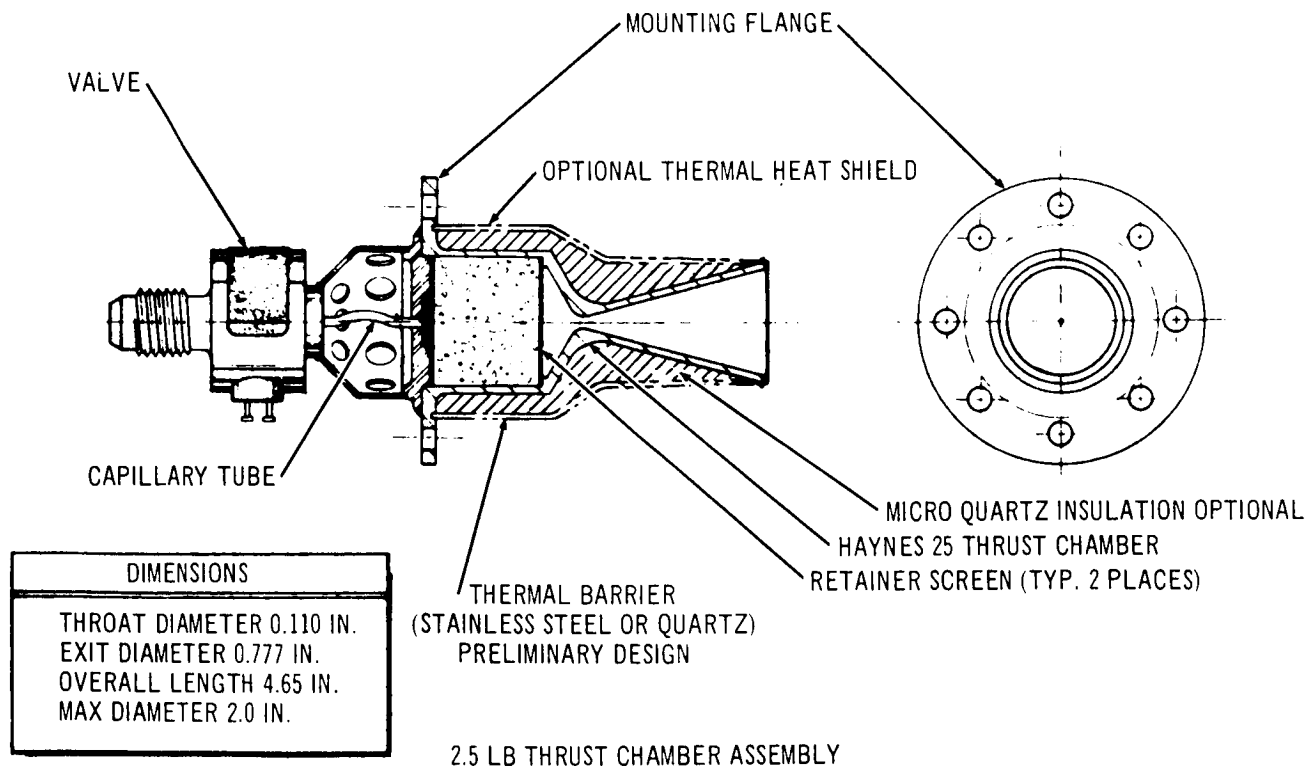


Figure 3-6. Catalytic Monopropellant Engine

rocket thruster assembly. A suitable monopropellant, such as liquid hydrazine, is valved to an injector plate and then to a catalyst bed where an exothermic decomposition takes place. The catalyst in the form of pellets, such as Shell 405, permits the heated gas decomposition products (hydrogen, nitrogen, and ammonia) to flow rapidly to the thruster nozzle where acceleration takes place. A specific impulse of 240 sec is attainable with gas chamber temperatures of 1,800°F. Ordinary materials of construction such as stainless steel or Hynes No. 25 alloy can be used. An engine developing 0.5 lb of thrust at a chamber pressure of 100 psia is estimated to weigh 0.25 lb. Problems associated with the thruster pertain to heat leak back through the valve and performance degradation caused by propellant hold-up volume. The former may produce instability due to the reaction taking place upstream of the bed. By proper thermal design, this effect may be minimized. Hold-up volume may be reduced by proper design of the feed tube and valve.

3.1.1.5 Arcjet

An arcjet converts electrical energy to thermal energy by heat transfer from an arc discharge struck between a tungsten cathode and a tungsten anode nozzle. The thermal energy in the steady state arc is produced by Joule heating and this energy is transferred to the outer propellant gas by conduction diffusion and convection. The propellant is finally expanded in a nozzle to convert the thermal energy into directed kinetic energy.

Figure 3-7 shows a typical design of a thruster module. The arc is generally unstable and strikes different parts of the anode during the course of firing. The nozzle and electrodes must be designed so as to prevent erosion pitting and overheating. The cathode which provides the electrons by thermionic emission is rod shaped and cooled by the incoming propellant. By forcing the arc to attach downstream of the throat in the low pressure region, a diffuse arc is formed thereby reducing point contact and overheating.

The arc heating produces very high gas core center line temperatures (to 10000°R), however the average propellant chamber temperature is lower, but still higher than that achievable with resistojets. As a result, a higher

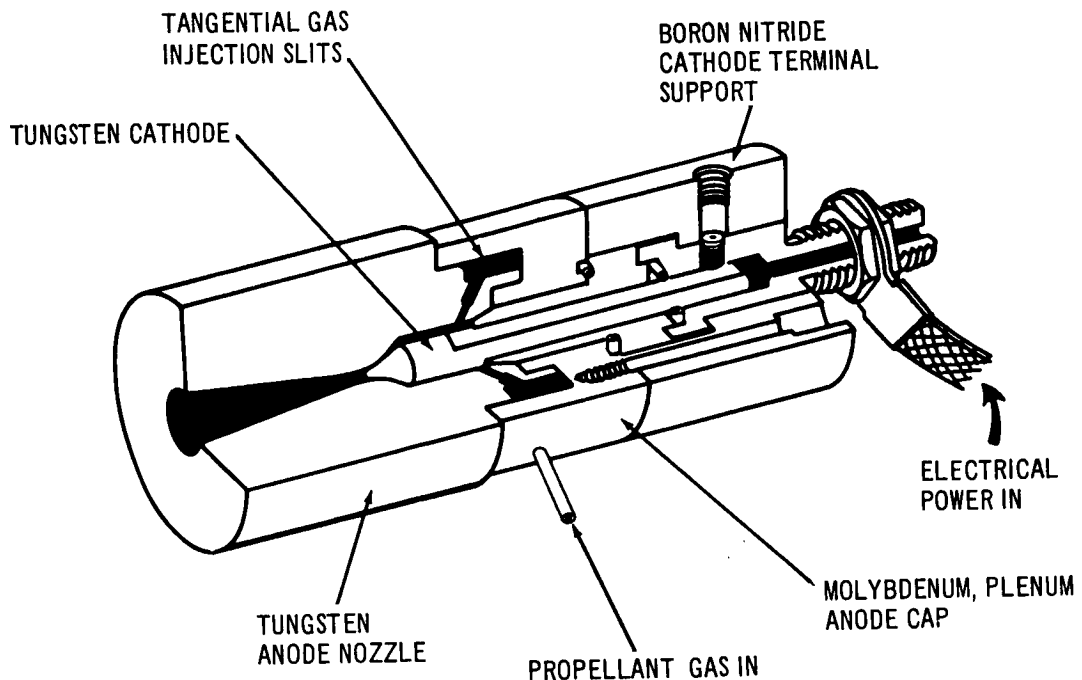


Figure 3-7. AVCO Radiation-Cooled Arc Jet

specific impulse is developed. However, because of the mode of heating, a large amount of dissociation and ionization occurs and the frozen flow efficiency, (μ_F) plays a major part in lowering the overall efficiency of the thruster system. Small arc jets are much more affected by dimensions, cathode and anode shape, pressure and flow rates. The nominal performance is given below:

NOMINAL ARCJET PERFORMANCE

Thrust, lb	.03
Specific impulse, sec	935
Efficiency, percent	30
Power, kw	2

3.1.1.6 Arc Jets, -- \bar{JXB} Accelerators

Other arc-jet techniques are being investigated. These include the application of a magnetic field perpendicular to the direction of flow of the electric current established by the arc. The interaction of the magnetic field, \bar{B} ,

with the electric current, \bar{j} , produces a force on the exhaust flow which results in an increase in specific impulse and efficiency. A specific impulse of 10,000 sec is predicted by this method using a variety of propellants.

3.1.2 Thruster Performance

In the following discussion of thruster systems performance, the information from the companies that participated in supplying information is used, where possible. Since guidelines were very loose in regard to the stabilization and control techniques and since the initial RFI called for feasibility investigations, the varied response received increased the difficulty of evaluating the systems on a common basis. The data are presented as received from each company, and the optimum-performing thruster of a class is selected for further comparisons.

3.1.2.1 Resistojets

Previous calculations had indicated that Resistojet performance makes it attractive for the MORL application. For this reason, a greater number of Resistojet designs were considered.

The Marquardt Corporation design (with a heat exchange element that consists of nested concentric tubes which are electrically connected in series) based their engine performance on the parameters shown in Table 3-5.

An individual thruster (1 of 14) for the zero-g solar power mode using hydrogen required 600 W and developed 0.0247 lb of thrust.

Table 3-5
MARQUARDT RESISTOJET PERFORMANCE

Jet Characteristics	Propellant	
	H ₂	NH ₃
Chamber temperature (°R)	4,350	4,350
Specific impulse (sec)	840	400
Efficiency	0.75	0.60
Thrust/power (lb/kWe)	0.0412	0.069

The Giannini Scientific Corporation Resistojet design uses the concept of electric contact resistance formed as a result of slightly pressing an inner electrode rod against an outer electrode tubular surface. The gas, flowing through narrow passages between the contact surfaces, picks up most of the heat at the points of contact near the throat. Table 3-6 summarizes the typical engine performance.

Table 3-6
GIANNINI RESISTOJET PERFORMANCE

Jet Characteristics	H ₂
Chamber temperature (°R)	3,600
Specific impulse (sec)	700
Efficiency	0.40
Thrust/power (lb/kWe)	0.0263

: The General Electric concept utilizes a thermal storage design, wherein a sealed heater element is isolated from the propellant flow but nevertheless maintains a constant stagnation temperature of $2,500^{\circ}\text{R}$, using NH_3 fed at 60°F (Figure 3-8). The propellant makes one pass through an annular passage over the heated core to the nozzle throat. The gas temperature approaches the body temperature within 20°F . Metal foil insulation is used to contain the heat and reduce radiation losses. Table 3-7 gives the performance of a typical thermal storage resistance jet.

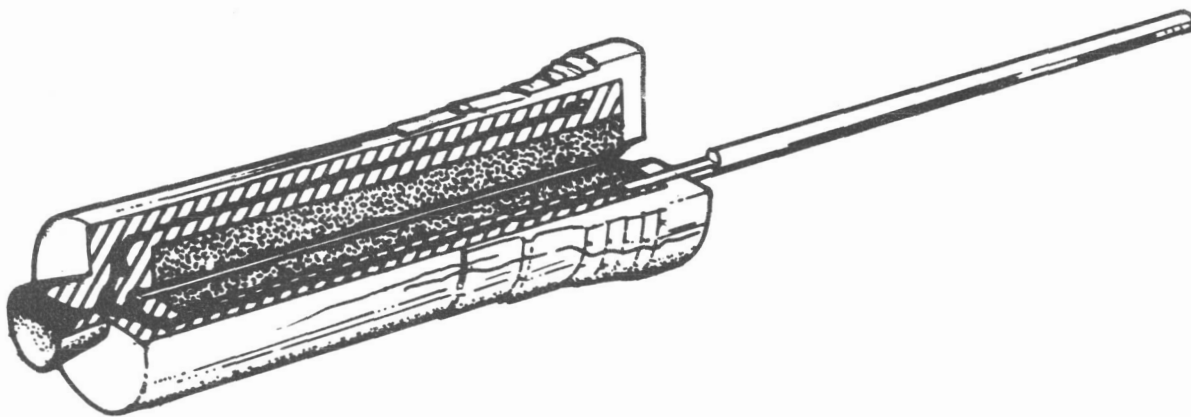


Figure 3-8. General Electric Resistance Jet

Table 3-7
GENERAL ELECTRIC RESISTANCE JET PERFORMANCE

Jet Characteristics	NH ₃
Chamber temperature (°R)	2,500
Specific impulse (sec)	270
Efficiency	0.518
Thrust/power (lb/kWe)	0.0882

The Avco Corporation design was based on a 3-kW concept which causes the propellant to enter a plenum at the aft end of the thruster, then to pass through a tube coiled about the engine exterior for regenerative cooling in a single or double pass. The gas then re-enters the engine near the aft end for passage into a central heater. This heater element consists of sections of molybdenum tube segments butted together but separated by boron nitride insulators. The tube segments are electrically connected in series by tungsten rhenium resistance heating coils which are placed across the tube diameter, normal to the gas flow; the alternate coils are also normal to each other. Figure 3-9 is a sketch of the design used in a 293-hour test. Table 3-8 lists the anticipated performance for typical engines.

Table 3-8
AVCO RESISTOJET PERFORMANCE (1 kW)

Jet Characteristics	H ₂	NH ₃
Temperature (°R)	4,680	4,680
Specific impulse (sec)	719	351
Efficiency	0.55	0.46
Thrust/power (lb/kWe)	0.0355	0.060

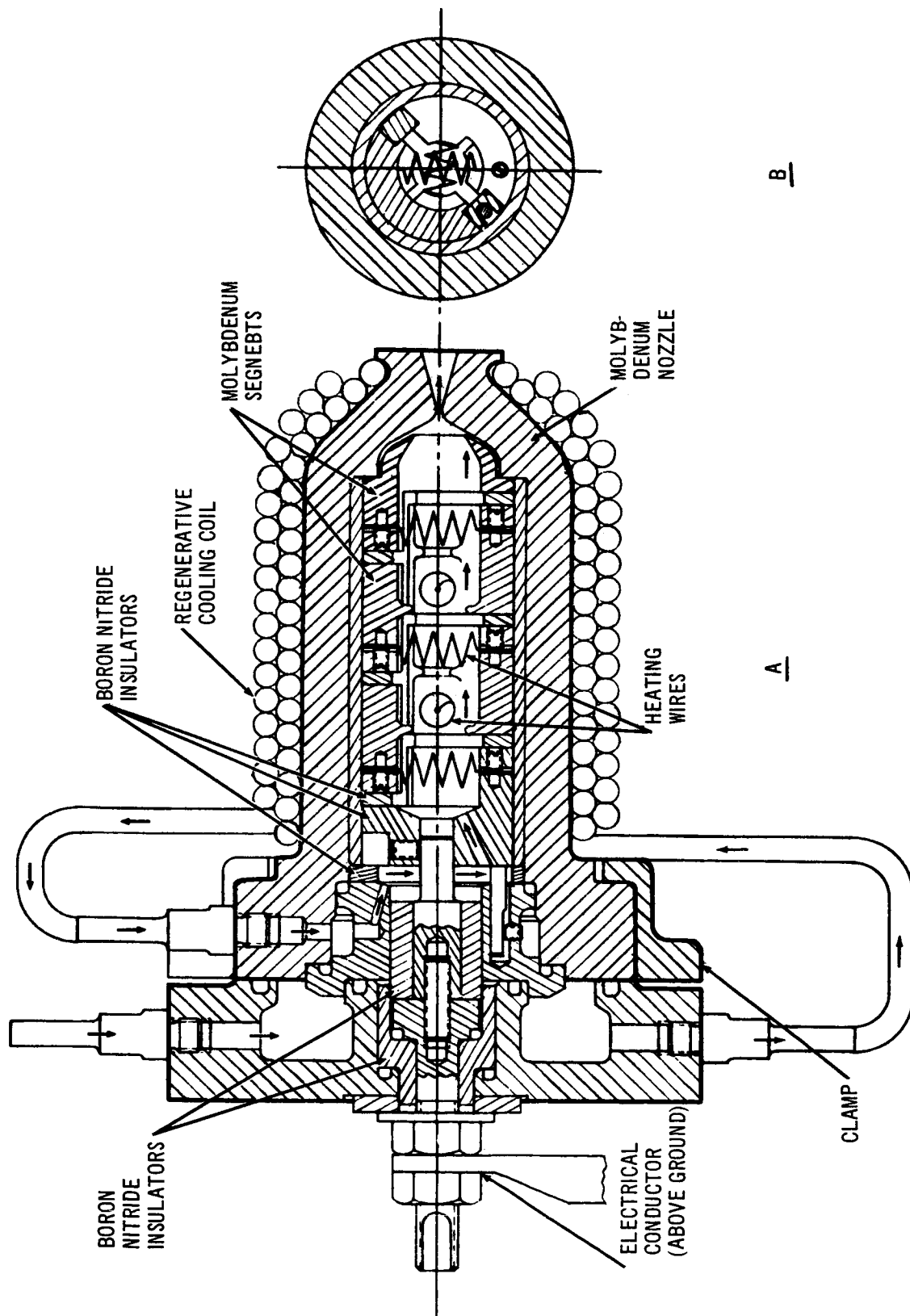


Figure 3-9. Avco 3kW Resistojet

3.1.2.2 Arc Jets

Arc jets have been developed in the 30-kW range which have run for 720 hours with H_2 propellant (Reference 2). However, the application to the MORL called for a much lower power level in the 1-kW range. Lack of time prevented contact with suitable engine manufacturers for information regarding the low-power arc jet. For that reason, the information regarding performance is based mainly on a survey conducted by NASA-Lewis (Reference 3) in which a wide range of arc jets are analyzed. The performance of engines in the 1-kW level are presented in Table 3-9.

Table 3-9
ARC-JET PERFORMANCE

Propellant	H_2	NH_3
Specific impulse (sec)	1,100	550
Efficiency	0.35	0.08
Power (kW)	1.0	0.920
Thrust/power	0.00991	0.00653

The data are quoted from Giannini Corporation reports on the development of low-power thrusters. However, it is the high-power (30 kW and greater) engines which have received greater attention because of their use in connection with materials and plasma studies. These engines have efficiencies over 50% and develop maximum gas core temperatures of 20,000°K.

3.1.2.3 Ion Engines

Ion engines were looked at briefly by the Hughes Research Laboratory. The Hughes engine is a cesium-contact type. To meet the thrust levels needed and still stay within a reasonable power demand the engine I_{sp} was selected at 4,000 sec. Unfortunately, the contact engine was developed for a higher I_{sp} , 10,000 sec, and therefore at the lowered I_{sp} the efficiency is drastically low (less than 20%) when the design curves are extrapolated (Figure 3-5).

Therefore, Hughes assumed that it would not be unreasonable to achieve a design at an engine for a higher efficiency at an I_{sp} of 4,000 sec. Figure 3-10 shows an orbit maintenance module and an attitude control module which provide for thrust in two opposite directions. Figure 3-11 is a cutaway showing the parts of the engine. Table 3-10 shows the performance of a typical engine.

Table 3-10
CONTACT ION ENGINE PERFORMANCE

Propellant	Cesium
I_{sp} (sec)	4,000
Efficiency	0.56
Power (kW)	2.5
Thrust/power (lb/kW)	0.0064
Thrust (lb)	0.016

Figure 3-12 shows a diagram of a typical ion engine propulsion system as proposed by Hughes.

3.1.2.4 Radiosotope Thrustor

Design considerations for the radioisotope thruster consisted of the evaluation of several radioisotope fuel forms for the mission as well as consideration of various propellants. TRW suggested a multiple-nozzle design in which propellant entered the aft end, circulated through a passage or tube coiled about radioisotope-heated cylinders, and then exited at a single nozzle. By standardizing radioisotope cylinder size, variation in thrust or heat output could be obtained by changing the fuel loading characteristics.

Figure 3-13 is a schematic diagram of two Pu-238 engine modules whose thrust levels are designed for the MORL application. The performance of a Po-210 and a Pu-238 engine with multiple nozzles is presented in Table 3-11.

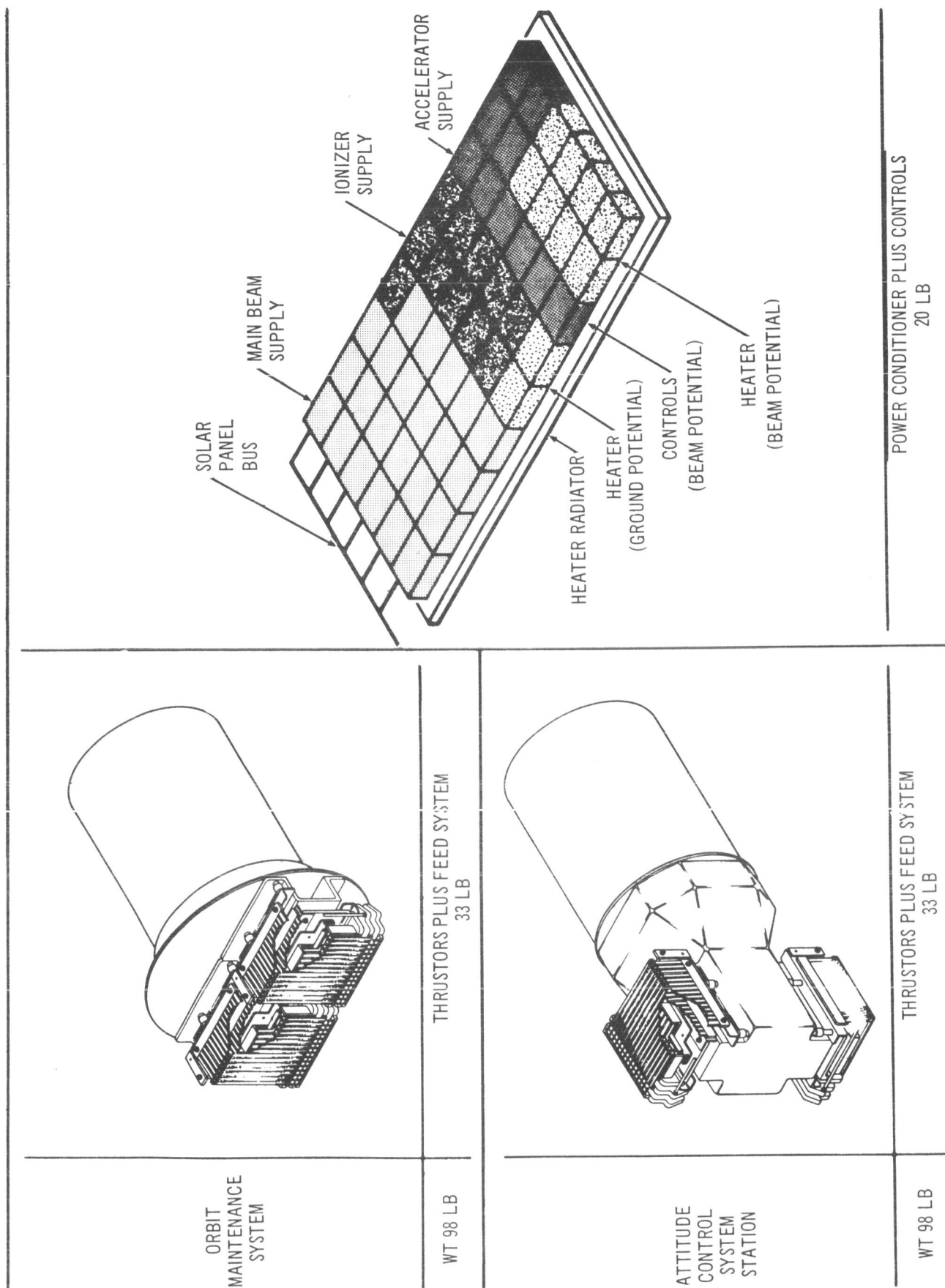


Figure 3-10. Ion Engine Space Control Systems

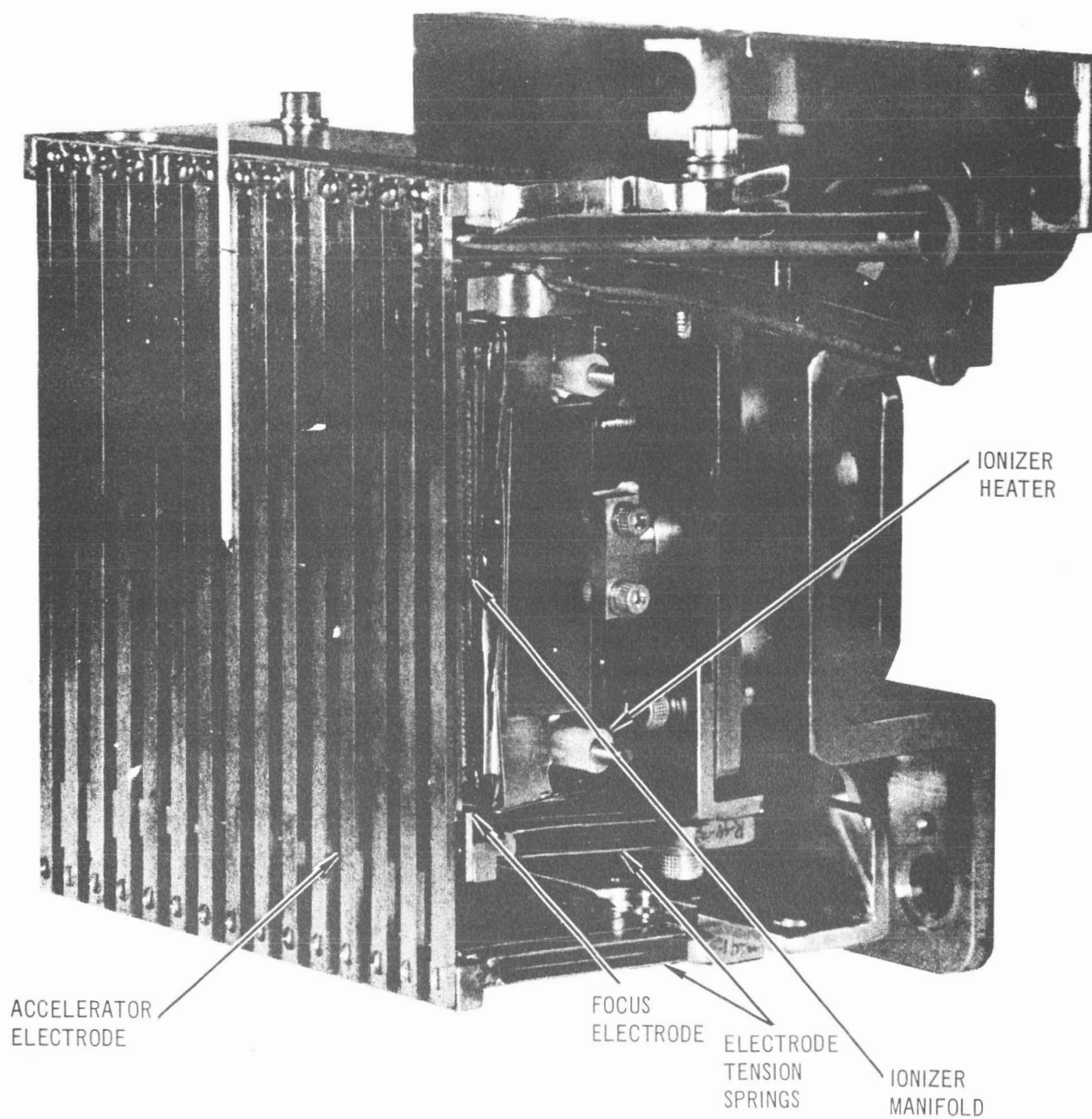


Figure 3-11. Linear Strip Ion Engine

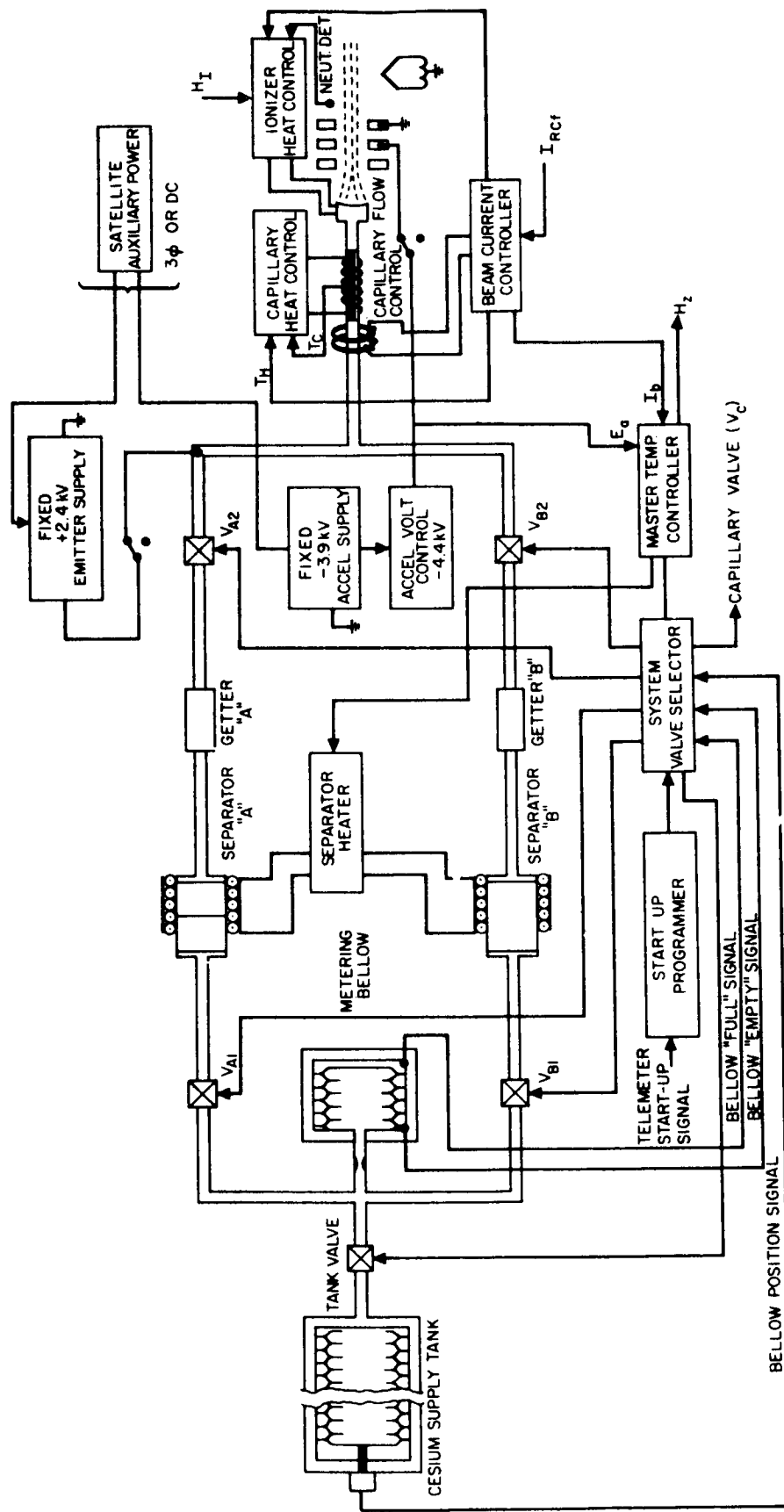


Figure 3-12. Cesium Ion Engine Block Diagram

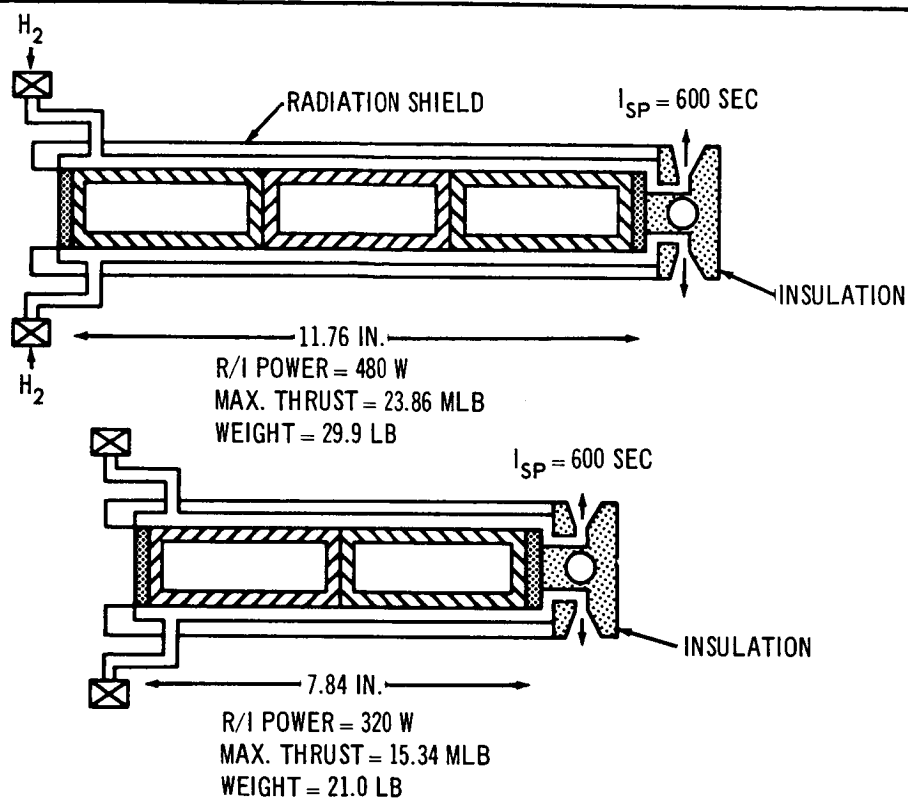


Figure 3-13. Typical Pu-238 Fueled Thrusters

Table 3-11
RADIOISOTOPE THRUSTOR PERFORMANCE

Propellant	H ₂	H ₂
Radioisotope	Po-210	Pu-238
Radioisotope power (W)	1,720	480
I_{sp} (sec)	650	600
Thrust (lb)	0.0234	0.0234
Weight (lb)	15	29.9
Replacement	147 days	5 years
Efficiency	0.525	0.637

The size of the modules varied from 1 to 2 ft in length, depending upon the number of capsules and thermal power needed for the mission. Figure 3-14 shows the variation in dimension with power.

Thermal Characteristics

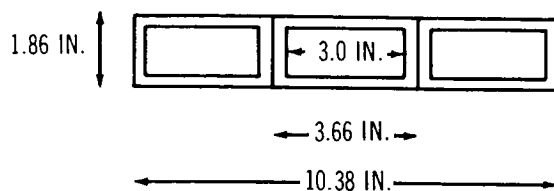
The estimated thermal characteristics of the thruster for both steady-state and no-flow conditions is shown in Figure 3-15, where the temperature is plotted as a function of distance along the thruster axis for a Pu-238-fueled engine using NH_3 propellant. The maximum fuel centerline temperature is at 3,700°F during flow and rises to a maximum of 4,100°F during no-flow conditions when heat removal is accomplished by radiation to the environment. This temperature is still below the melting point of the plutonium oxide microsphere fuel form (4,300°F).

Sublimation Considerations

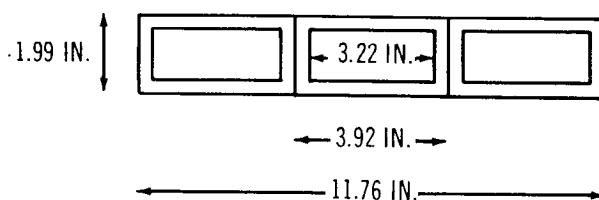
The high temperature to which the materials are raised, particularly in a hard vacuum, make them susceptible to sublimation. This is of concern to the radioisotope thruster and to the electric thrusters as well when operating in the 4,000°F range. Figure 3-16 is a plot of sublimation rate as a function of temperature for commercially pure tungsten. At 4,000°F, the evaporation rate is 10 mils, or 0.01 in./year. However, this rate decreases considerably when a gas pressure exists (as when propellant is flowing). Since the thrusters are designed to be in nearly continuous operation even if operation is only 30% of the time in 5 years (an extreme case), the amount of evaporation would be equal to $0.01 \times 5 \times 0.70 = 0.035$ in. This could be taken care of with extra thickness added to a tube or nozzle throat. On the other hand, the electric thrusters offer the advantage of dropping the temperature by cutting off the power during no-flow operation.

3.1.2.5 Catalytic Monopropellant Engine

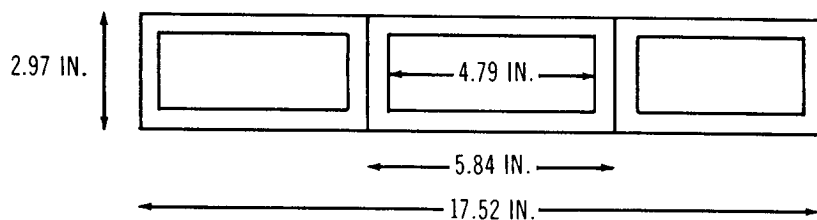
The catalytic monopropellant engine was considered because its use of hydrazine fuel provided a potential common tankage source with high-thrust systems already on board. Rocket Research Corporation surveyed the MORL requirements and suggested thrust levels varying from 0.25 to 20.0 lb.



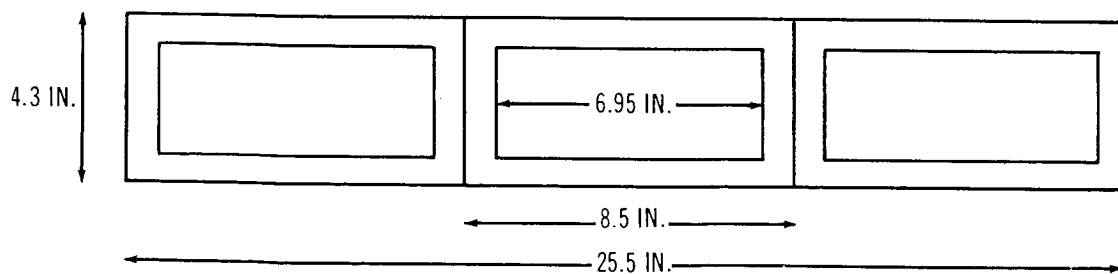
$P = 410 \text{ W}$
 $I_{SP} = 530 \text{ SEC}$



$P = 480 \text{ W}$
 $I_{SP} = 600 \text{ SEC}$



$P = 630 \text{ W}$
 $I_{SP} = 650 \text{ SEC}$



$P = 750 \text{ W}$
 $I_{SP} = 700 \text{ SEC}$

Figure 3-14. Dimensions of Pu-238 Heat Sources

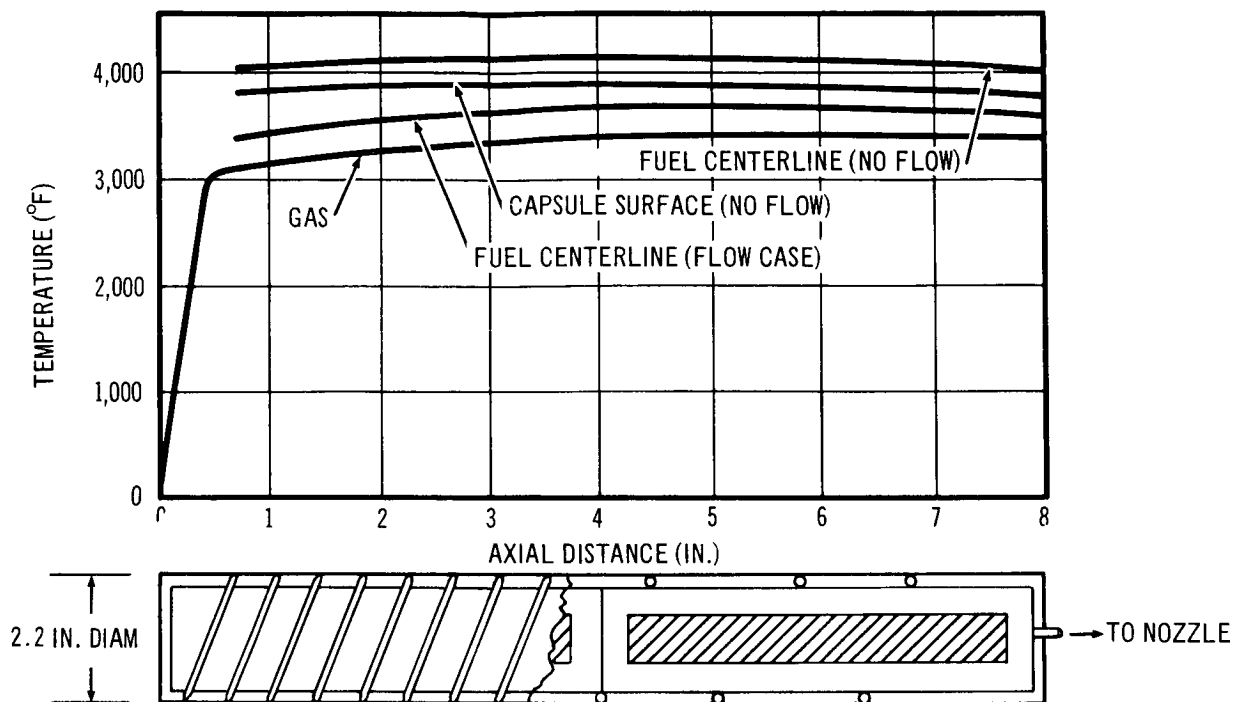


Figure 3-15. Temperature Distribution for 0.030-lb Thrust Engine

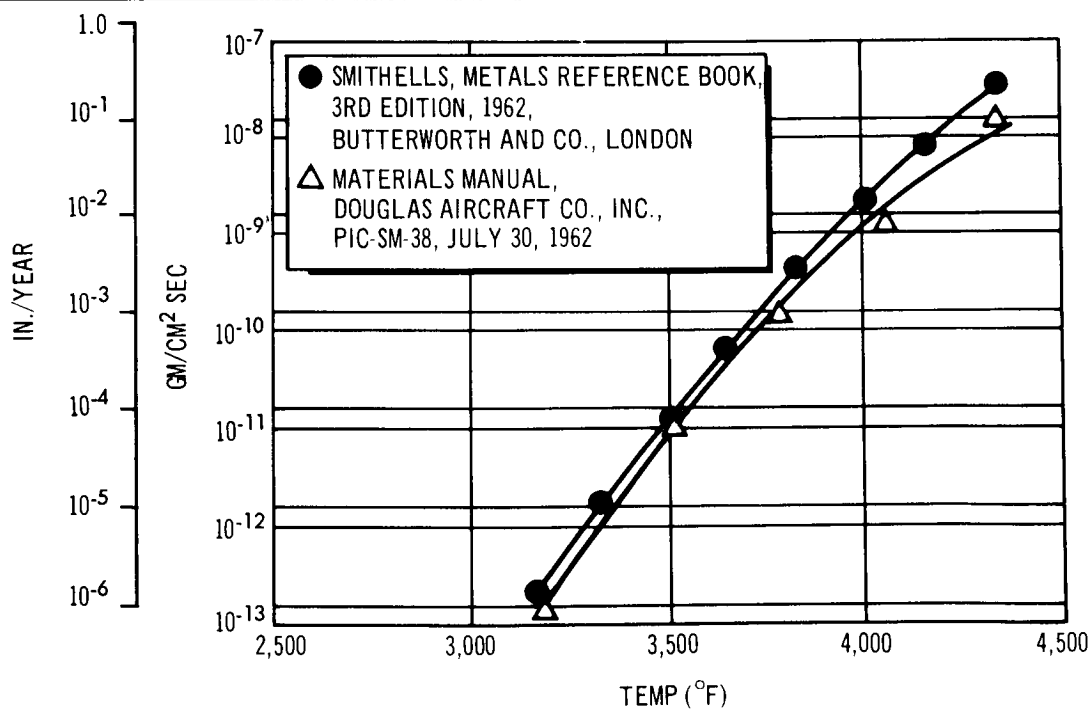


Figure 3-16. Sublimation Rate for Commercially Pure Tungsten

Figure 3-6 shows a typical thrust chamber assembly. Figure 3-17 shows the specific impulse as a function of pulse width with off time between pulses as a parameter. For the MORL application, the spin mode with 4 sec on-off operation represents the most severe manner of operation. A 4-sec off time with a 4-sec pulse width provides essentially steady-state performance, that is, $I_{sp} = 235$ sec.

Reactor Thermal Design

There are two primary aspects to the thermal design of a monopropellant hydrazine thruster. The first concerns obtaining the desired thermal environment within the reactor itself, particularly with regard to heat soak-back from the thrust chamber to the propellant valve. Adequate thermal isolation is necessary to allow close coupling of the propellant valve for minimum hold-up (for efficient short-pulse operation) and, at the same time, to avoid overheating the valve and the flow passages behind the injector face. The design accomplishes the isolation by a capillary tube flow element and a lightweight, perforated, stainless steel heat barrier.

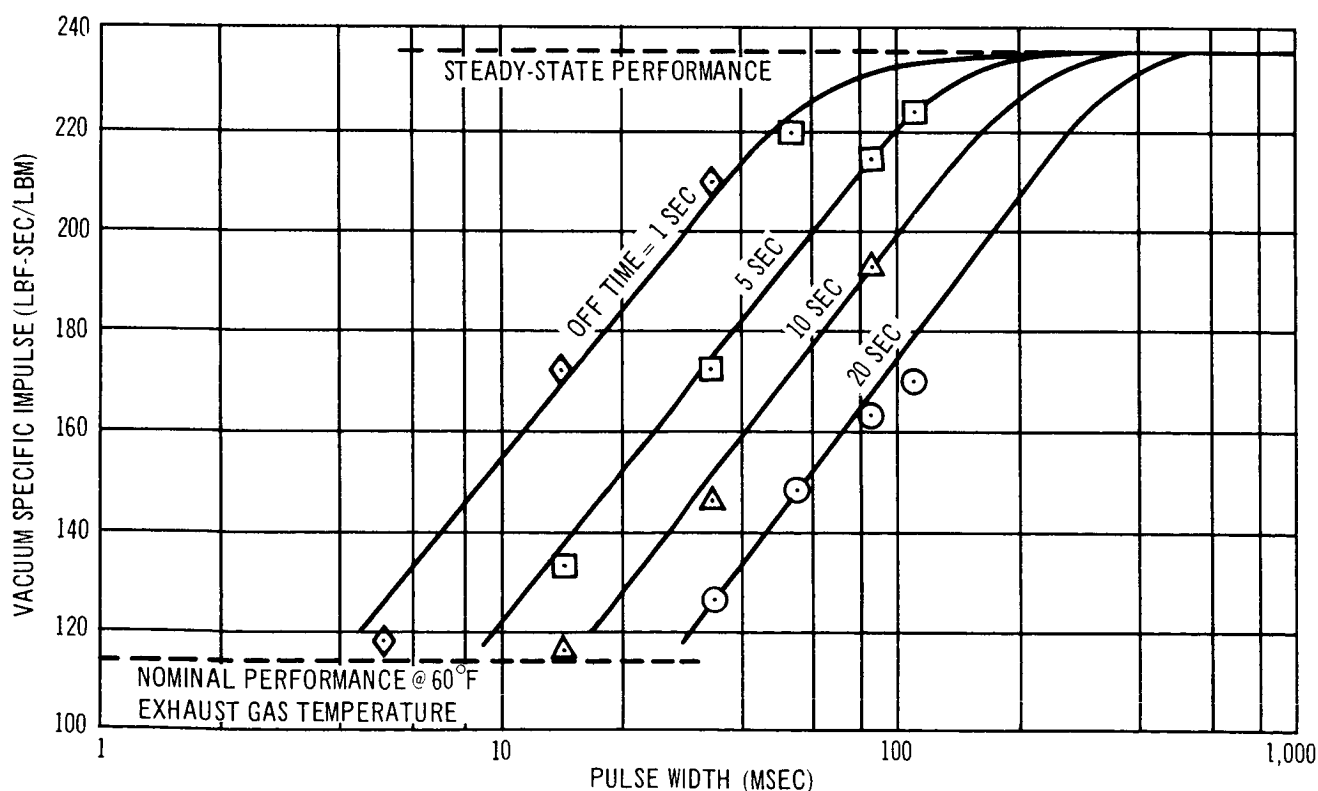


Figure 3-17. Vacuum Hot Pulse Performance for Catalytic Monopropellant Engine

The second factor in the thermal design of the reactor is the space environment encountered in operation. That is, since the freezing point of monopropellant hydrazine is approximately 34°F, the thermal environment of the thruster must be such that the propellant does not freeze at or behind the valve. In the present application, a small amount of electric power may be required to thermally condition the thrusters if they are mounted in exposed positions. This can be simply accomplished by using a few watts of electrical power or, in the case of the isotope power supply, by employing waste heat from the power supply system. In the latter method, use of this heat on a continuous basis will allow maintenance of catalyst bed temperatures of several hundred degrees (F), thereby slightly improving the overall average I_{sp} for the mission by eliminating the small heat loss caused by catalyst bed heating with the start of each cold pulse. A warm catalyst bed also will improve the transient response on a cold pulse. In order to conserve the heat generated during the firing period, an insulating covering is placed over the reactor, and the inside wall of the thrust chamber is coated with Rokide-Z to provide additional thermal insulation. This design approach is particularly desirable in the case of the pulsed operation required for the artificial-g spin mode configuration. Table 3-12 gives a typical thrust chamber assembly performance.

Table 3-12
CATALYTIC MONOPROPELLANT THRUSTOR PERFORMANCE

Propellant	Hydrazine (N ₂ H ₄)
Thrust (lb)	2.0
I_{sp} (sec)	235
Weight (lb)	0.55
Catalyst	Shell 405

System Schematic Diagram

Figure 3-18 is a schematic diagram of the system showing the hydrazine being pressure-fed via high-pressure gaseous nitrogen, which fills the space between the tank wall and a bladder containing the hydrazine. (Heaters are not shown in the diagram.)

3.1.3 Thruster Systems Comparisons

The advance thruster concepts are compared in terms of electric power and propellant weights for a 147-day total impulse. In the comparison, it was necessary to modify the thruster performance figures previously presented in order to take into account the varying thrust and power levels needed for a common basis of comparison (Table 3-13). The table reflects the best performance estimate over the range of performance requirements.

Table 3-13
THRUSTOR PERFORMANCE

	Specific Impulse (sec)	Efficiency (%)
Resistojet		
H_2	840	75
NH_3	400	60
Arc jet		
H_2	1,100	0.26
NH_3	600	0.26
Ion engine		
C_s	4,000	0.565
Isotope thermal		
H_2	650	54
NH_3	330	90
Monopropellant		
N_2H_4	235	

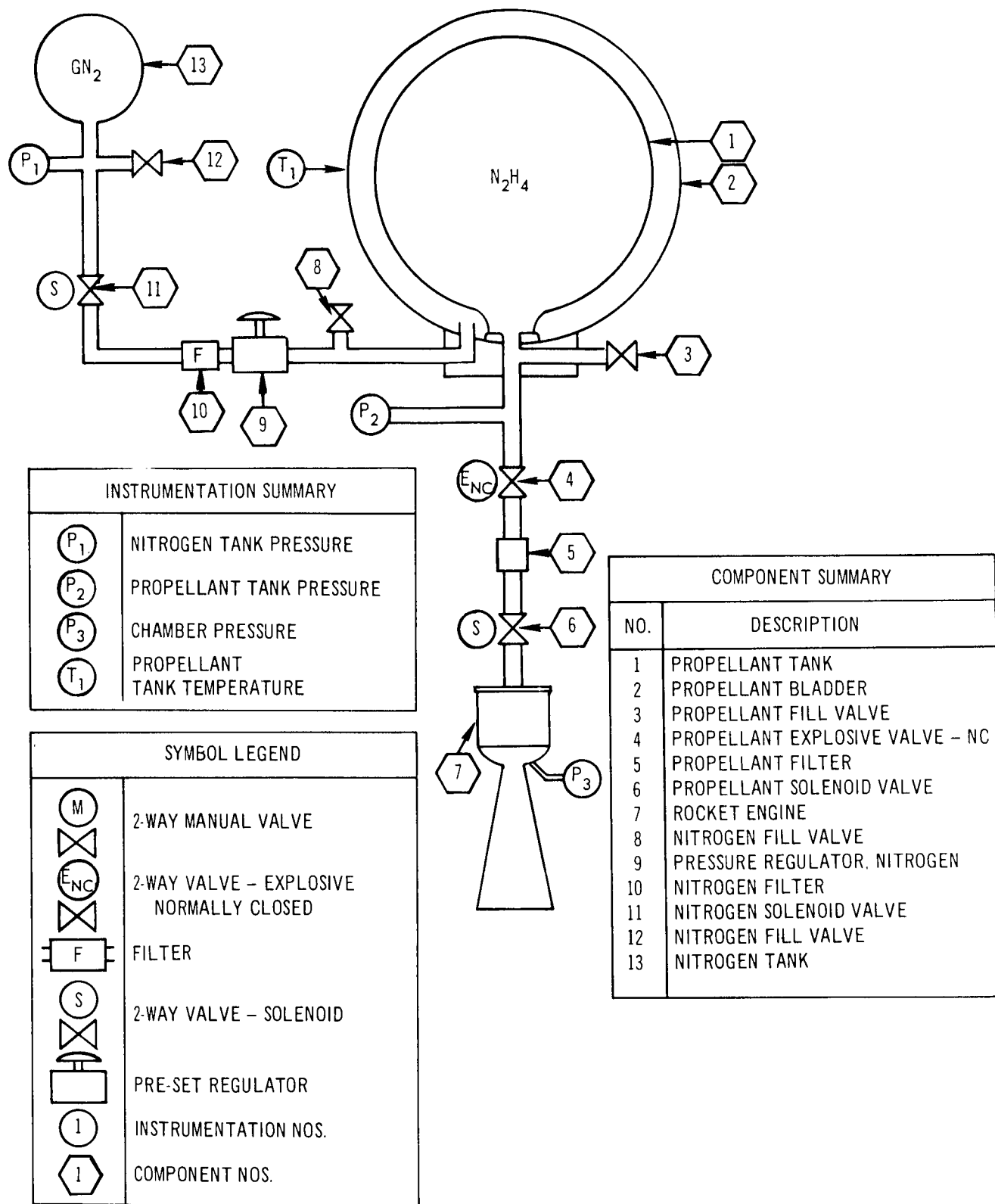


Figure 3-18. Pressure Fed Monopropellant Propulsion Thrustor Schematic

The duty cycle used for this analysis is given in Table 3-14; it is one of the earliest duty cycles submitted. The orbit injection requirements and the spin/despin impulse requirement for the artificial-g configuration, which must be performed every 90 days, are not shown. The fourth column lists the total impulse for 147 days. This will be used for designing the propellant tanks for the four configurations. For the zero-g mode solar panel power source, the impulse requirement is 0.714×10^6 lb-sec; for the Brayton Power Cycle, the impulse requirement is 0.262×10^6 lb-sec. The total drag and precession requirements for the artificial-g configuration, using the solar panel, is 2.34×10^6 lb-sec; with the Brayton Cycle, 1.97×10^6 lb-sec. In the case of the zero-g solar panel configuration, the drag, pitch, and yaw or the drag, pitch, and roll must be done at the same time. The minimum of these two controlling sequences produces a minimum total thrust of 0.0744 lb. For the zero-g configuration with the Brayton Cycle, the minimum thrust was 0.0314 lb; the artificial-g with a solar panel, 0.268 lb; and for the Brayton Cycle, 0.228 lb.

3.1.3.1 Electric Power Requirements

Figure 3-19 is a plot of electric power as a function of thrust for electric thrusters, assuming a simultaneous firing of thrusters. This results in an excessive instantaneous thrust level and power level, but nevertheless provides a conservative estimate of the power requirements should it be made available. It is evident that, to stay within the 3-kW power level imposed by the MORL specifications, the NH_3 arc jet and the Resistojet, using either H_2 or NH_3 , present the best potential. The ion engine, because of its very low thrust-to-power ratio, results in excessive power requirements (-9 kW for the Plutonium Brayton Cycle (PBC) zero-g configuration to 43 kW for the solar panel spin mode configuration). Also, the thrust-to-power ratio for the hydrogen arc jet results in an excessive power requirement for all modes except the PBC zero-g.

Table 3-14
RCS DUTY CYCLE (TYPICAL)

Mode	Power Config- uration	Control Function	Impulse Per Year (lb-sec)	Total Impulse Per 147 Days (lb-sec)	Duration of One Pulse (sec)	Per Orbit	Minimum Thrust (lb)	Total Thrust	
Zero-g	Solar panel	Drag	1.09×10^6	0.714×10^6	5,500	Continuous	0.0345	0.0744	
		Pitch	0.564×10^6		2,700	One	0.0300		
		Yaw	0.046×10^6		900	One	0.0089		
		Roll	0.144×10^6		2,500	One	0.01		
	Brayton Cycle	Drag	0.515×10^6	0.262×10^6	5,500	Continuous	0.016	0.0314	
		Pitch	0.046×10^6		133.3	One	0.015		
		Yaw	0.034×10^6		50	One	0.015		
		Roll	0.046×10^6		133.3	One	0.015		
Artificial-g	Solar panel	Drag	2.87×10^6	2.34×10^6	3.92	350	0.134	0.268	
		Pre- cession	2.87×10^6		1,370	2	0.134		
					3.92	350	0.134		
					1,370	2	0.134		
	Brayton Cycle	Drag	2.41×10^6	1.97×10^6	3.92	350	0.114	0.228	
		Pre- cession	2.41×10^6		1,370	2	0.114		
					3.92	350	0.114		
					1,370	2	0.114		

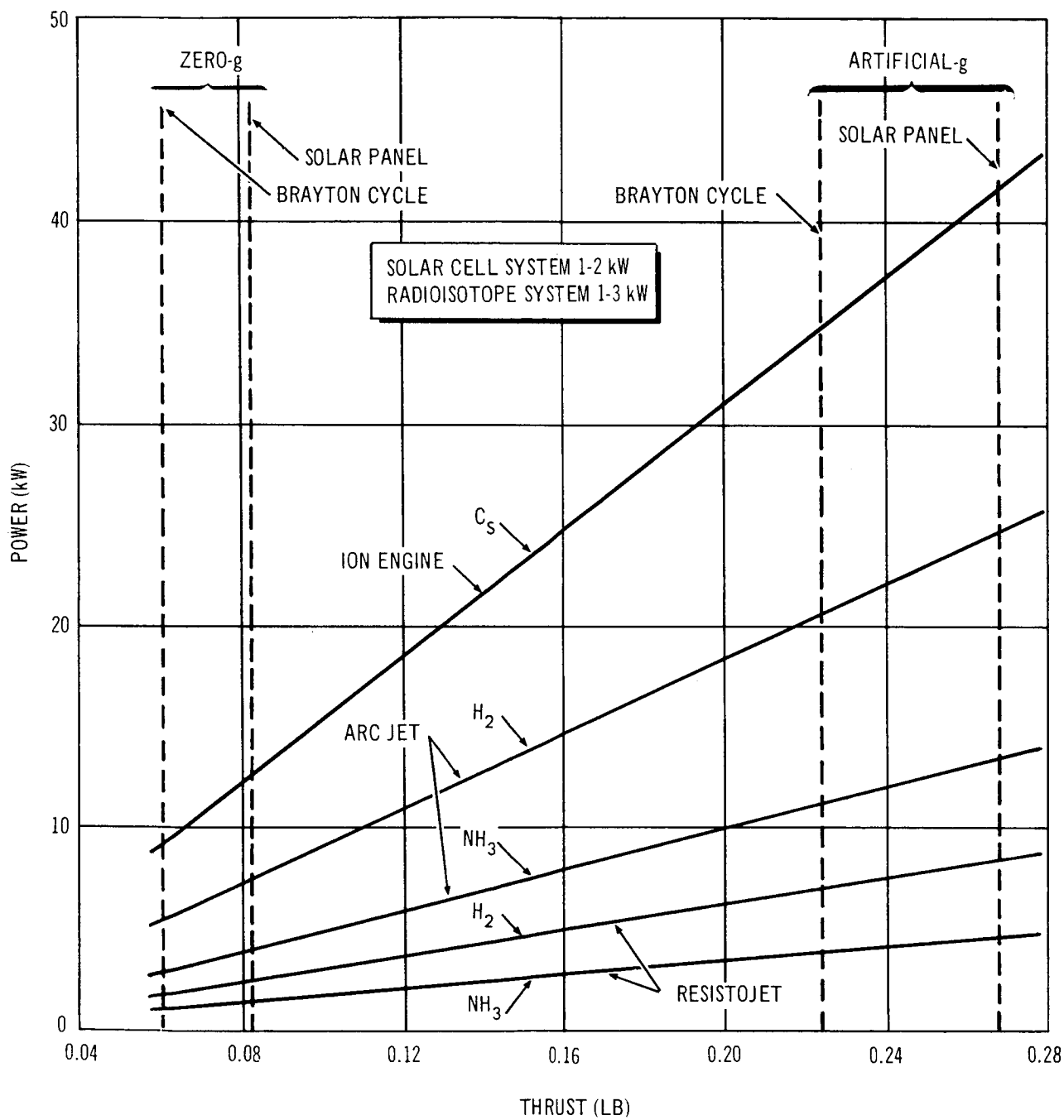


Figure 3-19. Power as a Function of Thrust

3.1.3.2 System Weight

The overall system weight is the sum of the individual weights of the electric power system propellant, tankage thruster, and feed systems. Figure 3-20 presents the results for the PBC configuration in the zero-g and spin modes. The systems considered were the iron engine, Resistojet, arc jet, catalytic monopropellant, and the radioisotope thruster. The Resistojet and radioisotope systems are the lightest; a discrepancy in system weight between the two is caused by the weight of the electric power system required by the former. A 5-year mission comparison, however, would bring the two system weights closer together, since the total propellant consumption by the Resistojet would be lowered by the ratio of the specific impulse, while the penalty for electric power weight stays the same as for the 147-day period.

Figure 3-21 shows the comparisons for the solar panel configuration. The Resistojet and radioisotope thruster systems are lightest; the previous statements regarding the discrepancy in system weights are applicable.

3.1.3.3 Systems Comparison

The results are presented in Table 3-15. In all cases, the artificial-g or spin mode results in a heavier system than the zero-g mode, because of the higher total impulse and thrust requirements. In the spin mode, the electric power requirements for the Resistojet were in excess of the 2 to 3 kW allowable. The analysis was a very rough, nonoptimized calculation which did not use impulse and thrust reduction techniques and scheduling. The purpose was to show system trends in order to aid in selection of one or more systems for further study.

3.1.3.4 Thruster Systems Selection

The selection criteria are discussed in detail in the following subsections.

Selection Criteria

The criteria for final selection were as follows:

1. Minimum weight.

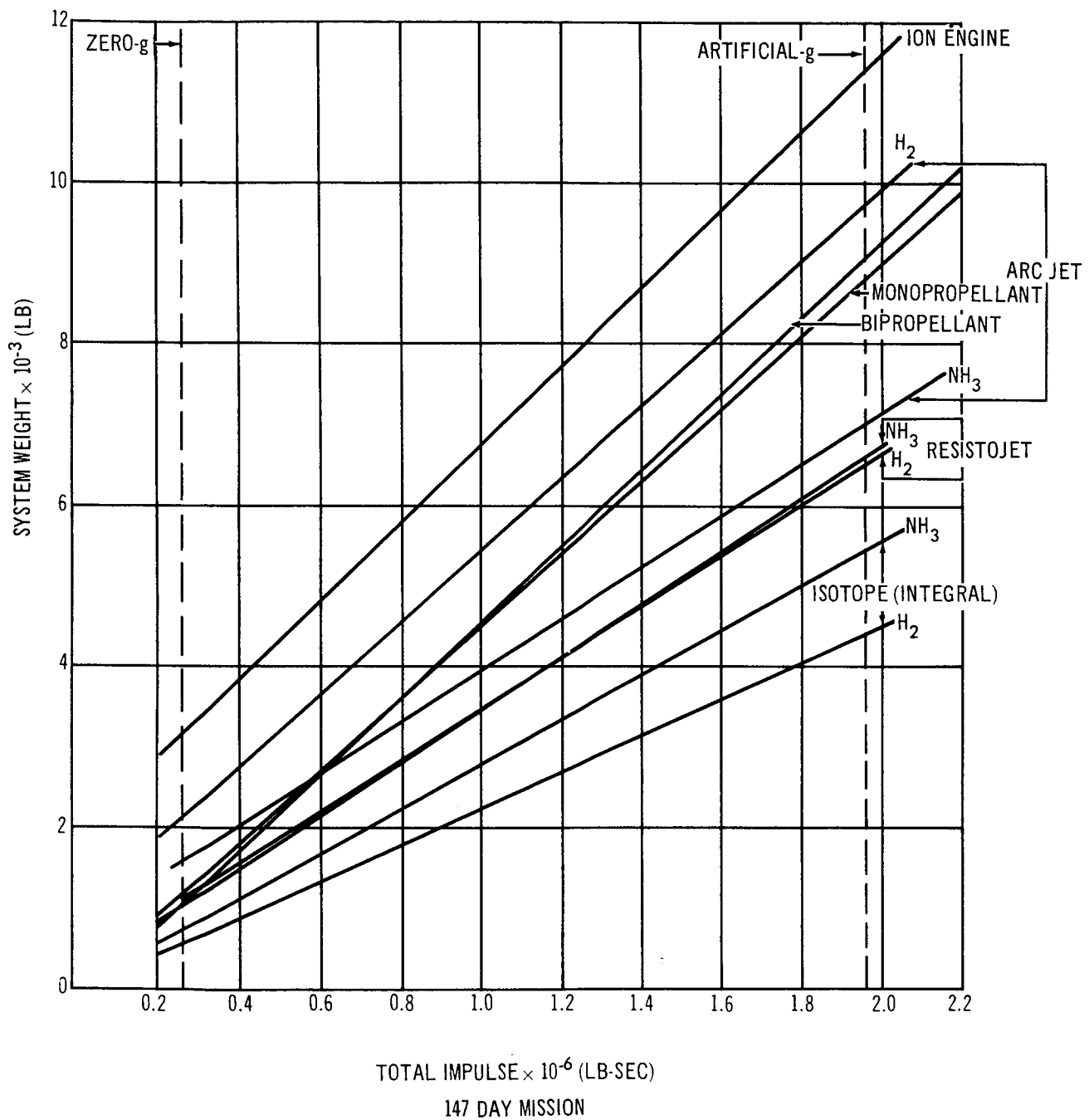


Figure 3-20. System Weight as a Function of Impulse – Brayton Isotope Configuration

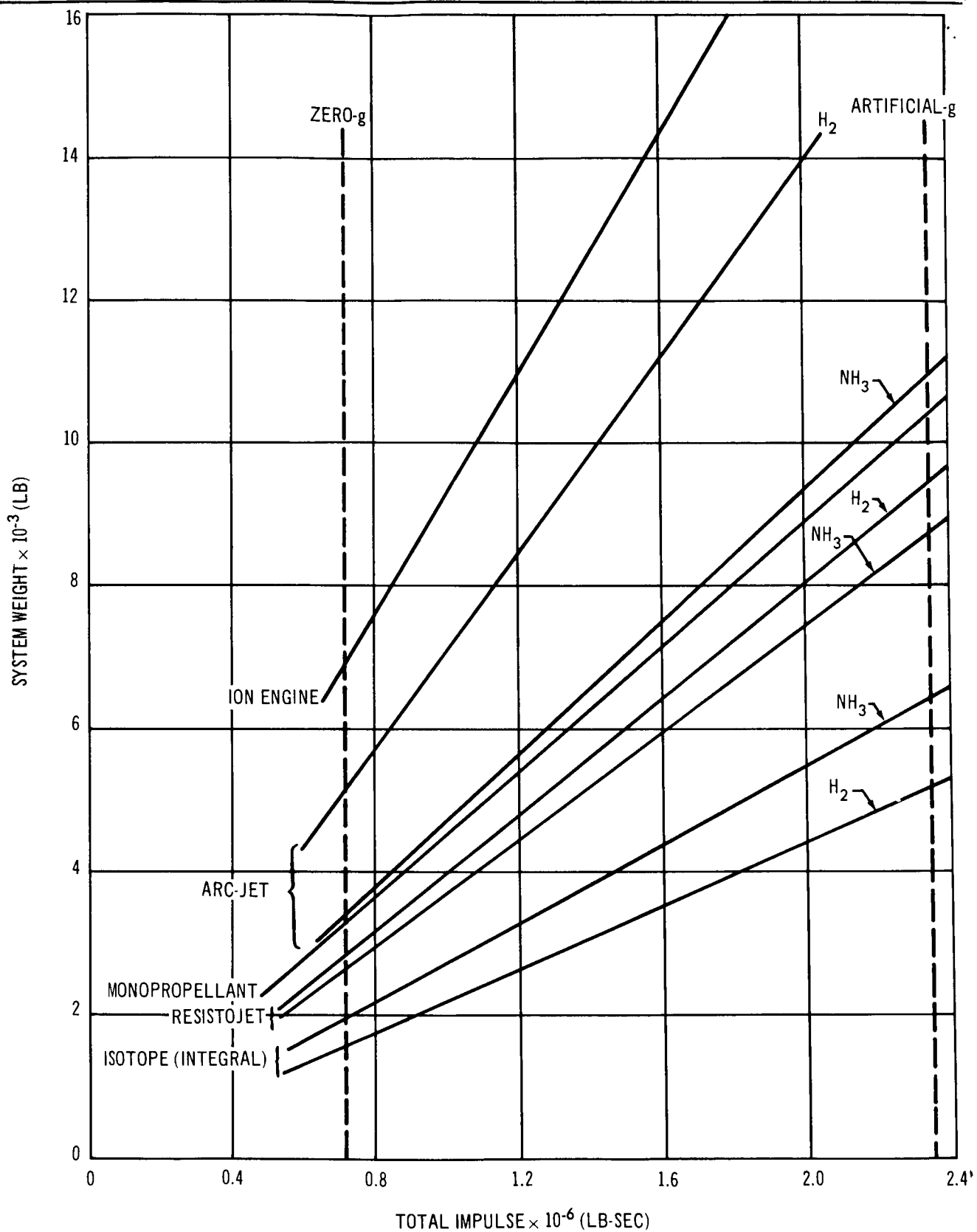


Figure 3-21. System Weight as a Function of Total Impulse – Solar Panel Configuration

Table 3-15

SYSTEM WEIGHT TABULATIONS
(147 Days)

	Zero-g				Artificial-g			
	Solar Panel		Brayton Cycle		Solar Panel		Brayton Cycle	
	Power (kW)	Weight (lb)	Power (kW)	Weight (lb)	Power (kW)	Weight (lb)	Power (kW)	Weight (lb)
Resistojet								
H ₂	1.8	2,740	0.75	866	6.52	8,965	5.55	6,489
NH ₃	1.1	2,548	0.46	875	4.98	9,070	3.40	6,556
Arc Jet								
H ₂	6.8	4,776	2.9	1,378	24.8	16,915	21.0	10,114
NH ₃	3.7	3,235	1.6	992	13.4	11,265	11.4	7,283
Ion Engine								
C _s	11.4	5,989	4.8	1,554	41.4	21,581	35.2	11,429
Isotope Thermal								
H ₂		2,550		953		8,470		7,160
NH ₃		2,656		1,707		8,823		7,432
Monopropellant								
N ₂ H ₄		3,344		1,227		10,945		9,240

2. Development risk.
3. Growth potential.
4. Life.
5. Reliability.
6. Integration potential.
7. Simplicity.
8. Safety.

Minimum Weight

A minimum weight system is important in order that the liftoff weight is within the booster capabilities and that the propellant resupply weight does not exceed the Apollo logistic vehicle carrying capacity.

Development Risk

The development risk is a measure of the ability to design, develop, and qualify a system in time to meet the MORL schedule.

Growth Potential

The development of an advance engine system must go beyond the immediate MORL requirements toward missions of greater scope and breadth. The development of a low specific impulse system may be worthwhile if some significant gain is achievable (for example, the utilization of biowaste for propellant).

Life

The life of an engine to meet the MORL specifications is an obvious factor. Frequent replacement of parts would place burden on the crew and complicate the logistics.

Reliability

MORL mission overall reliability demands a high subsystem reliability. The engine system selected must possess a demonstrable reliability which can meet these requirements.

Integration Potential

The engine system must be compatible with the MORL vehicle and must be adaptable for both the zero-g and spin modes. Interference with experiments must be kept to a minimum. It must also be compatible with other sub-systems and with all operational activities.

Simplicity

The engine system design must be simple enough to ensure that replacement, repair, adjustment, and control will require a minimum of crew time.

Safety

The engine system must meet the MORL safety specifications. This is a consideration particularly applicable to the radioisotope thruster, where fuel block safety considerations and radiation fields are paramount.

3.1.3.5 System Ratings

The characteristics and performance of the thruster systems were carefully reviewed and estimates were made of their general applicability in meeting the MORL overall criteria.

The Resistojet has the benefit of several years of development and test and appears to meet most of the criteria.

The radioisotope thruster, on the other hand, is a fairly new concept and, although tested, still requires a great deal of development. It needs no electric power but does depend on the availability of radioisotope. Its safety requirements regarding handling launch, abort, and disposal are comparable to those associated with the plutonium Brayton Power Cycle which has since become the baseline system.

Douglas, in concurrence with the NASA, has selected the Resistojet and radioisotope thruster concepts for further, more detailed studies.

3.2 PRELIMINARY DESIGN CONSIDERATIONS

The system concept evaluation described in Section 3.2 provided a basis for the selection of two propulsion concepts for further study: (1) the Resistojet and (2) the radioisotope thruster. The information generated in Section 3.2 was a tentative analysis based on preliminary performance data. Section 3.2 describes in more detail the analysis performed by Douglas and the engine subcontractors, the Marquardt Corporation for Resistojet and TRW Systems for radioisotope thruster, which resulted in a preliminary design definition of the advanced thrusters. Because the performance requirements were not yet completely decided, design information, in the form of parametric curves and tables, was generated to permit system sizing for a variety of thrust levels and propellant selections.

3.2.1 Impulse Requirements

Table 3-16 represents the vehicle's total impulse needs. The attitude-control requirement is really defined in terms of an impulse moment; the corresponding linear impulse will be a function of torque lever arm. Table 3-16 is expressed in terms of a linear impulse based on the representative moment arms. The station-keeping or propulsion requirement is a translational force and is represented by a linear impulse.

Table 3-16 presents the linear impulse needed per orbit for both the zero-g and spin modes and the solar power and Brayton Power Cycle configurations. In all cases, the spin mode has higher impulse requirement than that for the Isotope Brayton Cycle, primarily because of the drag that is created by the solar panels. It is understood (1) that the control functions of pitch, yaw, and roll are used to desaturate the control moment gyros using relatively long pulse duration and (2) that the CMG's were sized to control the vehicle for the cyclic disturbances only. The total impulse required of the reaction control thrusters to satisfy the vehicle's requirements may be greater or less than that given in Table 3-16, depending on factors of (1) thrust effectiveness, (2) actual lever arm used, and (3) extent of multiple accomplishment of functions by a single thruster. The fundamental principle of each of the three items is given below.

Table 3-16
REACTION-CONTROL SYSTEM REQUIREMENTS
(PRELIMINARY DESIGN PHASE)

Mode	Configuration	Control Function	Total Impulse per Orbit (lb/sec)	Couple Arm (ft)
Zero-g (Local horizontal)	Solar Power	Drag	150	20
		Pitch	100	20
		Yaw	113	20
		Roll	8	20
	Isotope Brayton Cycle Power	Drag	90	20
		Pitch	82	20
		Yaw	8	20
		Roll	8	20
Artificial-g (Spin axis solar)	Solar Power	Drag	500	
		Precession	500	280
	Isotope Brayton Cycle Power	Drag	420	
		Precession	420	280

Thrust effectiveness, ϵ , may be defined as the ratio

$$\epsilon = \frac{\text{impulse moment imparted to the vehicle}}{\text{impulse moment developed by thrusters}}$$

In high-thrust systems, this factor may be made generally equal to one because of the short firing times. In the low-thrust systems, the thrust direction generally does not coincide with the momentum vector to be removed over the extended firing time. A thrust effectiveness less than one is basically caused by the fact that the thrust vector, fixed to the laboratory reference system, may not coincide over the whole firing time with the momentum vector to be removed. For example, this may occur because momentum is stored in the inertial frame of reference (gyros), and the

desaturating thrust vector may be constrained to rotate because of the orbital or laboratory motion, in the case of the rotating laboratory.

Another example is the case of drag-makeup thrust. This is required along the orbital flight path but may be denied this direction because of a solar-fixed orientation. The manner in which thrust effectiveness enters the problem will be defined in each case as it is covered. The firing time is generally centered about the optimum point of thrust application. The net thrust effectiveness is the time-integrated average of the component in the optimum direction--the cosine term. Since we are dealing with uniform circular orbital or laboratory rotational motion (either Equation 3-1 or 3-2), it may also be treated as a sector angle integrated average.

$$\text{Orbital motion } \theta = \left(\frac{\tau_B}{2} \right) \cdot \frac{360}{5,500} \quad (3-1)$$

$$\text{Laboratory rotation } \theta = \left(\frac{\tau_B}{2} \right) (0.4) \frac{(360)}{2\pi} \quad (3-2)$$

where τ_B is thruster firing time and θ is defined by Figure 3-22. The resultant expression for effectiveness, ϵ , then, is shown in Equation 3-3.

$$\epsilon = \frac{1}{\theta} \int_0^\theta \cos \theta \, d\theta \quad (3-3)$$

Thrust effectiveness is shown as a function of arc firing angle (Figure 3-22). As an example, during orbit keeping, where thrust vectors are constrained to solar orientation and fired over an arc $\pm 45^\circ$ from the direction of orbital velocity factor, the effective impulse felt by the vehicle is 90% of the total impulse developed by the thrusters. The orbital velocity factor may also be applicable to the precession torque calculations, where the applied moment is rotating with the laboratory.

The total impulse required of the thruster may be reduced by the vehicle through two techniques. First, the moment arm may be increased. For example, a single thruster on the booster counterweight in the artificial-g mode may be used. This would accomplish the total precession torque because of the substantially larger momentum arm from the center of

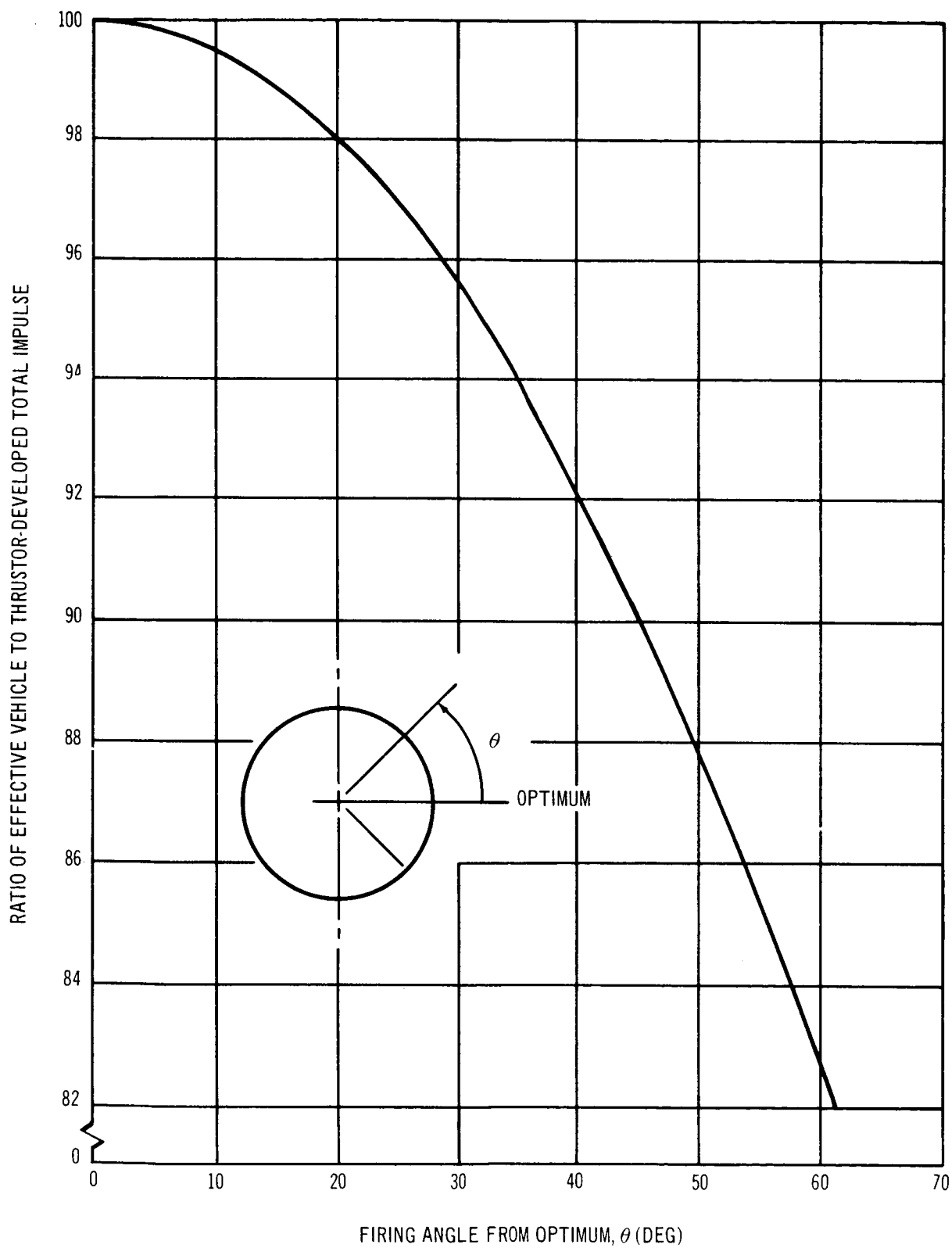


Figure 3-22. Thrust Effectiveness ϵ

rotation (CG) as contrasted to a thruster on the laboratory or a couple with one thruster located on each. Another example is the potential use of the longer moment arm in the longitudinal direction as contrasted to one corresponding to the vehicle diameter. Second, the torque may be developed not as a pure couple; hence, under certain circumstances, it may introduce favorable translational forces. This simultaneously accomplishes orbit keeping while doing the other attitude-control functions of pitch and yaw and, in the case of the rotating laboratory, precession.

It is noted again that requirements of attitude control, impulse, and so forth, are predicated upon reaction control jets operating in conjunction with control moment gyros, as discussed previously. The consideration of limit cycle operation for the reaction control system, as a secondary mode in the event of CMG failure, must be considered in a separate study. The detailed applications of these principles are described in each of the cases in Section 5.1.

The normal cruising requirements for use in the vehicle integration phase is a combination of the inertial frame of reference and the belly-down. This zero-g profile was considered to be 4 hours in the inertial frame, a short 30-min. transition period to and from the belly-down configuration, 19-1/2 hours belly-down per day. Each of the above phases is discussed in Section 5.

3.2.2 Thruster Logic and Impulse Reduction

Closer examination of the total impulse requirements for vehicle orbit keeping and stabilization and control indicated that it was possible to reduce the total impulse requirements (Table 3-16) by performing drag and pitch or drag and yaw simultaneously. This involved the elimination of oppositely directed thrusts needed to produce pure couples and thrusting off center along the velocity vector. Thus, only one drag motor, suitably located and sized for a sufficient thrust level, could provide the thrust along the velocity vector needed for drag, and simultaneously generate the torque needed to desaturate the pitch-control moment gyro without physically pitching the vehicle. The same reasoning holds true for the yaw function. A similar

technique was also used in the spin mode analysis; in addition to drag make-up, precession control was required. This was accomplished by pitching the vehicle about its CG to provide a torque perpendicular to the spin vector. By proper sequencing of the pitch motor firing times in the spin cycle and in the orbit sector, it was possible to do drag makeup at the same time. Therefore, both the zero-g and spin mode impulse requirements were greatly reduced. The net result was (1) a decrease in propellant consumed, (2) a lowering of the thrust level, and (3) a decrease in the electric power or radioisotope thermal power needed.

Table 3-17 shows the orbit impulse reduction which can be achieved by sharing drag makeup with pitch and yaw. However, it is not always possible to eliminate the operation of a pure couple in pitch and yaw during an orbit.

Table 3-17
REDUCED SPIN CYCLE REQUIREMENTS

Configuration	Initial Requirements (lb-sec/orbit)	Reduced Requirements (lb-sec/orbit)
Zero-g mode		
Solar power	371	222
Plutonium Brayton Cycle	188	98
Spin mode		
Solar power	1,000	801
Plutonium Brayton Cycle	840	672

Figure 3-23 shows a typical thrust allocation schedule for a Resistojet having approximately 20-millipound (mlb) thrust/engine. Figure 3-24 shows a schematic diagram of engine thrust direction. In Figure 3-23 it is seen that (neglecting the engines in parentheses) the firing of Engines P_1 and P_3 produces a pure couple for pitch makeup. The firing of Engines P_1 and D_1 simultaneously provides a thrust of 40 mlb for drag and develops torque used simultaneously for pitch. In a similar manner, the firing of D_2 and Y_1 simultaneously produces 40 mlb of thrust for drag and yaw. The last

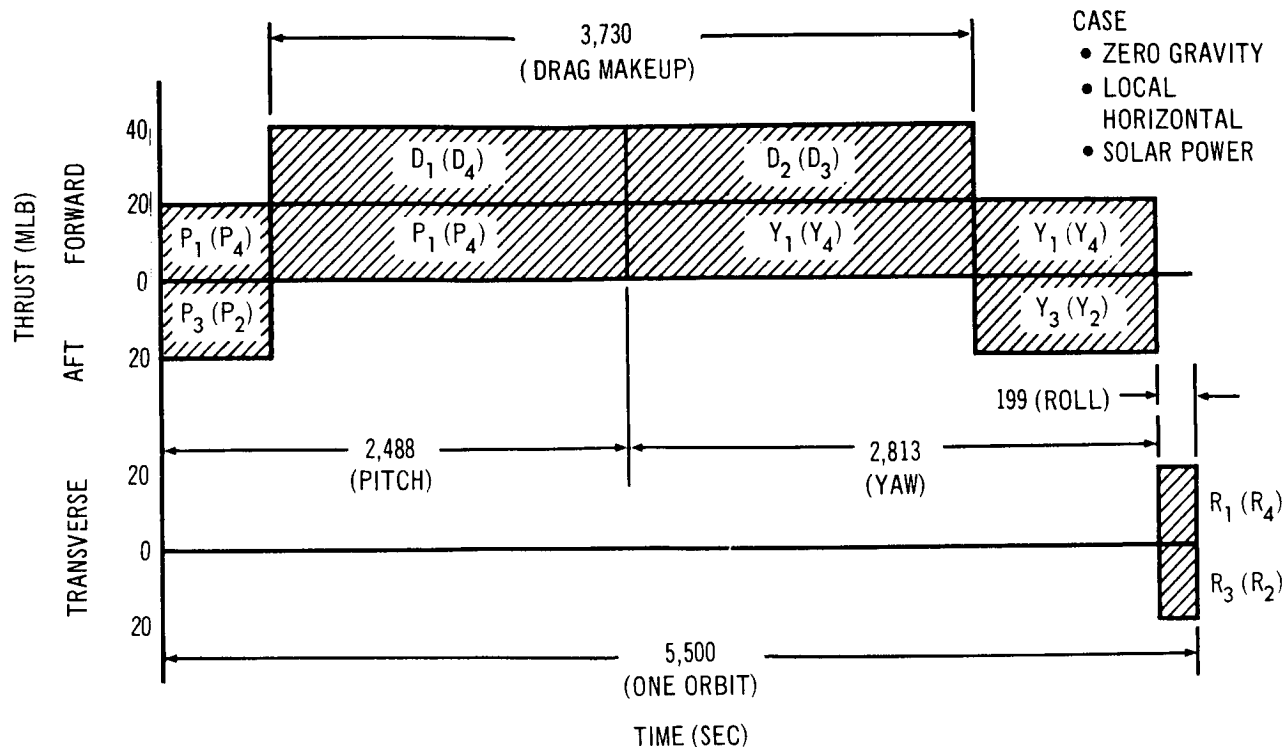


Figure 3-23. Thrust Allocation

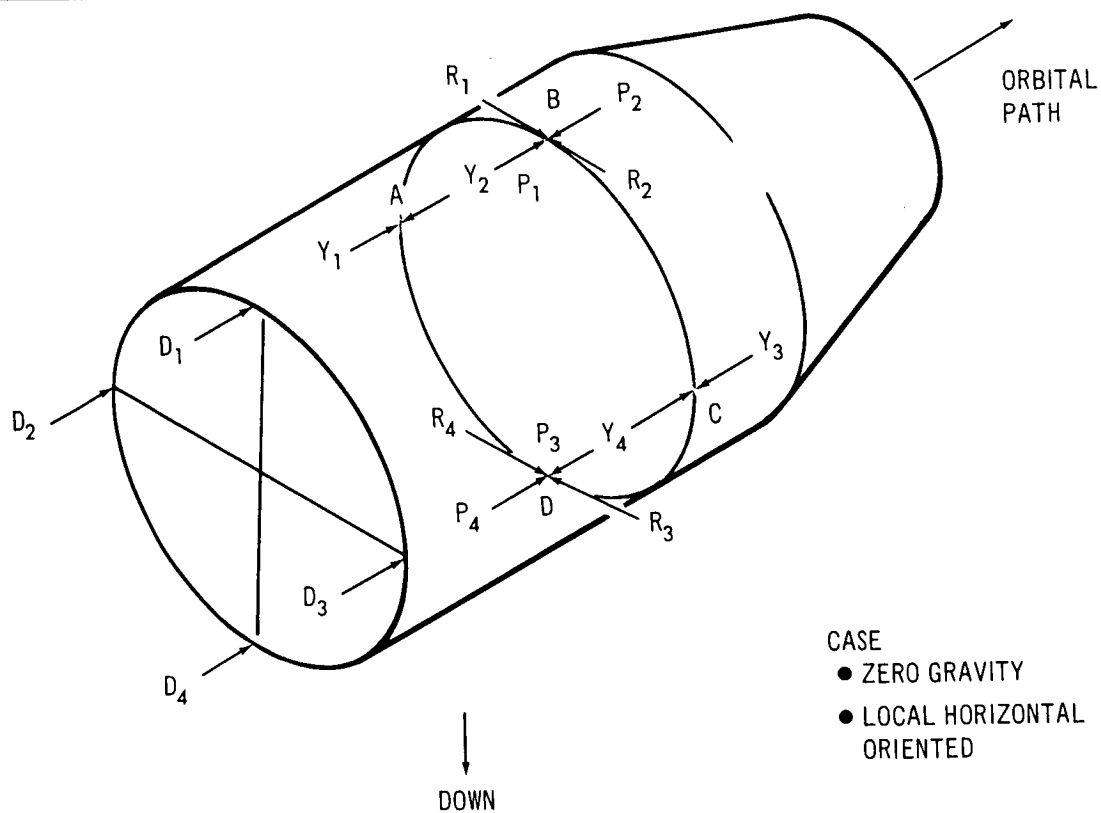


Figure 3-24. Resistojet Thrustor Locations

199 sec of orbit is reserved for a pure roll couple; no drag makeup is added.

Similar types of thruster schedules had to be worked out for each of the orbit modes and configurations. The thrusters were then designed to meet the thrust and energy levels needed to produce the impulse needed per orbit.

3.2.3 Propellant Characteristics

The choice of a propellant is generally restricted by the thruster requirements. In general, the thrusters are developed for maximum performance, the trend being towards a high specific impulse in order to reduce propellant consumption for a given total mission impulse. This is illustrated from the basic thrust equation

$$F = \dot{w} I_{sp} \quad (3-4)$$

one obtains the propellant weight

$$w_p = \frac{Ft}{I_{sp}} \quad (3-5)$$

where Ft (lb-sec) is the mission impulse requirement.

Figure 3-25 plots w_p opposed to I_{sp} for 90- and 147-day MORL mission impulse requirements. The solar power 147-day cycle requires 700 lb of propellant at an I_{sp} of 1,000 sec (developed, for example, by a hydrogen Resistojet), whereas a 300-sec chemical engine would require 2,400 lb of propellant; a savings in propellant weight of 1,400 lb is realized by using a high I_{sp} propellant.

The following propellants were selected for study with the advance thruster systems: (1) hydrogen, (2) ammonia, (3) hydrazine, (4) carbon dioxide, and (5) water. Hydrogen was selected because of its high specific impulse when used with the advance thrusters. Ammonia, on the other hand, has a lower specific impulse, but is more easily contained than the cryogenic hydrogen. Hydrazine was considered because of its compatibility with the high-thrust engine system. Carbon dioxide and water and gaseous hydrogen were the biowaste products of the EC/LS cycle. The potential performance of these

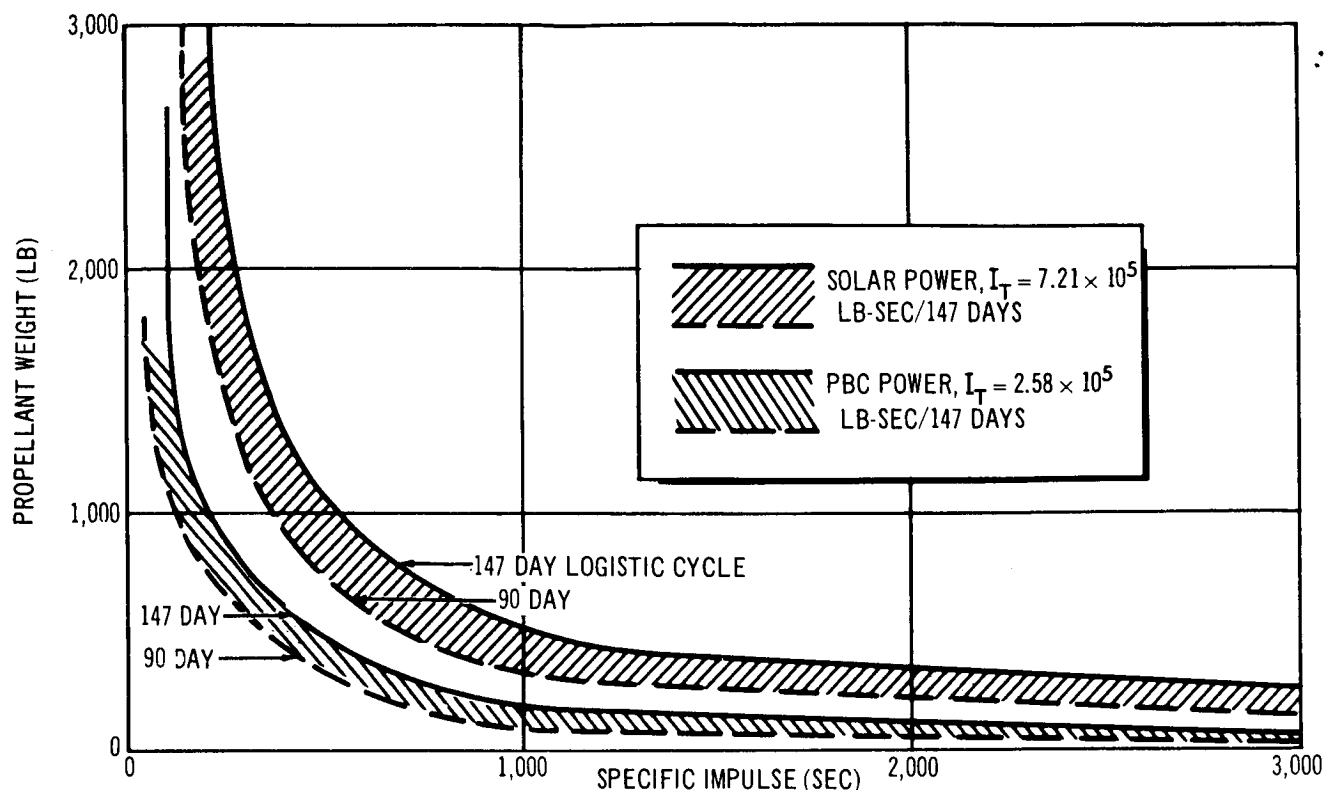


Figure 3-25. Propellant Weight as a Function of Mission Impulse

propellants are presented in Figure 3-26, which plots I_{sp} as opposed to temperature. Other propellants (not shown) are cesium and mercury, which were used in the ion engine.

3.2.3.1 Hydrogen

Hydrogen, although characterized by a high specific impulse and a low propellant consumption, is nevertheless difficult to store as a liquid. Studies have shown that, for the mission weights in question, it must be kept at its cryogenic temperature (37° to 55°R) and at a pressure of 1 to 10 atm in order to keep the tank weights at a minimum. This, in turn, requires insulation and careful tank support design in order to minimize heat leaks into the tank from the surrounding structure. The optimum design would reduce the heat leaks to a rate sufficient to boil off enough propellant to permit withdrawal of feed hydrogen at a constant pressure. Figure 3-27 plots the mass of hydrogen as a function of the mass ratio of hydrogen-to-tank for

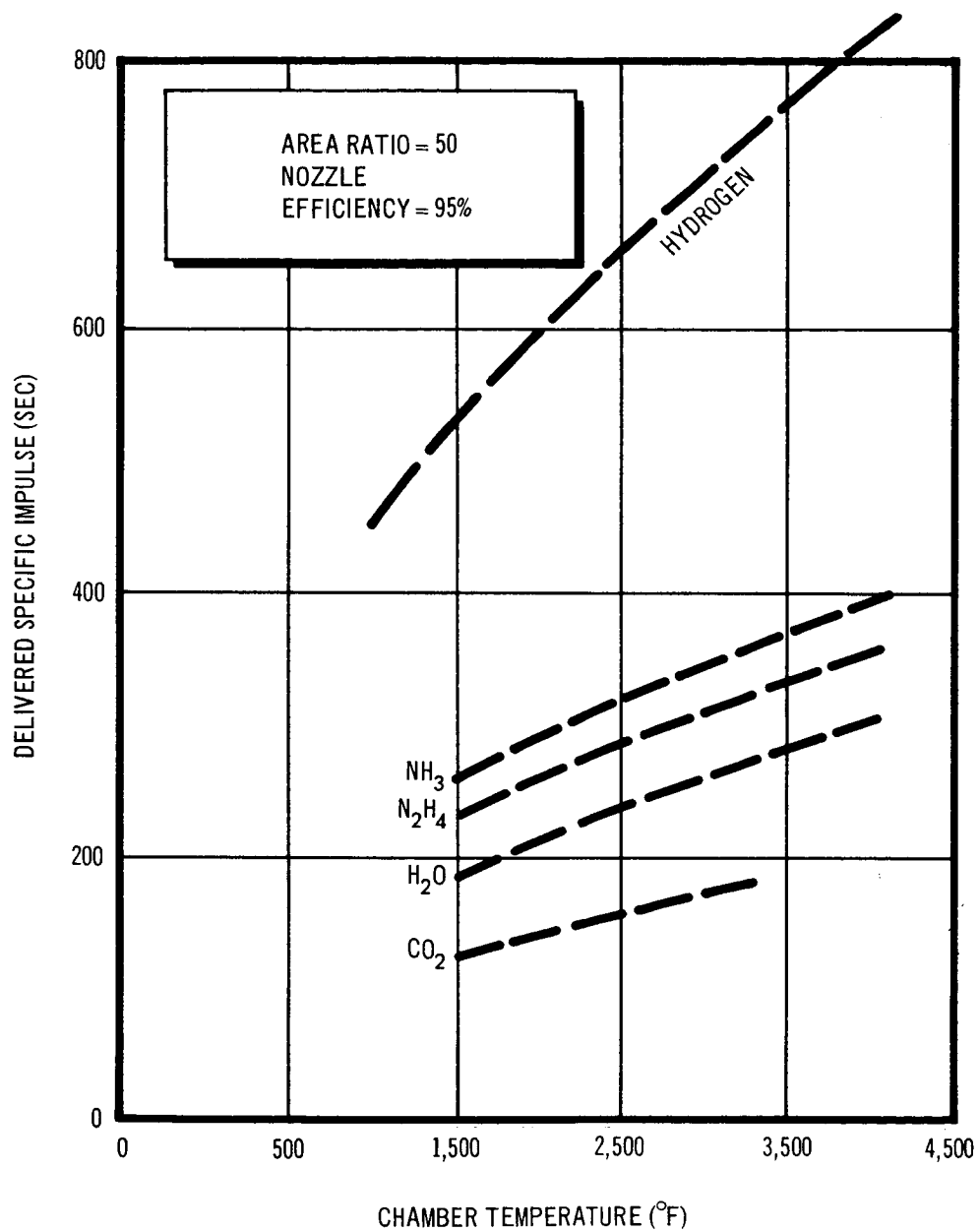


Figure 3-26. Specific Impulse as a Function of Temperature for Several Propellants

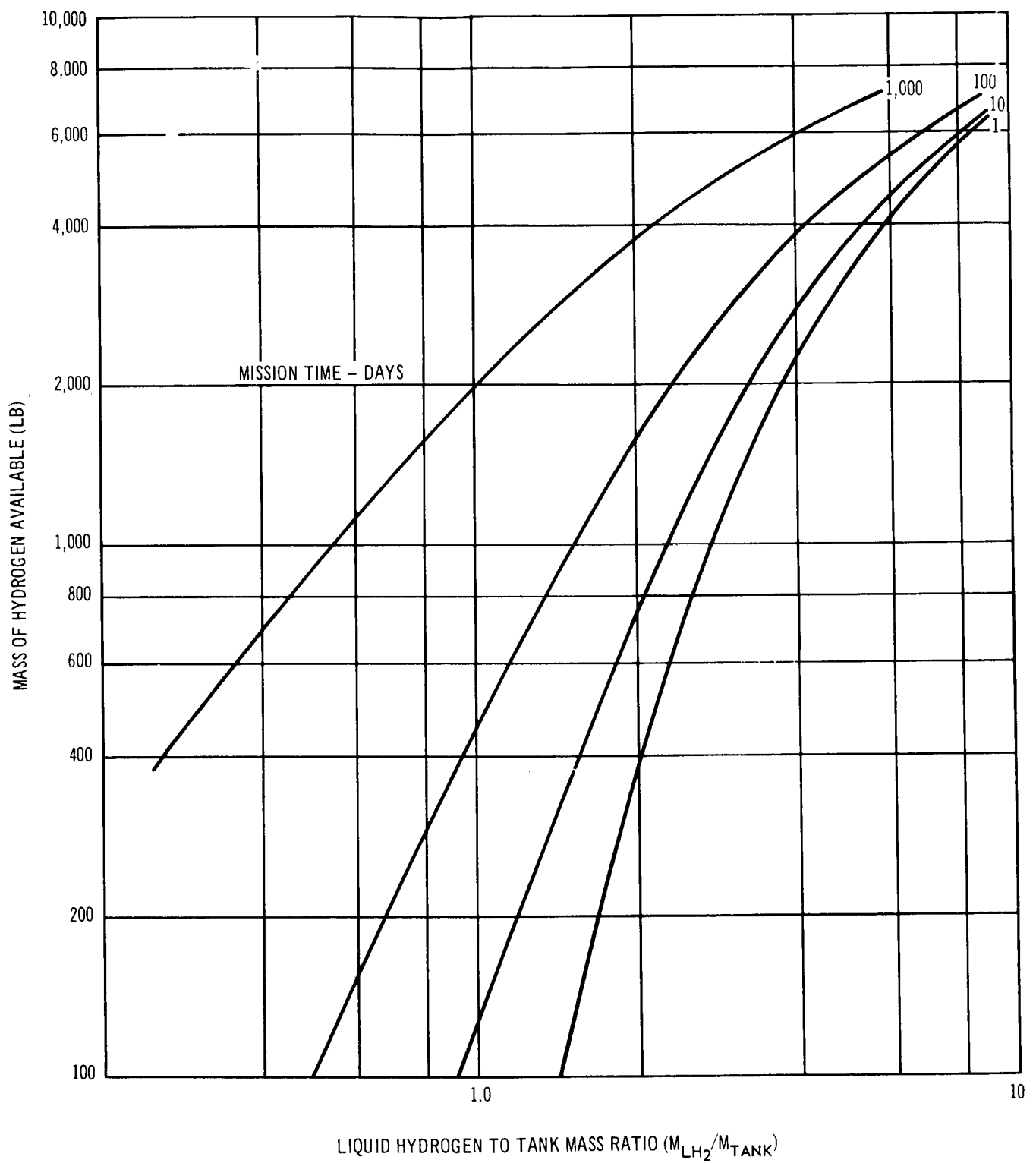


Figure 3-27. Estimated Liquid Hydrogen Storage Tank Weight for Low Thrust Missions

mission stay times of 1, 10, 100 and 1,000 days. As can be seen from Figure 3-27, 1,000 lb of hydrogen stored in space for 100 days shows a mass ratio of 1.55 and, therefore, would require a tank weighing 656 lb. These values were believed to be extremely conservative, and subsequent hydrogen tankage design for the MORL application showed the tank weights to be significantly less. Thus, 1,000 lb of cryogenic hydrogen are stored at 2 atm in a 260-lb tank using 100 sheets of high-performance insulation (Figure 3-28). The figure shows tank weight as a function of propellant weight for an insulated tank. Further discussion of the cryogenic tankage problem may be found in Section 5.4.

3.2.3.2 Ammonia

Ammonia in space storage presents no particular problem. Figure 3-29 shows the tank weight plotted as a function of propellant weight for varying tank pressures. One thousand pounds of propellant at a bulk temperature of 60 °F and a tank pressure of 200 psia would weigh only 28 lb.

3.2.3.3 Hydrazine

Hydrazine, stored as a liquid, has a freezing point of 35 °F and a normal boiling point of 236 °F. This temperature range is compatible with the MORL environment; the tank should not require excessive thermal shielding. However, freezing problems may arise during resupply. Also, propellant retained in the lines external to the vehicle during engine shutdown might freeze. Use of an additive, Aerozine 50, which has a freezing point of 18 °F, or line heating will alleviate the problem.

The hydrazine propellant can be pressure-fed with a high-pressure, nitrogen gas feed system. Tankage and feed system weight is similar to that of ammonia, that is, in the range of 10% to 15% of the propellant weight.

Table 3-18 lists some of the pertinent physical and thermodynamic properties of the propellants investigated. The water and CO₂ are recovered from the EC/LS system.

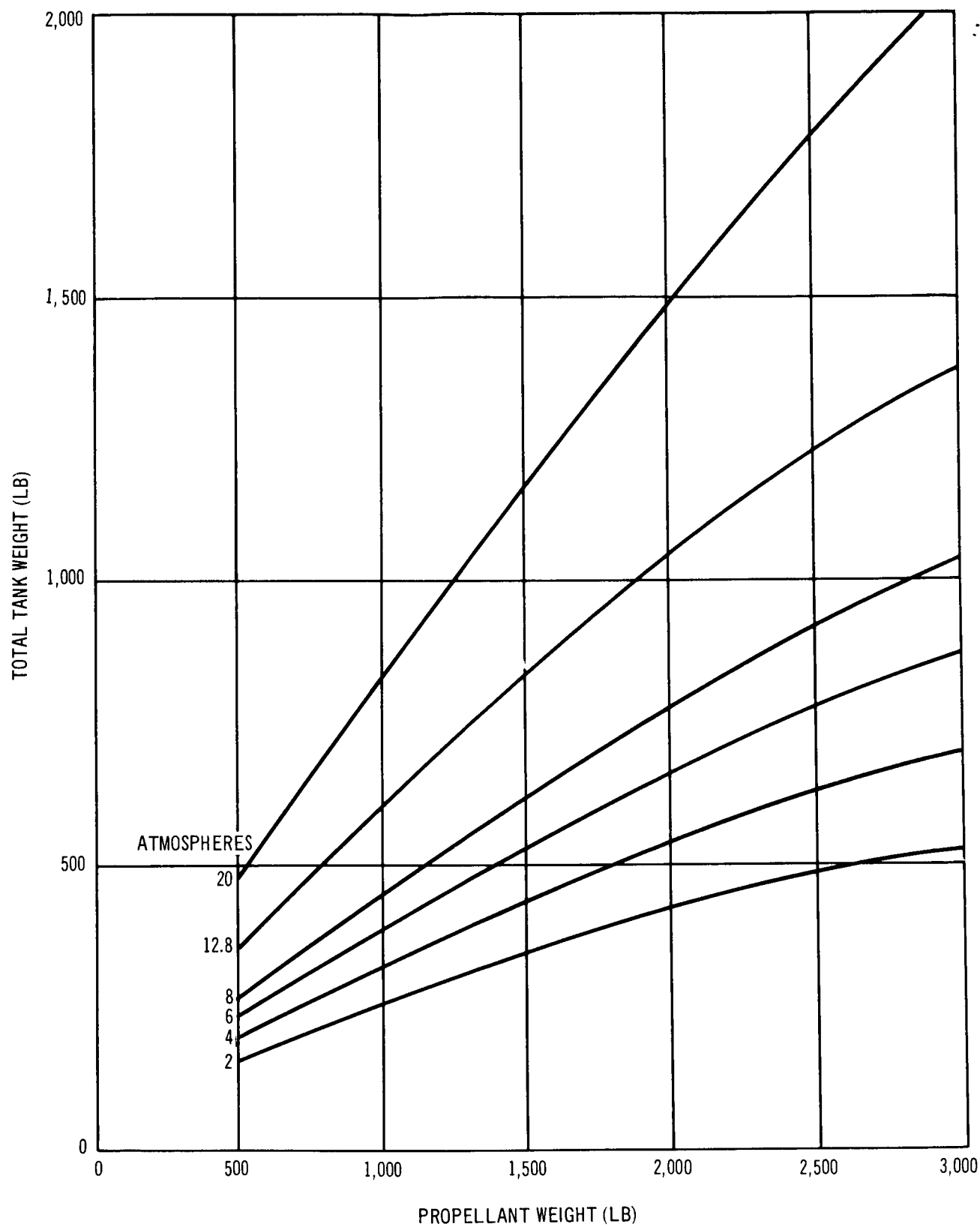


Figure 3-28. Total Hydrogen Tank Weight as a Function of Propellant Weight Using 100 Layers of HPI

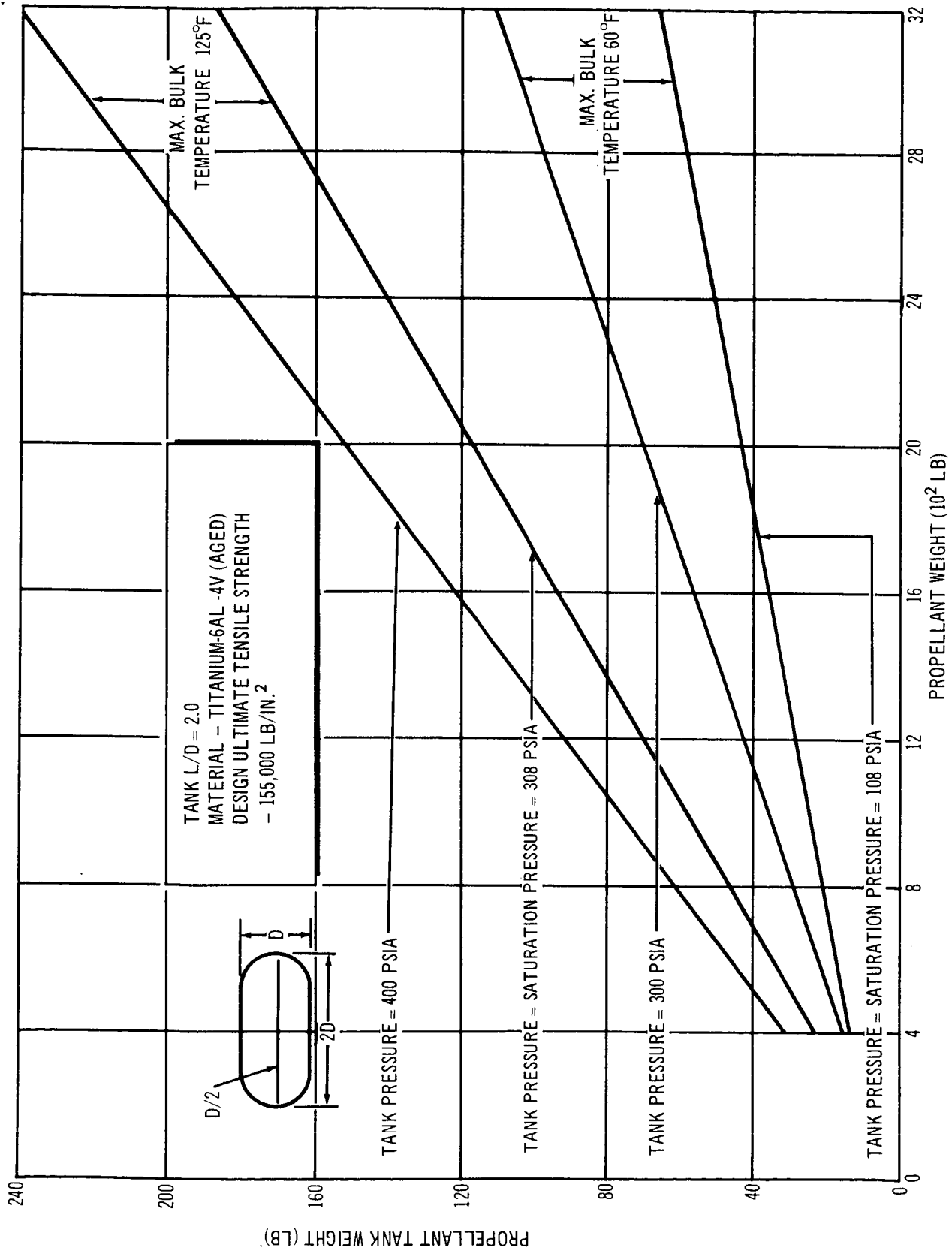


Figure 3-29. Tank Weight as a Function of Propellant Weight - Ammonia Propellant

Table 3-18
PROPELLANT PHYSICAL AND THERMODYNAMIC PROPERTIES

	H ₂	NH ₃	Hydrazine	CO ₂ (g)	H ₂ O
Storage temperature (°F)	-411	125	125	75	160
Storage pressure (psia)	80	325	1.01	35	7
Enthalpy of evaporation (Btu/lb)	155	450	540		1,002
Density (lb/ft ³)	3.72	35.7	63	0.25	61
Freezing point (°F)	-435	-108	34.7		32

3.2.3.4 Biowaste

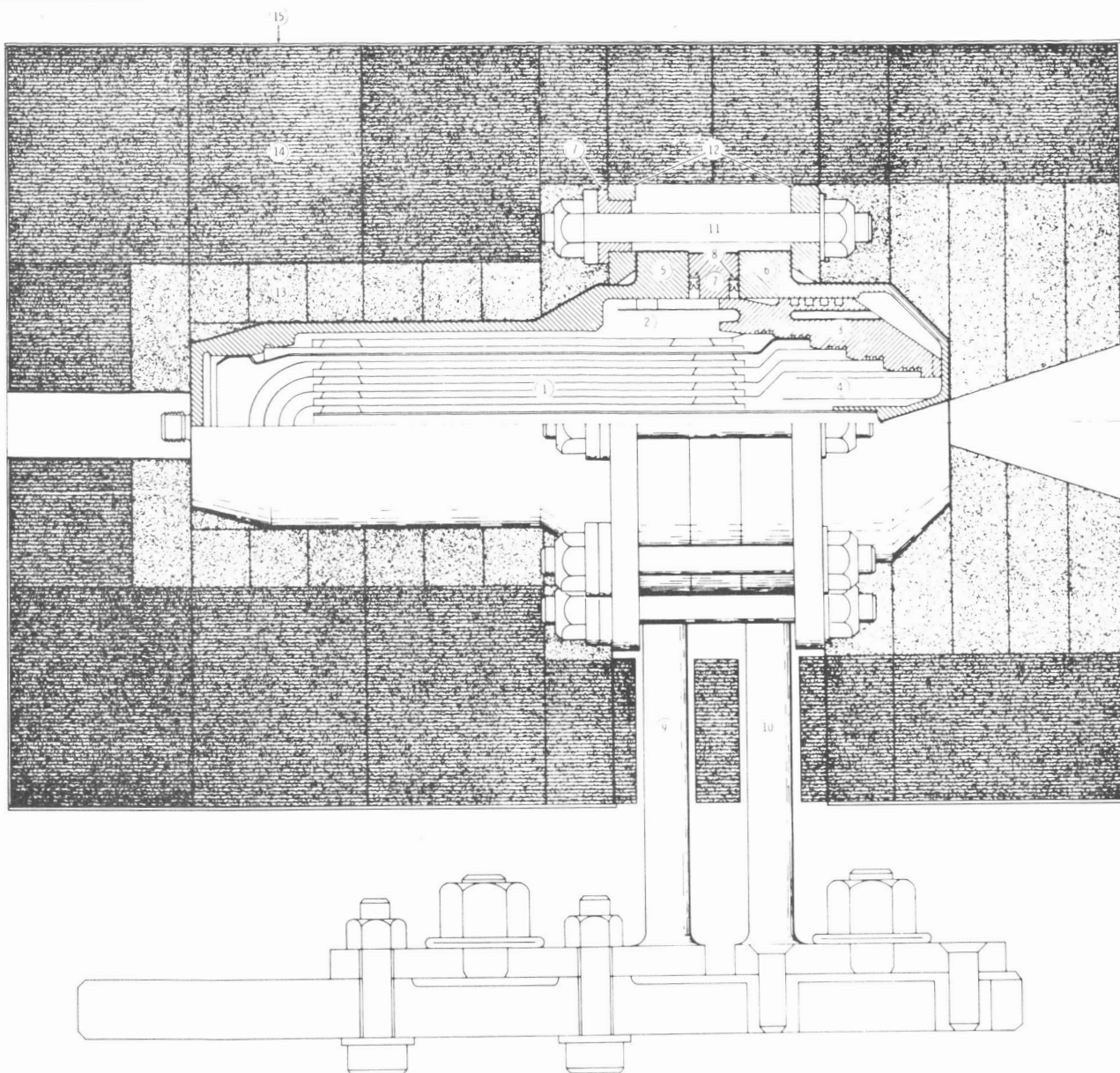
The quantity of stored biowastes depends on the processing technique used by the EC/LS system. Hydrogen gas may be evolved from a water electrolysis process; CO₂ gas is evolved from an adsorption system which purifies the cabin air. Excess liquid water is available from the metabolic process. These products are evolved on a more or less continuous basis; therefore, storage presents no significant problems other than maintaining a few atmospheres of pressure for feeding to the thrusters.

3.3 RESISTOJET PARAMETRIC STUDY

The Resistojet was selected in Section 3.1.3.4 as a primary candidate to replace the baseline bipropellant chemical reaction control system. The Resistojet was selected because of its ability to meet various selection criteria, such as minimum weight, low development risk, growth potential, long life, reliability, and so forth.

The Marquardt Corporation assisted Douglas in performing application studies of the Resistojet to the MORL vehicle based upon the experience accumulated by Marquardt with this engine and the experimental test data that have been produced under both Air Force and NASA sponsorship.

The Resistojet is an electrically heated rocket in which the propellant is heated by force convection from heat-exchanger wall. The energy is provided by Joule heating, and the thrust is generated by expansion of the heated propellant through a de Laval nozzle, Figure 3-30. Inasmuch as the



- | | |
|--|---|
| 1. I^2R HEATED EXCHANGER TUBES (9) - TUNGSTEN | 9. ELECTRICAL (+), PROPELLANT FEEDER, THRUSTOR SUPPORT - MOLYBDENUM - 0.3% TITANIUM |
| 2. REGENERATIVELY-COOLED SHIELDS (3) - TUNGSTEN | 10. ELECTRICAL (-), PROPELLANT FEEDER, THRUSTOR SUPPORT - TUNGSTEN - 2% THORIA |
| 3. HEAT EXCHANGER SUPPORT (ELECTRICAL INSULATOR) - BORON NITRIDE | 11. TIE BOLTS - MOLYBDENUM - 0.9% TITANIUM |
| 4. NOZZLE RADIATION SHIELD - TUNGSTEN | 12. COLLARS (2) - MOLYBDENUM - 0.9% TITANIUM |
| 5. FORWARD PRESSURE CASE - MOLYBDENUM - 0.9% TITANIUM | 13. THERMAL INSULATION - DYNAQUARTZ |
| 6. AFT PRESSURE CASE - TUNGSTEN - 2% THORIA | 14. THERMAL INSULATION - MIN-R-2000 |
| 7. ELECTRICAL INSULATIONS - BORON NITRIDE | 15. CASE - 321 STAINLESS STEEL |
| 8. METALLIC FACE SEALS (2) - INCOME X - SILVER-PLATED | |

Figure 3-30. Marquardt 3 kW Concentric Tube Resistojet

heat exchanger must at all times be at a higher temperature than the propellant, the Resistojet is basically a temperature-limited engine. The temperature limit is determined by the sublimation characteristics of the heat-exchanger material or by a reaction between the heat exchanger and the propellant. Figure 3-31 illustrates the specific impulse capability of the Resistojet as a function of the design electric power level for several propellants. Hydrogen, being the lowest molecular weight propellant material available, provides the highest specific impulse at the maximum chamber temperature limit of $4,356^{\circ}\text{R}$. The higher molecular weights of ammonia and hydrazine produce correspondingly lower specific impulses. Data are also shown in Figure 3-31 for water, carbon dioxide, and a mixture of these two propellants.

The lower temperature limit shown for these propellants is caused by their oxidation characteristics, thus more seriously limiting the temperature capability of the heat exchanger compared to the hydrogen, ammonia, and hydrazine. In Figure 3-31, the specific impulse level achievable is lower at the lower electric power level. This is caused by the larger viscous

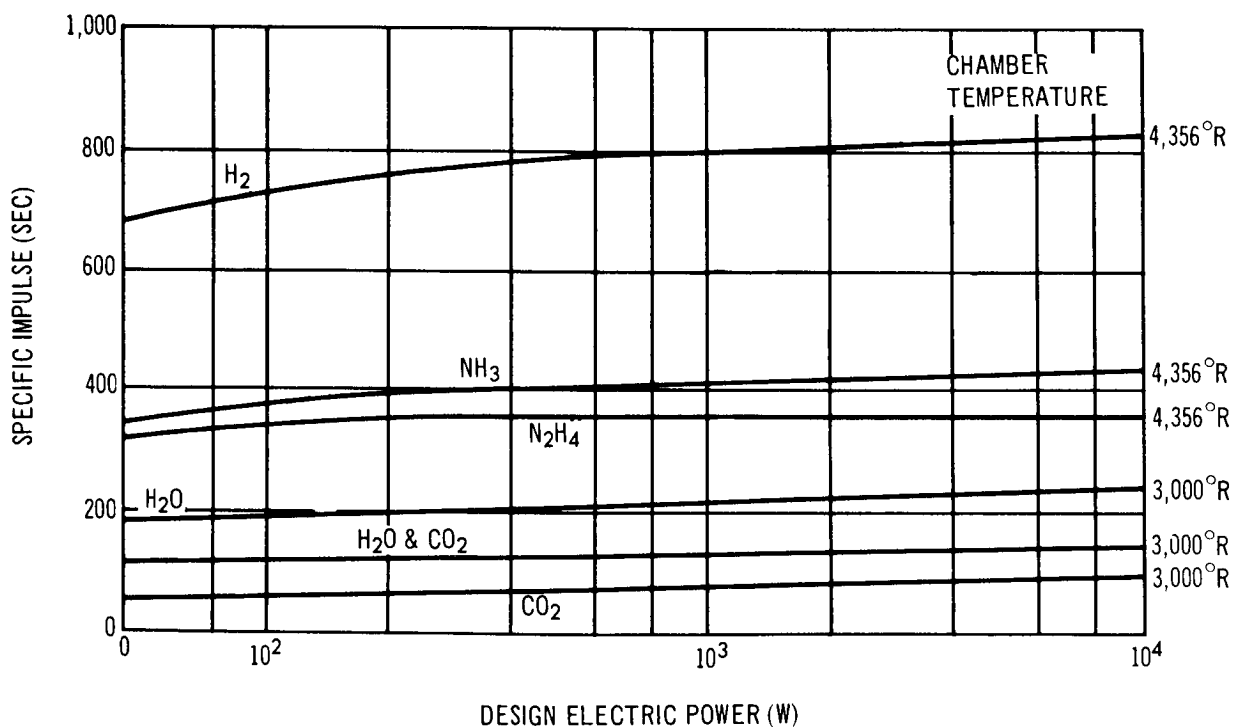


Figure 3-31. Resistojet Specific Impulse (as Influenced by Power Level)

effects associated with the smaller engine and results in a lower nozzle efficiency, which, in turn, manifests itself as a lower specific impulse and efficiency. The region of primary interest for the MORL vehicle is shown by the heavy lines for each of the propellants under consideration.

The electric power-to-thrust ratio requirements for the various propellants are shown in Figure 3-32 as a function of specific impulse. The dashed line presents the ideal value based upon 100% engine efficiency and the assumption that the propellant is introduced at the zero enthalpy level. As expected, the highest electric power-to-thrust ratio is required by the propellants which provide the highest specific impulse level.

It is apparent that the higher specific impulse capability of hydrogen will result in the lowest overall propellant requirement for the MORL vehicle. Hydrogen, however, results in the highest electric power requirement, thus penalizing this propellant with a larger power-supply weight. Furthermore, the cryogenic nature of hydrogen requires considerable insulation relative to the other propellants considered and results in heavier tank weight. A

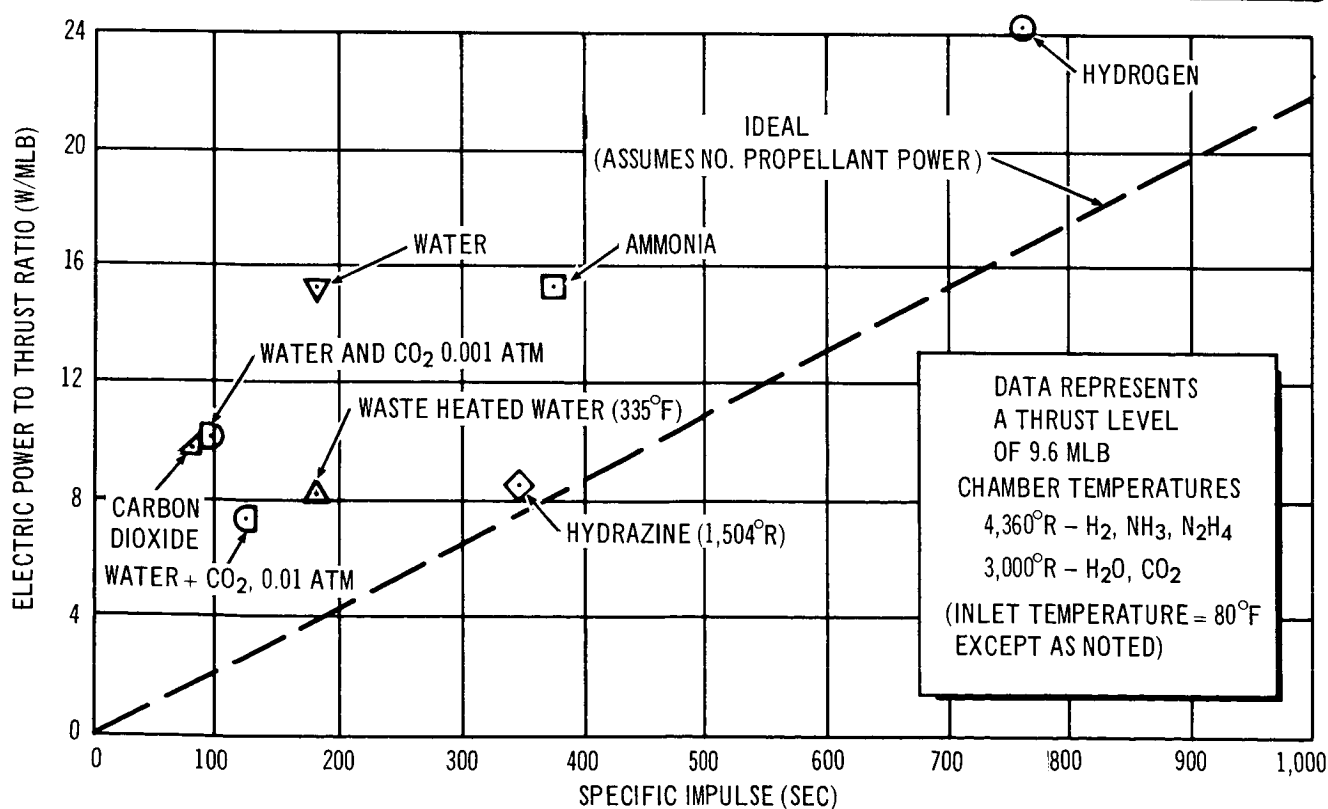


Figure 3-32. Electric Power to Thrust Ratio as a Function of I_{sp}

summary of the tank-to-propellant weight is shown in Figure 3-33. In view of these differences in specific impulse capability, tank weight, and electric power weight, it was not immediately apparent which of the propellants will produce the optimum performance for the MORL vehicle. Therefore, preliminary system weight studies were carried out for all of the propellants described above.

3.3.1 Determination of Thrust and Total Impulse Requirements

The following design criteria were established for the Resistojet reaction control system:

1. Design for a uniform system power level. This implies continuous thrusting in at least one of the various functions at all times. This results in the lowest possible power system size and weight.
2. Design all thrusters to be identical in size so that the firing time for each function is proportional to the total impulse requirement. This provides a simplification in the control system logic, reduces the logistic problems for replacement engines, and minimizes engine development costs.

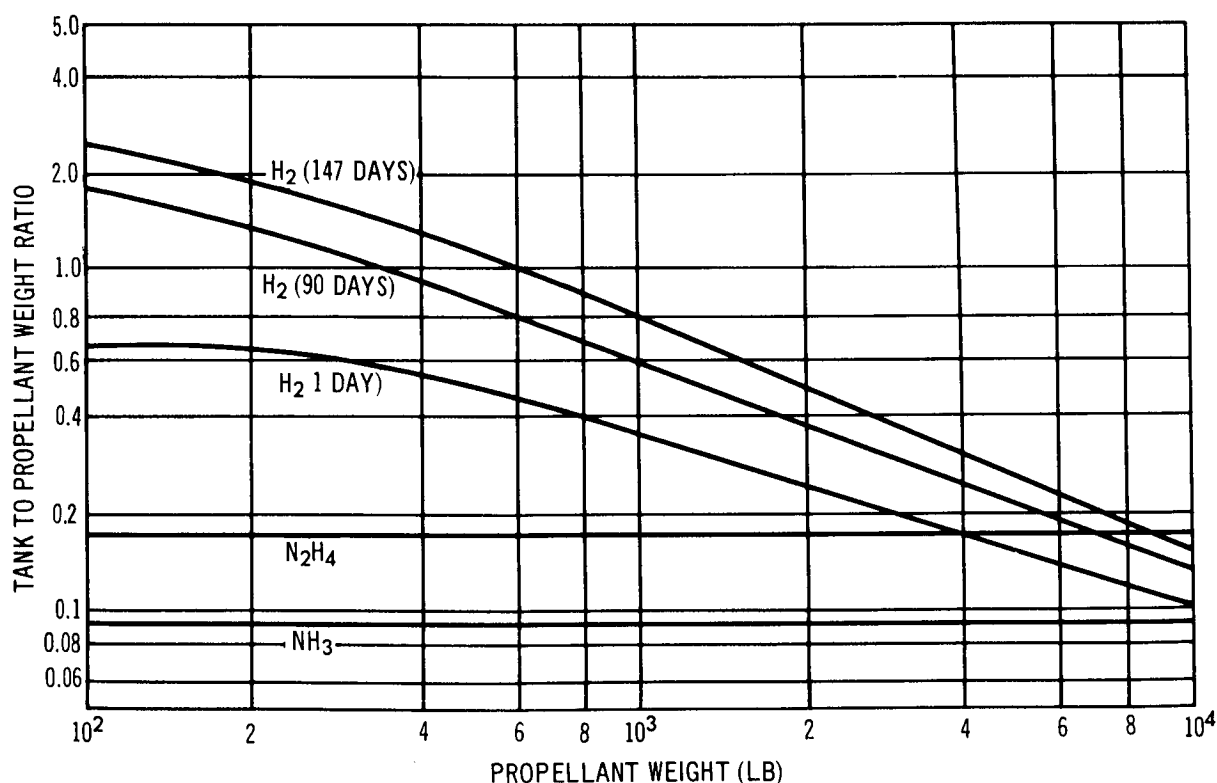


Figure 3-33. Tank to Propellant Weight Ratio Comparison

3. Wherever possible, drag makeup should be accomplished concurrently with either pitching or yaw. This would reduce the total impulse required for the vehicle. This is consistent with the discussion of this technique in Section 3.1.
4. Design the control system so that cold flow operation can fulfill the reaction control system requirements in the event of a power loss. This can be accomplished by increasing the propellant flow rate to offset the reduction in specific impulse.
5. Accomplish precession torque for the artificial-g mode vehicle by single-sided thrusting on the booster module because of the increased lever arm.

3.3.1.1 Zero-g Mode, Local Horizontal Orientation with Solar Panel Power Supply

The total impulse requirement per orbit, based on pure couples for pitch, yaw, and roll at a couple arm of 20 ft, are shown in Table 3-19. Compared with these are the total impulse requirements which take into account single-sided thrusting in pitch and yaw to introduce simultaneously a translational force which can simultaneously provide drag makeup.

Table 3-19
TOTAL IMPULSE REQUIREMENTS

Function	Vehicle I_t (lb-sec/orbit)	Thruster I_t (lb-sec/orbit)
Drag	150	---
Pitch	100	100
Yaw	113	113*
Roll	<u>8</u>	<u>8</u>
Total	371	221

*Note that there is an omitted thrust effectiveness factor of 0.88 which should have been applied to the yaw function, making it actually 128 lb-sec/orbit because of the nonconcurrency of the (CMG) momentum storage vector and the thrust-desaturating vector. This caused all systems for this case to be approximately 6% undersize. However, since this does not disturb the relative comparison between propellants, the minor correction was not included in the analysis.

Based upon the above criteria of continuous thrusting, the combined continuous thrust which must be provided then, is

$$F = \frac{I_t}{\Delta T \text{ orbit}} = \frac{221 \text{ lb-sec}}{5,500 \text{ sec}} = 0.0403 \text{ lb}$$

The individual thruster size based on two-thruster operation is, then 20.1 mlb.

It should be noted that 213 lb-sec/orbit can be supplied for drag makeup, while only 150 lb-sec are required. For this reason, the pitch and yaw thrusters can also be fired as pure couples when drag makeup is not required. Figure 3-34 illustrates the thruster locations required for the belly-down case. Figure 3-35 shows the orbital allocation of impulse for specific thrusters. The sequencing or scheduling of the control functions within the orbit is, of course, flexible, that is, the functional blocks of thrust may be broken up and fired in a number of subblocks as desired, as long as the total impulse requirement is satisfied.

The parenthetical thrusters shown are used for torques of the opposite sense. The drag compensation period shown in Figure 3-35 can be shifted as desired, so as to correspond more closely to the pitch or the yaw control periods. As mentioned earlier, two thrusters are scheduled at all times to present a continuous power loading to the electric system and all thrusters have the same thrust level.

Pitching can be performed in two ways. First, it can be done by thrusters P_1 and P_3 in pure couple with no resultant drag makeup occurring. The same pitching moment is accomplished by firing P_1 and D_1 , and concurrent drag makeup equivalent to the thrust of two D_1 is effected. The roll thrusters are always applied as pure couples.

It should be noted that the control system is not restrictive in that control functions may be accomplished simultaneously. As an example, pitch and yaw desaturation of the control moment gyro may be done simultaneously. To maintain constant power level, this is done at half rates while still providing full drag rate makeup.

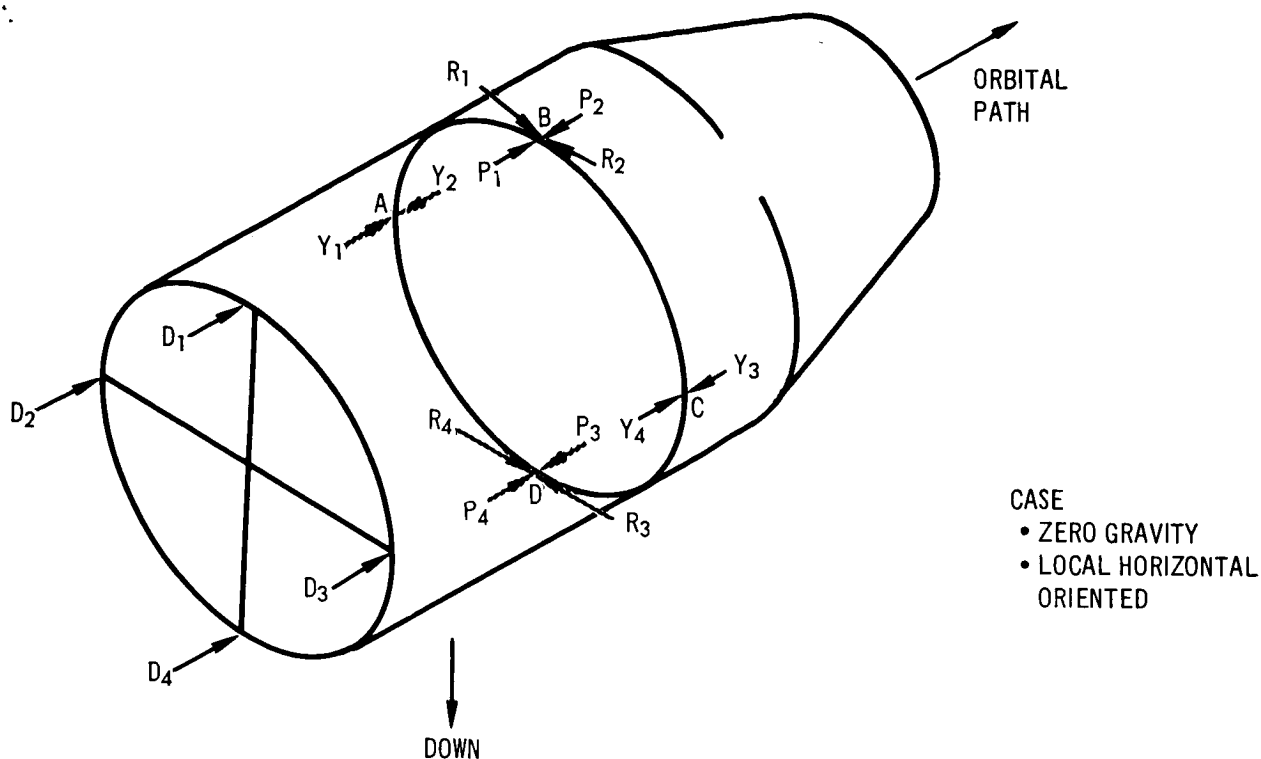


Figure 3-34. Resistojet Thruster Locations

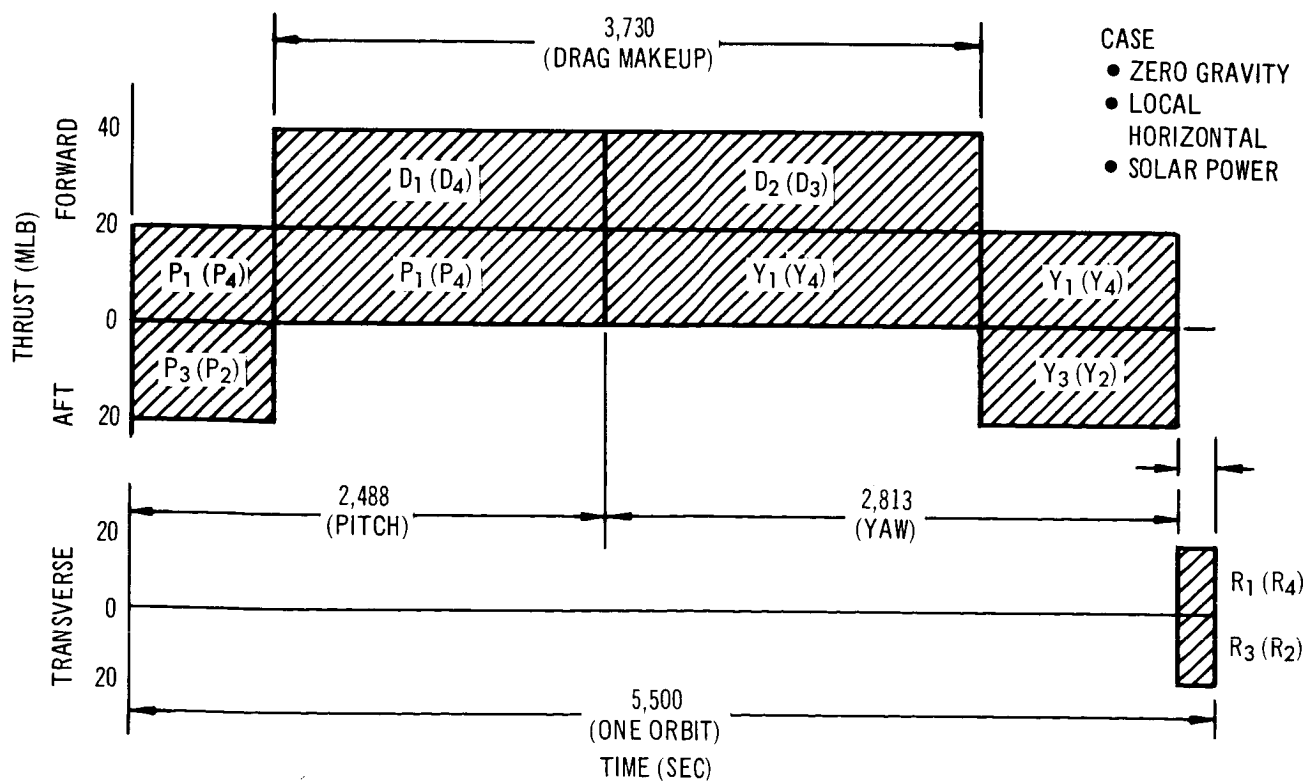


Figure 3-35. Thrust Allocation Zero G Solar Power

3.3.1.2 Zero-g Mode, Local Horizontal Orientation, Isotope Brayton Cycle Power Supply

The vehicle total impulse requirement per orbit, based on pure couples for pitch, yaw, and roll, is shown in Table 3-20. Also shown is the total impulse required per orbit when the various thrust functions are combined.

Table 3-20
TOTAL IMPULSE REQUIREMENTS
(COMBINED THRUST FUNCTIONS)

Function	Vehicle, I_t (lb-sec/orbit)	Thruster, I_t (lb-sec/orbit)
Drag	90	--
Pitch	82	82
Yaw	8	8
Roll	<u>8</u>	<u>8</u>
Total	188	98

The total thrust level for this case is

$$F = \frac{I_t}{\Delta T \text{ orbit}} = \frac{98 \text{ lb-sec/orbit}}{5,500 \text{ sec/orbit}} = 0.0178 \text{ lb}$$

The individual thruster size is 8.9 mlb. Figure 3-36 shows the resulting drag, pitch, yaw, and roll periods.

Again, by use of one-sided thrust for the pitch and yaw thrusters, translational forces are introduced which provide drag makeup. In this case, 90 lb-sec/orbit can be provided, which is just equal to the drag requirement.

3.3.1.3 Artificial-g Mode, Spin Axis Solar Oriented--Both Power-Supply Cases

The vehicle total impulse requirements of the artificial-g mode for both the solar panel and the Isotope Brayton Cycle power are similar. For this reason, these cases are treated together. The Isotope Brayton Cycle vehicle thrust levels are 80% of these for the solar panel mode.

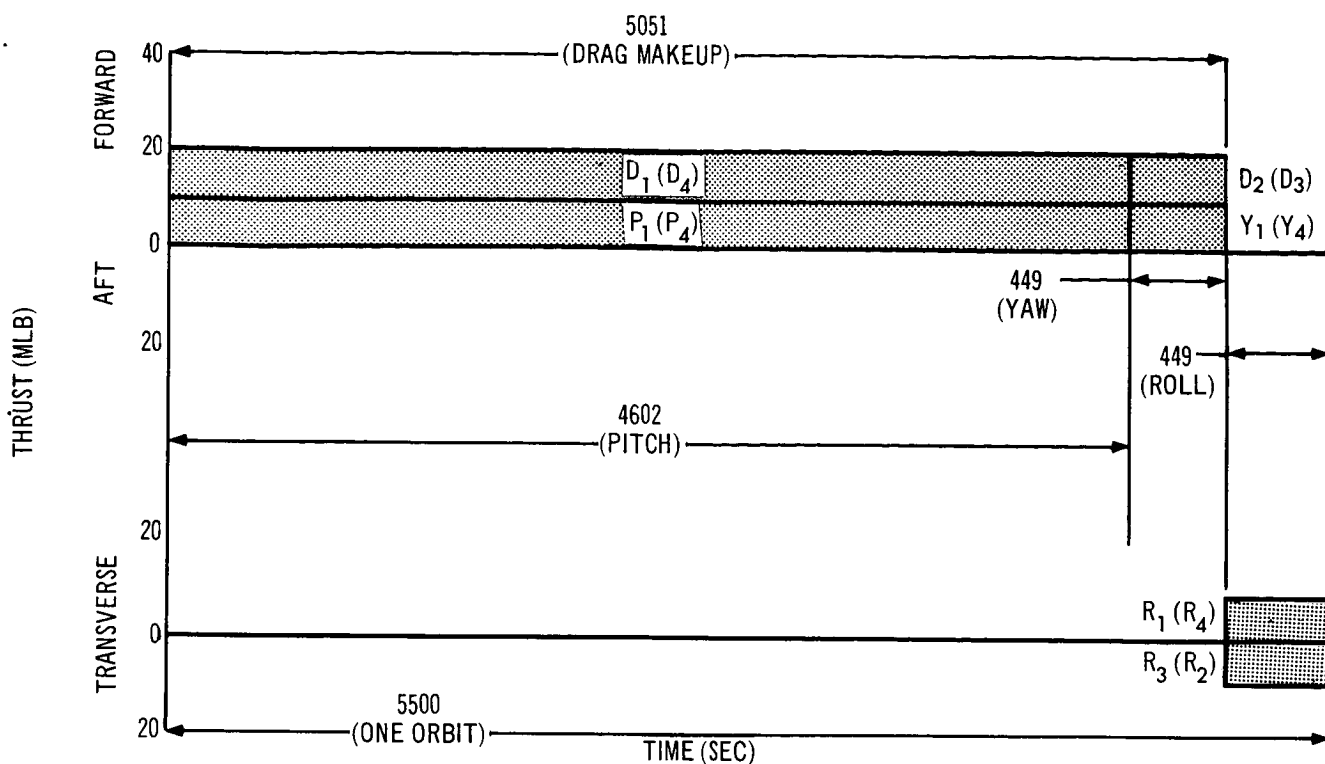


Figure 3-36. Thrust Allocation Zero G Brayton Cycle Power

The total impulse requirements per orbit, based on pure couples for precession (the thrusters are of equal thrust rating and have a 280-ft lever arm between them), are shown in Table 3-21.

Table 3-21
TOTAL IMPULSE REQUIREMENTS
(PRECESSION)

Function	Solar Panel (lb-sec/orbit)	Isotope Brayton Cycle (lb-sec/orbit)
Drag	500	420
Precession	<u>500</u>	<u>420</u>
Total	1,000	840

The orbital period is significantly more difficult to schedule in this case than in the zero-g cases. A uniform power expenditure over the laboratory is rotating about a spin axis, \bar{H} , which is sun oriented at a rate of 0.4

radians per sec. Precessional torques and drag makeup thrusts can only be accomplished during certain rotational positions of the laboratory. The laboratory and orbital relationships are shown in Figure 3-37. The required precessional torque vector, $\vec{\tau}$, required is always as shown.

As discussed earlier in Section 3.1, the total impulse required of the thrusters may be reduced by employing the largest available lever arms for torquing and introducing simultaneous translational drag makeup forces. For precession, a single thruster located on the booster, as shown in Figure 3-38, at a lever arm of 230 ft produces more favorable torque on the system than a couple at 280 ft (an effective lever arm of 140 ft based on the same total thrust expenditure). By these techniques, the vehicle precessional total impulse requirement was reduced to 61% of that of Table 3-21.

The thrust schedule shown in Figure 3-39 was developed with the intent of uniform power expenditure over the orbit. This ideal was approached rather closely with a maximum-to-minimum power ratio of 1.2. The reason for this nonuniformity is the constraint that less propulsion time is available for precessional control than for drag makeup.

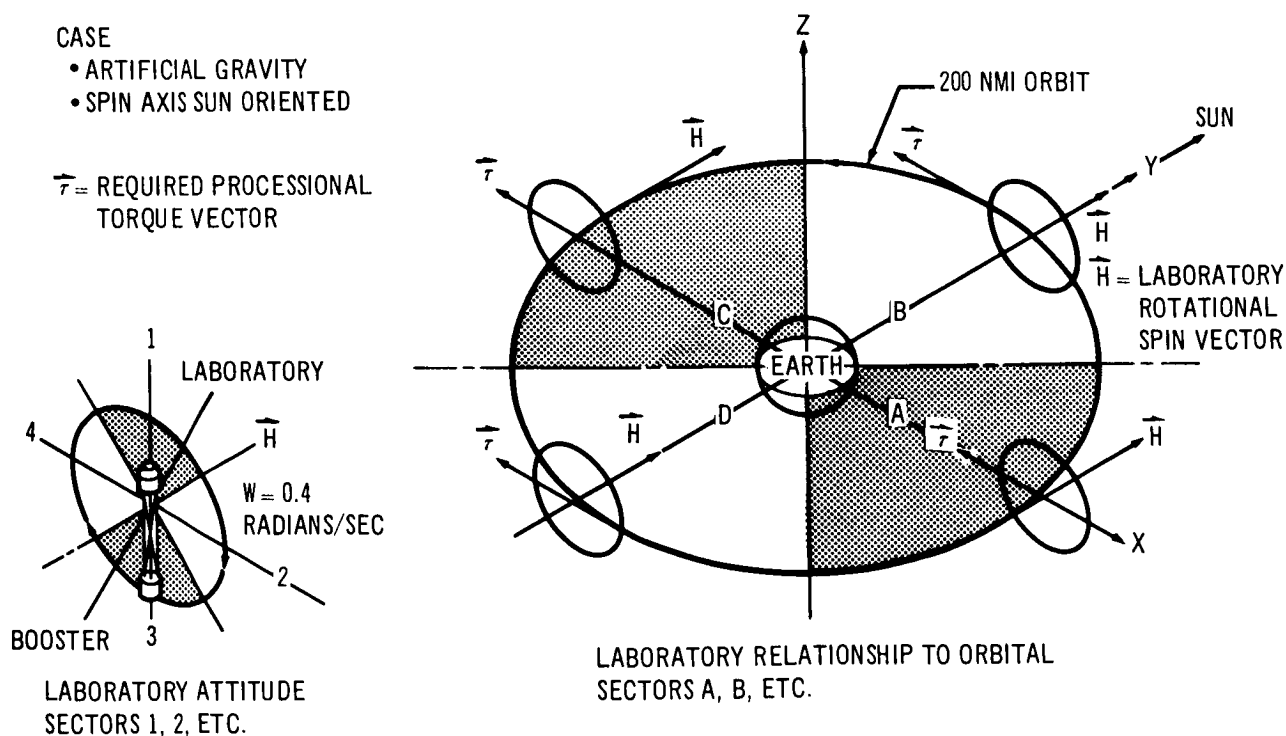


Figure 3-37. Laboratory Orbit Relationships, Spin Mode

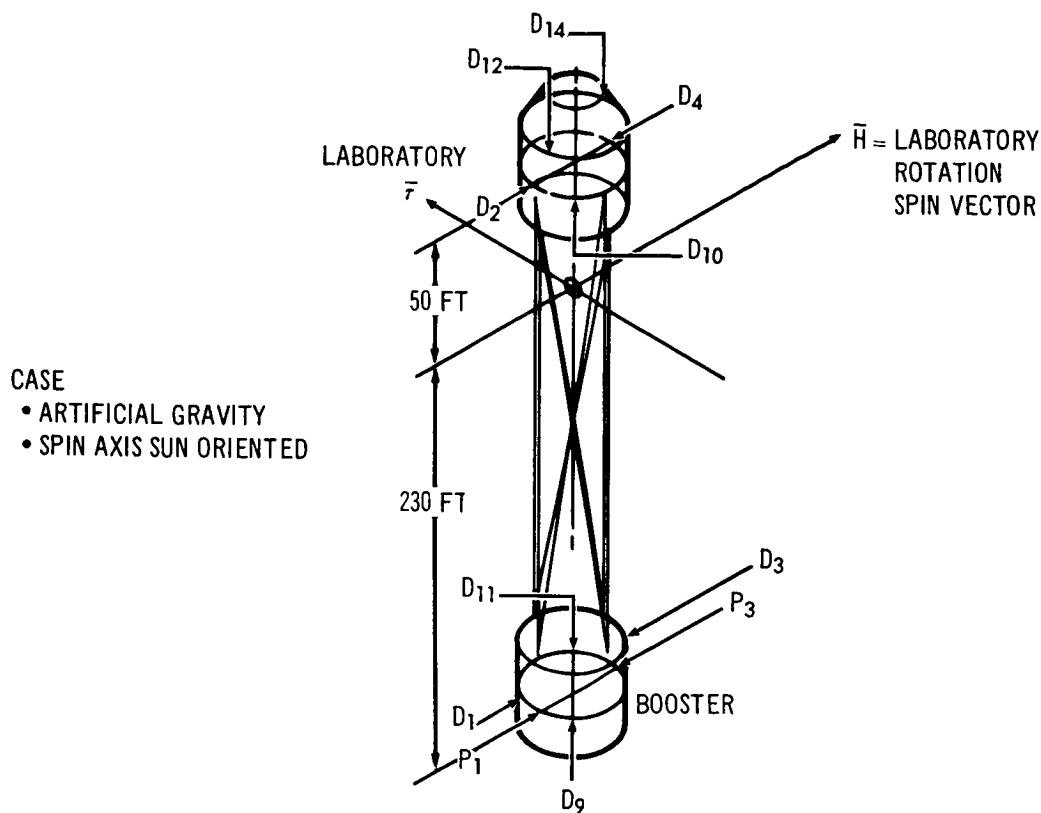


Figure 3-38. Resistojet Thrustor Locations, Spin Mode

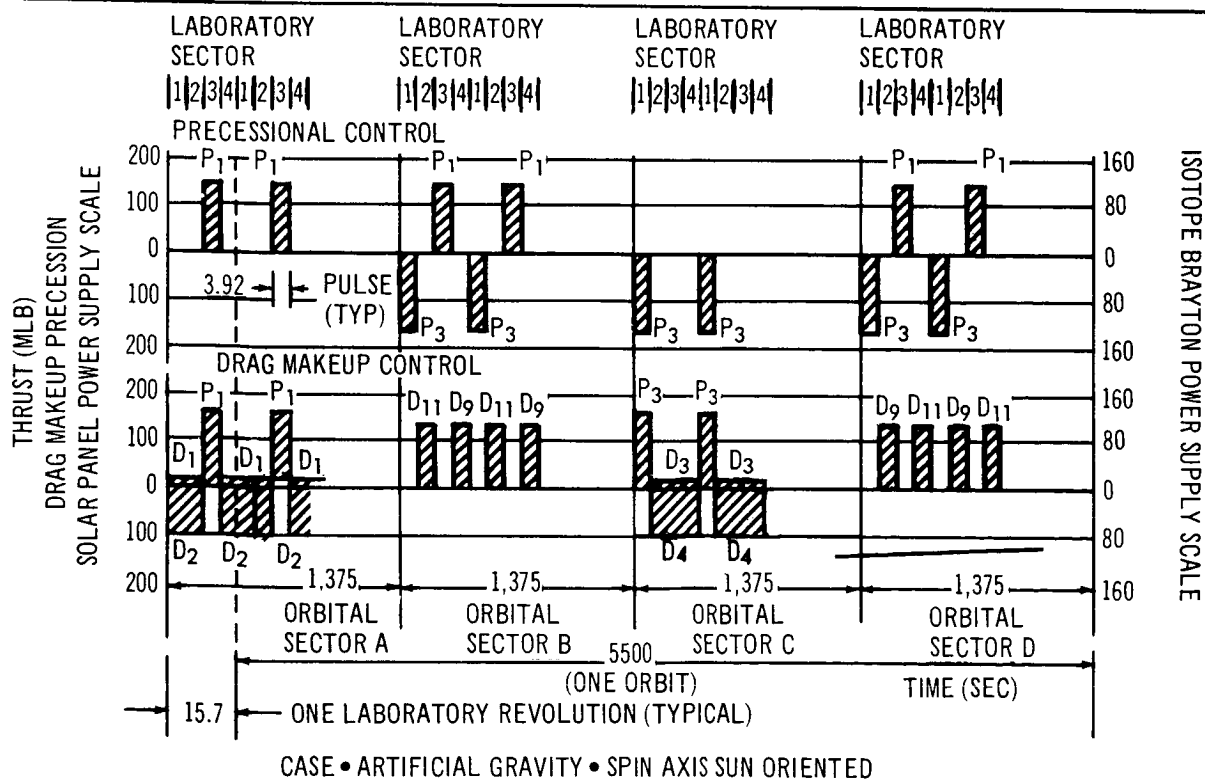


Figure 3-39. Thrust Allocation Sequence

Orbital Sector A (Figure 3-37)

Precessional control is accomplished in this sector by means of the precessional thruster, P_1 , when the laboratory is in its rotational sector 3. This pulse duration is 3.92 sec, occurring each laboratory revolution. It should be noted that since the precessional torque, $\bar{\tau}$, is made up of a single thruster, P_1 , a useful translational force is also introduced as drag makeup as shown in the second sequence of Figure 3-39. During the firing in Sector 3, the drag thrusters, D_1 and D_2 , are off, since the objective is a near-uniform power expenditure. The firing of this thruster over the 90° laboratory Sector 3 is accomplished at a thrust effectiveness of 0.9.

Drag makeup during orbital Sector A is accomplished by drag motors D_1 and D_2 . These are sized so as to represent a balanced thrust about the center of gravity. These similarly have an effectiveness factor of 0.9, since their firing angle over the orbit is 90° .

Orbital Sector B

Precessional control is accomplished at twice the orbital Sector A rate during this sector by the use of P_3 and P_1 while in the laboratory positions 1 and 3, respectively. This is done to cancel out any radial disturbances on the orbit.

During orbital Sector B, drag motors, D_{11} and D_9 , are fired while the laboratory is in Positions 2 and 4, respectively. Alternate motor locations might be D_{10} for D_9 and the sum of D_{12} and D_{14} for D_{11} . The small thrust levels involved, compared to the centrifugal tension loads in the cables, permits thrusting at low level. It should be noted that the thrust effectiveness is compounded by orbital and laboratory motion to be 0.81.

Orbital Sectors C and D

Orbital Sectors C and D are a repeat of their symmetrical counterparts, A and B, with opposite sense of the motor firings.

The table below summarizes the total impulse requirement on the basis of that actually demanded of the thruster and not necessarily that which is effected on the laboratory or orbit. That is, the thrust efficiency factors have been included. Therefore, these figures may be used directly for sizing motors.

Table 3-22
SUMMARY OF IMPULSE REQUIREMENTS

Function	Solar Panel (lb-sec/orbit)	Isotope Brayton Cycle (lb-sec/orbit)
Drag	463	388
Precession	<u>338</u>	<u>284</u>
Total	801	672

The resultant required thrust levels for each of these cases are:

Table 3-23
RESULTANT THRUST LEVELS

Function	Solar Panel (mlb)	Isotope Brayton Cycle (mlb)
$P_1 (P_3)$	164	131.2
$D_2 (D_4)$	110.8	93.1
$D_3 (D_1)$	24.1	20.3
$D_{11} (D_9)$	134.9	113.4

It should be noted that the artificial-g mode cases require engine sizes and locations considerably different from those of the zero-g case.

3.3.2 Resistojet Performance

The following paragraphs present a discussion of Resistojet performance.

3.3.2.1 Steady-State Performance

The summary of the steady-state test data obtained with a 3-kW Resistojet is shown in Table 3-24. As noted, this engine achieved a specific impulse of 838 sec and an overall efficiency of 79%. The thrust of 145 mlb is essentially that required for the artificial gravity mode vehicle. This engine was tested with hydrogen propellant for 25 hours and was delivered to the NASA Lewis Research Center. Although these data provide a reliable basis for predicting performance with hydrogen at this thrust level, it is necessary to compute the performance for other propellants and smaller engine sizes down to 10 mlb in order to cover the range of thrust and propellant requirements established in the previous section.

Table 3-24
RESISTOJET PERFORMANCE TEST (25 HOURS)

Test	Results
Electric power (W)	3,044
Vacuum specific impulse (sec)	838
Total power efficiency (%)	0.791
Electric power efficiency (%)	0.881
Mass flow (lb/sec)	1.75×10^{-4}
Thrust (mlb)	145
Total gas temperature (°R)	4,350
Chamber pressure (atm)	8.79
Cell pressure (mmHg)	0.7
Inlet temperature (°F)	86

The performance for the ammonia and hydrazine propellants was determined by assuming the same propellant temperature that was achieved by the 145 mlb test engine and computing the thrust and specific impulse performance by digital computer techniques.

Inasmuch as the thermodynamic characteristics of both ammonia and hydrazine are well known, the data obtained are considered accurate. It was possible to assume the same propellant temperature for ammonia and hydrazine

as achieved with hydrogen, since both of these materials are compatible with the tungsten heat exchanger at high temperature. In the case of the carbon dioxide and water vapor propellants, however, it was necessary to change the heat exchanger material and to lower the propellant temperature to 3,000°R to account for the oxidation that would be encountered with these two propellants.

The overall engine efficiency is determined by the product of the heat exchanger efficiency, η_h , and the nozzle efficiency, η_n . The heat exchanger efficiency is defined as the total power delivered to the gas at the nozzle divided by the total power input to the heat exchanger. The nozzle efficiency is defined as the specific thrust power in the jet divided by total gas enthalpy at the entrance to the nozzle. In the smaller sizes, the heat-exchanger efficiency is expected to be lower than that achieved for the 145 mlb thrust engine because of the much larger surface-to-volume ratio associated with the smaller engine. Therefore, the heat-exchanger efficiency was reduced with decreasing engine size.

The loss factors which were taken into account to determine nozzle efficiency are:

1. Incomplete recombination (F).
2. Incomplete expansion (E).
3. Exhaust divergence from axial (D).
4. Friction (V).

The method of determining nozzle efficiency is briefly described here. The nozzle efficiency is defined by

$$\eta_N = \eta_F \eta_E \eta_D \eta_V$$

Marquardt's experience has shown that frozen flow, rather than shifting equilibrium flow, exists in the small nozzle sizes. An existing IBM 7040 program was used to predict the specific impulse as a function of nozzle area ratio, which takes into account the first two loss factors above. A fixed divergence loss, η_D , of 0.96 was used with all propellants since the nozzle half-angle was fixed at 17°30', and this efficiency factor is relatively insensitive to Reynolds number.

The inclusion of the friction effect was a semiempiric one. For low thrust levels (order of millipounds) viscous effects become a significant factor in attempting to predict attainable nozzle performance. Various investigators (References 4 to 10) have attempted to define these losses, but insufficient empirical data are available to provide a complete answer. Viscous effects can usually be correlated as a function of Reynolds number (the ratio of inertia to viscous forces) and the Knudsen number--the ratio of the mean free path of the gas molecules to a characteristic length (for example, the nozzle throat diameter).

The probable trends of nozzle performance as a function of Reynolds number are shown in Figure 3-40 based on the limited data available. The lower curve (A) represents the ratio of the optimum I_{sp} to the I_{sp} for infinite expansion ratio. The range of values is from 0.42 (the free molecular limit) to about 0.95 for Reynolds numbers greater than 10^4 . This curve may be compared to the upper curve (B) where the reference I_{sp} is the isentropic (nonviscous) value that corresponds to the optimum area ratio nozzle based on Reference 4 results. Viscosity has a dual effect with decreasing

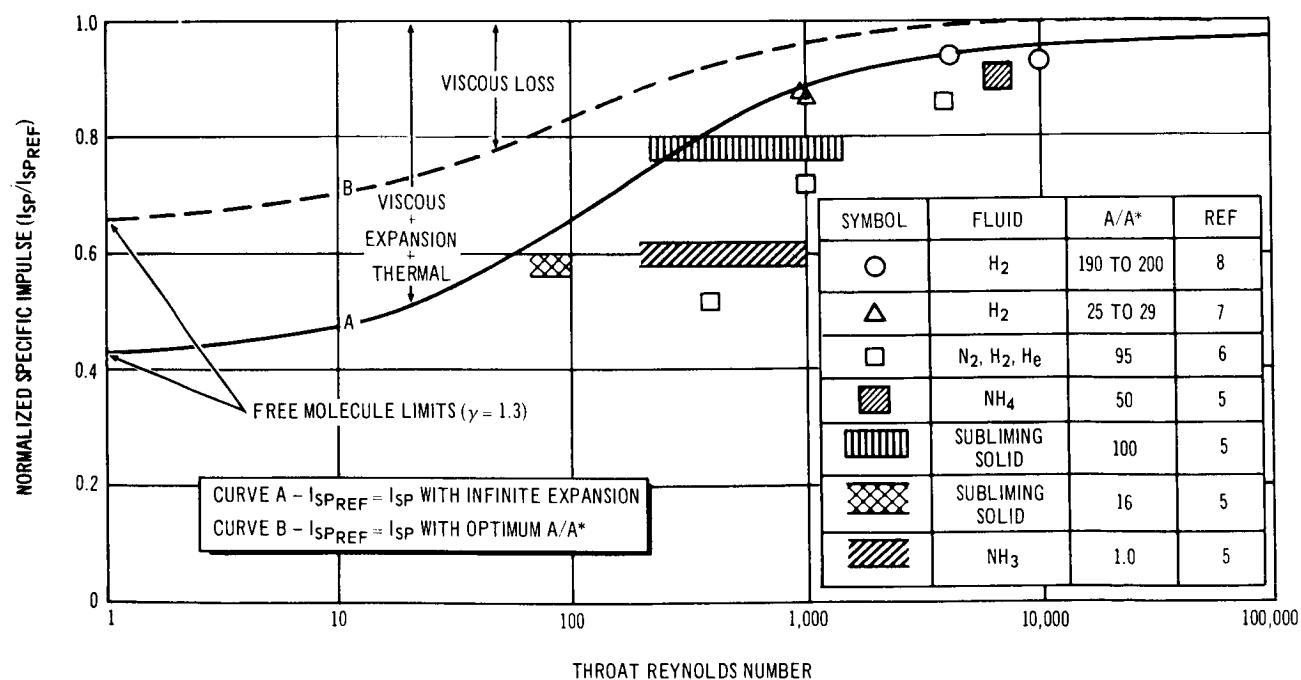


Figure 3-40. Viscous Effects on Low Thrust Nozzle Performance

Reynolds numbers--an increased viscous loss plus an increasing loss due to decreased expansion. The optimum area ratio becomes smaller and smaller and becomes just 1 in the free molecular limit. The data with the area ratio selected too small or too large tend to fall below the predicted optimum curve.

Viscous effects at very low Reynolds numbers are even more difficult to determine if the flow adjacent to the wall begins to slip and the wall streamline no longer has zero velocity. McAdams (Reference 11) and others have indicated that the various flow regimes correlate with Knudsen numbers as follows:

$N_{kn} < 0.001$	Continuum flow
$0.001 < N_{kn} < 2$	Slip flow
$N_{kn} > 2$	Free molecular flow

Milligan (Reference 12) indicated that slip effects in nozzle flows only become significant at Knudsen numbers of about 0.1.

For a 10-mlb water vapor rocket, for instance, at 0.2 atm at 2,500°F, it can be shown that

Throat Reynolds number ~ 500

Knudsen Number ~ 0.002

These values indicate that the viscous effects will be appreciable for the waste product Resistojet but can be predicted reasonably well. Also of special interest from Milligan's work is that continuum and slip flow regimes apparently merge smoothly with no discontinuity observed. This gives some substantiation to the smooth curve drawn in Figure 3-40. It should be pointed out, however, that these curves are largely based on a few scattered measurements and have not been experimentally verified at the low end of the Reynolds number scale.

The specific impulse achieved with each of the propellants of interest as a function of thrust level is given in Figure 3-41. Each point on this graph

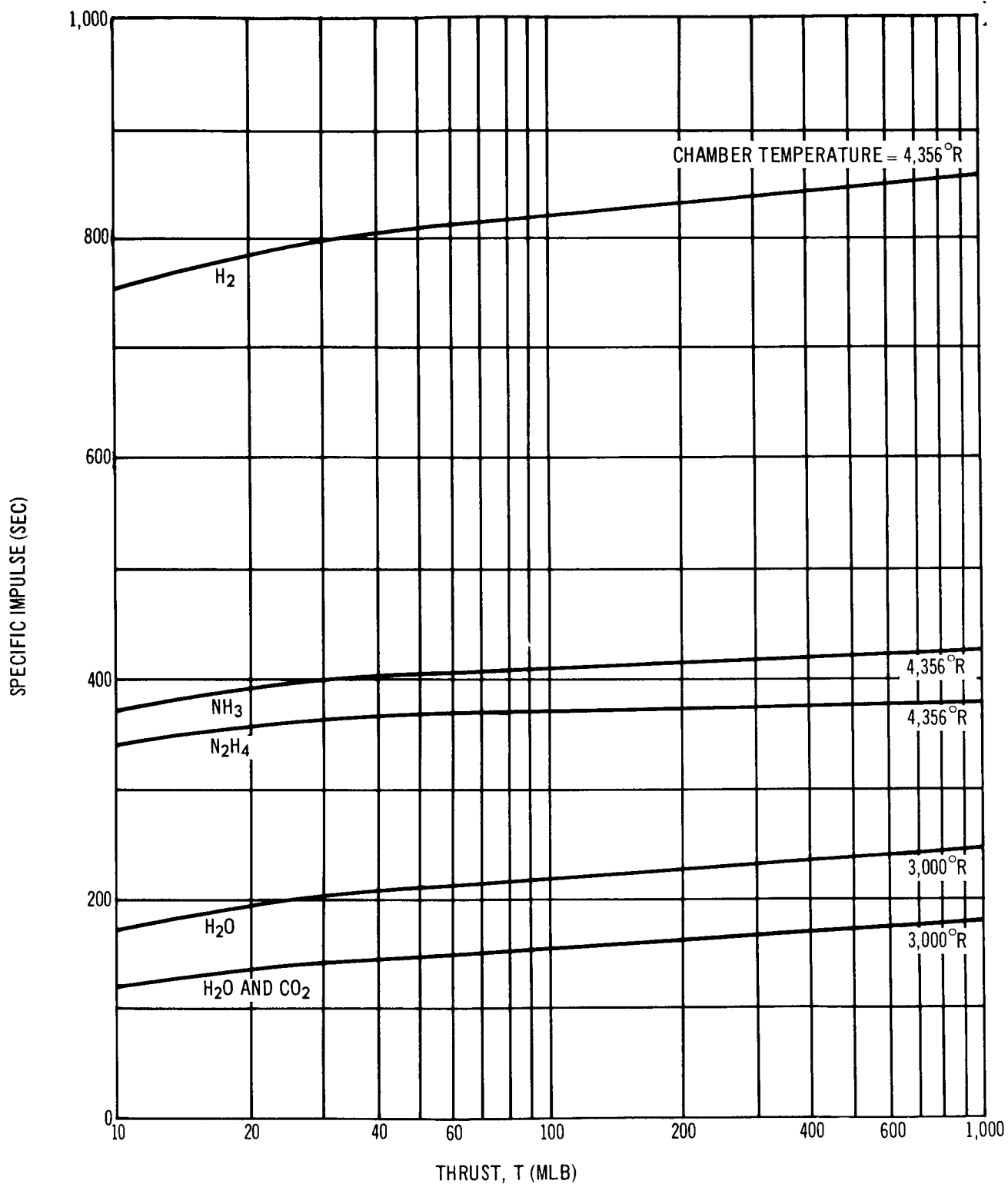


Figure 3-41. Estimated Resistojet Performance Specific Impulse as a Function of Thrust

represents a separate engine design. As previously noted, the decreasing specific impulse with decreasing thrust is caused by the higher viscous effects associated with the smaller engines.

Although increased chamber pressure was found to improve performance, primarily due to Reynolds number, a higher pressure has the undesirable trend of reducing the nozzle throat diameter and increasing propellant tank weight. A pressure optimization was performed for hydrogen and a pressure of 35 psia was selected. The optimum was quite broad. In the case of ammonia and hydrazine, tank weight considerations were less important, and chamber pressures of 45 psia were determined. For the biowaste, specifically carbon dioxide, the supply pressures were available at pressures less than 1 mm of mercury. Hence, low chamber pressures were used.

The overall electric power efficiency is shown as a function of thrust level in Figure 3-42 for the five propellant combinations of interest. The very high efficiency shown for hydrazine results from the exothermic chemical decomposition reaction that occurs, resulting in an overall electrical efficiency of more than 100%. Conversely, the overall efficiency of ammonia is low, because the energy required for dissociation is not returned to thrust energy during the expansion process.

The Resistojet thrust and propellant flow rates are shown as a function of design electric power level in Figures 3-43 through 3-48 for the various propellants of interest.

The estimated engine weight as a function of design electric power level is shown in Figure 3-49. The concentric tubular engine was employed to compute the estimate weight shown. The corresponding engine dimensions are given in Figure 3-50.

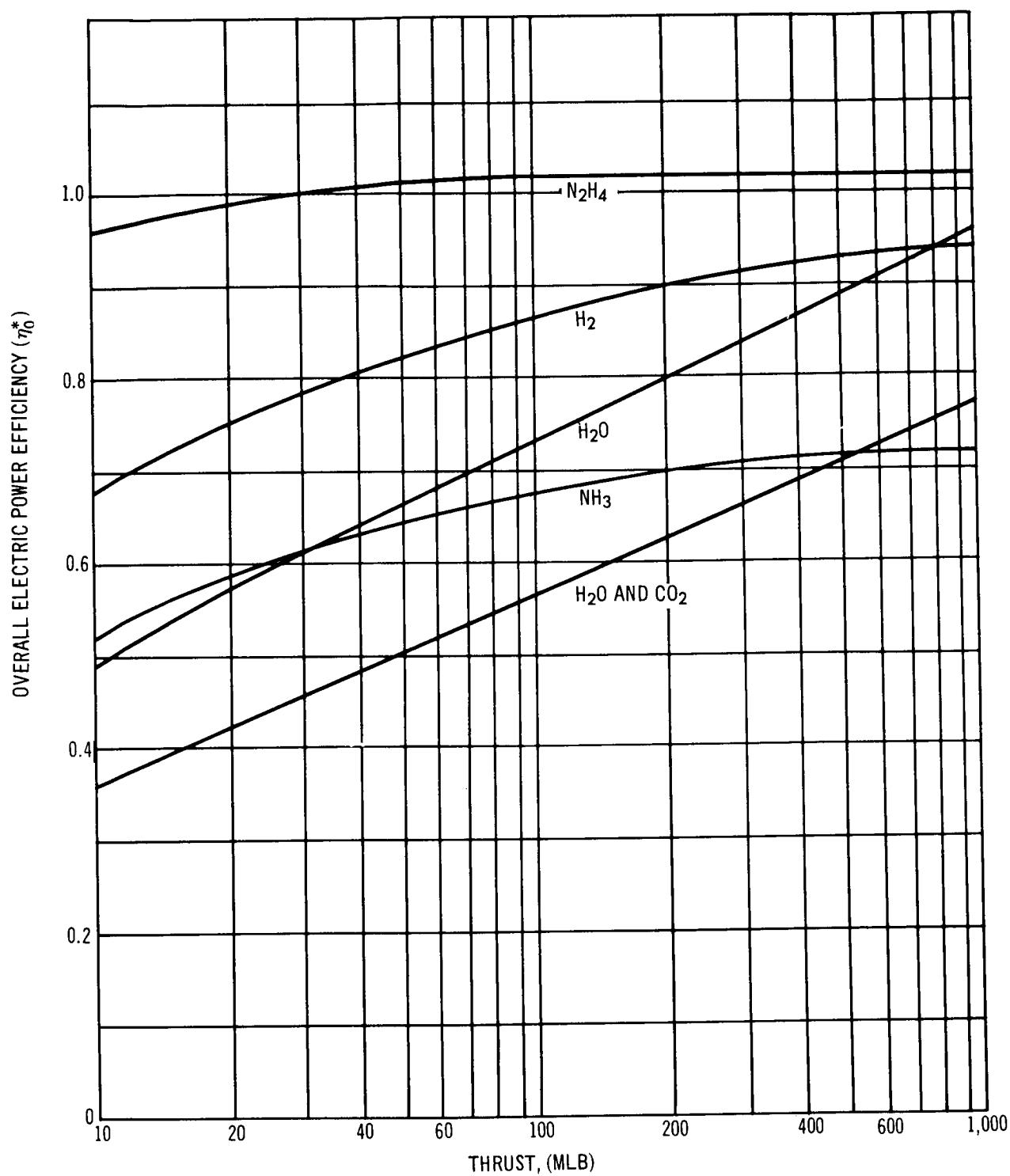


Figure 3-42. Estimated Resistojet Performance Overall Efficiency as a Function of Thrust

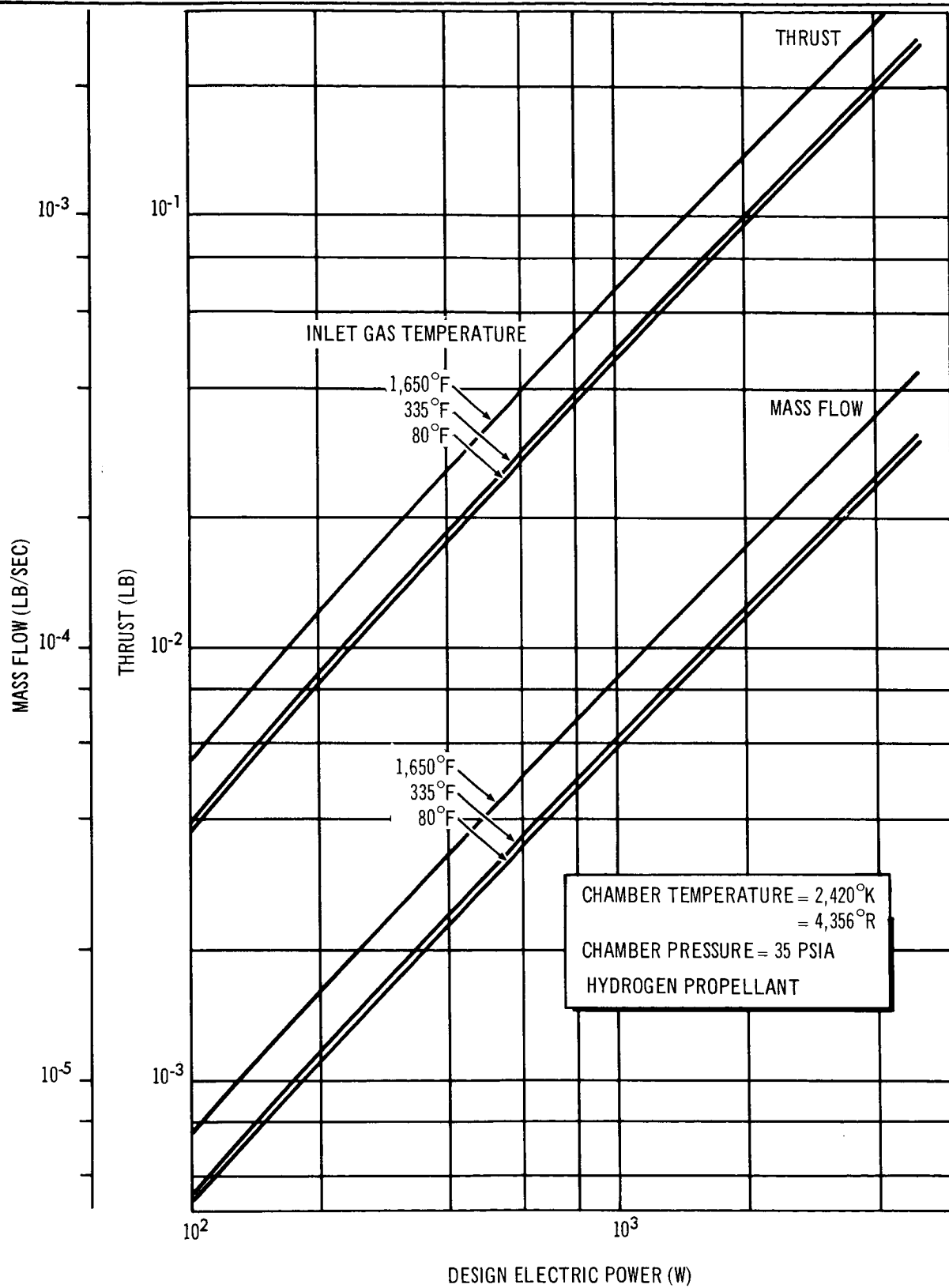


Figure 3-43. Resistojet Thrust and Propellant Flow Rate as a Function of Design Electric Power Level – Hydrogen

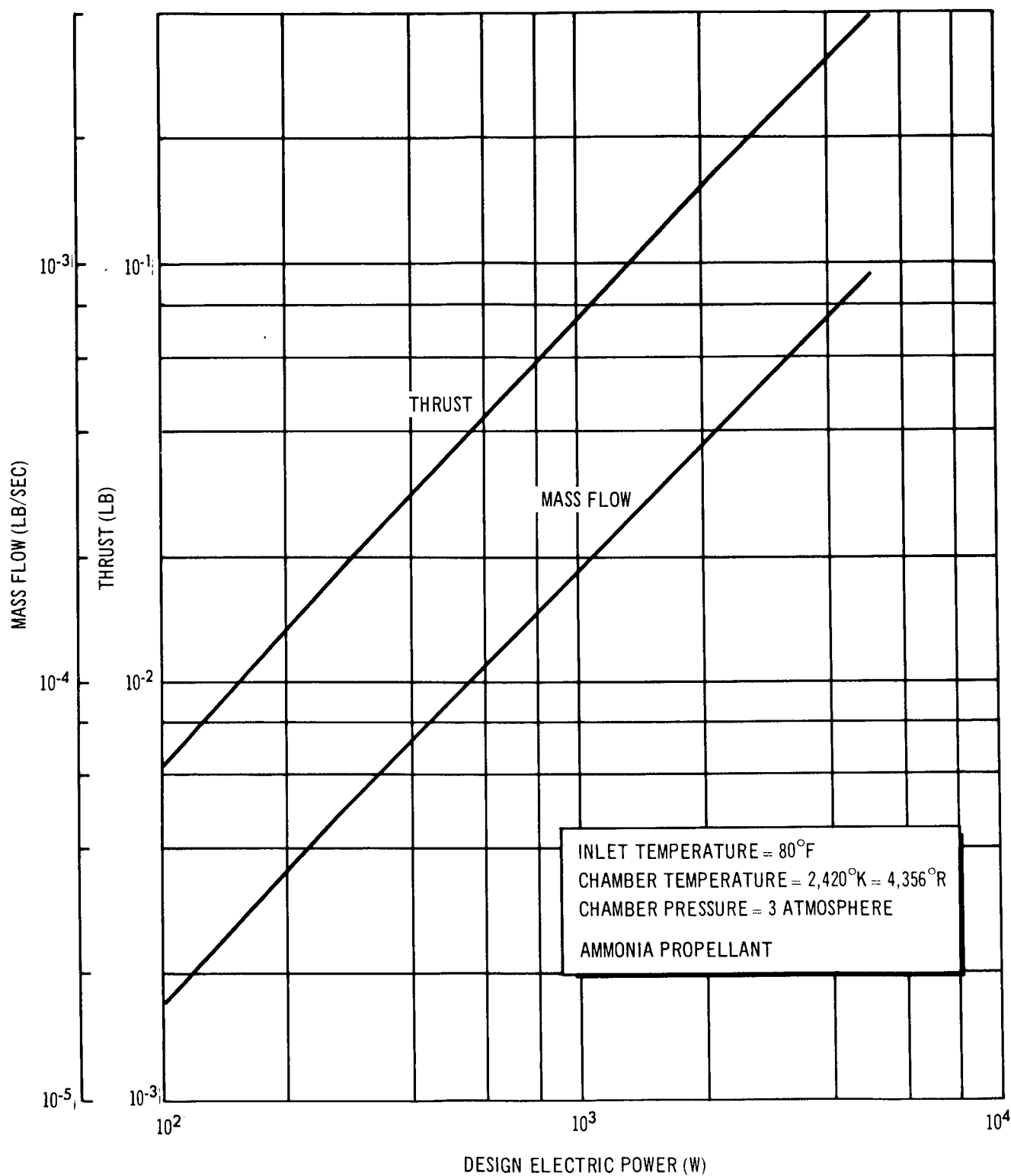


Figure 3-44. Resistojet Thrust and Propellant Flow Rate as a Function of Design Electric Power Level – Ammonia

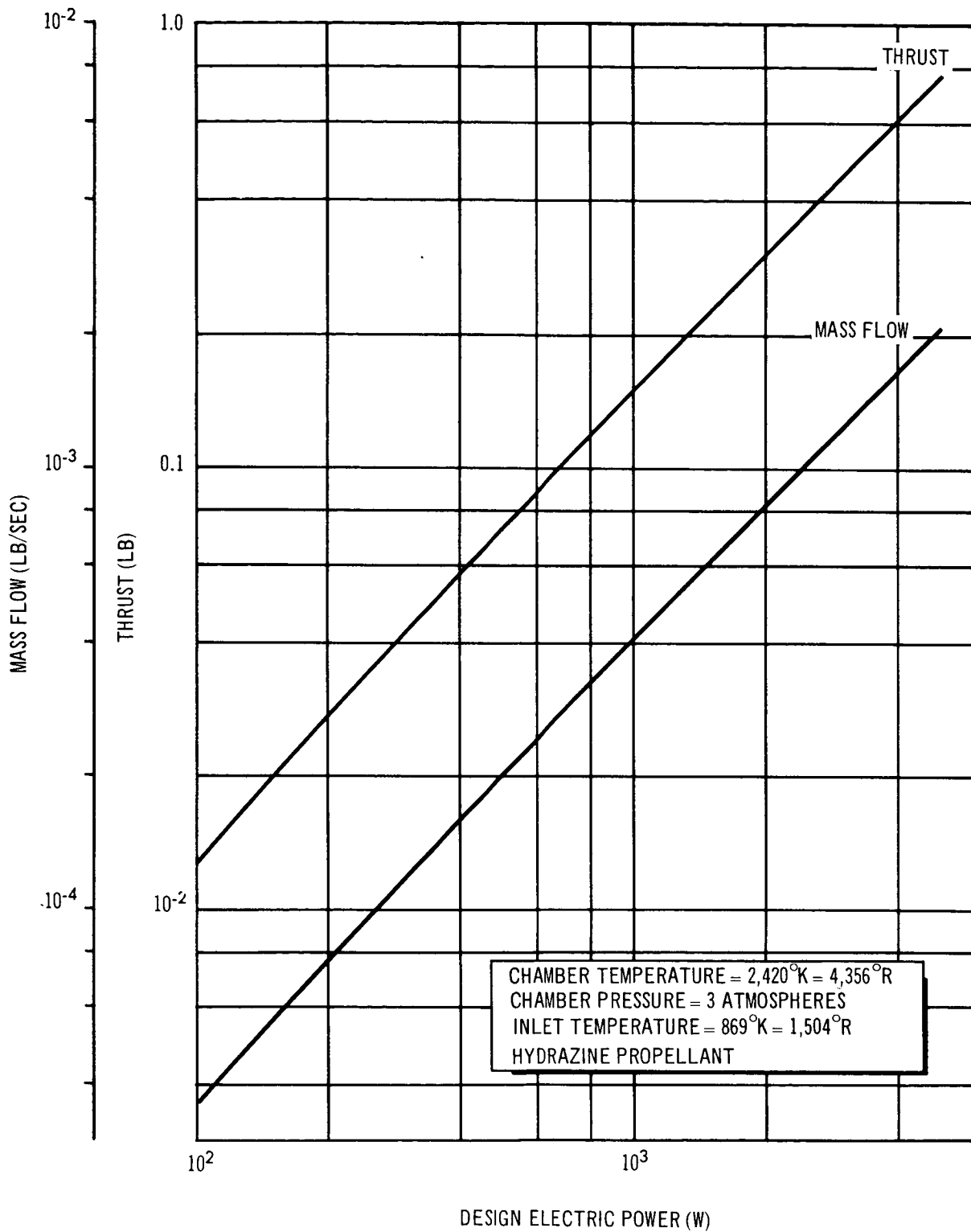


Figure 3-45. Resistojet Thrust and Propellant Flow Rate as a Function of Design Electric Power – Hydrazine

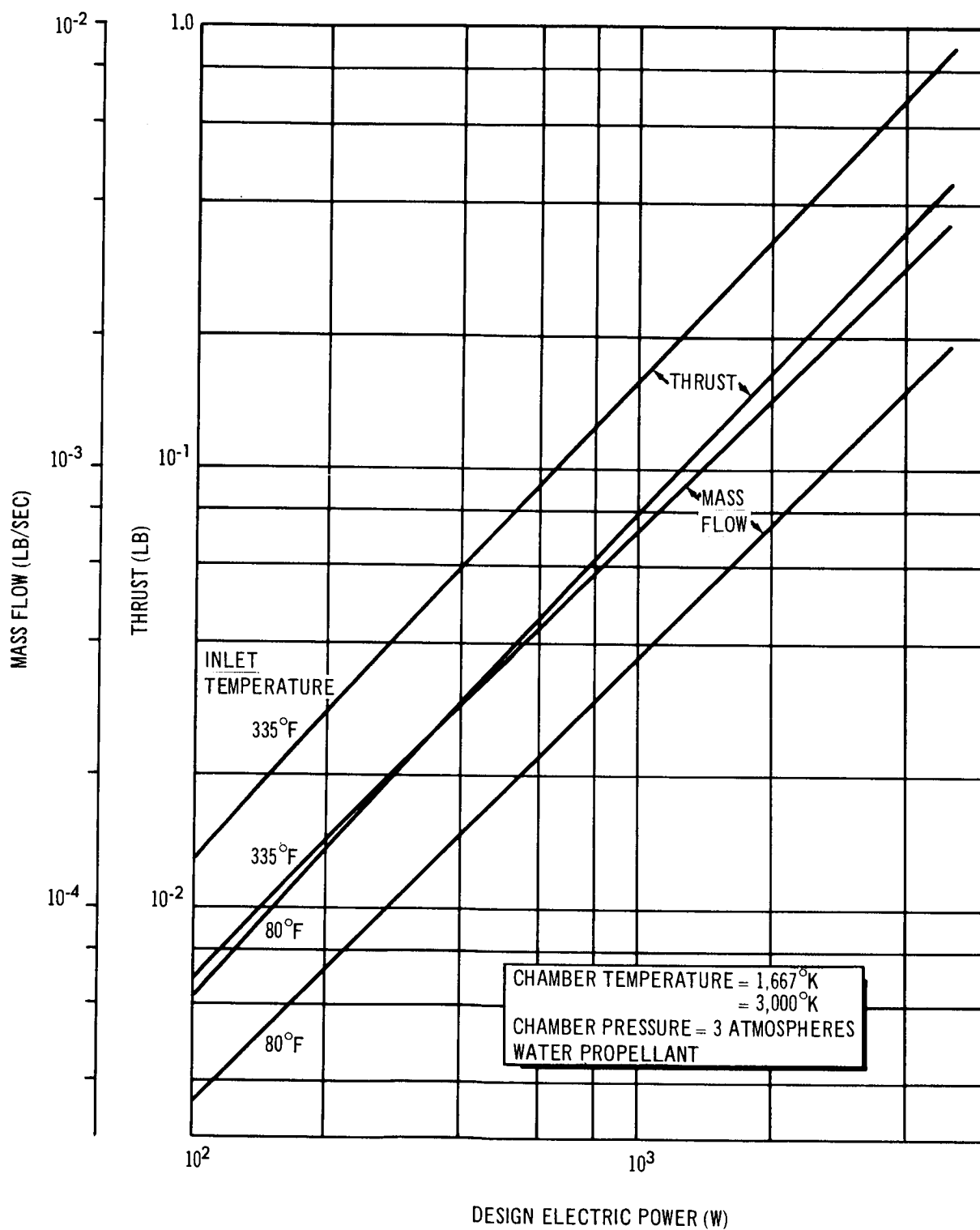


Figure 3-46. Resistojet Thrust and Propellant Flow Rate as a Function of Design Electric Power Level – Water

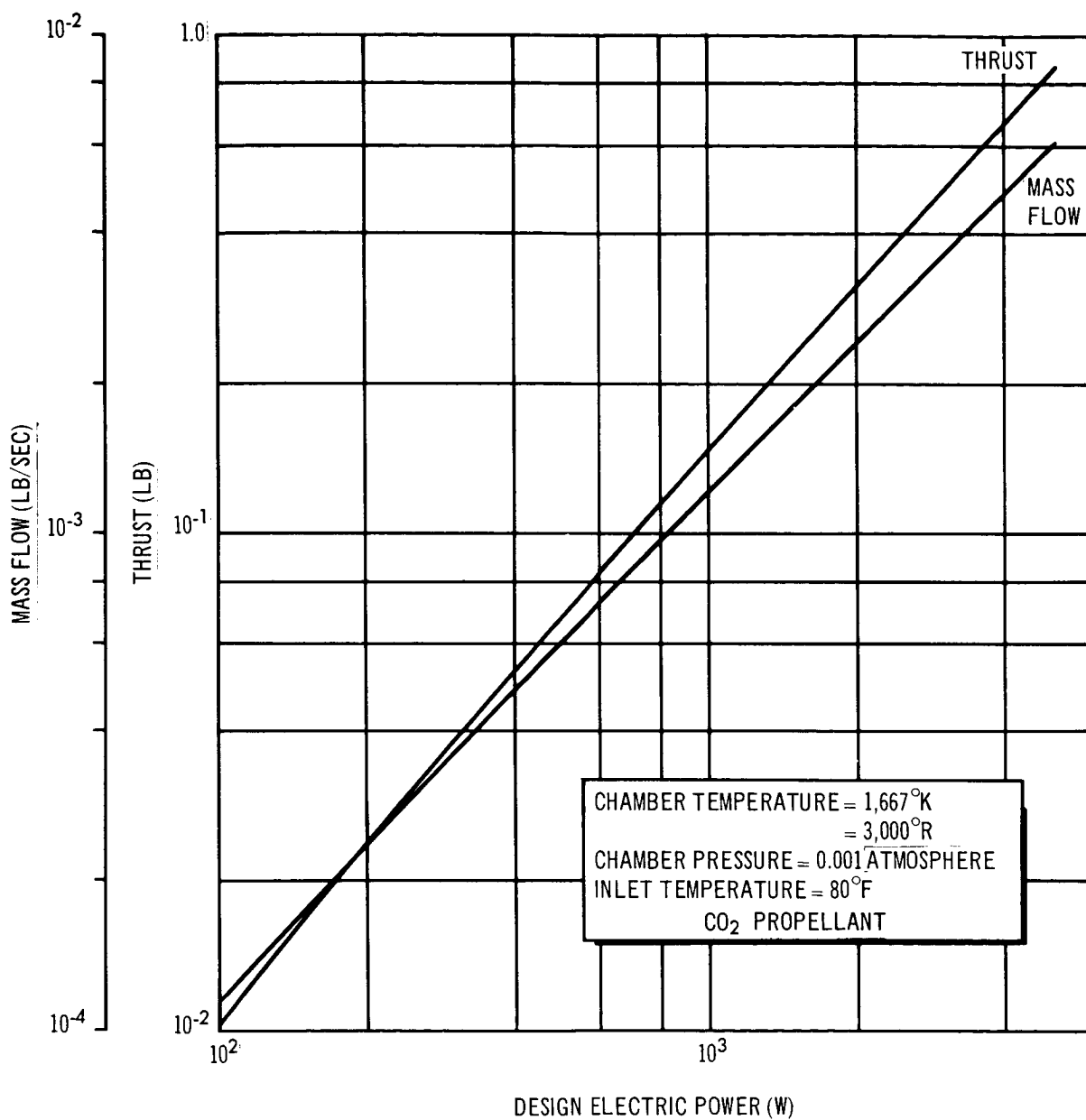


Figure 3-47. Resistojet Thrust and Propellant Flow Rate as a Function of Design Electric Power Level – Carbon Dioxide

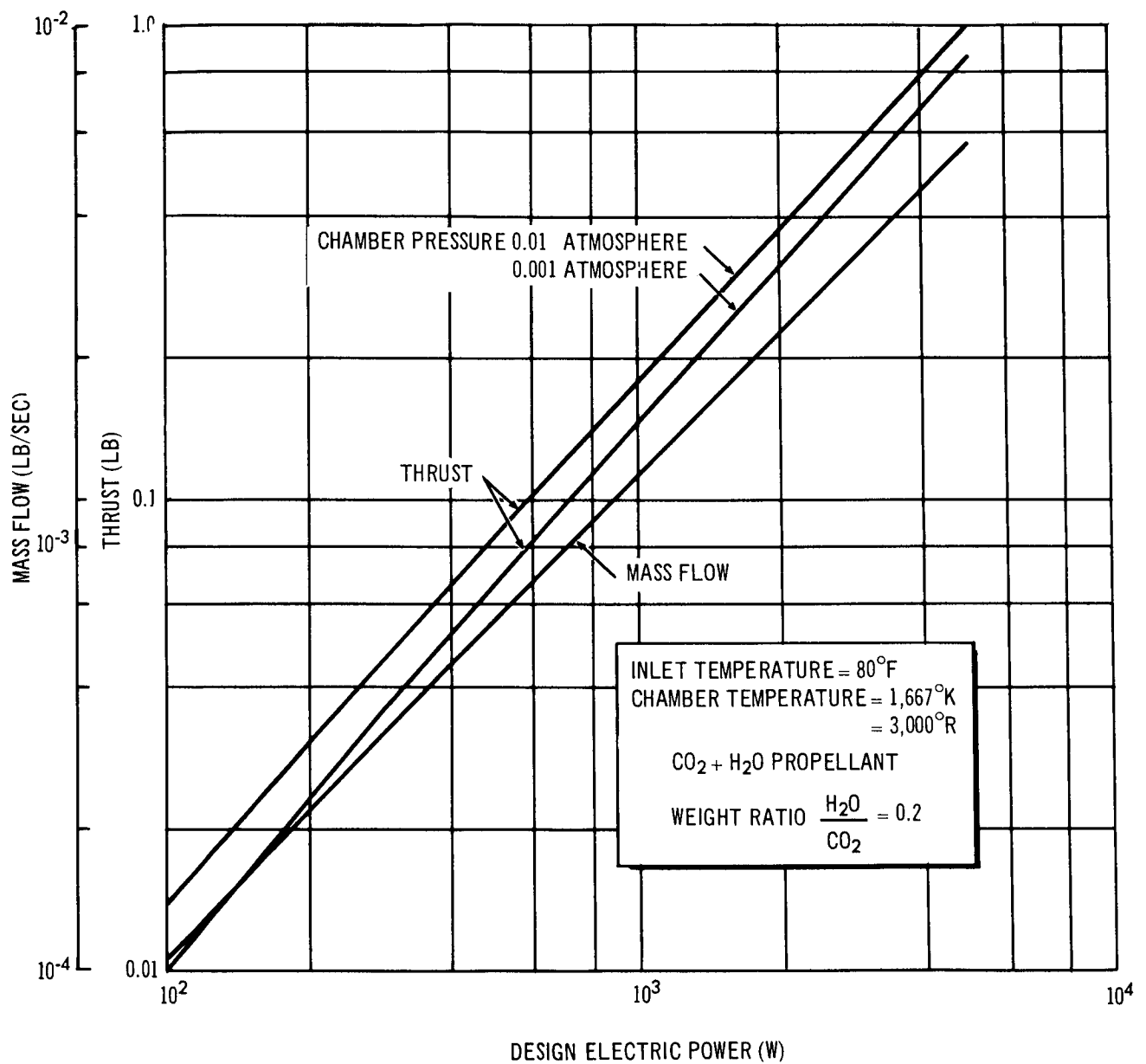


Figure 3-48. Resistojet Thrust and Propellant Flow Rate as a Function of Design Electric Power Level – Carbon Dioxide and Water

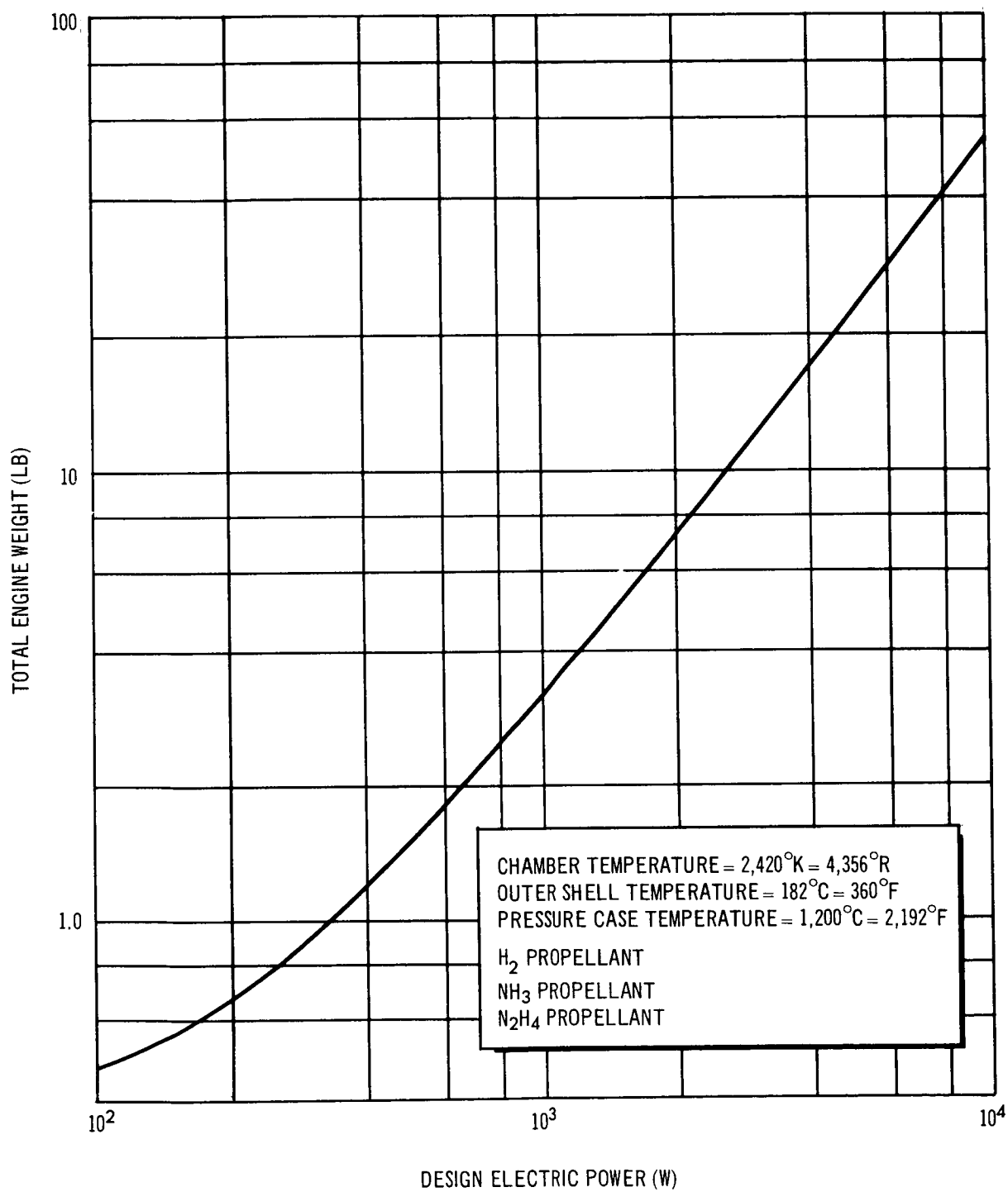


Figure 3-49. Total Engine Weight as a Function of Design Electric Power Level

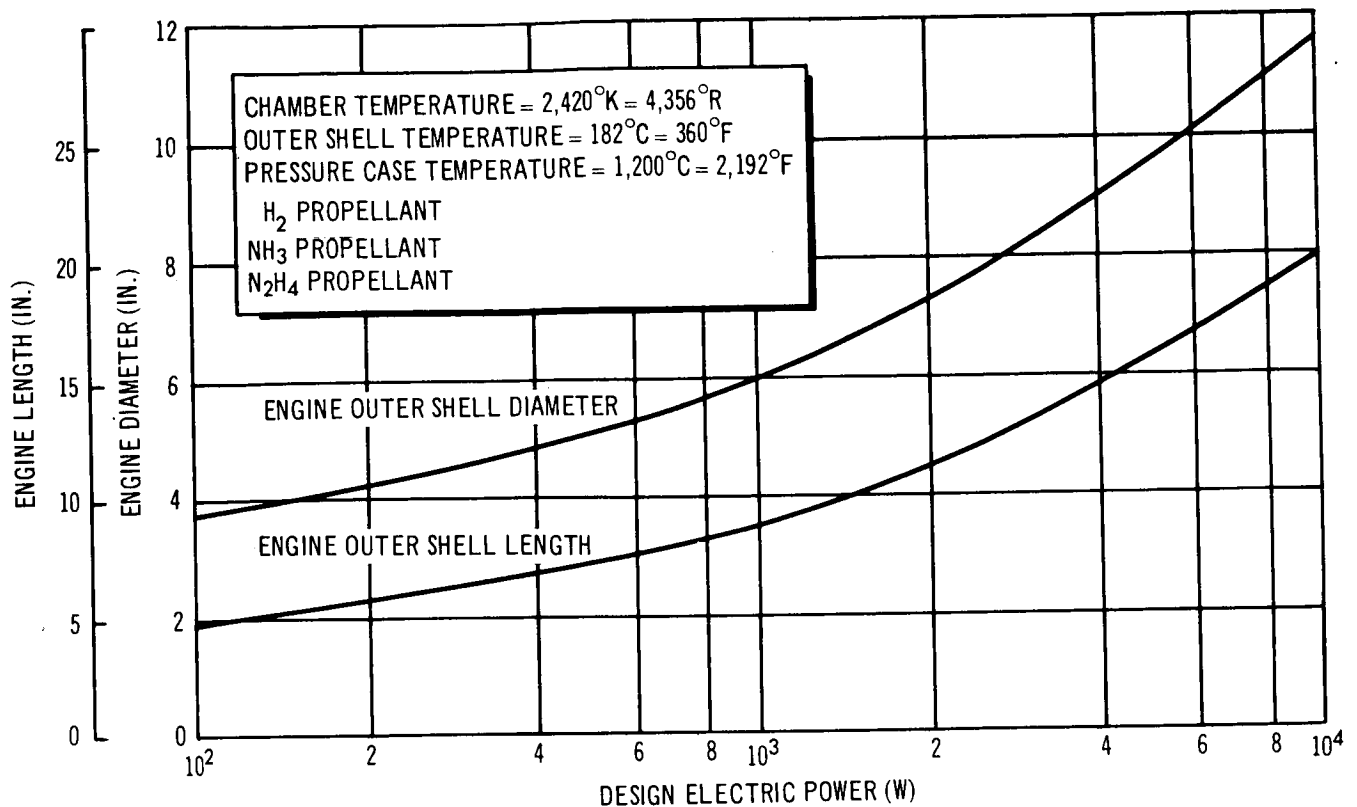


Figure 3-50. Engine Diameter as a Function of Design Electric Power Level

3.3.2.2 Ten-Millipound Resistojet Design

Figure 3-51 shows a layout of the 10 mlb thruster, designed for hydrogen, drawn approximately four times size. This design follows the construction philosophy of the concentric tubular 3-kW Resistojet as developed under the NASA Program of Reference 8 and is primarily a reduced scale version of that engine. Because of the small size of the 10-mlb thruster, however, some basic changes were necessary. To minimize the heat losses, it is desirable to make the engine as small as possible and still retain sufficient heat transfer area. To ensure optimum performance, the heat transfer area and heat transfer coefficient were found for the 3-kW Resistojet and applied to the following formula:

$$\frac{H \times A}{P_t} = K = \text{a constant}$$

where P_t is total power. The formula then determines the size of the 10-mlb engine heat exchanger and, hence, the engine. The unit will be made predominantly of tungsten or tungsten-rhenium, with boron nitride provided for

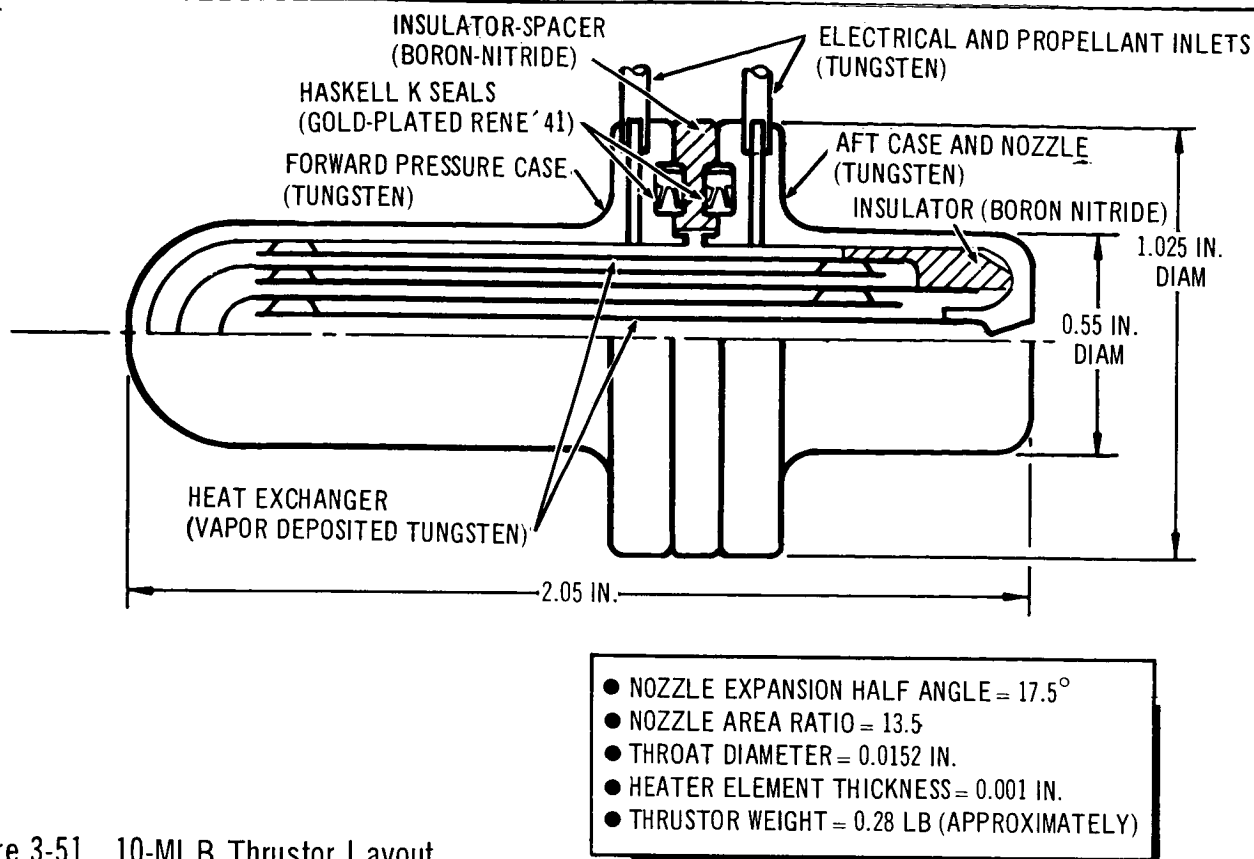


Figure 3-51. 10-MLB Thrustor Layout

electrical insulation. The heat exchanger concentric tubes will be fabricated by the tungsten vapor-deposition process and made to an element thickness of 0.004 in. as is shown. The cases will be machined or vapor deposited, and the nozzle shapes will be fabricated by Elox method. The forward and rear case will be held together by electrically insulated bolts (not shown).

3.3.2.3 High-Response Resistojet Design

Figure 3-52 shows the high-response Resistojet (HRR) concept. The advantages of this concept are as follows:

1. Low residence volume to facilitate high-pressure response.
2. Low thermal capacity to provide high-temperature response.
3. No high-temperature insulation is required in contact with the propellant gas.
4. The propellant heater and regenerative coil assembly are continuous and include no seals.
5. The voltage level may be set relatively independently of other limitations.
6. No pressure case is required. The interior of the thrustor, excluding the heater coils, is at space vacuum.

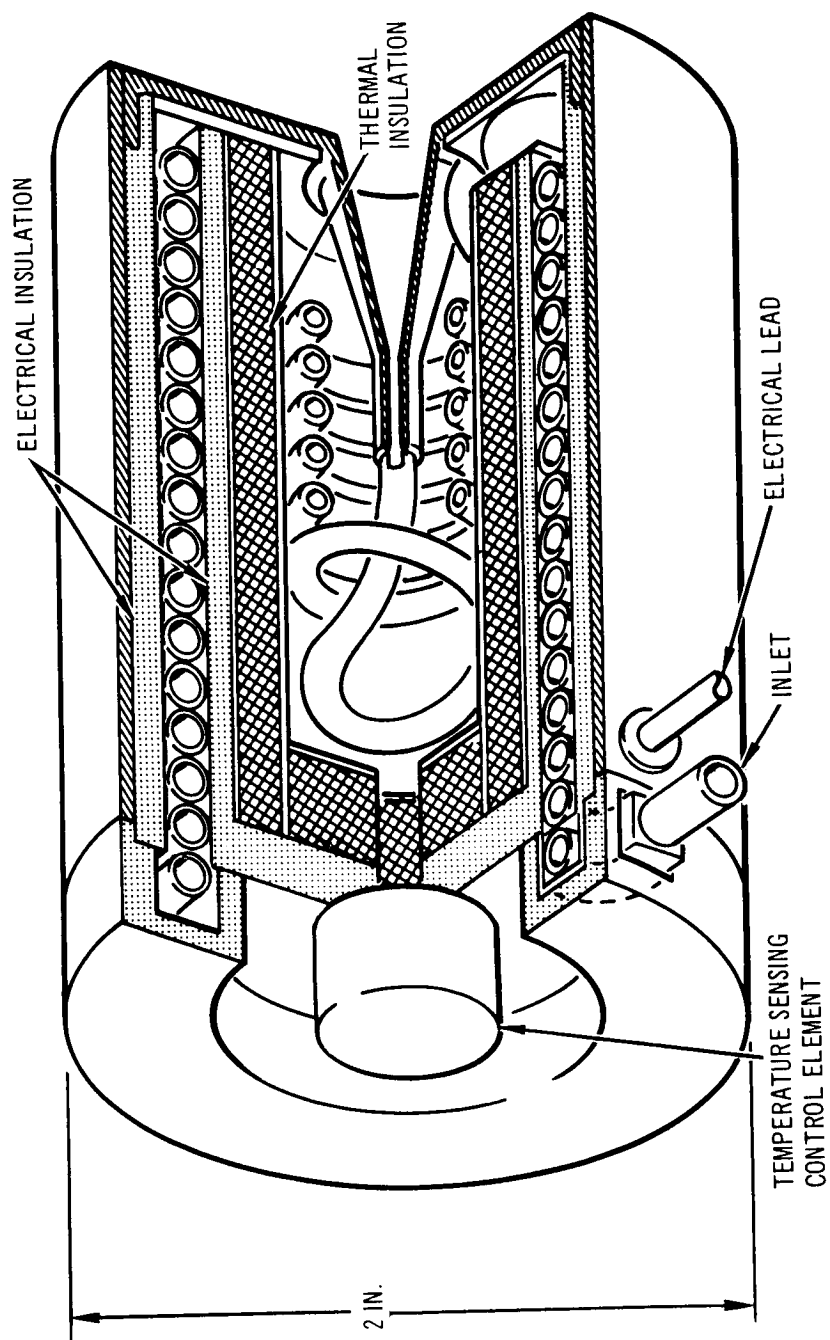


Figure 3-52. High Response Resistojet Concept

The propellant flow loop enters the regenerative molybdenum tubular coil. At the nozzle end, a tungsten-rhenium heater coil is joined by electron beam welding to form the highly resistant (for ohmic heating) heater loop. The heater loop is surrounded by electrical insulation to preclude lateral heater coil movement. The heater coil discharges into the de Laval nozzle. The electrical path parallels the gas path. The temperature-sensing control element is located at the rear of the thruster to monitor actual wall temperatures surrounding the nozzle entrance.

The concentric tubular Resistojet design is superior in steady-state performance to the high-response Resistojet concept in that it may operate at higher gas temperatures for the same life. This is true for two reasons: (1) the gas temperature approaches more closely the wall temperature in the case of the steady-state Resistojet and (2) the maximum temperatures may be limited on the HRR because of the exterior of the heater coil being exposed to a vacuum.

3.3.2.4 Off-Design Performance

The purpose of determining off-design performance is threefold: (1) to assist in the choice of system control variables; (2) to study the influence of unwanted variations of control variables on performance; and (3) to select the method of increased thrust potential under emergency conditions. The hydrogen engine for zero-g, belly-down, radioisotope case was chosen as an example. A design thrust of 8.9 mlb at an electric propulsive power input of 218 W was used. The conclusions reached here will be typical of the 9.8 mlb alternate Resistojet baseline engines used for hydrogen and ammonia.

The following cases are considered for the engine capable of being throttled under variable electric power: (1) constant specific impulse operation, for propellant economy; (2) constant maximum chamber temperature operation, as a physical limitation; and (3) constant chamber pressure operation for control simplicity and reliability.

Varying thrust at constant specific impulse is desirable. However, Figure 3-53 shows that this type of control results in a gas temperature which

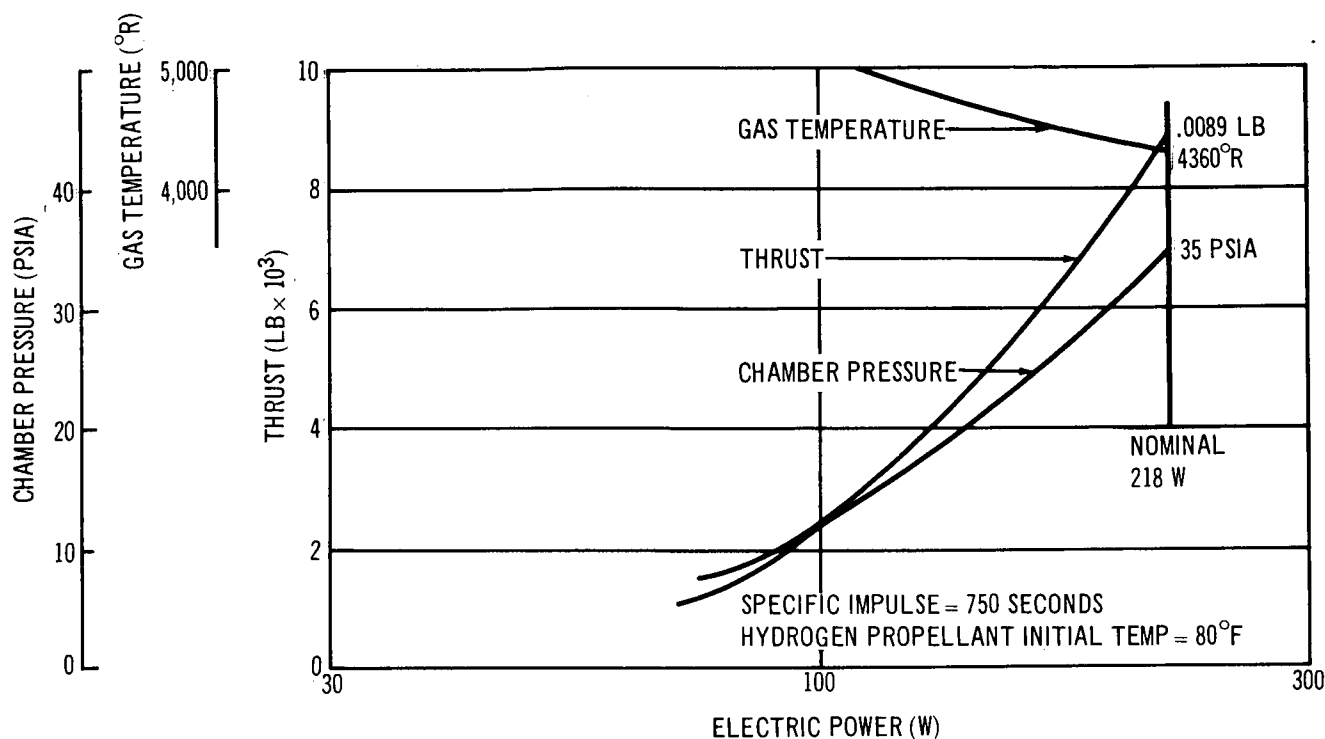


Figure 3-53. Resistojet Performance for Constant Specific Impulse

is greater than design. The requirement to reduce chamber pressure (to reduce flow) with electric power causes a decrease in nozzle efficiency. At half power, the chamber pressure is 13 psia for a thrust reduction to 31% of design. The gas temperature, however, had to be increased to 5,000°R to maintain constant specific impulse.

The second case considers an engine that can be throttled on the basis of constant gas temperature to overcome the problem of the previous example for thrust levels less than design. This is similar to the constant specific impulse operation and is really the most efficient method of reduced thrust operation although the control is not necessarily simple.

Constant chamber pressure operation and constant thrust operation at reduced electric power are almost synonymous. Figure 3-54 shows a constant thrust performance case. It should be noted that the required chamber pressure does not drop more than 4 psi from design to cold flow performance.

The cold flow (or zero electric power) performance is shown in Figure 3-55. The reason for the essentially one-to-one relation between thrust and chamber pressure is the following. As the gas temperature is reduced at constant

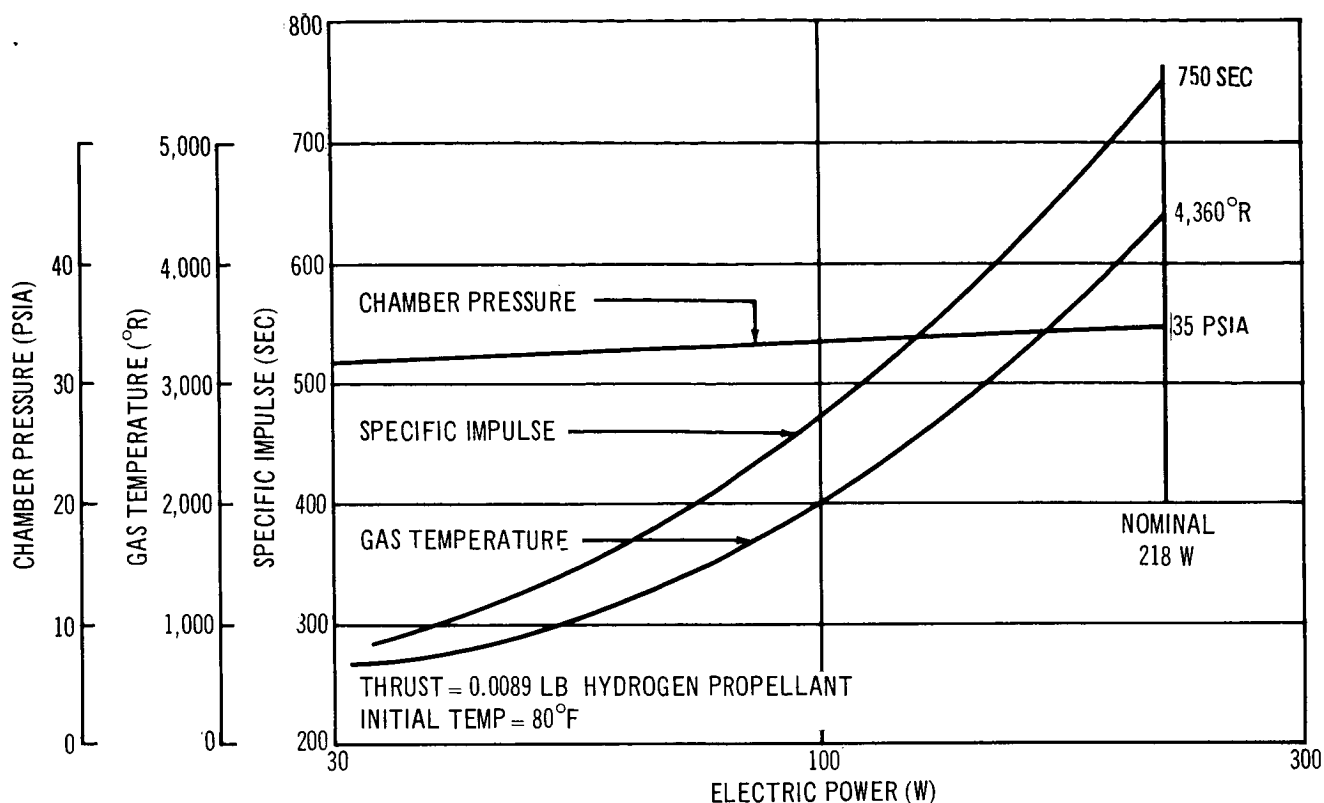


Figure 3-54. Resistojet Performance for Constant Thrust

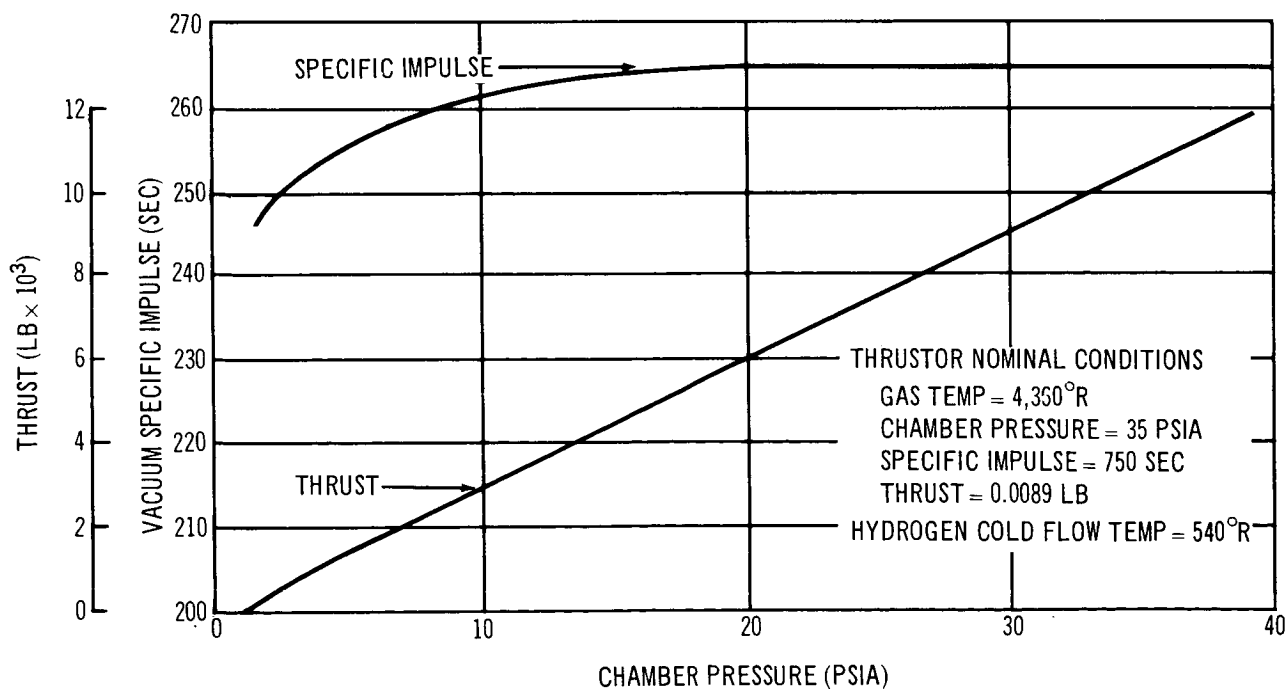


Figure 3-55. Resistojet Performance for Cold Flow

chamber pressure, the velocity or specific impulse is reduced essentially proportional to the square root of the absolute gas temperature. At the same time, however, propellant mass flow is increased approximately inversely proportional to the square root of temperature. The slight variation from proportions are real gas effects. Since thrust is proportional to the product of mass flow times velocity, it remains essentially constant.

Control sensitivity studies show that the constant chamber pressure controller produces essentially the performance shown in Figure 3-54 which is almost constant thrust independent of electric power level. This is useful to show the performance expected in the event of only partial power availability, either through a primary system failure or, for example, a single leg in the three-phase power feeder to an individual thruster becoming inoperative. It should be noted that such a failure does not interrupt thrust capability.

The cold flow performance as a function of pressure level is shown in Figure 3-55. Here the thrust is proportional to pressure and the specific impulse is constant. The specific impulse drops only slightly at the very low chamber pressures because viscous flow effects become more predominant.

In summary, the above off-design operation analysis shows that constant chamber pressure control is desired and that minor manual adjustment of thrust level may be accomplished by changing the chamber pressure and electric power proportionally. This latter, if desired, is effected by the intercoupling of a variable tap on the three-phase transformer in the power control with the pressure regulator through a dome-loading controller.

3.3.2.5 Thruster Life

The thruster life estimates are currently predicated on the sublimation rates of the tungsten heat-exchanger elements. Extensive life tests are required to establish this mechanism as the life-determining factor.

During engine operation, the heat-exchanger elements will be subjected to a pressure of 35 psia of hydrogen or a mixture of hydrogen and nitrogen, in the case of ammonia. This pressure, based upon Marquardt tests (Reference 13), strongly suppresses sublimation. The highest Resistojet

temperature encountered is $4,360^{\circ}\text{R}$ at the center element during thruster operation. The thermal control mode requires the central heat exchanger to be at a temperature of approximately $3,000^{\circ}\text{R}$, where the sublimation is trivial.

Based on the above, the sublimation of tungsten from the heat-exchanger elements is conservatively estimated at 2% of element thickness per year for the alternate baseline thruster size of 10 mlb. This produces a 2% increase in resistance and thus a 2% decrease in power, if the voltage is held constant and the engine temperature is reduced slightly. It should be noted, as previously shown, that the thrust level remains essentially constant. The change in performance may be accurately estimated from Section 3.3.2.4. The type of control was selected for simplicity and hence higher reliability.

3.3.2.6 Transient Response

The operating times required of the Resistojet thruster in the zero-g cases are so long that high-response capability is not a requirement. In the artificial-g case, however, operating periods are as short as 3.9 sec. Therefore, transient response must be considered for this application. The following is a study of the transient response of two Resistojet designs. The first is the concentric tubular type, specifically the Marquardt 3-kW unit developed under NASA contract. This design is referred to as the steady-state Resistojet (SSR). This type of design is discussed in Section 3.3.2.2. The second is the high-response design (HRR) described in Section 3.3.2.3. A 3-kW, $4,360^{\circ}\text{R}$ and 129 psia hydrogen Resistojet, typical of the MORL precession engine, P_1 or P_3 , was selected for analysis.

Pneumatic Response

Both filling and emptying of the thruster chambers of a high-response Resistojet (HRR) and the concentric-tubular (SSR) Resistojet are considered as first-order processes. Second-order effects, such as shock tube phenomenon during the start of the filling transient for an evacuated thruster and the viscous effects for the transient analysis from which chamber response is calculated, are not considered. Viscous effects are included with respect to nozzle efficiency and specific impulse.

Time constants are estimated to be of the order of 1 msec for the high-response Resistojet and of the order of 1 sec for the 3-kW concentric tubular Resistojet. For actual pulse widths as small as about 3 msec, an effective specific impulse of 750 sec or greater is predicted for the high-response Resistojet. For the concentric-tubular Resistojet, actual pulse width can be decreased to about 1 sec for an effective specific impulse of 750 sec. Ninety-nine percent of steady-state specific impulse is realized for actual pulse widths of about 2 msec and 7 sec, respectively, for the high-response and concentric-tubular Resistojets. In the limit of very small pulse widths, an effective specific impulse of 440 sec is realized in the latter case.

Time constants for ammonia Resistojets at a gas temperature of 4,360°R are about 1.6 times those for the hydrogen Resistojets with effective specific impulse varying between 200 and 410 sec (from very short to long pulse widths).

A quantitative comparison of bipropellant engine thrust response to the thrust response of Resistojets suggests considerably less noise and vibration would be emitted by Resistojet thrustors. In addition, modified flow controllers could permit very gradual thrust buildup and decays in Resistojet thrustors.

The Resistojet is considered to be a pressure divider (a volume between two choked nozzles) during the filling process. For the emptying process, only the exhaust nozzle is considered to be flowing. It is assumed that the thrustor volume can be divided into a cold and hot volume with an instantaneous heat release at the division plane. The ratio of cold to hot volume V_C/V_H is left to an empirical fit not yet performed. Values of 1 and 0.1 for V_C/V_H , respectively, for filling and emptying, are assumed for the calculations made here in this preliminary study.

A throat diameter of 0.029 in. equivalent to that of the Resistojet of Reference 8 is used with a discharge coefficient varying with Reynolds number, as shown in Figure 3-56. Total chamber volumes of 0.0274 cu in. and 11.2 cu in., respectively, are assumed for the HRR and the SSR.

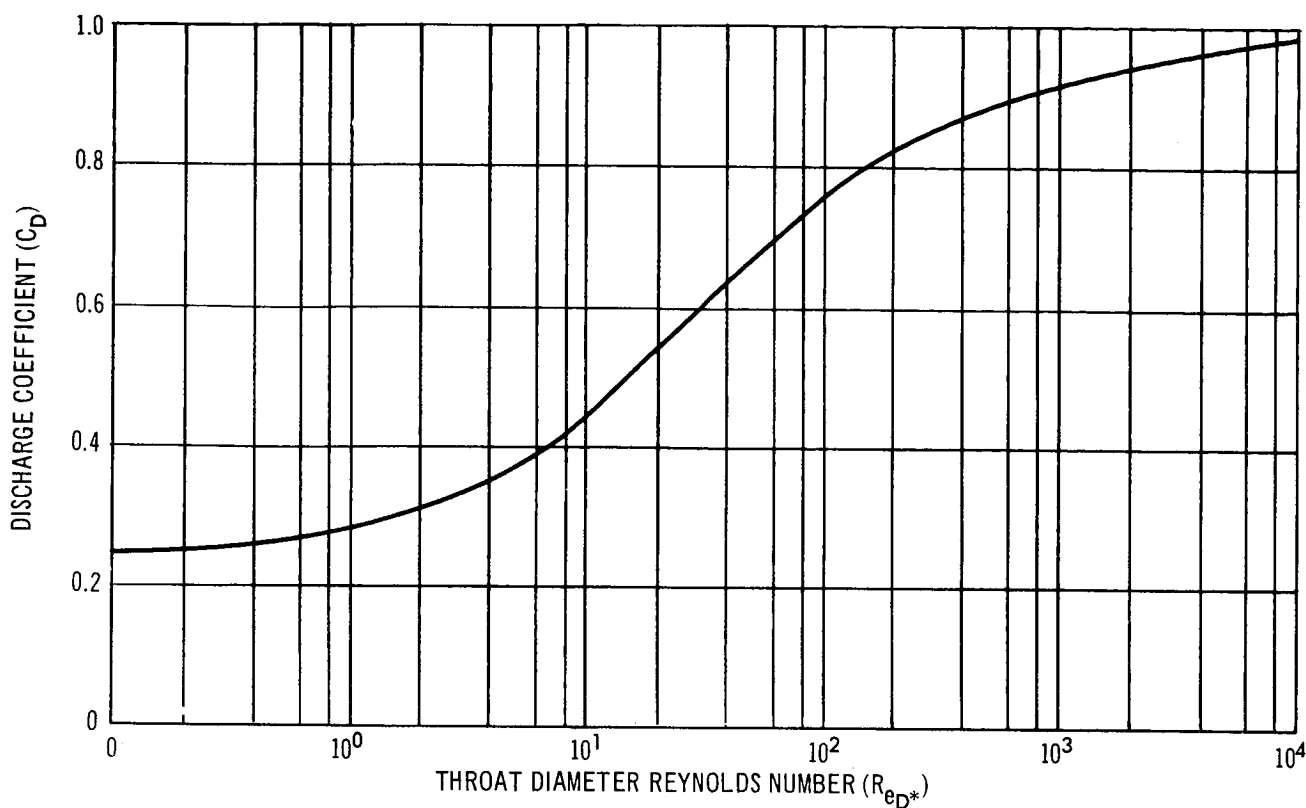


Figure 3-56. 3kW Resistojet Discharge Coefficient

Chamber pressure during the filling process is

$$P_{C_t} = P_{C_\infty} (1 - e^{-t/\tau_F})$$

where

P_{C_t} = the chamber pressure at time, t

P_{C_∞} = the steady-state chamber pressure

τ_F = the filling time constant

For the emptying process

$$P_{C_t} = P_{C_o} e^{-t/\tau_E}$$

where

P_{C_o} = the chamber pressure existing at the beginning of the emptying (closing of the propellant inlet nozzle)

τ_E = the time constant for the emptying process

Time constant (time to 63.2% of steady-state value) based on an initial propellant temperature of 540°R and a final gas temperature of 4,360°R are shown in Table 3-25.

Table 3-25
3 kW RESISTOJET TIME CONSTANTS

Thruster	HHR	SSR
τ_F , sec	0.0022	0.925
τ_E , sec	0.00082	0.331

The pressure ratios, P_{C_t}/P_{C_∞} and P_{C_t}/P_{C_0} for the filling and emptying processes are plotted in Figures 3-57 and 3-58 for the HHR and SSR, respectively. Emptying occurs in less than one-half the filling time. This is the direct result of the choice of V_C/V_H for each process and remains to be

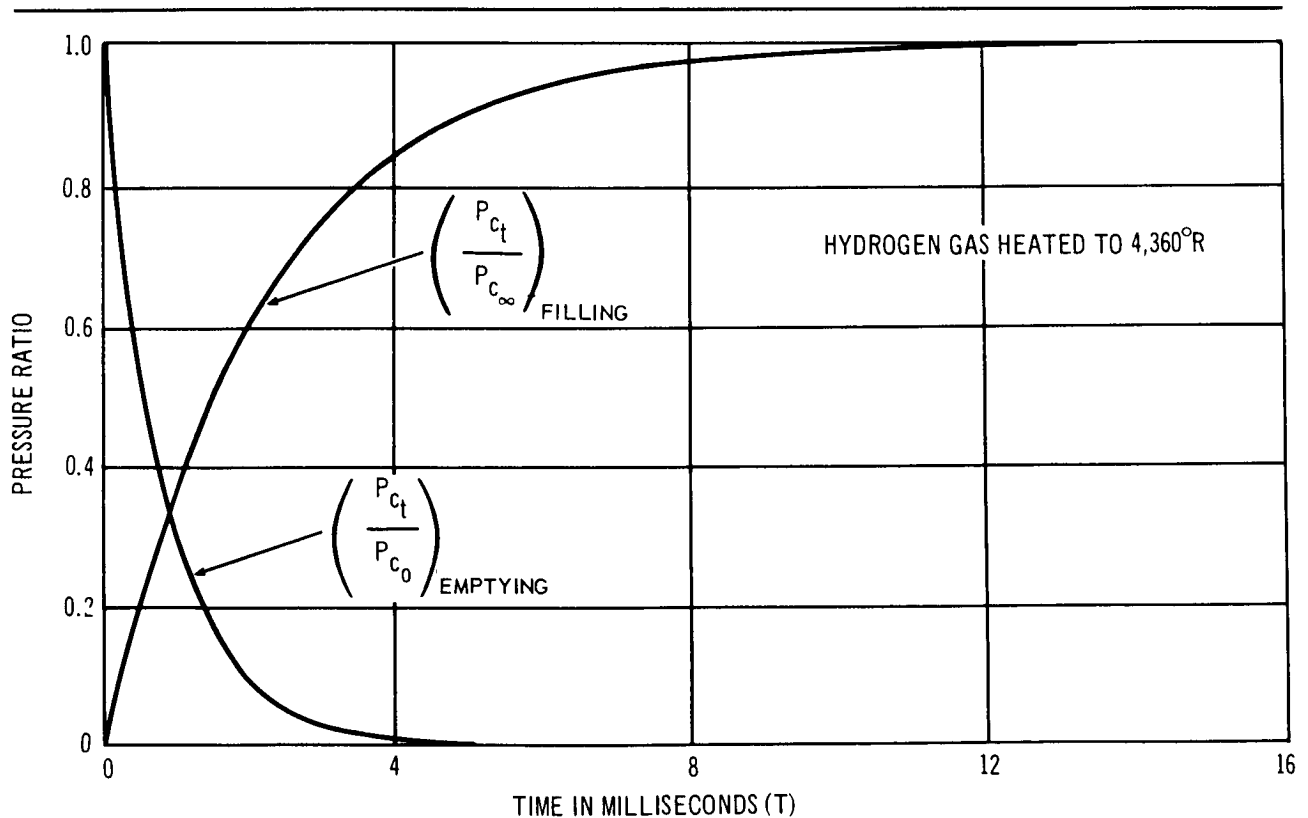


Figure 3-57. High Response Resistojet Chamber Pressure Time Response

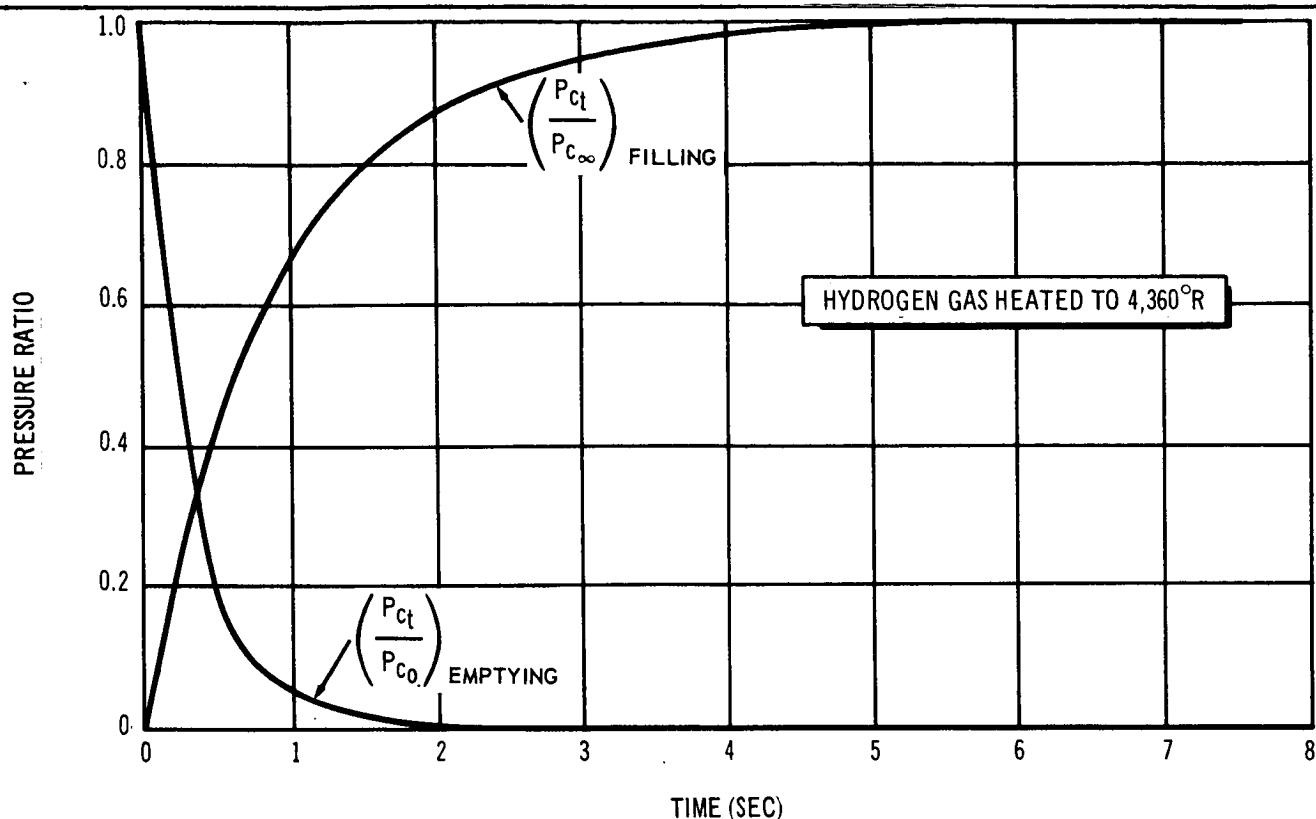


Figure 3-58. Steady State Resistojet Chamber Pressure Time Response

verified. With respect to the gas temperature distribution within the Resistojet, the emptying time constant would seem reasonable. However, it appears that the filling time constant is conservative, that is, longer than realistic.

Using the Resistojet of Reference 8 as a reference case, specific impulse changes with chamber pressure were estimated and are presented in Figure 3-59. Nozzle expansion, divergence, and thermal efficiencies were considered constants as follows:

$$\eta_E = 0.942$$

$$\eta_D = 0.96$$

$$\eta_T = 1.0$$

Then, specific impulse was calculated from using the procedures of Section 3.3

From Figures 3-57 and 3-58, the chamber pressure is found as a function of time, and mass flow rate, \dot{m} , is calculated for the chamber pressure

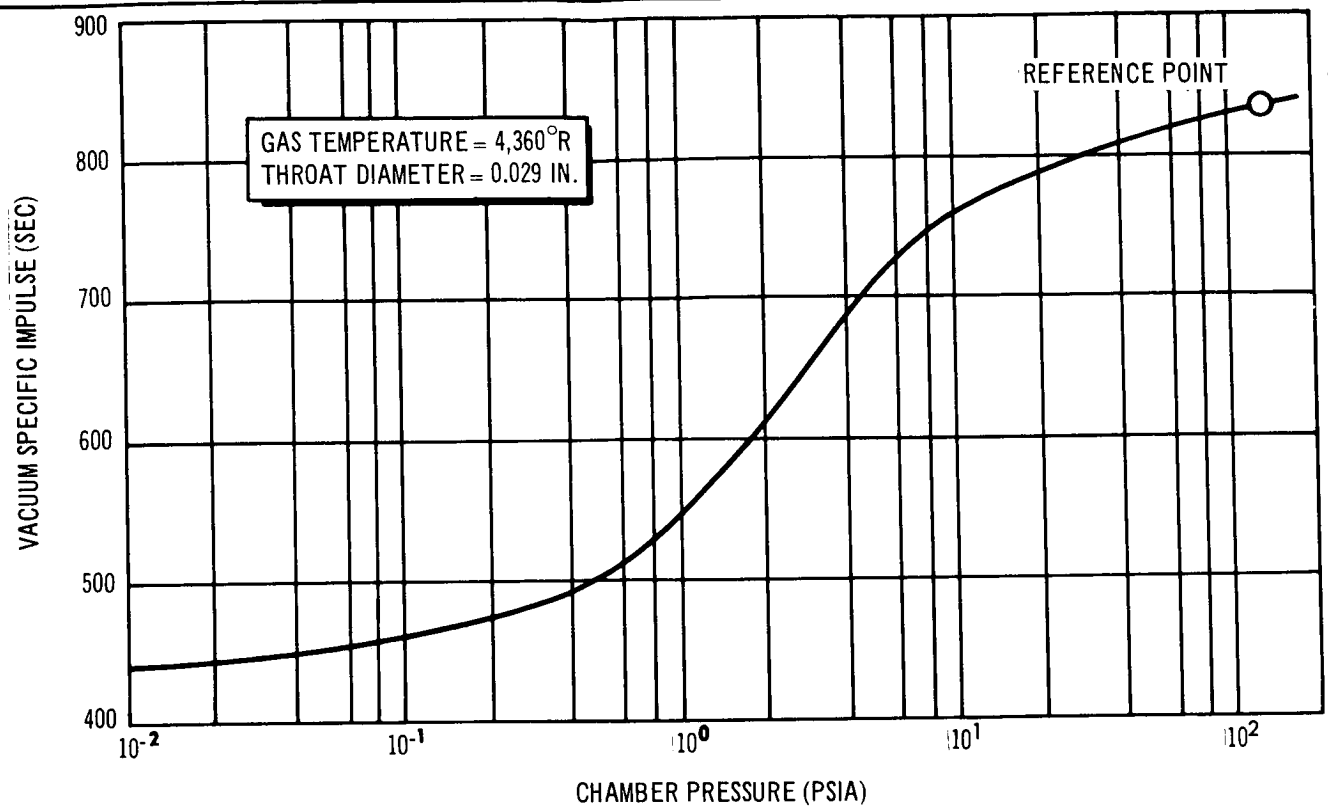


Figure 3-59. Hydrogen Resistojet Specific Impulse

and a gas temperature of 4,360°R. Specific impulse, I_{sp} , is found from Figure 3-59 and thrust is $\dot{m} I_{sp}$.

Figure 3-60 indicates how thrust varies for a Resistojet. Due to valve opening and fluid transport lag, thrust does not develop immediately following command signal initiation ($t = 0$). This time delay increment is typically of the order of 3 msec. Following this delay, thrust builds up rapidly at first and levels out at the steady-state thrust with a value of F_o . Thrust rise time response is defined as shown in Figure 3-60 for 90% of steady-state thrust.

A valve-closing delay and fluid transport lag occurs at the termination of the command signal. This delay is typically of the order of 3 msec. Thrust decay time is the increment of time shown in Figure 3-60 for a 90% decrease in the steady-state thrust.

The actual pulse width is taken from beginning of the thrust curve to the effective end. Figures 3-61 and 3-62 compare the effective specific impulse, $I_{sp_{eff}}$, and the impulse bit size, $F_o \bar{\Delta}t$, for the HRR and SSR. The effective specific impulse is given by

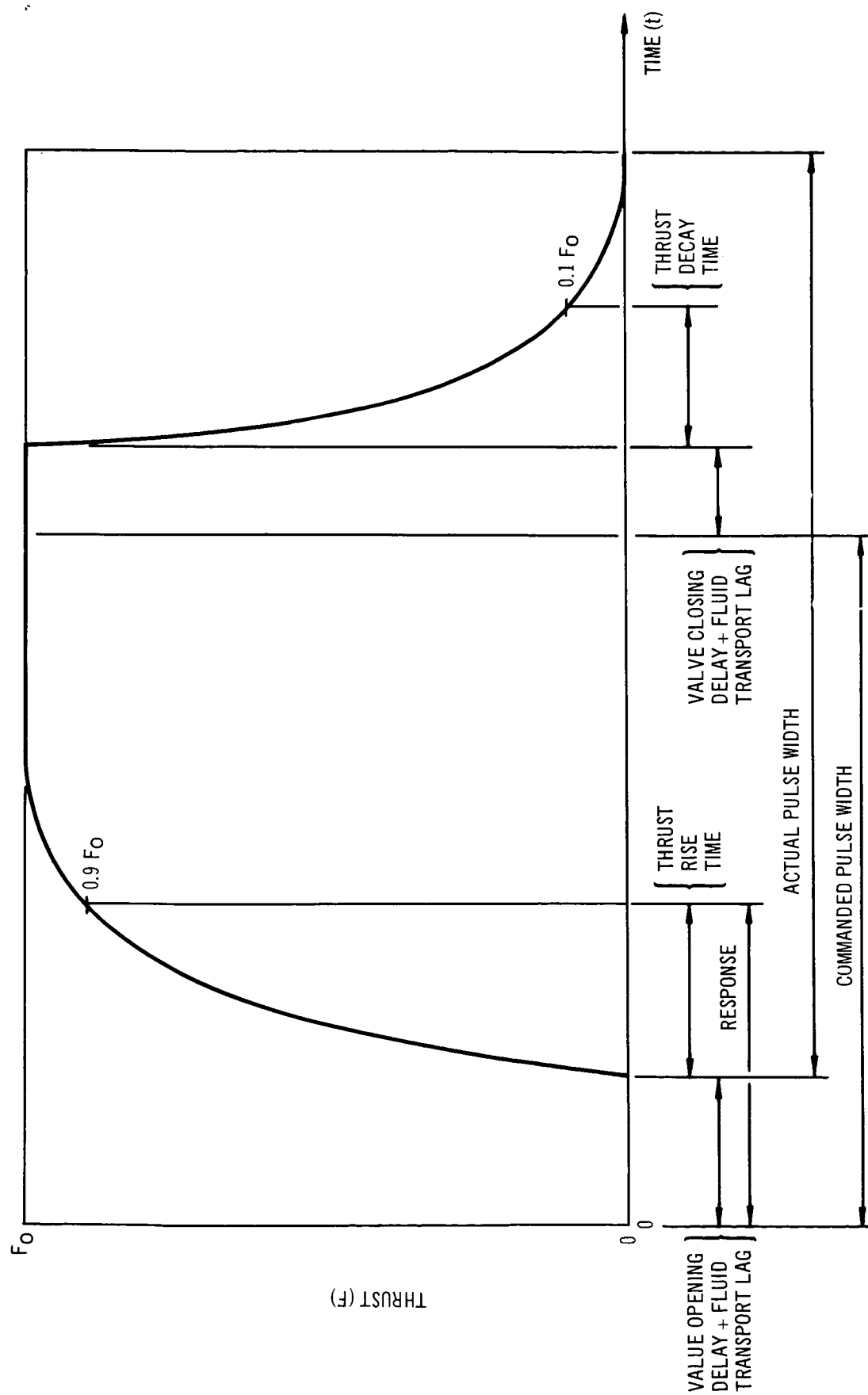


Figure 3-60. Resistojet Thrust Response

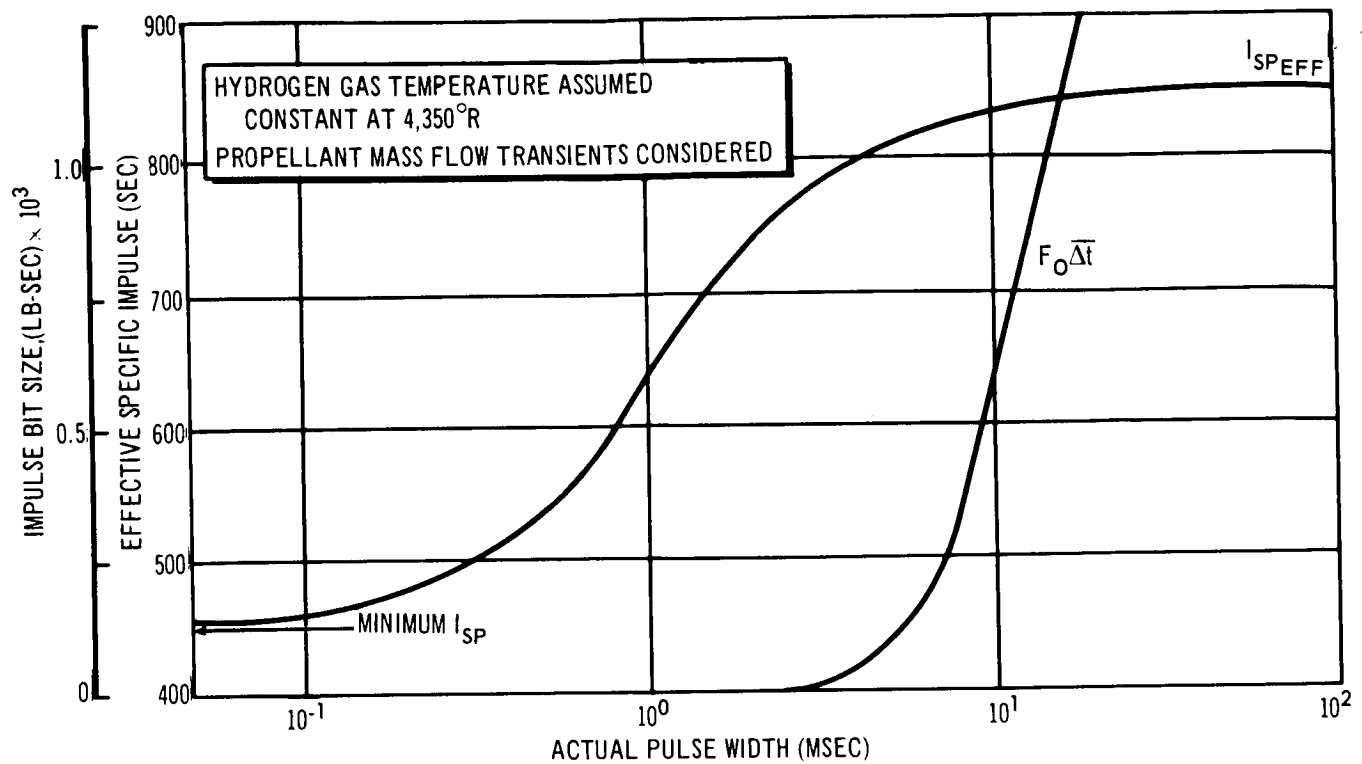


Figure 3-61. Estimated Transient Performance of High Response Resistojet 3kW

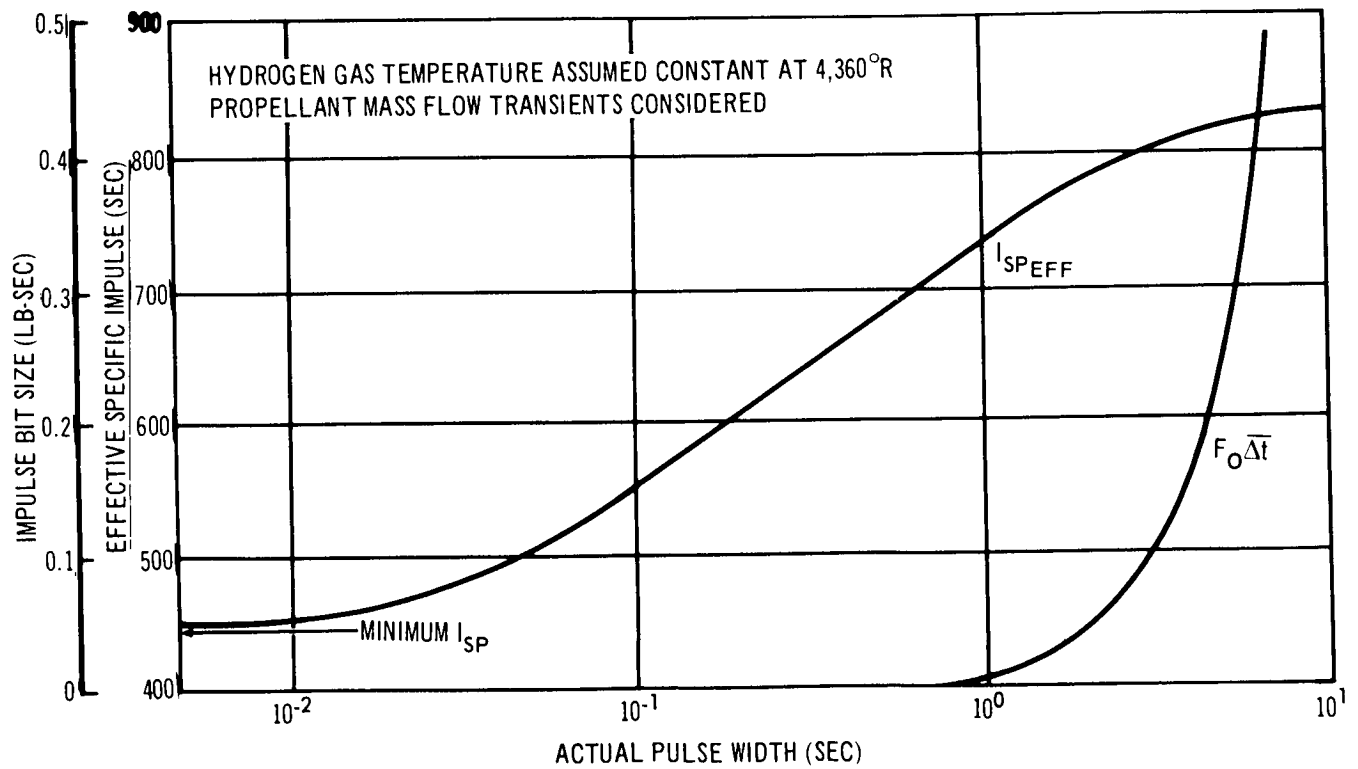


Figure 3-62. Estimated Transient Performance of Steady-State Resistojet 3kW

$$I_{sp_{eff}} = \frac{\int_0^t F dt}{\int_0^t \dot{m} dt}$$

and the impulse bit size by

$$F_o t = \int_0^t F dt$$

Therefore, the effective specific impulse becomes

$$I_{sp_{eff}} = \frac{F_o \bar{\Delta} t}{\Delta m}$$

where Δm = the amount of propellant consumed during the pulse. $\bar{\Delta} t$ = the effective pulse width and can be obtained by dividing $F_o \bar{\Delta} t$ by F_o which is 0.1467 lb. The effective square impulse bit, $F_o \bar{\Delta} t$, is the area under the curve of thrust as a function of time in Figure 3-60. Similarly, the propellant consumed is the area under a mass flow rate as a function of time plot. These graphical integrations were performed for several actual pulse widths (4, 6, and 14 msec for the HRR and 1.5, 2.5, and 5.7 sec for the SSR) to arrive at Figures 3-61 and 3-62. These actual pulse widths correspond to effectively filling to a chamber pressure of 40, 80, and 128 psia, respectively. At these fill points, the inlet valve is closed, and the emptying process follows. The emptying curves of Figures 3-57 and 3-58 apply with P_{C_o} equal to 40, 80, and 128 psia, respectively. A steady-state chamber pressure of 129 psia is used for all cases.

It should be noted that in the limit of the smallest conceivable impulse bit with 4,360°R hydrogen, a minimum specific impulse of 440 sec is guaranteed. This is the limiting specific impulse considering the gas leaving as free molecules.

A chamber pressure of 35 psia was selected for hydrogen Resistojets. At a 3-kW power level, a steady-state specific impulse of 829 sec (compare with 838 sec for the 129-psia reference point of Figure 3-59) is possible for a chamber pressure of 35 psia and gas temperature of 4,360°R. This curve of specific impulse as a function of chamber pressure would converge with the

curve on Figure 3-59 from 829 sec at 35 psia to 440 sec at 10^{-2} psia. The effect on the transient analysis would be small. A conservative correction on the effective specific impulse during pulsing would be a factor of $829/838 = 0.99$ applied to $I_{sp_{eff}}$ of Figures 3-61 and 3-62.

Ammonia propellant was considered as well as hydrogen. The time constant with ammonia is 1.6 times the time constant of hydrogen. This value is based on chamber pressures of 3 atm and 35 psia, respectively, for the NH_3 and H_2 Resistojets and a power level of 3 kWe. The effective specific impulse for an ammonia Resistojet would be about 410 sec for long pulse widths (longer than approximately 160 msec for the HRR and 16 sec for the SSR). For very short pulse widths, $I_{sp_{eff}}$ would approach a minimum value of 200 sec. S-curves similar to those shown in Figures 3-61 and 3-62 for the $I_{sp_{eff}}$ of hydrogen would extend from 200 to 410 sec for ammonia with 1.6 times the actual pulse widths shown.

In Figure 3-60 the Resistojet thrust buildup follows a first-order system response. In contrast, a bipropellant rocket thrust buildup can be represented (Figure 3-63A) by an under-damped second-order system for which a substantial thrust overshoot occurs (immediately following ignition) followed by damped oscillations. Noise and vibrations from the Resistojet thrustors (Figure 3-63B) would be considerably lessened over the noise and vibration from bipropellant thrustors. For manned space vehicles, where vibration from RCS thrustors may be a critical factor, thrust buildup and decay can be smoothed in the Resistojet (for example, Figure 3-63C) to any desired extent through modifications in a propellant flow controller. For instance, rather than the first-order filling and emptying curves depicted in Figure 3-60, more gradual S-shaped curves of thrust as a function of time would be possible (Figure 3-63C).

Thermal Response

Because of the large thermal capacitance associated with the concentric tube Resistojet, it is necessary to maintain nearly a constant temperature at all times in the thrustor module. However, in spite of the thermal storage design there are thermal transients. That is, the heater element

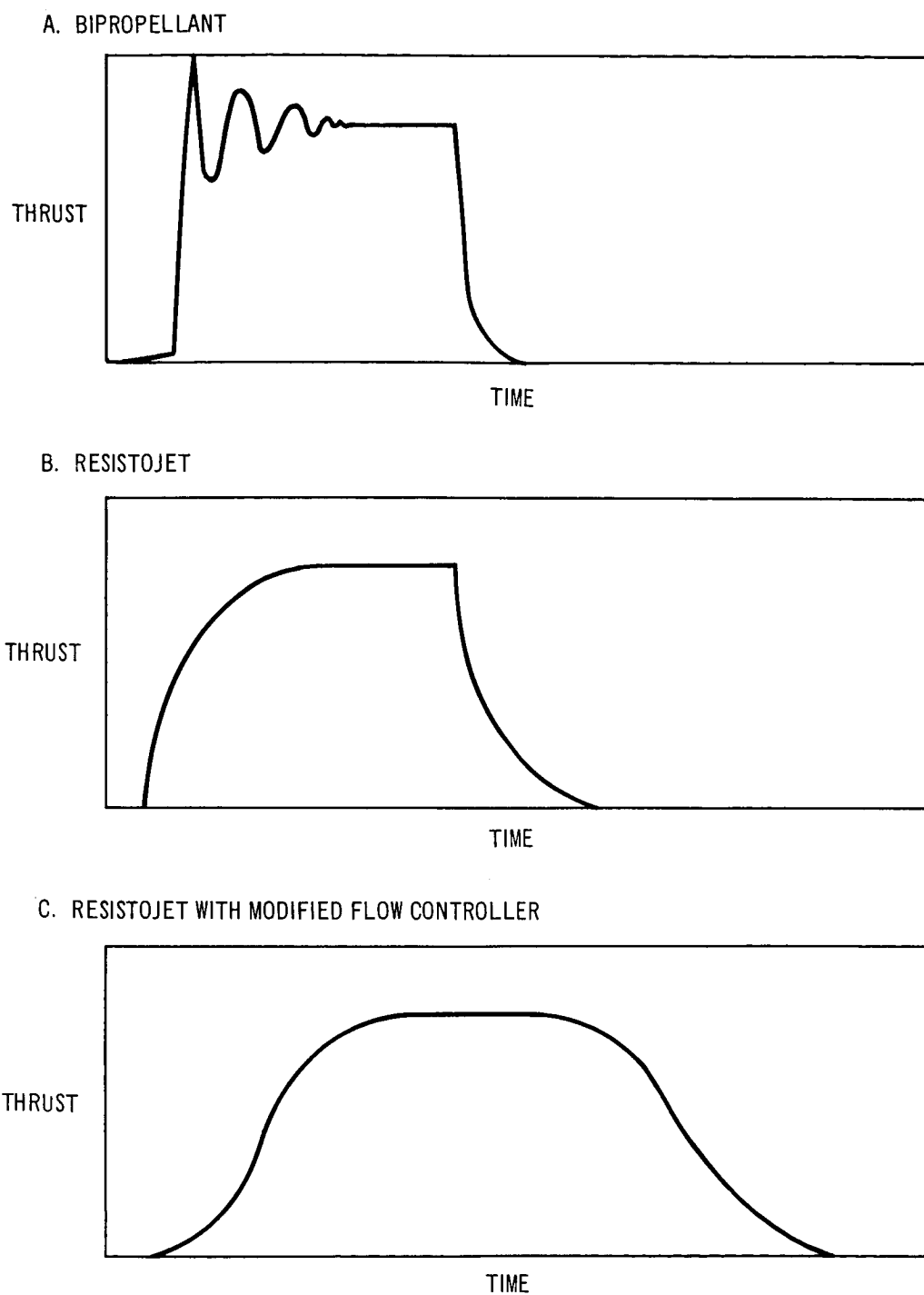


Figure 3-63. Typical RCS Thrust Response

temperature distribution is relatively uniform when shut down; however, it involves strong temperature gradients under operation with the propellant flowing. Since the heater element constitutes a small mass, its thermal inventory is small, requiring approximately 15 sec with the 10-mlb engine to heat to operating temperature. Realistically, times of the order of 1 min. may be required for the heater element to come to full temperature. Because the firing times are large, this is not considered a serious limitation in the zero-g operating mode.

The HRR is designed to minimize the thermal capacity of the engine and thus, to increase the response time. This engine will probably be required for the artificial-g vehicles.

3.3.3 Reaction Control System Description

The Resistojet reaction control system consists of the elements shown in Figure 3-64. The biowaste propulsion system is described in Figure 3-65. The differences are primarily concerned with the propellant pressurization and intermediate storage considerations. Thrustor locations for the various modes are shown in Figures 3-34 and 3-38.

Figure 3-64 is typical of the zero-g configuration. Its extension to the artificial-g case is evident. The propellant feed system is pressure-regulated and subsequently flow-controlled. The pitch module set is shown in Figure 3-64. Dual propellant feeders, also serving as electrical terminals, were used for each Resistojet.

The electric power adapter shown conditions the electric power to its proper voltage level and waveform for the case considered. The power was considered to be metered before switching it to a thrustor. An enthalpy (in effect, temperature) level controller sensing flow and power and controlling flow rate was used. This system was later simplified to use a fixed engine voltage (manually adjustable) and pressure regulator as described in Section 5. The important system operating parameters and weights are summarized for each propellant and condition in Tables 3-26 and 3-27.

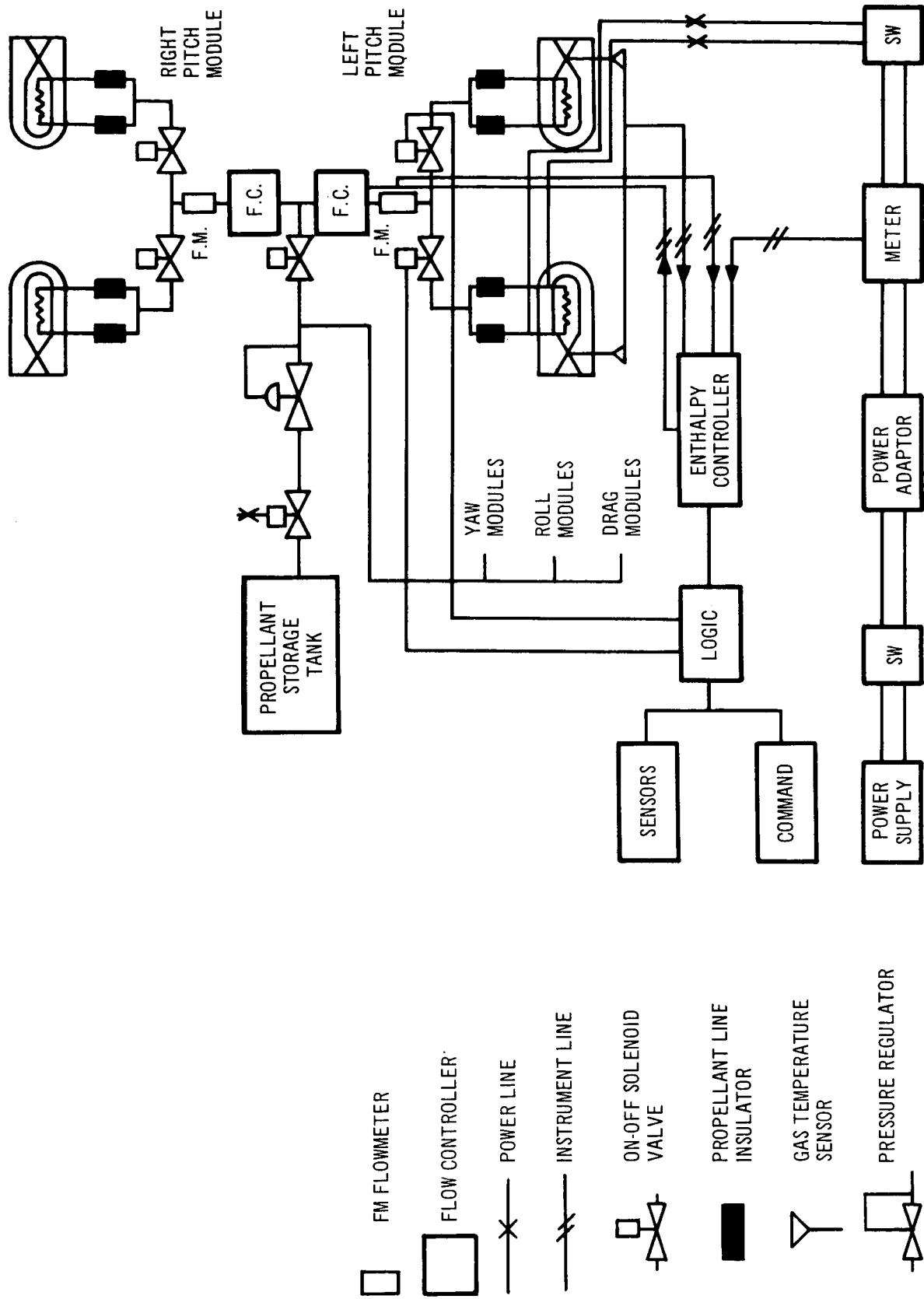


Figure 3-64. RCS Schematic

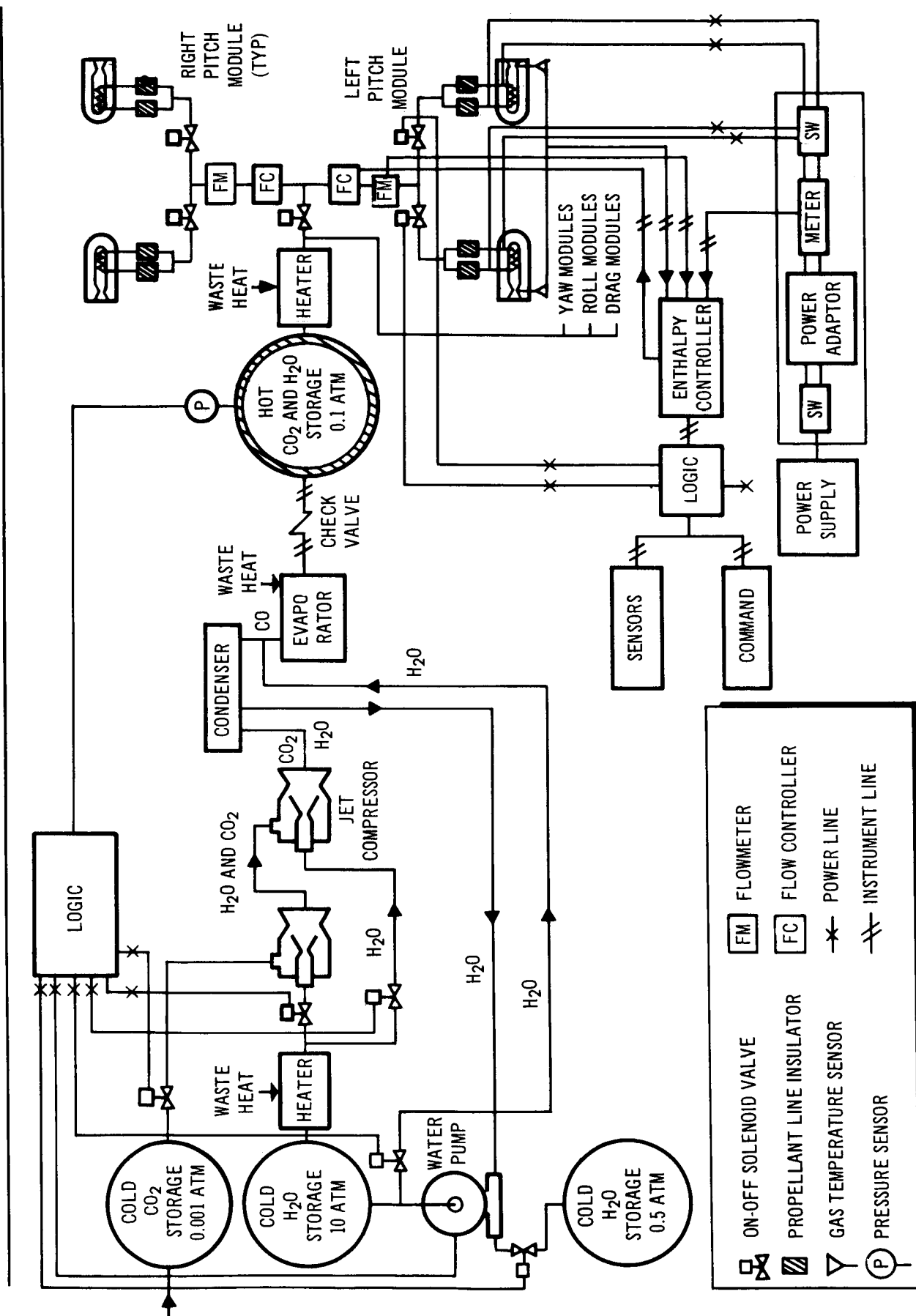


Figure 3-65. Biowaste RCS Schematic

Table 3-26
PRELIMINARY DESIGN SUMMARY
(ZERO-G MODE--LOCAL HORIZONTAL ORIENTED)

Design Characteristics	Solar Panel (500 lb/kWe)				Isotope Brayton (300 lb/kWe)			
	H ₂	NH ₃	N ₂ H ₄	H ₂ O and CO ₂	H ₂	NH ₃	N ₂ H ₄	H ₂ O and CO ₂
Average electric power (W)	1,149	734	412	356	574	379	231	195
Average total mass flow ($\dot{w} \times 10^4$ lb/sec)	0.52	1.04	1.14	2.935	0.236	0.474	0.522	1.44
Thrustor chamber pressure (psia)	35	44.1	44.1	0.147	35	44.1	44.1	0.147
Thrustor chamber temperature (°R)	4,360	4,360	4,360	3,000	4,360	4,360	4,360	3,000
Propellant storage pressure (psia)	50	80	250	-	50	80	250	-
Propellant storage temperature (°R)	45.7	504	530	530	45.7	504	530	530
Thrusts/engine (lb)	0.0201	0.0201	0.0201	0.0201	0.0089	0.0089	0.0089	0.0089
Propulsive power/engine (W)	457	288	151	138	216	137	73.53	68
Specific impulse (sec)	777.6	388.1	353.8	134.7	750.7	375.3	344	124

Table 3-27
PRELIMINARY DESIGN SUMMARY
(ARTIFICIAL-G MODE--SPIN AXIS SUN ORIENTED)

Design Characteristics	Solar Panel (500 lb/kWe)				Isotope Brayton (300 lb/kWe)			
	H ₂	NH ₃	N ₂ H ₄	H ₂	NH ₃	N ₂ H ₄	N ₂ H ₄	
Average electric power (W)	3,399	2,150	1,138	2,829	1,814		962	
Average total mass flow rate ($\dot{w} \times 10^4$ lb/sec)	1.82	3.58	3.99	1.47	2.96		3.29	
Thruster chamber pressure (psia)	35	44.1	44.1	35	44.1		44.1	
Thruster chamber temperature (°R)	4,360	4,360	4,360	4,360	4,360		4,360	
Propellant storage pressure (psia)	50	80	250	50	80		250	
Propellant storage temperature (°R)	45.7	504	530	45.7	504		530	
Thrusts/engine(lb)								
Precession (P ₁ , P ₃)	0.164	0.164	0.164	0.1312	0.1312		0.1312	
Drag (D ₁₁ , D ₉)	0.1349	0.1349	0.1349	0.1134	0.1134		0.1134	
(D ₂ , D ₄)	0.1108	0.1108	0.1108	0.0931	0.0931		0.0931	
(D ₁ , D ₃)	0.0241	0.0241	0.0241	0.0203	0.0203		0.0203	
Propulsive power/engine (W)								
Precession (P ₁ , P ₃)	3,360	2,120	1,100	2,720	1,710		890	
Drag (D ₁₁ , D ₉)	2,800	1,740	910	2,370	1,480		770	
(D ₂ , D ₄)	2,300	1,460	755	1,940	1,225		632	
(D ₁ , D ₃)	540	338	178	462	290		152	
Specific impulse (sec)								
Precession (P ₁ , P ₃)	825.8	409.5	366.5	822.3	408.6		366.1	
Drag (D ₁₁ , D ₉)	822.7	408.6	366.2	819.8	407.5		365.8	
(D ₂ , D ₄)	819.4	407.3	365.8	816.3	406		365.3	
(D ₁ , D ₃)	783	390.6	355.8	778	388.3		353.9	

The biowaste propulsion pressurization system uses CO_2 and H_2O mixture as propellant. Initially, it was expected that the CO_2 waste would only be available at pressures of less than 1 mm Hg (~ 0.001 atm). Further, a usable water-to-carbon-dioxide weight ratio of 0.2 was fixed by the ecological balance of the spacecraft with water initially at cabin pressure. A miniature steam ejector system, similar to those which pump up the exhaust pressure to atmospheric pressure from open cycle wind tunnels, was devised. A small steam generation system is provided. This system pumps water to the boiler and uses waste heat for steam generation. The latent heat of the water is a significant portion of the specific impulse capability of superheated steam but can be supplied, for example, from waste heat, at 150°F at 4 psia. The steam pumps the CO_2 in two stages to 0.1 atm. In the system shown, H_2O is condensed and recycled to improve performance. If CO_2 can be made available at cabin pressure, then the pressurization system is omitted, and the system corresponds to Figure 3-65.

3.3.4 System Weight Comparison

The vehicle impulse requirements and engine performance data developed in the previous sections were combined to determine the total and component weights of the various Resistojet reaction control systems. Computations were made for hydrogen, ammonia, hydrazine, and biowaste propellants in combination with the four MORL vehicle modes.

3.3.4.1 Resupply Launch Weight

The propellant resupply weight that must be provided each 90 days is shown in Figure 3-66. It is apparent from this figure that the higher specific impulse capability of hydrogen more than compensates for its higher tank weight. The system employing biowaste propellant requires no resupply with the Isotope Brayton zero-g vehicle, inasmuch as the entire reaction control system function can be provided by waste products from the environmental control system. The solar power supply zero-g vehicle has a higher total impulse requirement than can be supplied by the biowaste materials and, therefore, some resupply is required. The biowaste systems are not shown for the artificial-g mode vehicles, because the impulse required far

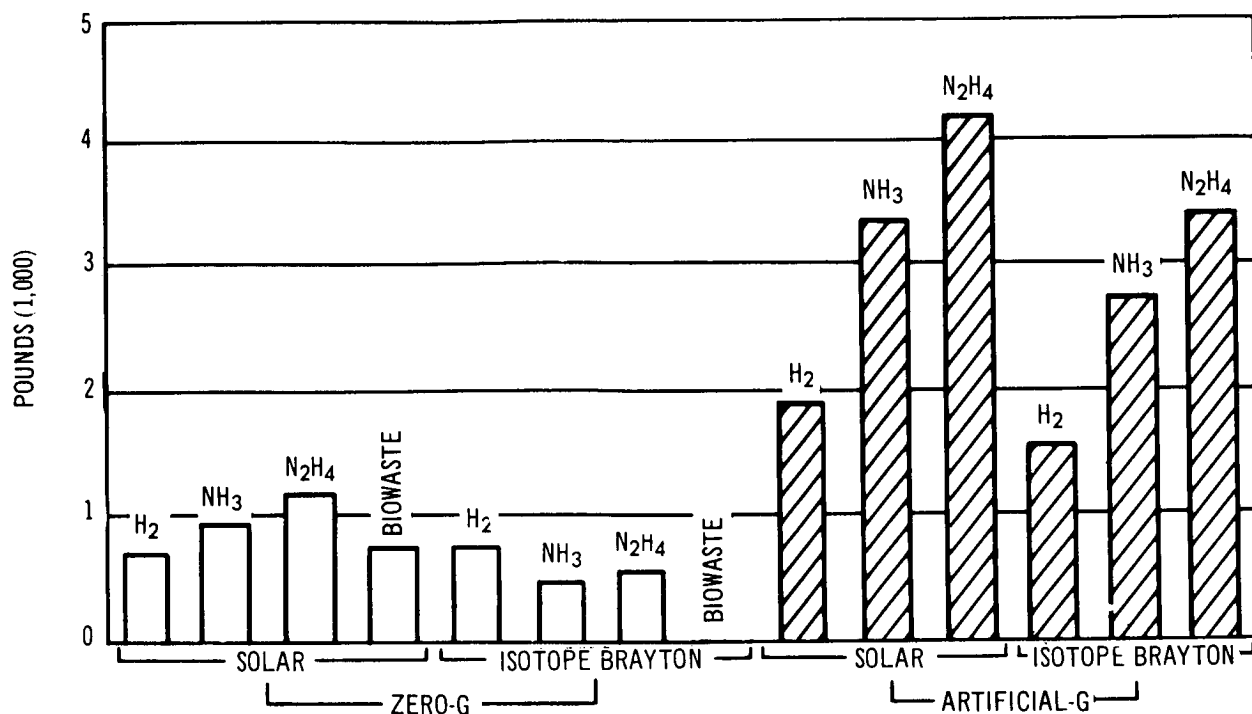


Figure 3-66. Resupply Launch Weight 90 Days

exceeds the availability of the biowaste propellant and, thus, makes this system less attractive than the three reaction control systems shown.

3.3.4.2 Power Supply Weight

The power supply weight for each of the systems is shown in Figure 3-67. As expected, the propellant combinations that supply the highest specific impulse capability require the highest power supply weight.

3.3.4.3 Initial Launch Weight

The initial launch weight of the complete reaction control system, including sufficient tankage for 147 days of operation and 20 days propellant supply, is shown in Figure 3-68. Hydrogen has the highest initial launch weight as a result of the higher power supply and tank weight for the cryogenic material. The total initial launch weight for the other systems are from 500 to 1,000 lb less than the hydrogen case and are at about the same level.

3.3.4.4 Initial Plus Resupply Weight

The entire weight lifted for each system over the 5-year life of MORL is shown in Figure 3-69. The long period of operation causes the higher

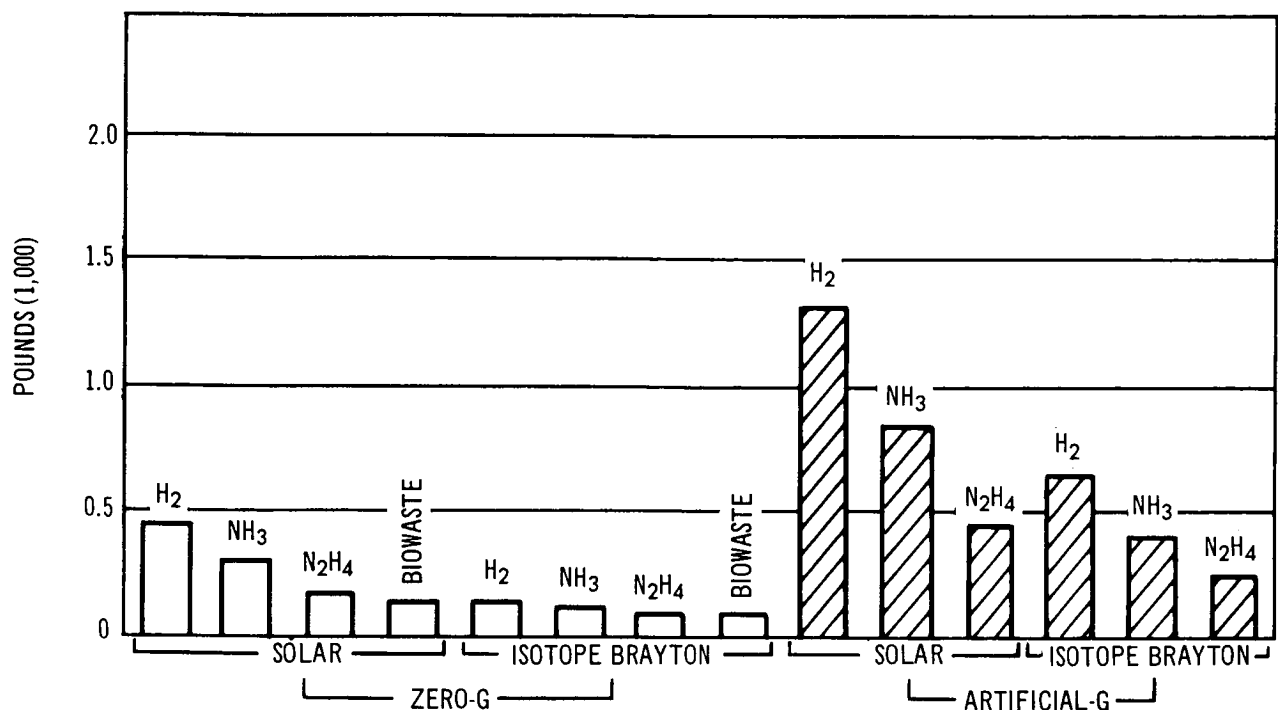


Figure 3-67. Power Supply Weight

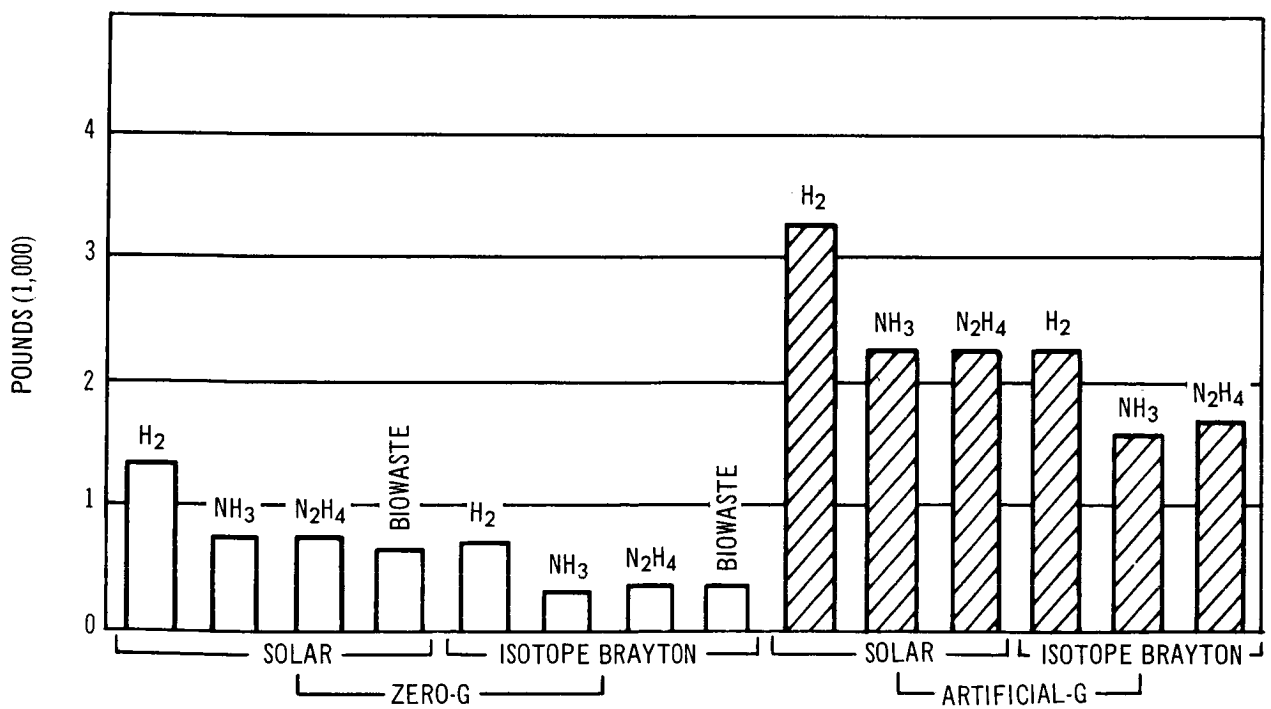


Figure 3-68. Total Initial Launch Weight

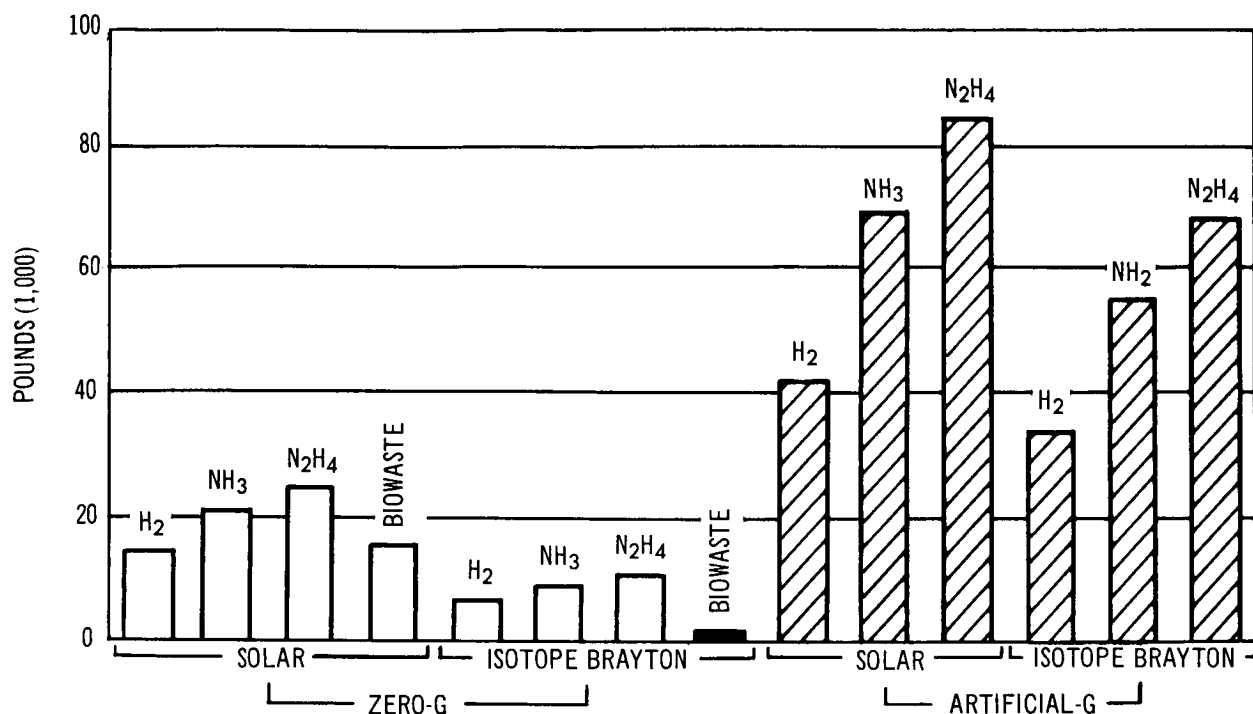


Figure 3-69. Grand Total Launch Weight (Initial and Resupply) - 5 Years

specific impulse capability of hydrogen to have predominance over the high initial-plus-resupply weight, thus providing the lowest weight of the nonbiowaste systems. The biowaste propellant combination is shown to be particularly attractive for the Isotope Brayton zero-g mode vehicle, inasmuch as sufficient waste products are potentially available from the environmental control system to accomplish the entire reaction control system requirement. The biowaste system provides approximately the same total system weight that is required for the hydrogen system for the solar zero-g mode vehicle. Inasmuch as the resupply of water might represent an easier logistic task than the resupply of cryogenic hydrogen, this system might be considered seriously, even though the biowaste products are not sufficient to do the entire reaction control system requirement for this vehicle.

Tables 3-28 and 3-29 present the detailed component weight breakdown for all of the reaction control system and vehicle mode combinations studied. The detailed engine data for each combination is presented in Tables 3-26 and 3-27. Tables 3-28 and 3-29 show that the engine thrust levels range from 9 mlb for the Isotope Brayton zero-g mode vehicle up to 164 mlb for the solar artificial-g mode vehicle.

Table 3-28

SYSTEM WEIGHTS (ZERO-G MODE/LOCAL HORIZONTAL ORIENTED)

Weight Breakdown		Solar Panel (500 lb/kWe)				Isotope Brayton (300 lb/kWe)			
Elements	H ₂	NH ₃	N ₂ H ₄	H ₂ O and CO ₂ **	H ₂	NH ₃	N ₂ H ₄	H ₂ O and CO ₂ **	
Propellant tank and associated subsystems	580	127	258	37	413	63	118	37	
Propellant feed system	30	30	30	30	30	30	30	30	
Resistojet thrusters	22	14	9	3	11	8	7	2	
Electric power feed system	24	17	13	12	15	12	10	9	
Power supply system	575	367	206	178	172	114	69	59	
Propellant (147 days*)	690	1,384	1,517	1,158	317	691	692	-0-	
Propellant (20 days*)	94	188	206	403	43	94	94	187	
Propellant (90 days*)	422	847	929	709	194	423	424	-0-	
Summary									
Total system dry weight	1,231	555	516	260	641	227	234	137	
Total initial launch weight (20 days*)	1,325	743	722	663	684	321	328	324	
Total wet weight (147 days*)	1,921	1,939	2,033	1,418	958	918	916	137	
Resupply launch weight (90 days*)	623	974	1,187	746	310	486	542	-0-	
Grand total resupply weights	12,806	20,017	24,328	15,369	6,371	9,988	11,108	-0-	
Grand total launch weights	14,131	20,760	25,050	16,032	7,055	10,309	11,436	324	
*All propellants include 5% reserve									
**Wastes are not shown charged as propellants (2,426 lb for 147 days). Solar Panel Case requires supplemental water. Isotope Brayton Case must reject 509 lb excessive waste opposing thruster									

Table 3-29
SYSTEM WEIGHTS
(ARTIFICIAL-G MODE--SPIN AXIS SUN ORIENTED)

Weight Breakdown Elements	Solar Panel (500 lb/kWe)				Isotope Brayton (300 lb/kWe)			
	H ₂	NH ₃	N ₂ H ₄	H ₂ O and CO ₂	H ₂	NH ₃	N ₂ H ₄	H ₂ O and CO ₂
Propellant tank and associated subsystems	1,028	436	904		966	361	746	
Propellant feed system	27	27	27		27	27	27	
Resistojet thrusters	70	40	19		57	32	15	
Electric power feed system	56	37	22		48	32	20	
Power supply system	1,700	1,075	569		849	544	289	
Propellant (147 days*)	2,427	4,772	5,319		1,960	3,947	4,387	
Propellant (20 days*)	330	649	724		267	537	597	
Propellant (90 days*)	1,486	2,922	3,257		1,200	2,417	2,686	
Summary								
Total system dry weight	2,881	1,615	1,541		1,947	996	1,097	
Total initial launched weight (20 days*)	3,211	2,264	2,265		2,214	1,533	1,694	
Total wet weight (147 days*)	5,308	6,387	6,860		3,907	4,943	5,484	
Resupply launch weight (90 days*)	1,922	3,358	4,161		1,587	2,778	3,432	
Grand total resupply weights	39,500	69,010	85,282		32,616	57,090	70,341	
Grand total launch weights (5 years)	42,711	71,274	87,547		34,830	58,623	72,035	

*All propellants include 5% reserve.

3.4 RADIOISOTOPE THRUSTOR

Radioisotope-heated thruster systems are substantially capable of meeting the selection criteria discussed in Subsection 3.1.3.4. As a result, TRW Systems was placed under contract by the Douglas Aircraft Company to establish the feasibility of using radioisotope thrusters for the MORL mission. The technology of these devices has been pursued at TRW Systems for the past 2-1/2 years under the continuing AEC-funded POODLE program. In early 1965, under joint AEC/Air Force sponsorship, TRW Systems successfully demonstrated a radioisotope-fueled POODLE thruster at the AEC's Mound Laboratory. Much of the technology developed under these programs is directly applicable to the design and development of a radioisotope RCS for MORL.

The first phase of the study was a comparative parametric evaluation of various candidate radioisotope fuel forms and propellants for the MORL RCS requirements, as defined by Douglas during the first few weeks of the study. From the various weight and performance trends established during this phase, all but one radioisotope fuel form and two propellants were eliminated from further consideration. During this first phase, effort was also expended on combining the roll, pitch, yaw, and drag-makeup thrust vectors so as to minimize the total impulse requirement per orbit.

During the second phase of this study, the results of these analyses were used to generate preliminary designs of a MORL RCS system, which included detailed computer thermal analyses, feed system evaluation and selection, and further biological shielding calculations. Both of these phases are described in Section 3.4. The third phase of the study which involved details of the system integration is described in Section 5.

The preliminary analysis phase of the study was conducted to establish the following:

1. The magnitude of thrust level and impulse requirements.
2. The selection of propellant(s).
3. Weight characteristics of the RCS utilizing the various isotope candidates.
4. The selection of the most promising form of radioisotope fuel.

The typical duty cycle and system design criteria employed for the initial parametric study are shown in Tables 3-1 and 3-16, respectively. As indicated in Table 3-16, two possible mission modes and two possible electrical power supplies were specified for MORL. The zero-g mode is the baseline mode for MORL and is the most straightforward in terms of specifying the thrust vector requirements. Because the requirements for the zero-g mode were much more clearly defined early in the study, the zero-g mode was emphasized for the comparative performance analysis of the various RCS concepts.

The propellants considered for RCS applications were ammonia, hydrogen, and hydrazine. In addition, the use of biowastes (CO_2 and water) were considered.

3.4.1 Thrust Level Determination

The duty cycle, defined in Table 3-16, represents the separate impulse requirements associated with each orbit-keeping function, without regard for the total impulse reductions associated with the simultaneous performance of these functions. To determine appropriate thrust levels while minimizing total impulse requirements, a tradeoff study was conducted. In addition, an optimum yaw burn time was calculated for the configuration using a solar cell electric power supply.

The zero-g mode, illustrated in Figure 3-70, can be visualized as a belly-down mode of operation where the yaw axis is always parallel with the Earth radius vector. A schematic drawing of the MORL with a radioisotope RCS is shown in Figure 3-71. As shown in Table 3-16, the propulsive efficiencies for all of the zero-g mode control functions, except yaw in the solar-powered configuration, are independent of the pulse duration over the ranges specified. Thus, excluding the yaw control function for a solar-powered MORL, the longest possible pulse duration is selected and minimum thrust levels are obtained. This criterion is based on keeping the radioisotope RCS weight and radioisotope inventory as low as possible because the thrust weight and radioisotope inventory are roughly proportional to the thrust level for a given specific impulse.

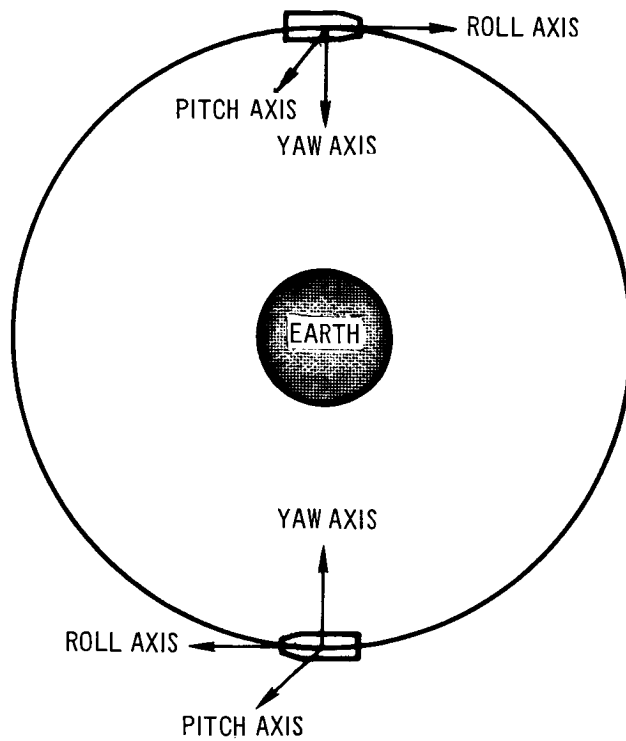


Figure 3-70 MORL in the Zero G Mode

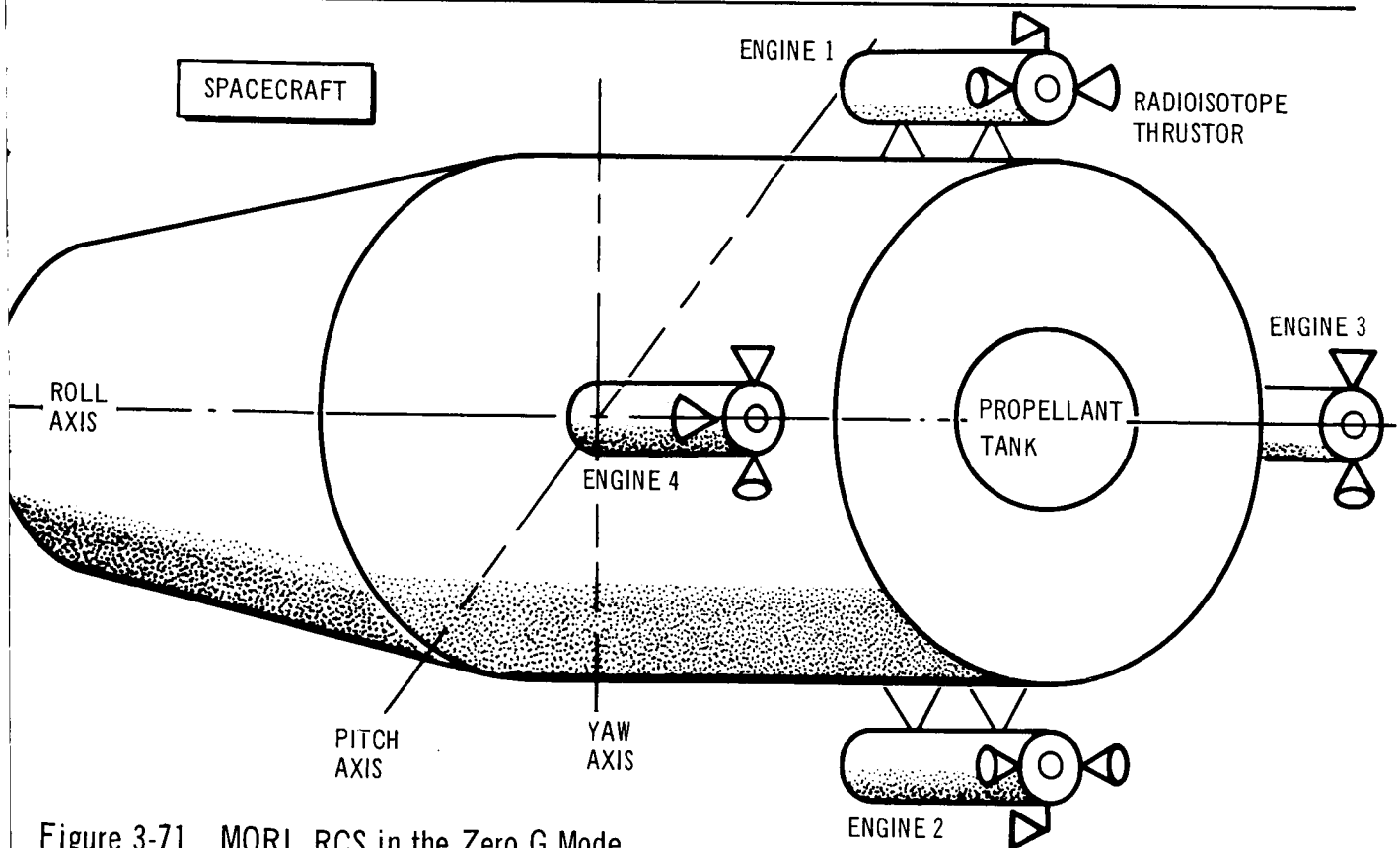


Figure 3-71. MORL RCS in the Zero G Mode

In the case where the propulsive efficiency can vary significantly over the range of permissible pulse duration, the total impulse and propellant requirements also vary. A simple minimization of thrust level does not lead to an overall system minimum weight. A simplified analysis, minimizing the system weight, was performed to determine near-optimum pulse durations for the yaw control function of a solar-powered MORL in the zero-g mode. The results for Pu-238-fueled thrusters are presented in Table 3-30 for hydrogen and ammonia propellants.

Table 3-30
NEAR-OPTIMUM YAW THRUST LEVELS AND BURN TIMES
FOR THE SOLAR-POWERED MORL IN THE ZERO-G MODE
(Pu-238-FUELED THRUSTORS)

Propellant	I_{sp} (sec)	Mission Time (years)	Total Burn Time per Orbit (sec)	Firing Duration (sec)	Total Thrust (lb)
Hydrogen	761	5.0	1,820	910	0.0655
Ammonia	364	5.0	1,520	760	0.0770

Higher thruster weights would tend to lower the optimum yaw thrust levels, as would any cost penalty associated with the cost of the radioisotope inventory. Although not optimized, these effects were considered in the selection of the yaw thrust level to be used in the preliminary analysis, and resulted in the selection of a yaw thrust requirement of 0.0574 lb at a firing duration of 1,050 sec/orbit for the solar-powered MORL in the zero-g mode. This thrust level was applied to all propellants and all radioisotope fuels for the purposes of the preliminary analysis.

To establish thrust level requirements associated with each of the four radioisotopes, it was necessary to evaluate the firing sequence associated with all of the orbit-keeping functions. Total thrust levels for each engine were established by distributing the total thrust requirement nearly equally among the four engines, and by performing orbit-keeping functions, such as drag/pitch and drag/yaw, simultaneously with appropriate engines.

Tables 3-31 and 3-32 present the results of this analysis for three drag/pitch and drag/yaw firing configuration.

Configuration 1, reflecting the lowest thrust requirement, uses Engines 1 and 2 (Figure 3-71) for both drag and pitch thrusting. Each of these two engines provides one-quarter of the total drag makeup thrust of 0.0164 lb (or 0.0041 lb), and one-half of the total pitch thrust of 0.0149 lb (or 0.0075 lb). In addition, each engine provides one-quarter of the total roll thrust of 0.015 lb (or 0.00375 lb). Therefore, the maximum thrust demand for either Engine 1 or 2, depending on the pitch direction, is 0.0153 lb.

The pitch demand consists of a couple, with Engines 1 and 2 each providing a thrust of 0.00745 in opposite directions. As a result, one of the two pitch engines always fires in the direction of drag makeup, while the other engine fires against it. The net impulse delivered by Engines 1 and 2, without roll, is

$$\text{Impulse} = \left[|F(\text{Drag}) + F(\text{Pitch})|_{\text{Eng 1}} + |F(\text{Drag}) - F(\text{Pitch})|_{\text{Eng 2}} \right] \times \text{Burn Time}$$

An identical relationship exists between Engines 3 and 4 which were used for drag and yaw functions.

Tables 3-31 and 3-32 present the total impulse requirements for each of the three configurations examined. Configurations 2 and 3 require successively lower impulse with somewhat higher thrust levels than that shown for Configuration 1. However, for the parametric analysis of RCS structure factors, the impulse requirements of Configuration 1 were used for both the RBP and solar power configurations.

A schematic illustration of the spin mode orbital characteristics is shown in Figure 3-72. The spacecraft, consisting of the MORL capsule and a spent Saturn IVB as its counterweight, is to rotate at an angular velocity of 0.4 radians/sec about the spacecraft's center of gravity. The spacecraft configuration is presented in Figure 3-73. This mission mode is characterized by the constraint that the spin vector is always sun-oriented. As a result, RCS requirements consist of precession thrusting, as well as orbit-keeping drag makeup.

Table 3-31
THRUST AND IMPULSE REQUIREMENTS FOR THE RBP
CONFIGURATION ZERO-G MODE

Config- uration	Engines	Control Function per Engine	Thrust per Engine (lb)	Max. Thrust per Engine (lb)	Total Firing Time per Orbit (sec)	Impulse per Orbit (lb-sec)	Total Impulse per Orbit (lb-sec)
1	1 and 2	1/4 Drag	0.0041		5,500	86	
		1/2 Pitch	0.0075		5,500		
		1/4 Roll	0.0038		533		
				<u>0.0153</u>			
	3 and 4	1/4 Drag	0.0041		5,500	53	
		1/2 Yaw	0.0075		533		
		1/4 Roll	0.0038		533		
				<u>0.0153</u>			<u>139</u>
2	1 and 2	1/4 Drag	0.0082		5,500	90	
		1/2 Pitch	0.0075		5,500		
	3 and 4	1/2 Yaw	0.0075		533	16	
		1/2 Roll	0.0075		533		
				<u>0.0150</u>			<u>106</u>
	1 and 2	9/20 Drag	0.0075		5,500	86	
		1/2 Pitch	0.0075		5,500		
		1/4 Roll	0.0038		533		
				<u>0.0187</u>			
	3 and 4	1/20 Drag	0.0075		533	12	
		1/2 Yaw	0.0075		533		
		1/4 Roll	0.0038		533		
				<u>0.0187</u>			<u>98</u>

Table 3-32

THRUST AND IMPULSE REQUIREMENTS FOR THE
SOLAR-POWERED CONFIGURATION
ZERO-G MODE

Config- uration	Engines	Control Function per Engine	Thrust per Engine (lb)	Max. Thrust per Engine (lb)	Total Firing Time per Orbit (sec)	Impulse per Orbit (lb-sec)	Total Impulse per Orbit (lb-sec)
1	1 and 2	1/2 Drag	0.0137		5,500	158	
		1/2 Pitch	0.0091		5,500		
		1/2 Roll	0.0075		533		
				<u>0.0303</u>			
	3 and 4	1/2 Yaw	0.0287	<u>0.0287</u>	2,100	120	<u>278</u>
2	1 and 2	1/3 Drag	0.0091		5,500	180	
		1/2 Pitch	0.0091		5,500		
		1/2 Roll	0.0075		533		
				<u>0.0257</u>			
	3 and 4	1/6 Drag	0.0046		5,500	151	
		1/2 Yaw	0.0287		2,100		
				<u>0.0333</u>			<u>259</u>
3	1 and 2	1/3 Drag	0.0091		5,500	108	
		1/2 Pitch	0.0091		5,500		
		1/2 Roll	0.0075		533		
				<u>0.0257</u>			
	3 and 4	1/6 Drag	0.0119		2,100	120	
		1/2 Yaw	0.0287		2,100		
				<u>0.0406</u>			<u>228</u>

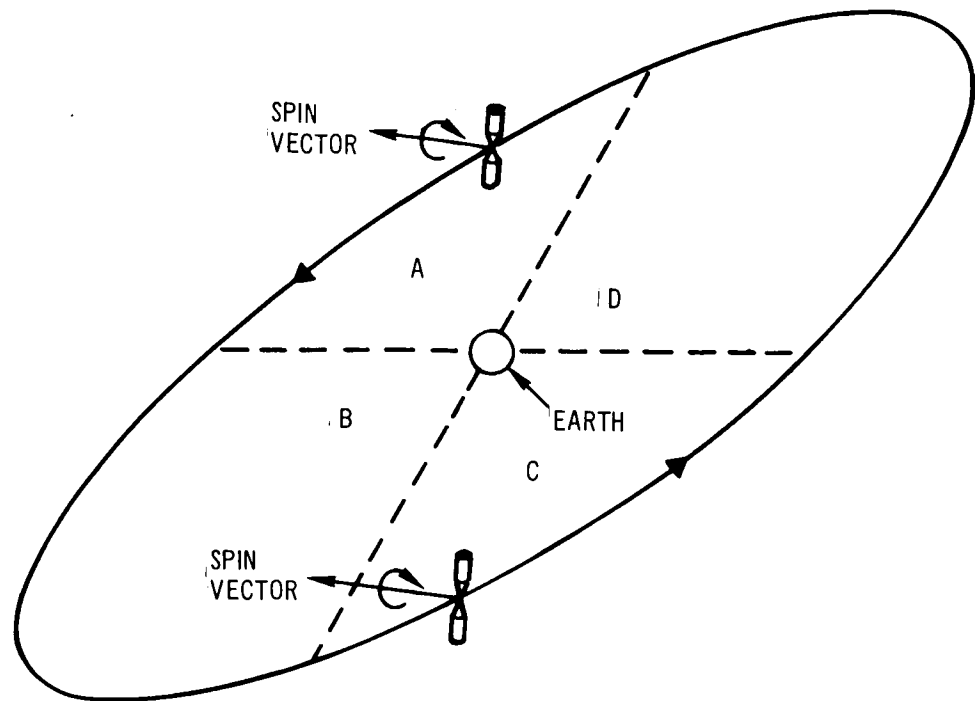


Figure 3-72. MORL in the Spin Mode

As in the case of the zero-g mode firing sequence, a tradeoff between drag and precession, where both requirements are satisfied by the same force vector, is possible in Quadrants A and C of Figure 3-72. As a result, Engines 5 and 6 perform both drag and precession functions while Engines 1 and 2 perform drag makeup only. In Quadrants B and D, while Engines 5 and 6 continue to perform precession functions but no longer in the direction of drag makeup, Engines 3 and 4, and 7 and 8 perform the drag makeup as they achieve proper orientation in the appropriate spin quadrant.

As indicated in Table 3-33, the total impulse requirements for the spin mode are considerably greater than for the zero-g mode. The firing sequence is also much more complex. Because of time limitations, only a small analytical effort was exerted in this area and, therefore, the values shown in Table 3-33 should not be considered as necessarily optimum.

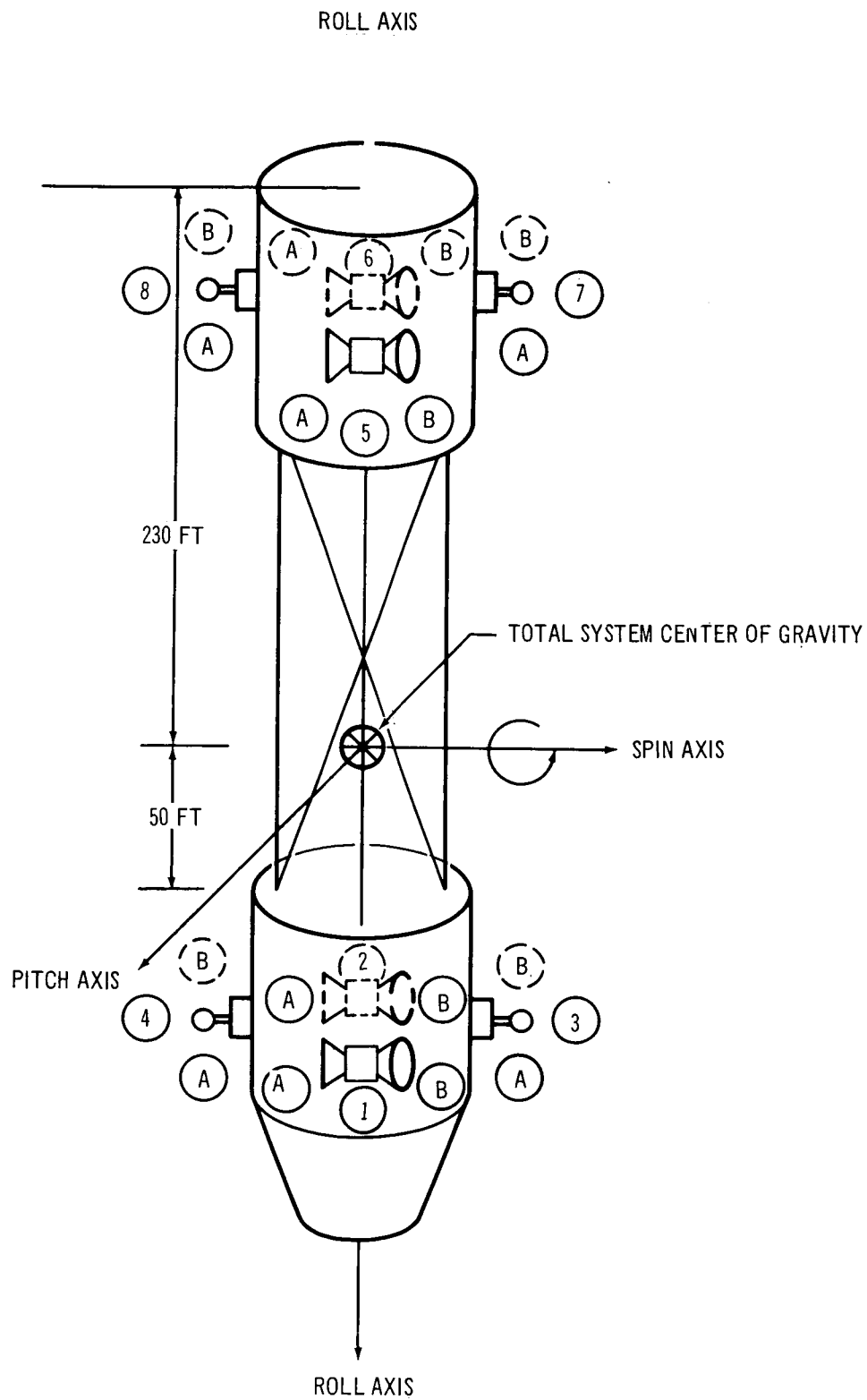


Figure 3-73. MORL Spin Mode Configuration

Table 3-33

IMPULSE REQUIREMENTS FOR THE MORL
IN THE SPIN MODE

Power Supply	Engines	Control Function per Engine	Thrust per Engine (lb)	Max. Thrust per Engine (lb)	Total Firing Time per Orbit (sec)	Impulse per Orbit (lb-sec)	Total Impulse per Orbit (lb-sec)
Solar	1 and 2	Drag	0.0430	0.0430	2,060	177	
	3 and 4	Drag	0.0575	0.0575	1,375	158	
	5 and 6	Drag	0.0093		2,060		
			0.0615		1,375		
		Precession	0.1230	<u>0.1230</u>	688	376	
	7 and 8	Drag	0.0125	0.0125	1,375	34	
							<u>745</u>
Isotope	1 and 2	Drag	0.0365	0.0365	2,060	150	
	3 and 4	Drag	0.0485	0.0485	1,375	133	
	5 and 6	Drag	0.0079		2,060		
			0.0515		1,375		
		Precession	0.1030	<u>0.1030</u>	1,688	316	
	7 and 8	Drag	0.0106	0.0106	1,375	29	
							<u>628</u>

3.4.2 Propellant Evaluation

Three potential propellants, hydrogen, ammonia, and hydrazine, in addition to the MORL biowastes (water and CO_2) were considered for possible application in a radioisotope-fueled RCS for MORL. The specific impulse for each of these propellants is shown in Figure 3-74 as a function of thruster chamber temperature for a nozzle efficiency of 0.95 and an expansion ratio of 50. The ideal specific impulse data were generated by means of the standard TRW rocket nozzle performance computer program for frozen flow and for hydrogen, and are essentially the same as those suggested in References 14 and 15.

Temperature constraints of radioisotope thrusters are based on the radioisotope fuel form melting points and the strength characteristics of the encapsulating materials. Thruster chamber gas temperatures of up to $3,500^\circ\text{F}$ have been found to be feasible with the use of refractory metals.

Temperature constraints for radioisotope thrusters fed by water or CO_2 are also based on materials compatibility between the thruster flow tube material and the propellant. For operating temperatures in excess of $1,650^\circ\text{F}$, either superalloy or noble metals may be required, depending on the upper limit of operating temperature.

Use of hydrogen as the propellant for a radioisotope RCS is very attractive from the standpoint of propellant mass required to deliver a specified impulse. The low propellant weight associated with hydrogen-fed systems is, however, somewhat offset by the tankage weights required for hydrogen. To avoid large tankage weight penalties, the hydrogen must be stored as a liquid, thus introducing problems associated with propellant thermal control. Despite the potential disadvantages, however, hydrogen is a very attractive propellant candidate.

Both ammonia and hydrazine offer the advantage of a propellant that can be stored easily in the MORL environment. The specific impulse of ammonia is higher than that of hydrazine for a given thruster chamber temperature. In addition, hydrazine is shock-sensitive when heated and would introduce

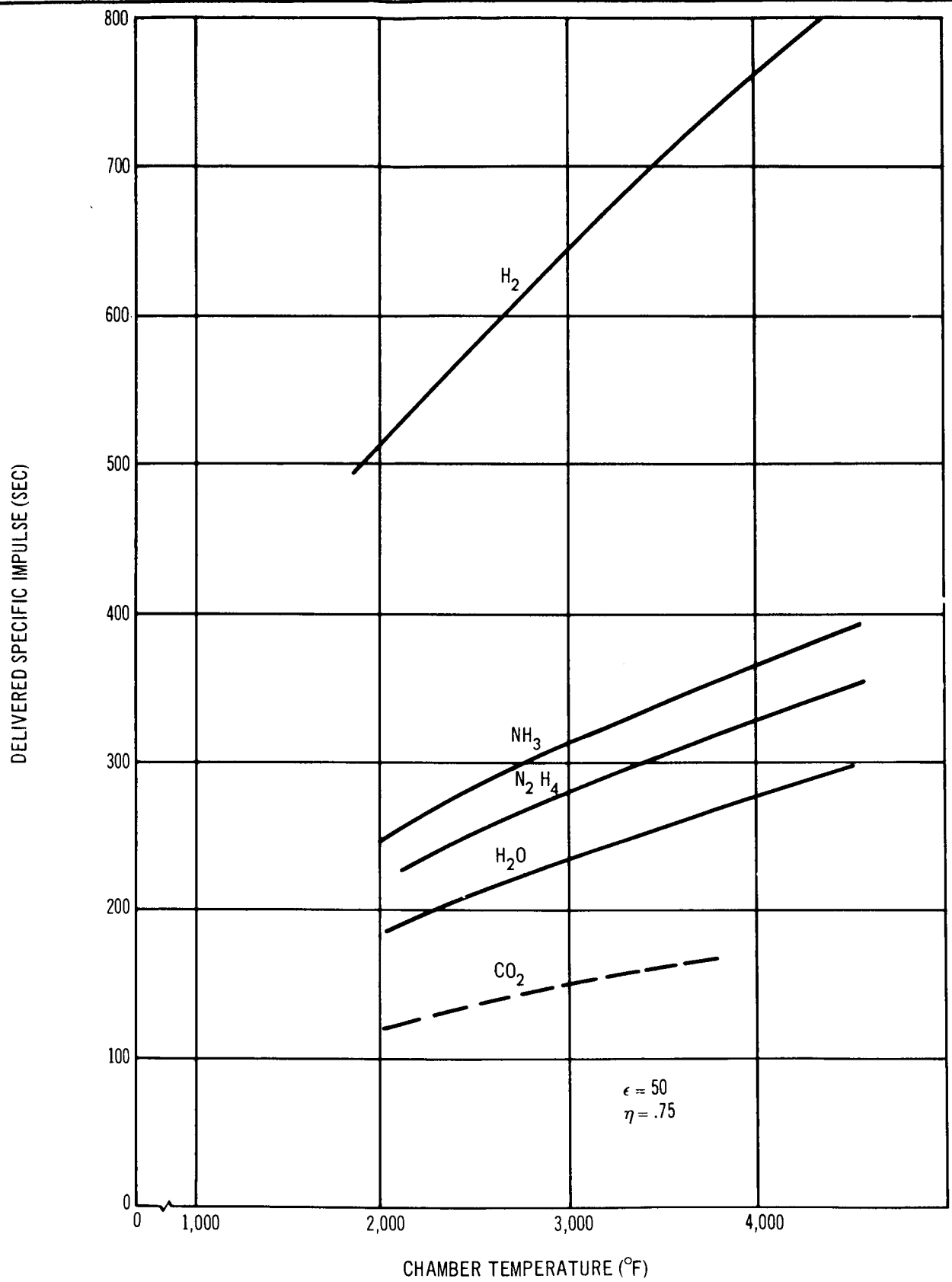


Figure 3-74. Specific Impulse as a Function of Temperature

some complexity into the propellant feed system. There appears to be no real justification for considering hydrazine for more detailed designs.

For the purposes of the preliminary RCS evaluation, ammonia and hydrogen were considered as the propellant candidates. In addition, the use of CO₂ and H₂O biowastes for propulsion purposes was described in Section 3.4.3. A thruster for use with CO₂ was discussed in Section 3.4.4.

3.4.3 Biowaste Utilization

Biowaste products of the MORL life support system consist of CO₂ and H₂O. Both of these products can be used for propulsion in a radioisotope-fueled RCS. Table 3-34 presents their availability and propulsion capability.

Table 3-34
POTENTIAL PERFORMANCE CAPABILITY
OF BIOWASTE PROPELLANTS

	Biowaste Propellant	Availability (lb/day)	Supply Pressure (psi)	I _{sp} (sec)	Gas Temp (°F)	Impulse per Orbit (lb-sec)
Baseline	H ₂ O	3.15	7	192	1,650	36
Phase IIa (cryogenic oxygen)	CO ₂	13.9	low	122	1,650	108
Baseline	CO ₂	14	low	122	1,650	108
with H ₂ O electrolysis	H ₂	1.6	7	761	3,500	78

The baseline biowaste availability can provide a total of 136 lb-sec of impulse per orbit, of which 108 lb-sec is available with CO₂ only. Therefore, the entire impulse requirements of RBP Configurations 2 and 3 of Table 3-31 corresponding to 106 and 98 lb-sec respectively, can be satisfied by the CO₂ biowaste operating at 1,650°F.

Biowaste use for propulsion purposes would require that the CO₂ be available at pressures of the order of cabin pressure. This would necessitate an on-board compression capability with its associated weight penalty.

Table 3-35 summarizes the baseline biowaste utilization capability for both RBP and solar configurations for impulse requirements of 106 and 259 lb-sec respectively. To partially satisfy the propulsive requirements of Engines 3 and 4 of the solar configuration, the CO_2 temperature would have to be raised to $3,200^\circ\text{F}$. The H_2O available would only partially satisfy the requirements of Engines 1 and 2 at a temperature of $3,000^\circ\text{F}$. Supplemental water would be required to provide an additional impulse of 32 lb-sec.

Biowaste availability with H_2O electrolysis would provide gaseous hydrogen. With the available CO_2 again satisfying impulse requirements for the RBP configuration, supplemental hydrogen would be needed to satisfy requirements in the solar configuration.

3.4.4 Thrustor Analysis

A number of radioisotope fuels and design approaches for each fuel was evaluated to establish the most promising thrustor configurations for the MORL application. Radioisotope fuel form, half-life, permissible operating temperature, thrustor size, thrust level, biological shielding requirements, and materials compatibility must be considered in the thrustor design. These criteria are discussed in the following paragraphs.

A schematic drawing of a typical radioisotope-heated reaction control thrustor installation is shown in Figure 3-75. The device consists of a radioisotope fuel form, encapsulated in a metallic cylinder around which a series of propellant flow tubes are coiled. Each tube is connected to a separate exhaust nozzle. The number of nozzles depends upon mission requirements. An additional tube is provided for prelaunch cooling water. A concentric shell, with thermal insulation attached to its outer surface, encloses the entire assembly. Biological shielding is provided around the thrustor periphery. Four longitudinal fins are attached to the thrustor and act as re-entry aids in the event of mission abort. A solenoid valve is attached to each propellant tube upstream of the thrustor inlet to control propellant flow through each nozzle. The thrustor operates by heating the propellant as it passes through the propellant flow tube. The propellant is then expelled through a converging-diverging nozzle to create propulsive thrust.

Table 3-35
BIOWASTE PROPELLANT UTILIZATION
ZERO-G MODE

		Maximum Impulse Available per Orbit (lb-sec)	Total Impulse Req PBC Configuration		Additional Impulse Required	Total Impulse Req Solar Configuration		Additional Impulse Required
			Engines 1 and 2	Engines 3 and 4		Engines 1 and 2	Engines 3 and 4	
Baseline	CO ₂	152 (3,200°F)	90	16	None	—	151	—
	H ₂ O	76 (3,000°F)	—	—	None	108	—	32
Baseline with H ₂ O electrolysis	CO ₂	152	90	16	None		151	
	H ₂	78 (3,500°F)	—	—	None	108		30

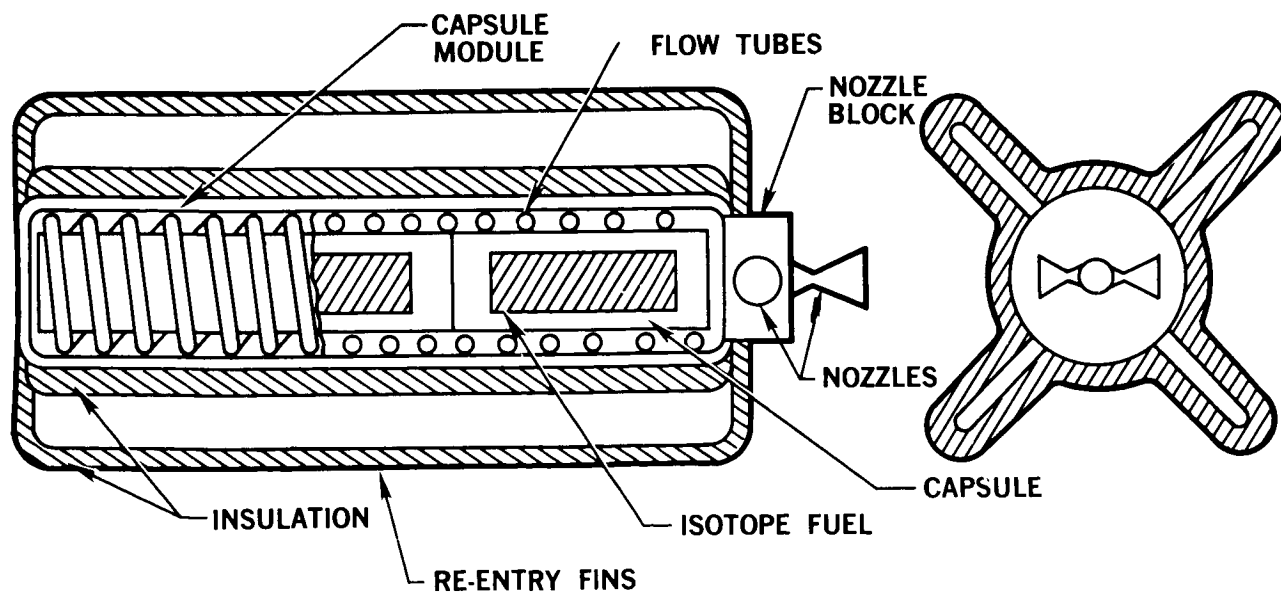


Figure 3-75. Radioisotope Thrustor for MORL Mission

The first item considered in the design of the thruster assembly is the radioisotope container or capsule. The capsule contains and positions the isotope fuel so as to achieve the most efficient use of the heat generated by the isotope decay process. The capsule must be designed to allow safe handling of the isotope and to contain fuel, and to prevent undue biological hazard under all normal and emergency conditions. Since emergency conditions may involve mission abort resulting in re-entry and high velocity impact, the capsule must be designed to withstand the associated environmental stresses.

The propellant flow tubes, carrying propellant from the flow control valve to each nozzle, are coiled around the capsule to provide the required heat transfer area to the propellant. The tubes must be sized so as not to exceed the allowable pressure drop and, in the case of the ammonia propellant, adequate surface area must also be available to permit complete decomposition.

The remainder of the thruster consists of the enclosing shell which surrounds the radioisotope capsule and the coiled propellant tubes. The nozzle assembly, insulation, and re-entry fins are connected to this structure. The fins, by increasing the aerodynamic drag on the thruster during abort re-entry, decrease the ballistic coefficient and impact velocity. The fins also induce a spinning motion about the longitudinal axis of the thruster during re-entry which decreases effective re-entry aerodynamic heating. In this manner the severity of the re-entry environment is significantly reduced, which permits the design of a capsule capable of surviving re-entry and impact.

Thermal insulation is required to achieve desired operating temperatures with moderate radioisotope fuel inventories. Since heat is being generated continuously the insulation scheme selected must be appropriate for both propellant flow and no-flow conditions. During no-flow conditions, the entire isotope heat must be transferred to space without exceeding material strength and fuel form temperature limitations. Previous thermal analyses of larger radioisotope thrusters indicate that thrusters can be designed for passive thermal control. For this type of thermal control the heat loss through the insulation is tailored to permit the dissipation of the total heat generated to space with only a nominal increase in thruster temperature during no-flow conditions. Thermal insulation requirements were computed

for a fuel centerline temperature differential of 300°F between the flow and no-flow condition at the hottest point in the radioisotope capsule for both conditions. The temperature differential between flow and no-flow conditions decreases as the thruster thermal efficiency decreases. During flow conditions insulation heat losses result in a reduced thermal efficiency which is defined as the percent of the total heat generated that goes into the propellant.

A compilation of radioisotope heat sources, published periodically by C. A. Rohrmann of the Hanford Laboratories, was used to establish the initial list of potential radioisotope fuel forms. Of the 14 radioisotopes listed, almost half can be eliminated immediately because of the large nuclear radiation shielding weight requirements. The remaining candidate radioisotopes considered are shown in Table 3-36. The first four radioisotopes listed are alpha emitters; the latter three are essentially pure beta emitters. These radioisotopes were considered in the light of their nuclear radiation shielding requirements and in terms of their estimated availability in 1970.

Cm-244 was eliminated from further consideration because of its relatively large neutron radiation field when compared with the remaining radioisotopes in Table 3-36. Tm-170 and Tl-204 were eliminated since there appears to be insufficient production capability for these two isotopes. Cm-242 was also eliminated as a candidate fuel because it offers no apparent advantage over Po-210. The half lives and total radiation fields of the two isotopes are very similar, but the Po-210 fuel forms have been developed and used much more extensively than Cm-242. In addition, Cm-242 has a significantly larger neutron radiation field than does Po-210 and thus must be shielded by more bulky neutron shields. The latter consideration is primarily one of compact design rather than weight, since the total shielding weight required for Po-210 is about the same as for Cm-242.

Even though the total mission lifetime is 5 years, periodic resupply missions to the orbiting laboratory allow consideration of shorter half-lived isotope thrusters which could be replaced at prescribed intervals. Thus, the isotopes which appear most applicable to the MORL RCS requirements are: plutonium-238, promethium-147 and polonium-210.

Table 3-36

RADIOISOTOPE RADIATION FIELDS AND AVAILABILITY

Isotope	Half Life	Radiation/kWt ¹		Radiation/kWt		Estimated Production ² per yr in 1970 in kWt
		in mrem/hr at 10 ft Bare Capsule	0.4 in U	in mrem/hr at 10 ft Bare Capsule	8 in LiH	
Po-210	138 days	10	1.5	0.3	0.02	140
Pu-238	89.8 year	0.08	0.02	9.0	1.1	20
Cm-242	163 days	0.8	0.3	13	1.4	120
Cm-244	18.4 year	9	4.5	365	50	129
Pm-147	2.67 year	15.5	1.6	-	-	14
Tm-170	127 days	1.1×10^4	22	-	-	Limited
Tl-204	3.9 year	200	1	-	-	Limited

¹ORNL-3576, Handbook of Shielding Requirements and Radiation Characteristics of Isotope Power Sources For Terrestrial, Marine and Space Applications. E. D. Arnold.

²Present and Potential Annual Availability Isotopic Power Fuels. Division of Isotopes Development, USAEC (1963).

Since the MORL will be a man-rated system, the nuclear radiation fields within the spacecraft must be kept at a tolerable level. For the MORL configuration containing a Radioisotope Brayton Power (RBP) system, the combined radiation dosage contribution from the Brayton Cycle radioisotope heat source and the radioisotope-powered thrusters must not exceed this tolerable level. Once the maximum permissible dose rate is established the optimum shield configuration should be evaluated on the basis of minimum overall system weight. However, specification of the optimum shield configuration requires a tradeoff between thruster shielding and RBP heat source shielding to determine the shielding requirements for each radiation source which results in the lightest overall system weight. Since this evaluation could not be performed as part of this study, the allowable radioisotope thruster nuclear radiation contribution was taken to be 10% of that contributed by the RBP radioisotope heat source. The radiation fields surrounding the RBP heat source are shown in Figure 3-76. This figure shows that the dose rate 5 ft from the vehicle skin is about 5 mrem/hour. For the purpose of preliminary analysis the allowable thruster dose rate contribution for the RBP mode was taken to be 0.5 mrem/hour at 5 ft.

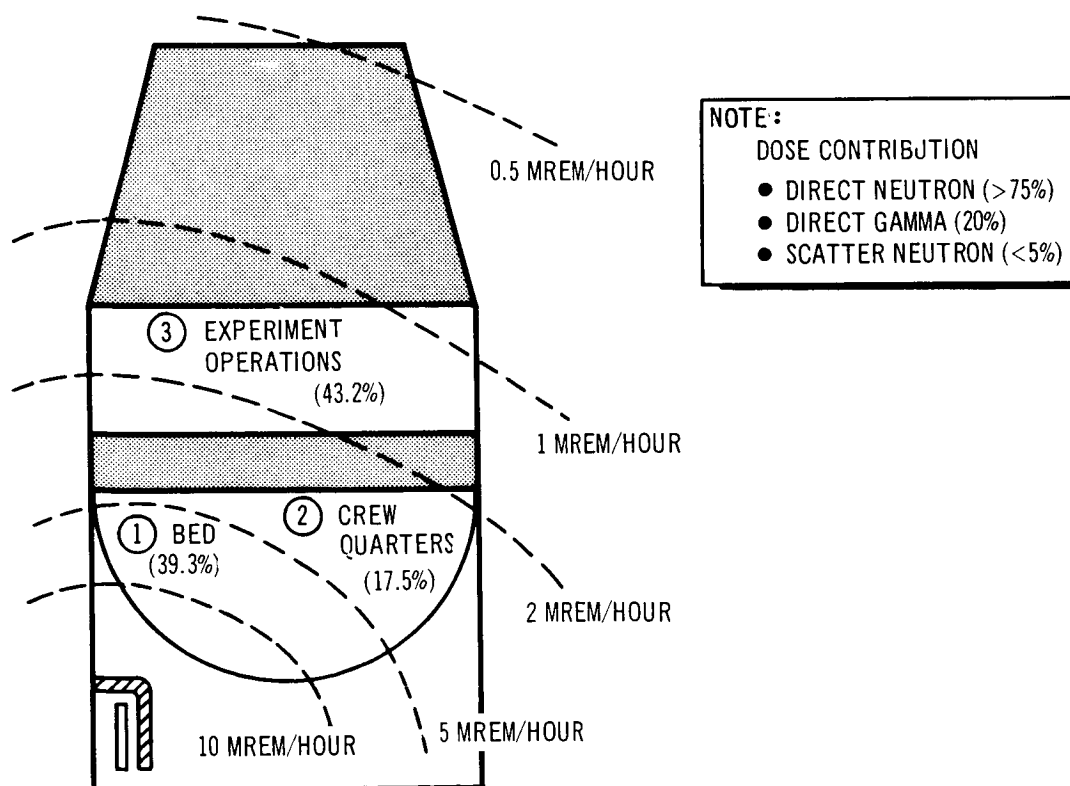


Figure 3-76. Radiation Dose Rate - RBP Function

In the case of the solar-powered configuration the radioisotope thrusters are the only sources of on-board radiation and the allowable thruster radiation dose rate was selected as 5 mrem/hour at 5 ft.

The RCS thrusters are to be located at four positions, 90° apart, around the periphery of the MORL capsule. To simplify the preliminary analyses, dose contributions from adjacent thrusters were not considered when establishing the shield thickness requirements for a selected thruster.

Shield thicknesses and weights were determined for the three most promising radioisotope fuel candidates. Since the purpose of the analysis was to produce preliminary parametric results, the method of calculation was necessarily simplified as previously described. Thus, the shield weights are approximate and were used primarily to compare shielding requirements for polonium-210, promethium-147 and plutonium-238. No attempt was made to optimize combined neutron and gammas shield weights for polonium-210 and plutonium-238. (An optimization would result in shield weight saving.) In addition, the weight of end shields was neglected for this analysis. A more detailed shield design was completed for the isotope selected for use in system design described in Section 5.4.3.

3.4.4.1 Design Criteria and Assumptions

To evaluate the various fuel forms, thrusters were sized for the following isotope-propellant combinations:

<u>Fuel Forms</u>	<u>Propellants</u>
Pu-238 O ₂	H ₂ , NH ₃ CO ₂
Pm ₂ -147 O ₃	H ₂ , NH ₃
Po-210 rare earth compound	H ₂ , NH ₃

Thrust level of 0.015 and 0.030 lb represent nominal thrust requirements for the RCS system parametric study for the exit propellant temperature range of 1,500° to 3,500°F. Temperature levels above 3,500°F were not considered because of problems during no-flow conditions.

The following criteria were established for design calculations and for determining thruster physical characteristics:

1. The diameter of the fuel capsule must be such that the fuel center-line temperature remains several hundred degrees Fahrenheit below the melting point of the fuel.
2. The thruster must be capable of surviving re-entry intact.
3. The length to diameter ratio, L/D , of the capsule should be less than five. Impact studies conducted at TRW and Sandia have indicated that an L/D ratio greater than five increases impact damage.
4. The overall thruster thermal efficiency is assumed to be approximately 70%.
5. Capsule structural material will be W-25Re.

The total quantity of isotope required for any single thruster depends on thrust level and, for the short half-life isotopes, the I_{sp} requirements at the end of mission life. A 60-day period from time of isotope encapsulation to start of the mission was assumed for all systems. The thruster design consists of determining the following parameters:

1. Thrust requirements.
2. Isotope power level required to achieve the desired thrust and I_{sp} , including the effect of the isotope half-life.
3. Volume occupied by the isotope.
4. Capsule inner dimensions required to contain the fuel within the constraints of fuel centerline temperature and the required L/D ratio.
5. Capsule wall thickness required for impact survival.
6. Previous experience indicates that the following wall thicknesses (as functions of exit gas temperatures) are reasonable for W-25Re:

<u>Exit Gas Temperature (°F)</u>	<u>Thickness (in.)</u>
1, 500	0.20
2, 000	0.20
3, 000	0.25
3, 500	0.30

7. The weight of the capsule and fuel to obtain the loaded capsule weight.

8. The total weight of the thruster including fins, capsules capsule module; and thruster components. The weight of nozzle, braze, insulation, flow tubes, and other hardware can be estimated from previous studies of similar sized thrusters as follows:

- A. Nozzles--0.35 lb
- B. Nozzle block--0.50 lb
- C. Insulation--0.05 lb/capsule
- D. Flow tubes--0.15 lb/capsule
- E. Braze--0.15 lb/capsule
- F. Fins--20% of total thruster weight

3.4.4.2 Po-210 Thruster Design

Polonium fuel forms have been under development for space applications at Mound Laboratory for 8 years. The SNAP-3 generator built in 1959 was Po-210-fueled.

Pure polonium has the highest specific power of any of the radioisotope fuels currently under development by the AEC. As a result of its low melting point it can only be considered as a useful form for high temperature applications when combined with other high-temperature materials. A classified high-temperature fuel form is presently available which is stable at the operating temperatures of interest for radioisotope thruster applications. A program is underway at Mound Laboratory to raise the permissible operating temperature even higher.

The pyrophoric and respirable nature of the fuel form necessitates the use of completely sealed capsules. Since polonium fuel forms are alpha emitters, helium pressure buildup occurs within the sealed fuel container. Major programs are being conducted by TRW Systems, NASA, and the AEC to determine long-duration high-temperature creep properties of capsule materials.

At higher temperature, the low strength of the container material coupled with a continuous pressure buildup, results in a thick walled container design with its correspondingly large mass. The capsule design criterion calls for an allowable stress level resulting in less than 5% creep during the life of the capsule. The isotope service life was projected to be 207 days (60-day shelf life and 147-day mission life).

With the half-life of Po-210 at 138 days the launch to end-of-mission-power ratio is 2. The Po-210 thruster would operate initially at temperatures 1.2 times that of the end-of-mission temperature. The thrusters were designed with an allowable creep stress at the higher initial temperature.

Typical results of the preliminary analysis of Po-210 capsule characteristics are shown in Table 3-37 for ammonia and hydrogen propellants. Figures 3-77, 3-78, 3-79 and 3-80 present thruster weights as a function of I_{sp} .

Polonium-210 is an attractive candidate for use in a MORL RCS because the radiation fields associated with this isotope are relatively low. Nearly 100% of the disintegrations of polonium-210 produces lead-206 and results in the release of a single 5.3 MeV alpha particle which is absorbed in the source compounds and thruster capsule walls. However, $1.2 \times 10^{-3}\%$ of the disintegrations produce a 4.5 MeV alpha plus a 0.803 MeV gamma from lead-206. Although 0.8 MeV gammas constitute the entire gamma field for pure polonium-210, the fuel form compound produces neutrons by alpha-neutron reactions. Po-210 powered thrusters therefore require both gamma and neutron shielding.

For the purposes of this shielding study the neutron production rate was assumed to be 200 neutrons/sec-Curie. This figure is believed to be conservative since Reference 16 indicates about 100 neutrons/sec-Curie for the neutron production rate.

To establish shield thickness requirements, the point source of the gamma and neutron dose rates were determined to be 7.79×10^{-2} mr/hour-W and 3.32×10^{-3} mrem/hour-W respectively.

Depleted uranium was selected as the gamma shield material because of its large photon absorption cross-section. Shield thickness requirements were calculated to permit half of the dose to be from gammas. Thus, gamma shielding requirements were based on the uranium thickness necessary to reduce the point source gamma dose at 5 ft to 50% of the total allowable dose, that is, 0.25 mrem/hour for the RBP mode and 2.5 mrem/hour for the solar power mode. Gamma transmission factors for the capsule walls were applied, and the required thickness of uranium was established using the absorption coefficients indicated by curves of dose rate as a function of

Table 3-37
TYPICAL CAPSULE DIMENSIONS AND WEIGHTS
Po-210 ISOTOPE--207-DAY CAPSULE LIFE
F = 0.015 LB

T _{gas} Exit (°F)	Watts per Capsule	Length (in.)	ID (in.)	Wall Thickness (in.)	Overall Length (in.)	OD (in.)	Fuel (lb)	Weight of Capsule (lb)	Total Weight (lb)	No. Capsules Required
Hydrogen Propellant										
1,500	837	1.6	0.63	0.17	1.94	0.98	0.14	0.690	0.830	1
2,000	945	2.8	0.92	0.25	3.28	1.4	0.16	2.44	2.60	1
3,000	575	6.4	1.8	0.50	7.48	2.9	0.10	23.4	23.5	2
3,500	417	8.8	2.2	0.60	10.0	3.4	0.07	41.6	41.7	3
Ammonia Propellant										
1,500	606	1.9	0.48	0.12	2.15	0.71	0.10	0.360	0.460	1
2,000	640	2.9	0.72	0.18	3.24	1.1	0.11	1.29	1.39	1
3,000	355	4.9	1.5	0.38	5.70	2.3	0.06	12.1	12.2	2
3,500	187	5.6	1.7	0.43	6.45	2.6	0.03	18.1	18.1	4

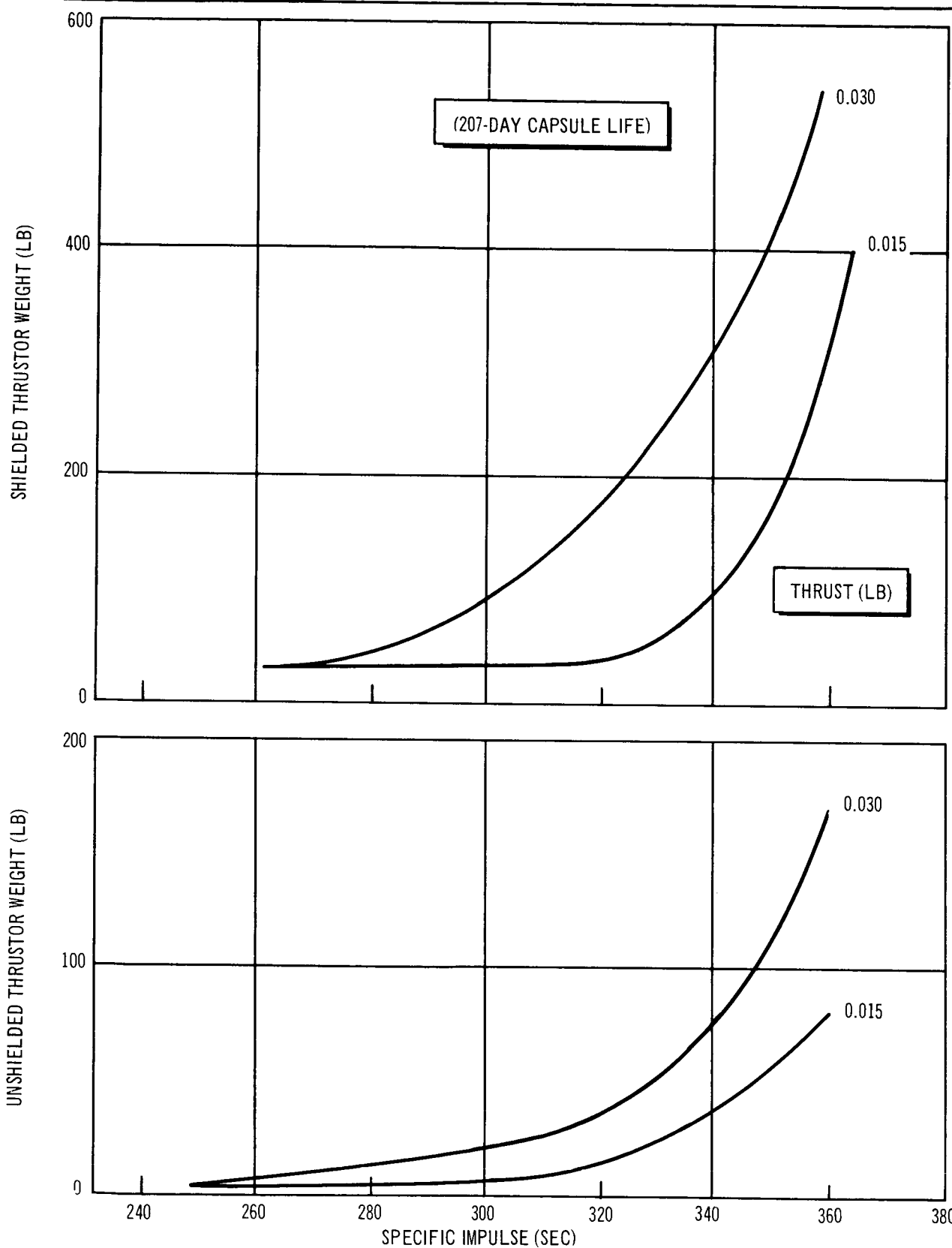


Figure 3-77. Po-210 Thrustor Weight as a Function of Specific Impulse, RBP Configuration, Ammonia Propellant

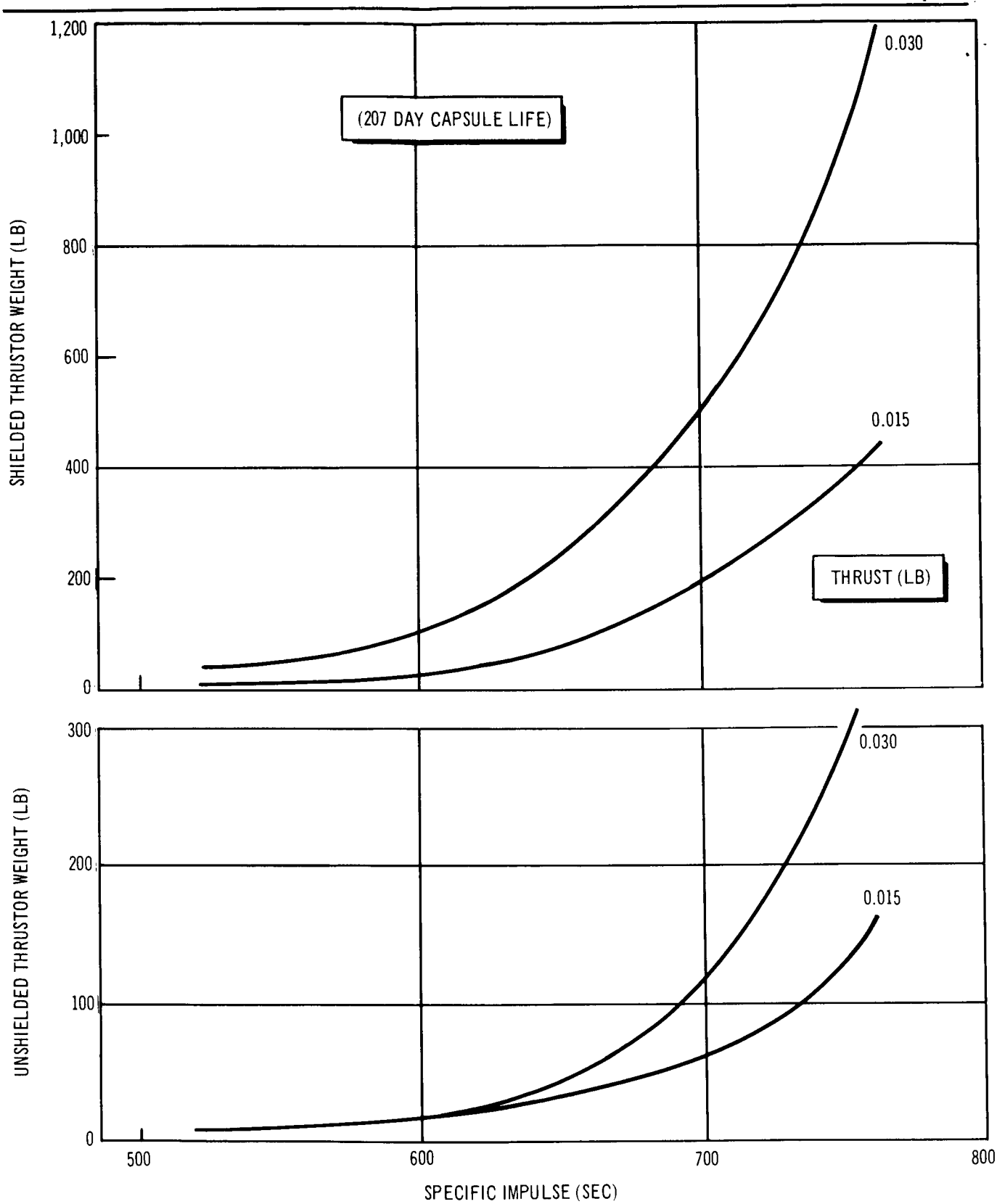


Figure 3-78. Po-210 Thrustor Weight as a Function of Specific Impulse, RBP Configuration, Hydrogen Propellant

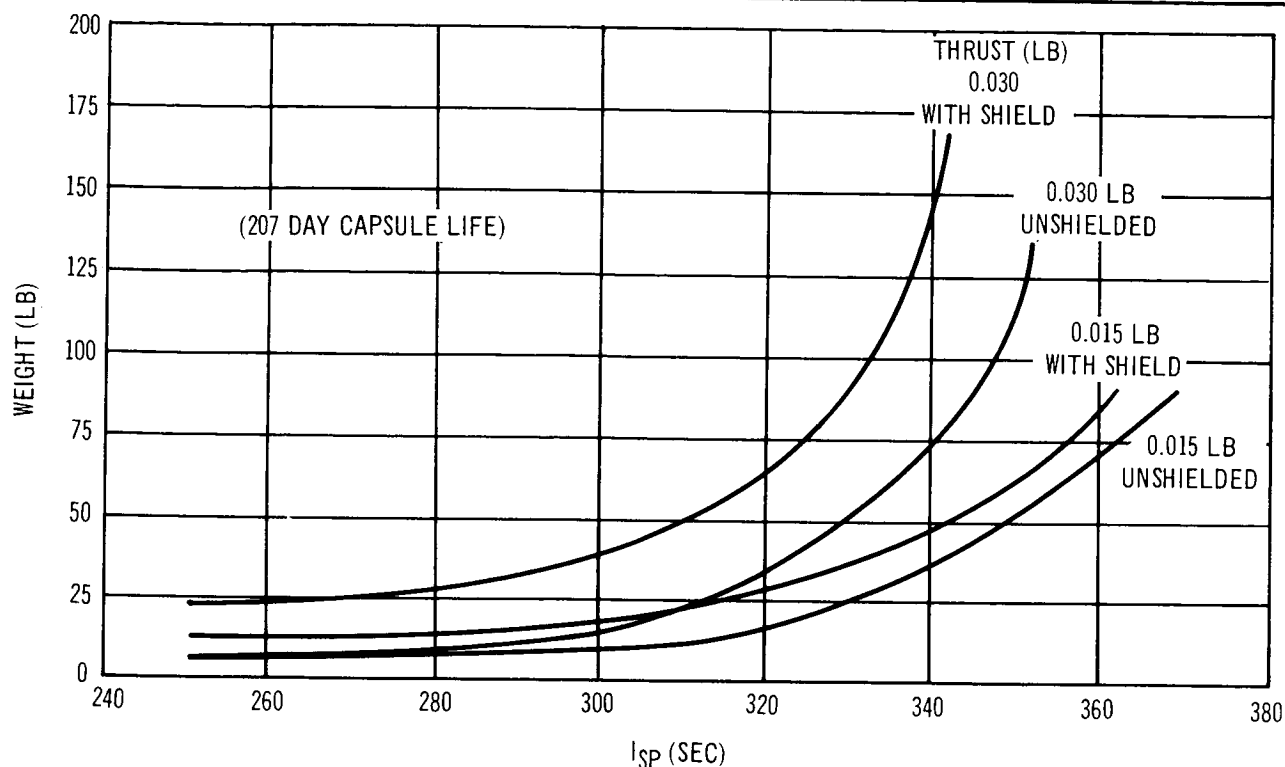


Figure 3-79. Po-210 Thrustor Weight as a Function of Specific Impulse, Solar Powered Configuration, Ammonia Propellant

uranium thickness for Po-210 gammas presented in Reference 16. Uranium thicknesses range from 1.0 to 3 cm depending on the MORL operating mode. To give a conservative estimate, the gamma shielding effect of the LiH neutron shield was not included.

The neutron shield material selected was lithium hydride because of its light weight and large neutron removal cross-section. The lithium hydride thickness required to reduce the point source neutron dose rate at 5 ft to 50% of the allowable dose (0.25 mrem/hour and 2.5 mrem/hour for the RBP and solar modes, respectively) was determined by using the curve of transmission factor as a function of lithium hydride thickness, shown in Figure D-1 of the Appendix. Thicknesses ranged from 10 to 39 cm, depending on MORL operating mode.

Since the neutrons mean free path in tungsten is about 5 cm and the isotope capsule walls are characteristically 1 cm thick, a capsule wall neutron transmission factor was not applied. The attenuation factor for neutrons

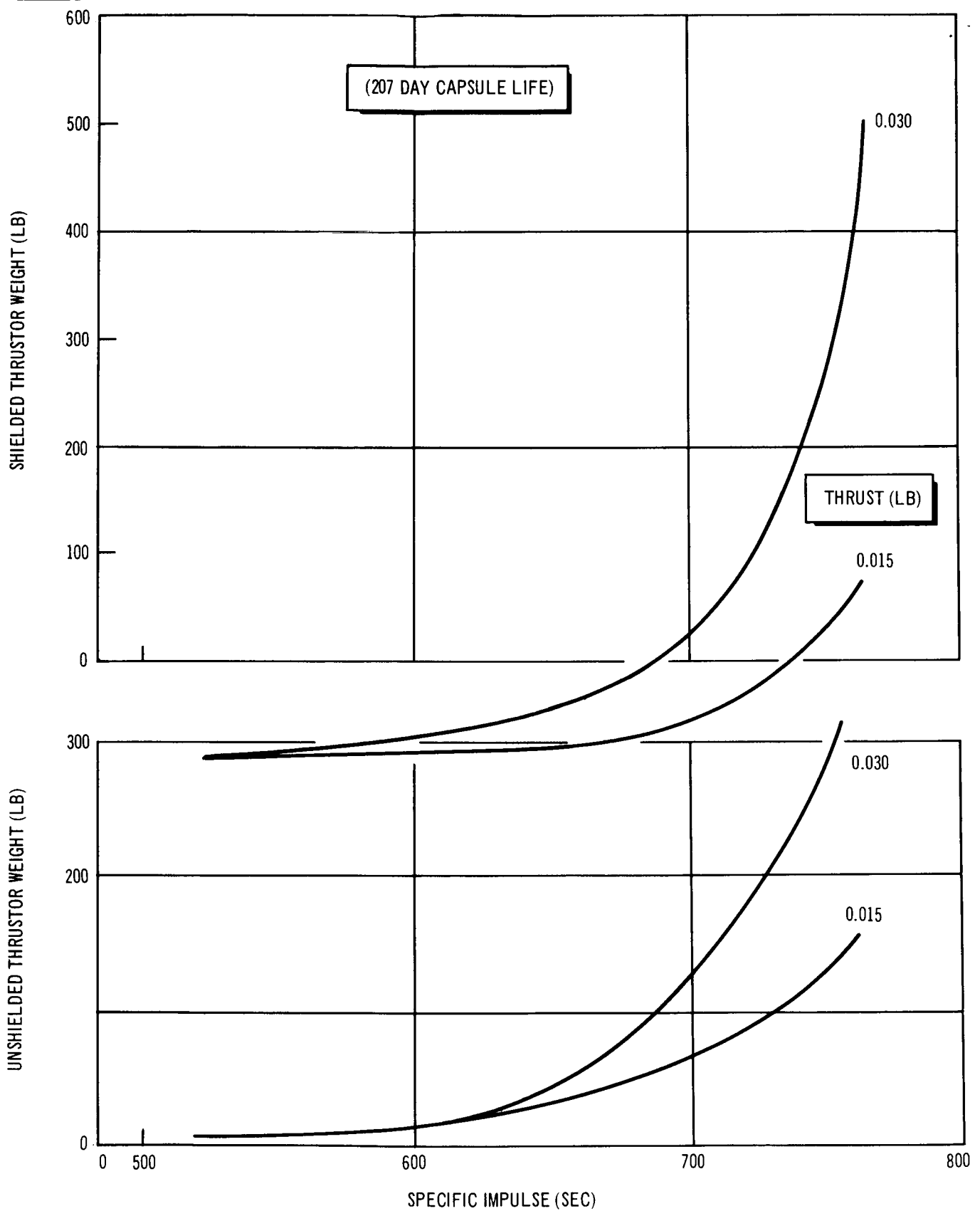


Figure 3-80. Po-210 Thrustor Weight as a Function of Specific Impulse, Solar Powered Configuration, Hydrogen Propellant

passing through the uranium gamma shield was also neglected since the shield thickness represented less than one neutron mean free path.

Figures 3-77, 3-78, 3-79, and 3-80 present shielded and unshielded thruster weights as a function of I_{sp} .

3.4.4.3 Promethium-147 Thruster Analysis

In contrast to alpha emitters, Pm-147 emits low-energy beta particles and thus generates no helium gas. This eliminates the problem of pressure buildup at high temperatures and the necessity of using porous media to relieve capsule pressure. The oxide form, Pm_2O_3 , has a melting point of 4,100°F.

Pm_2O_3 may be less inert and more prone to chemical attack than PuO_2 . Battelle-Northwest has revealed that this fuel form decomposes after exposure to either fresh water or sea water for a period of a few months. Present material compatibility information interpreted from preliminary tests with the rare earths, neodymium and samarium, two nonradioactive elements which are chemically similar to promethium, indicate that at 2,000°F Pm_2O_3 exhibits excellent compatibility with molybdenum while the cobalt-based alloys reveal some evidence of chemical attack.

Pm_2O_3 powder with a packing fraction of 90%, an effective specific activity of 1.88 W/cm³ and an effective density of 6.5 gms/cm³ was used for the promethium thruster analysis. With the half-life of Pm-147 at 2.67 years, the ratio of the initial power level and end-of-mission power level would be approximately 4. To obtain propellant exhaust temperatures of 3,500°F toward the end-of-mission, the fuel loading would provide exhaust temperatures of the order of 4,900°F during the early phases of the mission when power generation is highest. Since the Pm_2O_3 fuel form melts at 4,100°F, the maximum allowable fuel centerline temperature should be nominally restricted to 3,900°F. Therefore, the exit gas temperature of the thruster cannot exceed 3,500°F during any phase of the mission since there is a 100° to 200°F temperature increase across the fuel, and the fuel temperature will increase 300°F in going from the flow to the no-flow case. For a 3,500°F initial exit gas temperature, the end of mission exit gas temperature would

decay to 2,400°F. To assure a constant thrust during the mission, the propellant flow rates would have to be adjusted to compensate for the lower I_{sp} . Table 3-38 presents typical results of the Pm-147 thruster analysis with ammonia and hydrogen propellants for a 5.17-year mission life. Figures 3-81, 3-82, 3-83, and 3-84 present thruster weights as a function of I_{sp} . To alleviate the temperature limitations described above, the possibility of thruster replacement during a normal resupply mission approximately mid-way through the 5-year mission, was considered. A preliminary design analysis of a Pm-147 thruster with a 2.98-year life was performed. The 2.98-year mission life assumed replacement of the thrusters on the 12th resupply trip. For the 2.98-year capsule life, the temperature level at the end of the mission is 0.83 times the temperature level at the beginning of mission. The end-of-mission exit gas temperature is then 2,850°F. Table 3-39 presents typical results of the Pm-147 thruster analysis for a 2.98-year capsule life. Figures 3-85, 3-86, 3-87, and 3-88 present thruster weights as a function of I_{sp} .

Promethium-147 is a pure beta emitter which decays to samarium-147 with a half-life of 2.6 years. Two betas are emitted: one at a maximum energy of 0.225 MeV (with a yield fraction of nearly 100%) and a second one at a maximum energy of 0.10 MeV (with a yield of $10^{-2}\%$). In the 0.10 MeV beta decay, a 0.121 MeV gamma is, in turn, emitted with a yield of $3.5 \times 10^{-3}\%$ for each Pm-147 disintegration.

Two impurities, Pm-147 and Pm-148, are usually present in Pm-147. Promethium-148 has a 42-day half-life and, therefore, aging Pm-147 for a half-life (2.6 years) results in radiation field reduction to that characteristic of Pm-147 and Pm-146 only. The Pm-146 activity in Pm-147 source was assumed, in accordance with Reference 16, to be $5 \times 10^{-5}\%$ by beta activity.

Promethium-146 decays in two modes. Some 35% of the disintegrations occur by beta emission which result in samarium-146. And 65% of the Pm-146 disintegrations occur by electron capture which result in neodymium-146. Gammas having energies of 0.75 MeV and 0.45 MeV are emitted in the electron capture process. The half-life of Pm-146 has been reported as 1.94 and 4.4 years, with the latter value being the one most recently reported in the literature.

Table 3-38

TYPICAL CAPSULE DIMENSIONS AND WEIGHTS
(Pm-147 ISOTOPE--5.17-YR CAPSULE LIFE) F = 0.015 LB

T _{gas} Exit (°F)	Watts per Capsule	Length (in.)	ID (in.)	Wall Thick- ness (in.)	Overall Length (in.)	OD (in.)	W Fuel (lb)	Weight of Capsule (lb)	Total Weight (lb)	Number of Capsules Required
Hydrogen Propellant										
1,500	590	4.8	2.25	0.20	5.2	2.65	4.5	7.0	11.5	2
2,000	665	5.4	2.25	0.20	5.8	2.65	5.1	7.6	12.7	2
3,000	810	6.5	2.25	0.25	7.0	2.75	6.2	11.4	17.6	2
Ammonia Propellant										
1,500	895	7.3	2.25	0.20	7.7	2.45	6.6	9.7	16.3	1
2,000	904	7.4	2.25	0.20	7.8	2.45	6.9	9.8	16.7	1
3,000	1,010	8.3	2.25	0.25	8.8	2.75	7.8	13.7	21.5	1

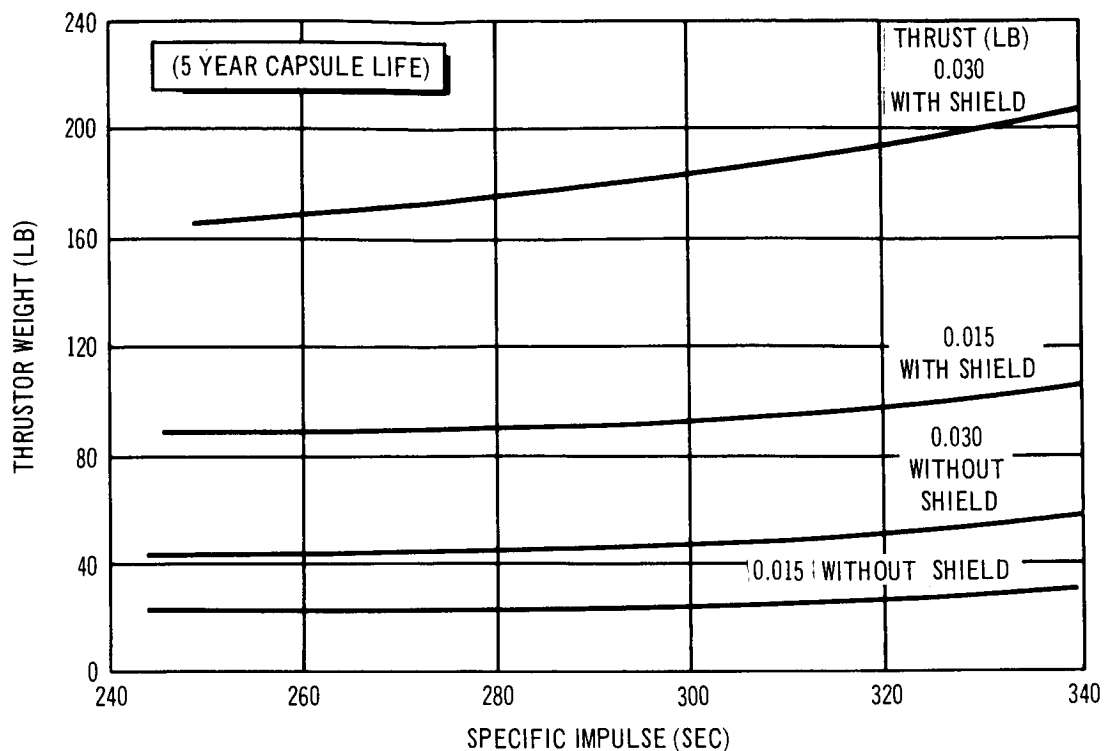


Figure 3-81. Pm-147 Thrustor Weight as a Function of Specific Impulse, RBP Configuration, Ammonia Propellant

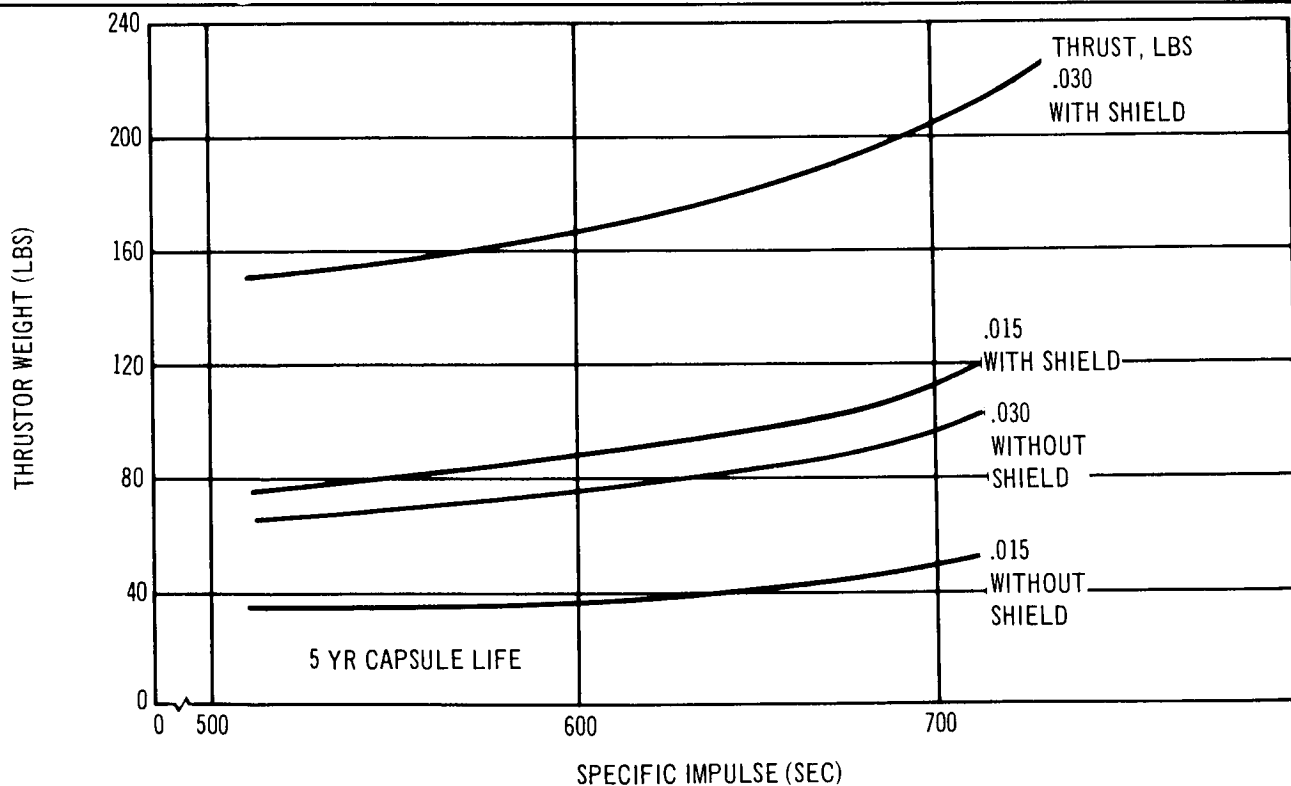


Figure 3-82. Pm-147 Thrustor Weight as a Function of Specific Impulse (Hydrogen Propellant RBP Configuration)

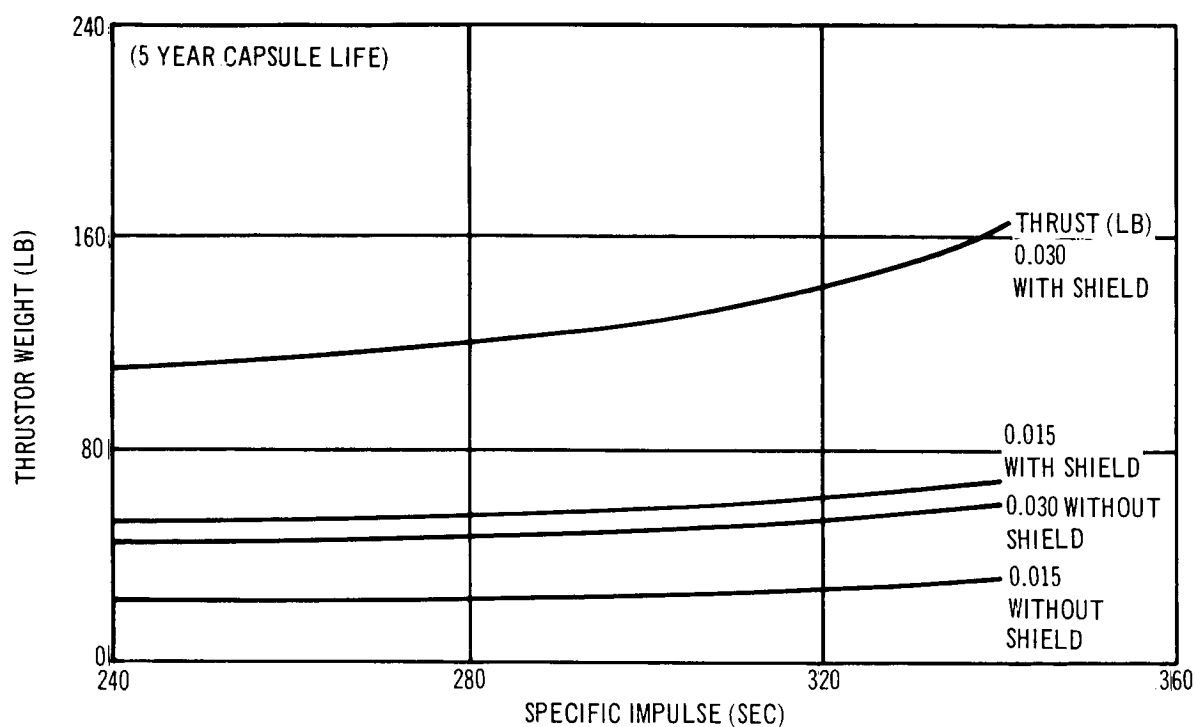


Figure 3-83. Pm-147 Thrustor Weight as a Function of Specific Impulse, Solar Power Configuration, Ammonia Propellant

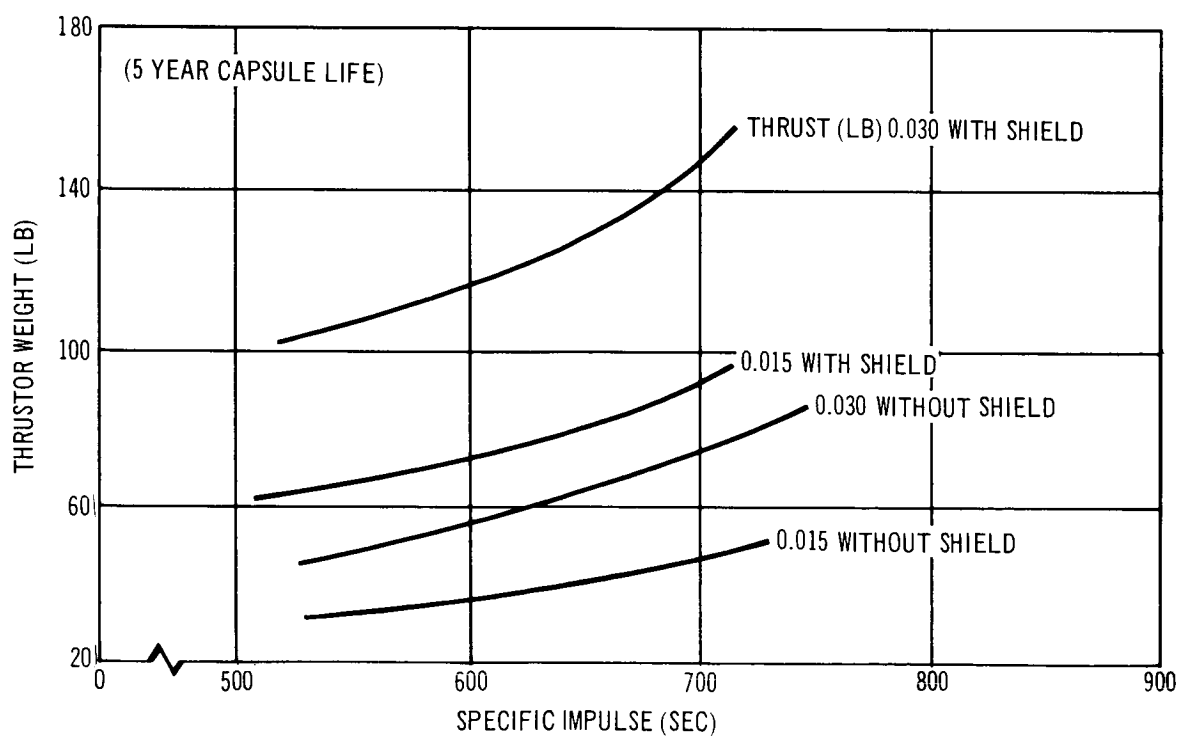


Figure 3-84. Pm-147 Thrustor Weight as a Function of Specific Impulse, Solar Power Configuration, Hydrogen Propellant

Table 3-39
TYPICAL CAPSULE DIMENSIONS AND WEIGHTS
(Pm-147 ISOTOPE--1,090-DAY CAPSULE LIFE) F = 0.015 LB

T _{gas} Exit (°F)	Watts per Capsule	Length (in.)	ID (in.)	Wall Thick- ness (in.)	Overall Length (in.)	OD (in.)	Fuel (lb)	Weight of Capsule (lb)	Total Weight (lb)	Number of Capsules Required
Hydrogen Propellant										
1,500	651	5.3	2.25	0.20	5.7	2.65	5.0	7.4	12.4	1
2,000	735	6.0	2.25	0.20	6.4	2.65	5.7	8.3	14.0	1
3,000	870	7.3	2.25	0.25	7.8	2.75	6.8	12.4	19.2	1
Ammonia Propellant										
1,500	470	4.9	2.0	0.20	5.3	2.4	3.6	6.1	9.7	1
2,000	497	5.2	2.0	0.20	5.6	2.4	3.8	6.4	10.2	1
3,000	553	5.7	2.0	0.25	6.2	2.5	4.2	9.0	13.2	1

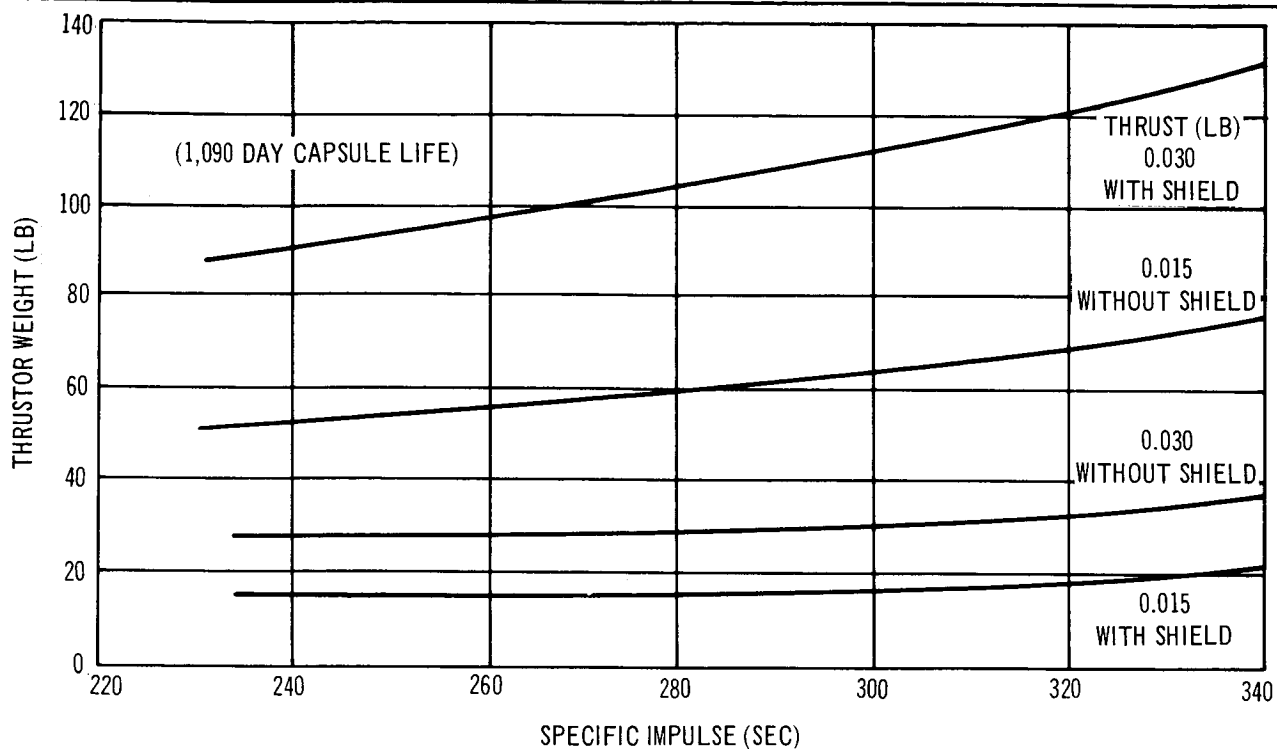


Figure 3-85. Pm-147 Thrustor Weight as a Function of Specific Impulse, RBP Configuration, Ammonia Propellant

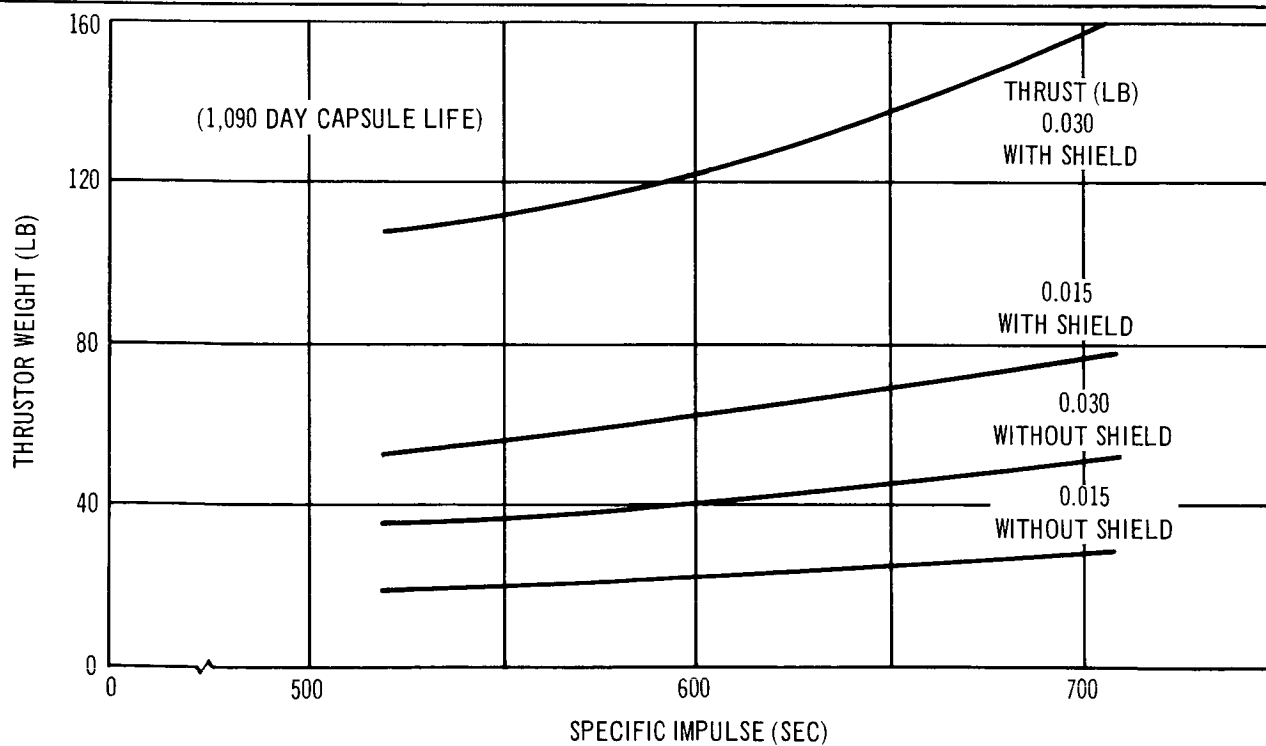


Figure 3-86. Pm-147 Thrustor Weight as a Function of Specific Impulse, RBP Configuration, Hydrogen Propellant

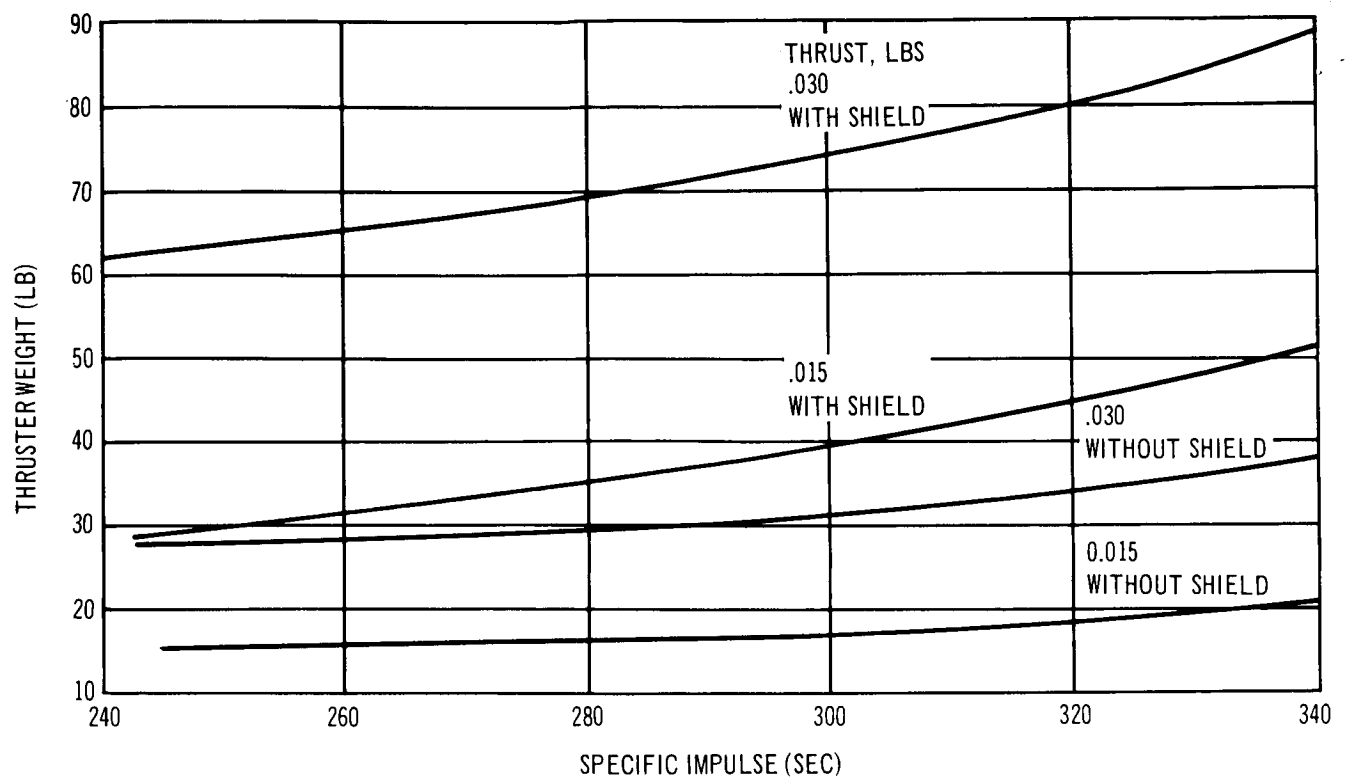


Figure 3-87. Pm-147 Thruster Weight as a Function of Specific Impulse, Solar Power Configuration, Ammonia Propellant

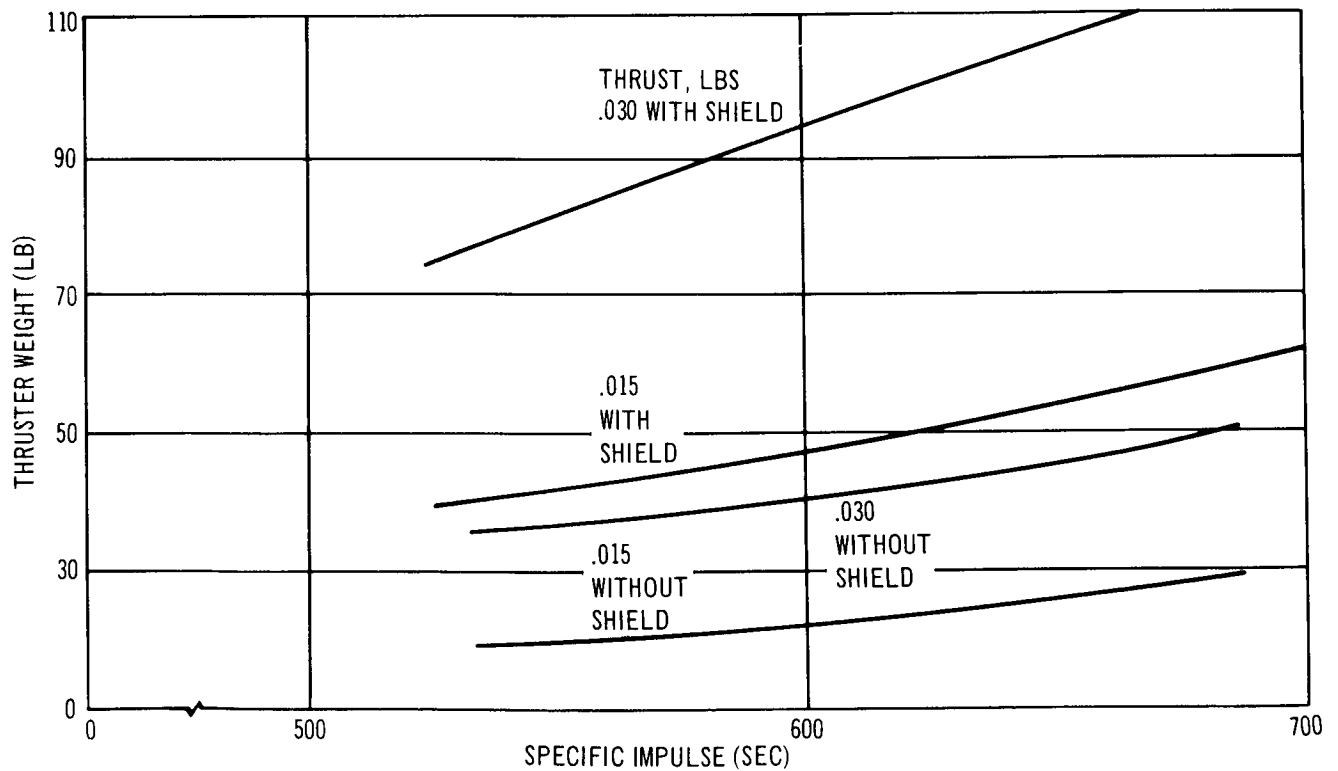


Figure 3-88. Pm-147 Thruster Weight as a Function of Specific Impulse, Solar Power Configuration, Hydrogen Propellant

The radiation fields associated with promethium-147 are caused by bremsstrahlung from the Pm-147 and Pm-146 betas and the above mentioned 0.121 MeV, 0.75 MeV and 0.45 MeV gammas.

TRW Systems developed a computer code to calculate the radiation fields associated with radioisotopes such as Pm-147.

The computer program, called DECAY, permits an accurate analysis of the energy release and the photon radiation fields associated with radioisotopes. Although many codes which calculate the radiation fields surrounding radioisotopes do not take into consideration bremsstrahlung from not-allowed beta transitions, the basic equations employed in this program to compute the average energy factor for beta emission and the bremsstrahlung associated with such beta emission do permit inclusion of not-allowed beta transitions. The relativistic form of the coulomb correction factor is also employed. The inclusion of not-allowed beta transitions and the relativistic form of the coulomb correction factor can result in significant increases in the accuracy of calculations for certain isotopes. The bremsstrahlung spectrum from any arbitrary source material is divided into twenty energy groups. Energy-dependent transmission calculations are performed with these groups. For photon transmission in the energy range where Compton scattering becomes predominant, tables of buildup factors as a function of shield thickness, mass attenuation coefficient, and energy are provided and are used in the calculations. As a result, the program performs a relatively detailed analysis of radiation fields surrounding radioisotopes.

DECAY was used to generate the dose rate from pure Pm-147 and pure Pm-146. The bremsstrahlung spectrum obtained using DECAY is plotted for the Pm-147, 0.225 MeV maximum energy betas in Figure D-2 of the Appendix. A plot of the dose rate at 1 m from a Pm-147 source with a Pm-146 impurity of $5 \times 10^{-5}\%$ by beta activity is presented in Figure D-3 of the Appendix as a function of tungsten shield thickness. Tungsten was selected as the shield material because of the availability of DECAY shield calculation results. Figure D-3 of the Appendix shows that the dose rate from bremsstrahlung is negligible when considering tungsten thicknesses greater than about 0.1 cm, and that the dose rate as a function of thickness curve has a slope characteristic of gamma transmission. For tungsten

thicknesses greater than 0.2 cm the Pm-146 gammas can be considered to contribute the entire radiation field.

In summary, the radiation field surrounding a radioisotope Pm-147 source with a Pm-146 impurity of $5 \times 10^{-5}\%$ by beta activity, consists primarily of the 0.45 MeV and the 0.75 MeV gammas originating from Pm-146. Reference 17 presents a method for determining a self-shielding factor, which was used in the calculations. The factor applied was conservatively based on the mean free path of the 0.75 MeV Pm-146 gamma when considering spherical source geometry. The thruster self-shielding factor ranged from 0.2 to about 0.35 depending on source size.

After applying the source self-shielding factor and the transmission factor for the capsule walls, the additional tungsten thickness required to reduce the dose rate at 5 ft to 0.5 mr/hour for the RBP power mode and to 5 mr/hour for the solar power mode was determined from Figure D-3 of the Appendix. The thicknesses ranged from 2 cm to 4.8 cm depending on the mode of operation. Figures 3-81 through 3-88 present shielded and unshielded thruster weights as a function of I_{sp} .

3.4.4.4 Plutonium-238 Thruster Analysis

Fuel forms of Pu-238 have been developed and flight qualified for various SNAP applications. Because of the low-radiation level and long half-life, plutonium may well be the most suitable isotope for long-lived missions. The low melting point (1,180°F) and pyrophoricity of the pure metal favor its use in the oxide form, (PuO_2). Recent investigation at Mound Laboratory with plutonium dioxide microspheres indicate that this fuel form shows promise for high temperature applications. In addition, the microsphere diameters are well above the respirable size range (10μ). This characteristic, coupled with their extreme insolubility and inertness to chemical attack, makes PuO_2 one of the most biologically safe fuel forms available today.

Plutonium fuel forms, as well as all other alpha-emitting radioisotopes, produce helium atoms when the alpha particles (helium nuclei) are slowed down and allowed to capture their missing orbital electrons. This results in a helium gas pressure buildup within a closed or sealed heat source capsule and introduces the problem of high temperature creep of the capsule

materials at the typical radioisotope thruster operating temperatures. One method of relieving this pressure involves the design and use of a porous plug, permeable to helium but not to the microspheres. Mound Laboratory has shown promising results in a long duration test during which it was demonstrated that fine PuO_2 powder can be contained in a vessel fitted with a series of frits (in this case stainless steel) which allow only helium release.

The PuO_2 fuel form is presently available for reliable operation at temperatures of up to approximately $2,000^\circ\text{F}$. Mound Laboratory indicates that experiments are presently under way at higher temperatures to ascertain the detailed fuel form characteristics. They estimate that, by late 1966, $2,700^\circ\text{F}$ fuel form technology will be available for routine application and that, by 1967, the operational technology will be extended to approximately $4,000^\circ\text{F}$. It is also of interest to note that Mound Laboratory is investigating the feasibility of coating the microspheres with metals to increase their thermal conductivity and further enhance their inert characteristics. Preliminary results show promise of achieving both objectives. In addition, an extensive compatibility program is under way at Mound Laboratory to determine which containment materials are best suited for use with PuO_2 microspheres.

The design of the PuO_2 thruster capsules was based on the use of a porous plug, designed to vent helium gas generated by isotopic decay. The fuel form has a specific activity of 2.93 W/cm^3 and an effective microsphere density of 7.5 gm/cm^3 . The fuel centerline temperature during no-flow conditions was restricted to $4,100^\circ\text{F}$, 200°F below the melting point. For a $4,100^\circ\text{F}$ fuel centerline temperature, the fuel diameter can not exceed 1.76 in. for an exit gas temperature of $3,500^\circ\text{F}$ at full flow.

The design of the thrusters (which took into account fuel power decay) was to achieve a specified I_{sp} at the end of the mission. Over the 5-year mission life the Pu-238 power level decreases by 4%.

Typical results of the design analysis for a Pu-238 O_2 thruster with hydrogen and ammonia propellants as a function of end-of-mission I_{sp} are presented in Table 3-40. Pu-238-fueled thrusters were also sized for use with CO_2 biowaste as the propellant. These thrusters were designed for $1,650^\circ\text{F}$ exhaust temperatures at thrust levels of 0.0257 and 0.0156 lb corresponding to the baseline RBP configuration. The exhaust temperature of $1,650^\circ\text{F}$ was

Table 3-40

TYPICAL CAPSULE DIMENSIONS AND WEIGHTS
(Pu-238 ISOTOPE--F = 0.015LB)

T _{gas} Exit (°F)	Watts Per Capsule	Length (in.)	ID (in.)	Wall Thick- ness (in.)	Overall Length (in.)	OD (in.)	W Fuel (lb)	Weight of Capsule (lb)	Total Weight (lb)	Number of Capsules Required
Hydrogen Propellant										
1,500	154	2.60	1.25	0.20	3.00	1.65	0.80	2.2	3.1	2
2,000	167	2.83	1.25	0.20	3.21	1.65	0.90	2.4	3.3	2
3,000	202	3.43	1.25	0.25	3.93	1.75	1.1	3.3	4.4	2
3,500	221	3.75	1.25	0.30	4.35	1.85	1.3	4.4	5.7	2
Ammonia Propellant										
1,500	213	3.60	1.25	0.20	4.0	1.65	1.2	3.0	4.2	1
2,000	226	3.83	1.25	0.20	4.23	1.65	1.3	3.1	4.4	1
3,000	250	4.23	1.25	0.25	4.73	1.75	1.4	4.4	5.8	1
3,500	264	4.47	1.25	0.30	5.07	1.85	1.5	5.8	7.3	1

selected because the corresponding I_{sp} will satisfy the impulse requirements of 106 lb-sec orbit when utilizing all available CO_2 generated by the life support system. CO_2 thrusters can be designed for temperatures of up to 3,000°F. Table 3-41 presents the results of a CO_2 thruster design with CO_2 as the propellant. It should be noted that CO_2 may attack W-25Re above this temperature and noble metal flow tubes, such as platinum-rhodium would be required.

PuO_2 thrusters, using sealed capsules to contain the helium generated from isotopic decay, were sized during a previous study. These results were used in the overall system weight analysis.

Since the radioisotope provides a continuous source of heat, the thruster assembly must be designed to accommodate this energy during both propellant flow and no-flow conditions. High thermal efficiency is desired during flow to minimize thruster weight and isotope inventory. However, during no-flow conditions, the entire isotope heat must be transferred to space without exceeding the maximum design temperature limitation imposed by the isotope fuel melting point. For a PuO_2 thruster, a safe limiting temperature at the fuel centerline during no-flow conditions was estimated to be 4,100°F, approximately 200°F below the isotope melting point.

An analysis was conducted using the TRW thermal analyzer digital computer program (TRW/TAP) which simulates a heat transfer system by means of an electrical analog network. The network is a series of solid and fluid nodes, representing the thruster and propellant respectively, interconnected by thermal resistances representing the various heat transfer paths between nodes. The steady-state solution to a given network is obtained by the use of a modified relaxation technique on a system of simultaneous finite difference equations. The solution provides the temperature of each node in the network. The code includes temperature-dependent thermal transport properties, thermal conductivity, specific heat, and emissivity.

Circumferential symmetry was assumed except at the fin. The asymmetric effect of the fin was included by connecting the node in the module of the thruster to the fin and then appropriately interconnecting the nodes within the

Table 3-41
TYPICAL CAPSULE DIMENSIONS AND WEIGHTS
(Pu-238 ISOTOPE--CO₂ PROPELLANT)

Typical Thrustor Weights						
T _{gas} Exit (°F)	I _{sp} (secs ⁻¹)	Thrust Level (lb)	Number of Capsules	Total Capsule Weight (lb)	Capsule Module Weight (lb)	Total Thrustor Weight (lb)
1,650	122	0.016	1	2.2	0.3	5.5
1,650	122	0.026	1	3.2	0.4	6.8

Typical Capsule Dimensions						
T _{gas} Exit (°F)	Total Watts	Length (in.)	ID (in.)	Wall Thickness (in.)	Overall Length (in.)	OD (in.)
1,650	83	2.2	1.0	0.2	2.6	1.4
1,650	136	3.7	1.0	0.2	4.1	1.4

Weight Fuel (lb)	Weight Capsule (lb)	Total Weight (lb)
0.5	1.7	2.2
0.8	2.4	3.2

fin. The flow area of the coiled propellant flow tubes was simulated by an annular flow passage with the correct heat transfer area of the coiled tube. An approximate two dimensional model of the exhaust nozzle was included in the network. However, nozzle heat losses at the low flow rates of interest represent an area where considerable effort must still be expended.

In a thruster designed for ammonia propellant, ammonia decomposition in the propellant flow tube results in a net radial velocity component near the wall which produces a turbulent boundary layer. The heat transfer coefficient must be calculated from the turbulent relationship even though the bulk Reynolds number indicates laminar conditions. Preliminary mass transfer calculations indicate that the ammonia would be completely decomposed at temperatures of approximately 2,000°F. Therefore, turbulent heat transfer coefficients were used in the temperature region below 2,000°F with a laminar coefficient used above 2,000°F. In the case of the hydrogen thruster, the heat transfer coefficient was evaluated at a constant Nusselt number (laminar flow) using temperature-dependent thermal conductivity. The isotope thermal conductivity was estimated to be 1.2 Btu/hour-ft-°F. Because of lack of data it was assumed to be independent of temperature.

The thruster thermal insulation consisted of multiple refractory radiation shields. The effective thermal conductance of these shields was calculated previously with the TRW/TAP program as a function of thruster surface temperature.

The effective thermal conditioning of the thruster insulation was varied until the fuel centerline temperature during no-flow conditions was approximately 4,100°F. Propellant flow rates were then varied to obtain corresponding exit gas temperatures so that the efficiency of the thruster, as a function of exit gas temperature, could then be calculated.

The insulation required for the ammonia thruster was found to be equivalent to 35 concentric molybdenum foil shields while for the hydrogen thruster 28 molybdenum shields were required. It should be noted that these values of thermal conductance were computed on the assumptive basis of radiative heat exchange only, and that in the computation, the effect of conduction

between adjacent shields was neglected. If conduction between adjacent shields cannot be eliminated, a slightly larger number of shields will be required to obtain the required insulation effectiveness.

Temperature profiles were obtained for the following thrusters for an exit gas temperature of 3,500°F:

1. Hydrogen thrustor with 420°F inlet gas temperature.
2. Hydrogen thrustor with 125°F inlet gas temperature.
3. Ammonia thrustor with 125°F inlet gas temperature.

The profiles are presented in Figures 3-89, 3-90, and 3-91. The gas temperature profiles are all flat with the exception of a very large temperature increase near the thrustor inlet. This type of profile illustrates the effect of axial conduction. Previous computer calculations of radioisotope thrusters, while neglecting the effect of fins, also showed axial conduction of heat, but to a lesser extent. The axial heat flow is primarily through the capsule wall, thrustor module, and fins.

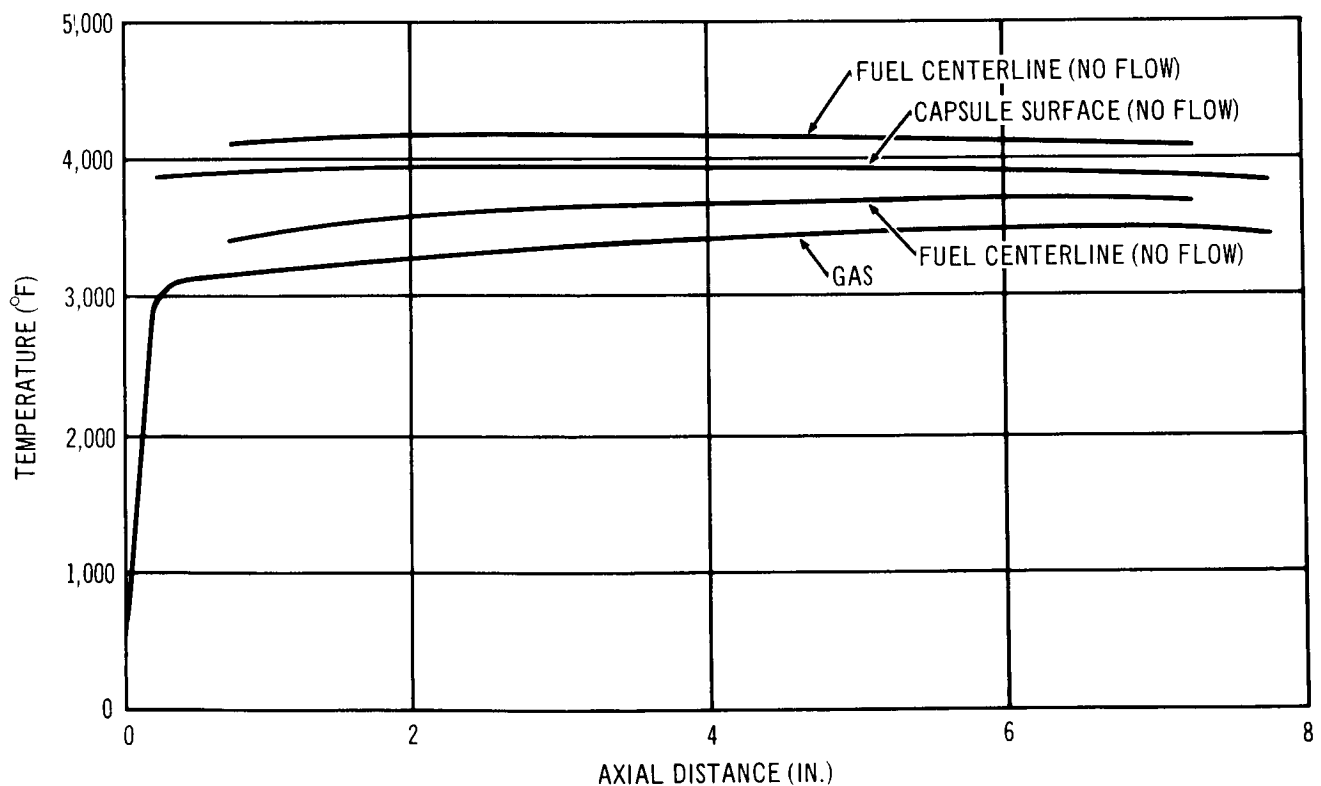


Figure 3-89. Temperature Profiles, Ammonia Thrustor 125°F Gas Inlet

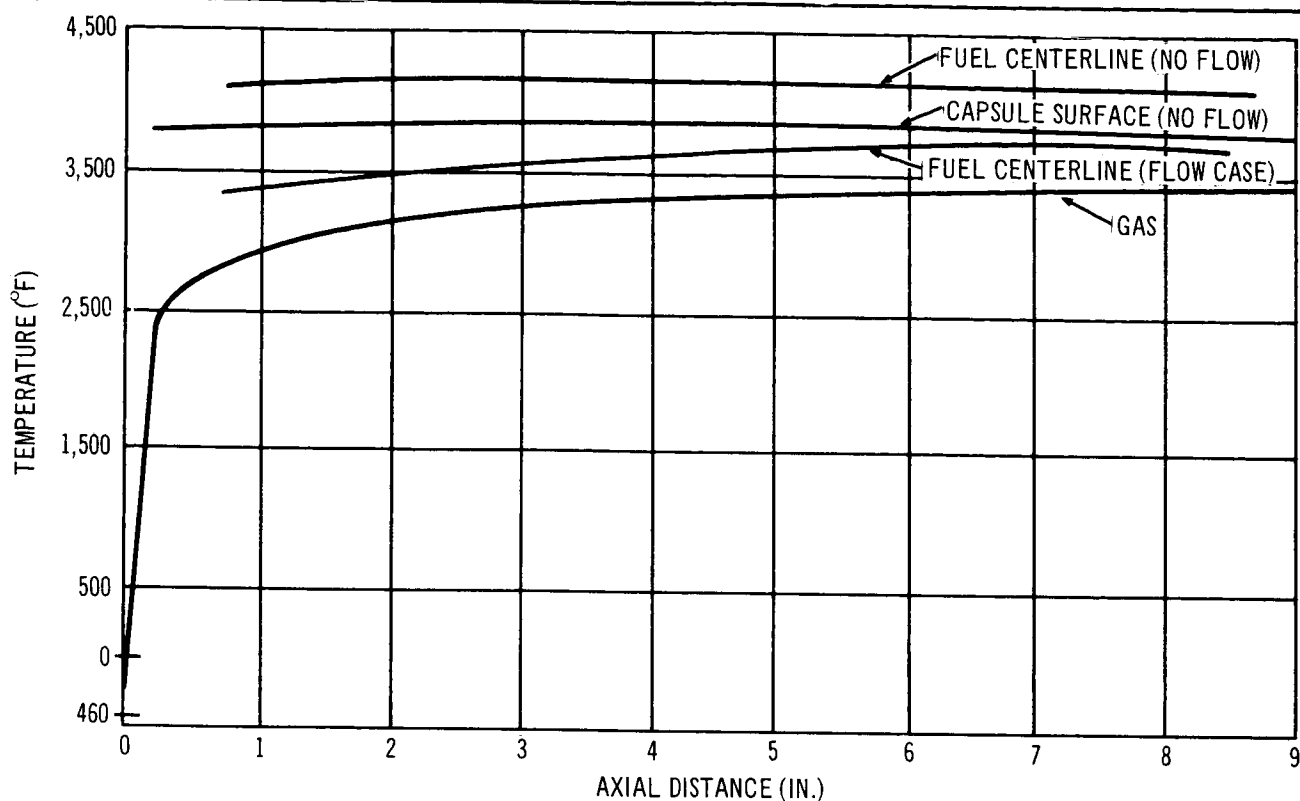


Figure 3-90. Temperature Profiles, Hydrogen Thrustor, -420°F Gas Inlet

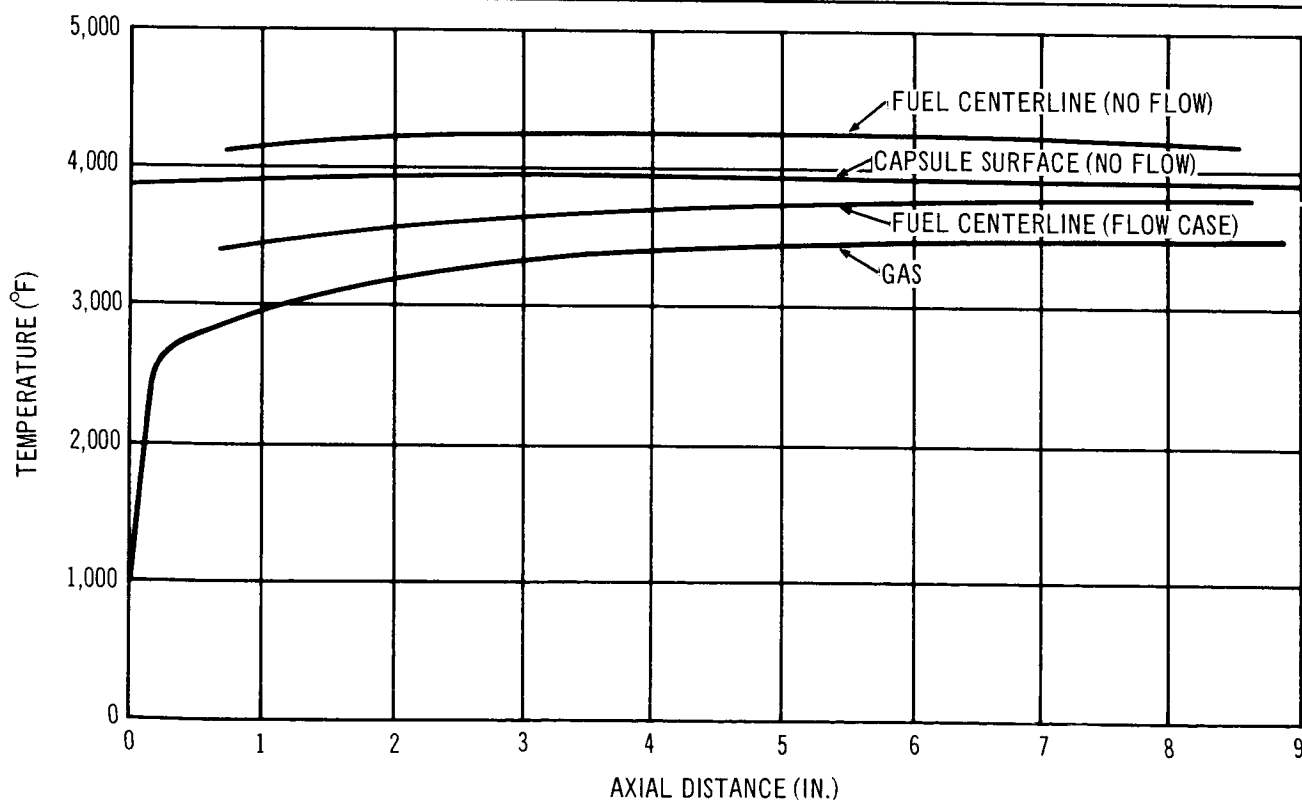


Figure 3-91. Temperature Profiles, Hydrogen Thrustor, 125°F Gas Inlet

By varying the propellant flow rates to each of the two thruster configurations, it was possible to determine the changes in thruster thermal efficiency as a function of mass flow rate. Figure 3-92 illustrates that the thermal efficiency decreases as the propellant flow rate diminishes, while the propellant exit temperature increases. It is apparent that a thruster thermal efficiency of approximately 50% is required to obtain a 3,500°F exit gas temperature without exceeding a fuel centerline temperature at 4,100°F during no-flow operation.

Thruster weight and performance characteristics over a range of thrust levels were obtained by performing a detailed design on several typical thrusters using vented PuO_2 capsules with propellant exit temperatures of 3,500°F. Thrust levels of 0.019, 0.026, and 0.042 lb were selected. A nominal thermal efficiency of 50% was chosen, based on the results of the thermal analysis.

It was necessary to select materials of construction for the thrusters which are capable of maintaining their strength at the operating temperature and are chemically compatible with the propellant during operation. In addition, the material must be capable of surviving the re-entry environment and landing impact in the event of an abort. W-25Re was chosen as the material to construct the thruster, capsule, and fins. W-25Re does not react with the propellants, has adequate strength, and is relatively ductile for a refractory alloy. Preliminary tests, conducted at TRW under the POODLE program, indicate that W-25Re appears to have adequate impact resistance for capsule applications. However, W-25Re does react with oxygen to form a volatile oxide. An oxidation-resistant cladding such as Rh-Ir alloy must, therefore, be used to ensure survival during and after re-entry. Should impact occur in the ocean, the reaction between the W-25Re and the sea water is negligible and the capsule integrity should be maintained for relatively long periods of time.

Figure 3-93 presents isotope thermal power requirements as a function of thrust level for ammonia and hydrogen propellants at 50% thermal efficiency. Figure 3-94 presents total unshielded thruster weight as a function of thrust level.

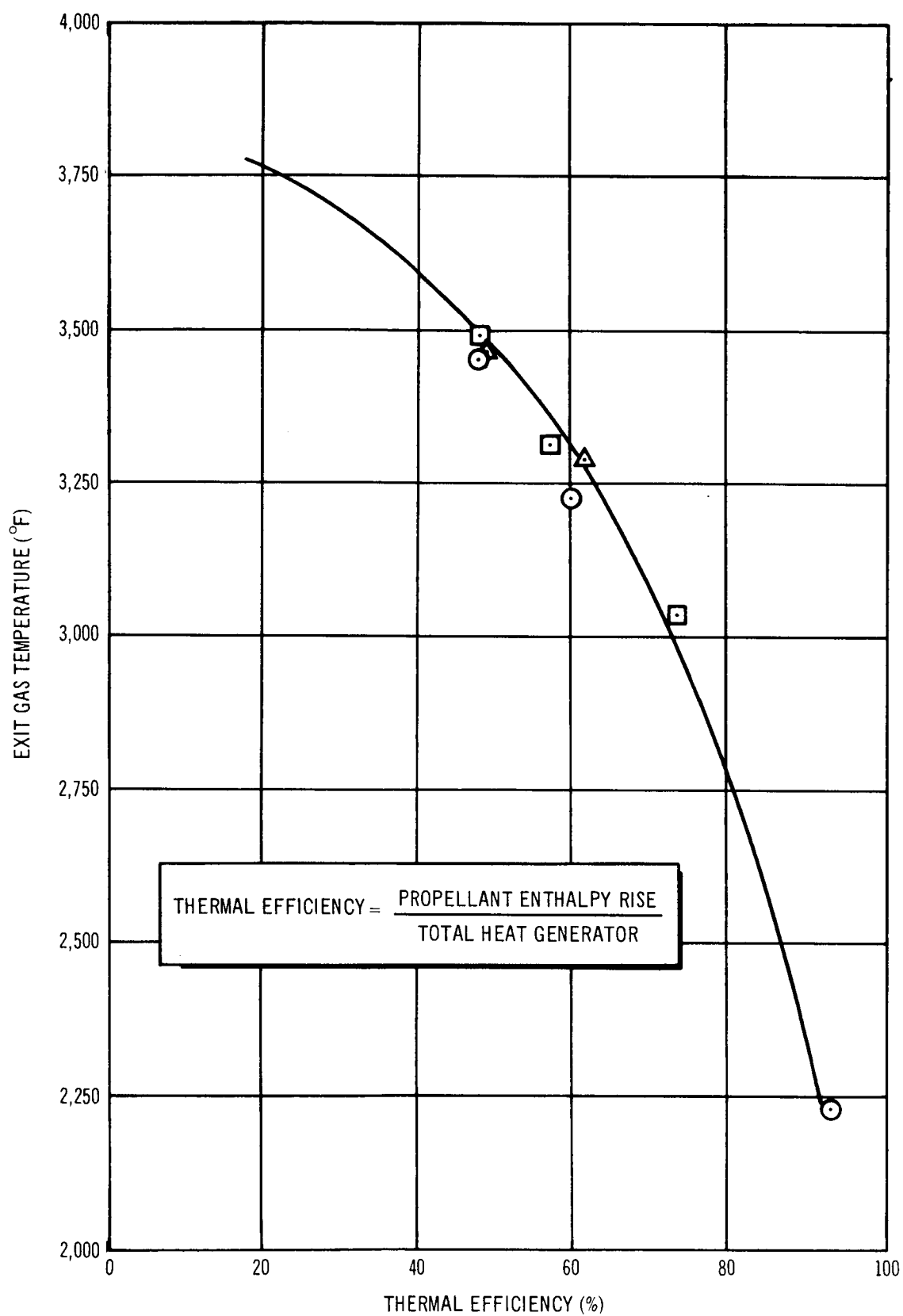


Figure 3-92. Thrustor Thermal Efficiency as a Function of Exit Gas Temperature

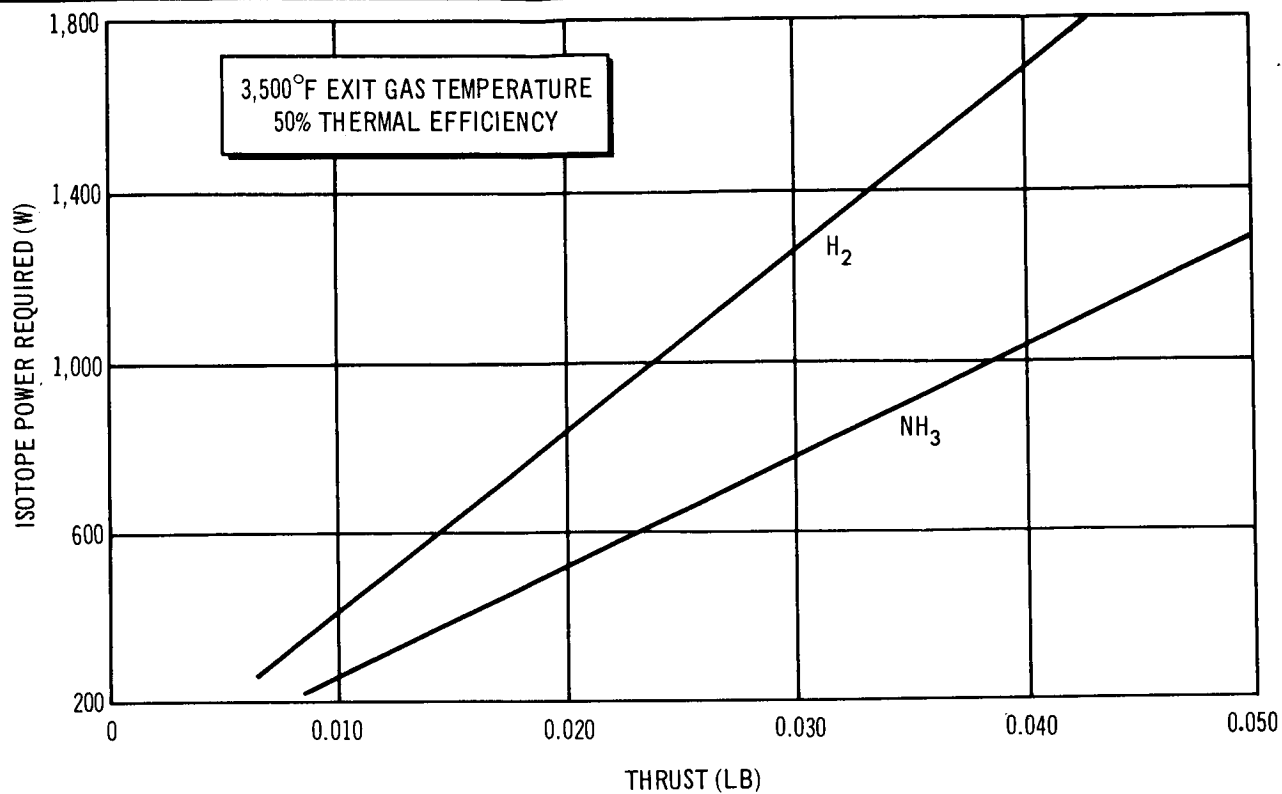


Figure 3-93. Pu-238 Isotope Power as a Function of Thrust Level

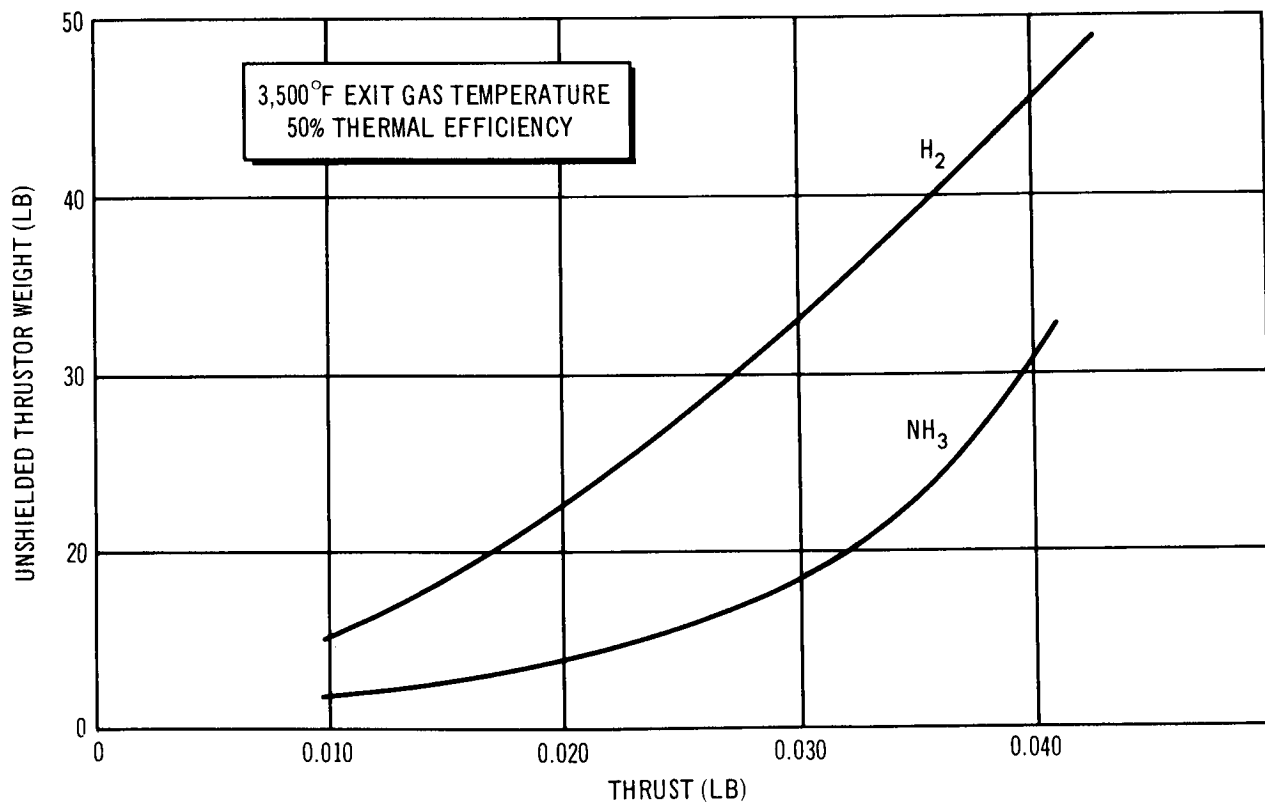


Figure 3-94. Unshielded Pu-238 Thrustor Weight as a Function of Thrust Level

Approximately 80% of the total radiation dose from a PuO_2 heat source is contributed by neutrons with the remaining 20% contributed by gammas. The neutron field from plutonium-238 decay is the result of spontaneous fission of Pu-238 and alpha-neutron reactions with the oxygen within the fuel form. The corresponding neutron source strengths are 2.53×10^3 and 1.76×10^4 n/sec-gm Pu-238 respectively. Based on this neutron production rate, the neutron dose at 5 ft from the bare PuO_2 point source is 15.1×10^{-3} mrem/hour-W.

Plutonium-238 decays to uranium-234 with a half-life of 2.5×10^5 years. Alphas at six energies are emitted in the decay of plutonium-238 with five of the six accompanied by gamma emissions of various energy levels. In addition, the continuous gamma spectrum associated with the prompt fission gammas and the fission product gammas resulting from the spontaneous fission of plutonium-238, must also be considered. From tables showing the gamma energy groups, the basic gamma source terms and the radiation fields at 1 m from a bare plutonium-238 source and neglecting gamma contributions below 0.20 MeV, the gamma dose rate at 5 ft from a bare point source is 4.73×10^{-3} mrem/hour-W.

U-238 and LiH were considered for gamma and neutron shielding, respectively. The gamma transmission factor for uranium shielded Pu-238 heat sources is shown in Figure D-4 of Appendix . This figure was used along with the plot of the neutron transmission factor as a function of lithium hydride thickness presented in Figure D-1 of Appendix , to determine the gamma and neutron shielding requirements. Since neutrons were considered to yield 80% of the total dose rate at 5 ft, their contribution was 0.4 mrem/hour and 4.0 mrem/hour for the RBP and solar modes, respectively. The gamma attenuation in the lithium hydride and neutron attenuation in the uranium were not taken into account, which resulted in a conservative shield thicknesses determination. Uranium gamma shield thicknesses ranged from zero to 1.8 cm, and lithium hydride neutron shield thicknesses ranged from 1.5 cm to 34 cm, depending on the MORL configuration. Figures 3-95, 3-96, 3-97, and 3-98 present shielded thruster weights as a function of I_{sp} .

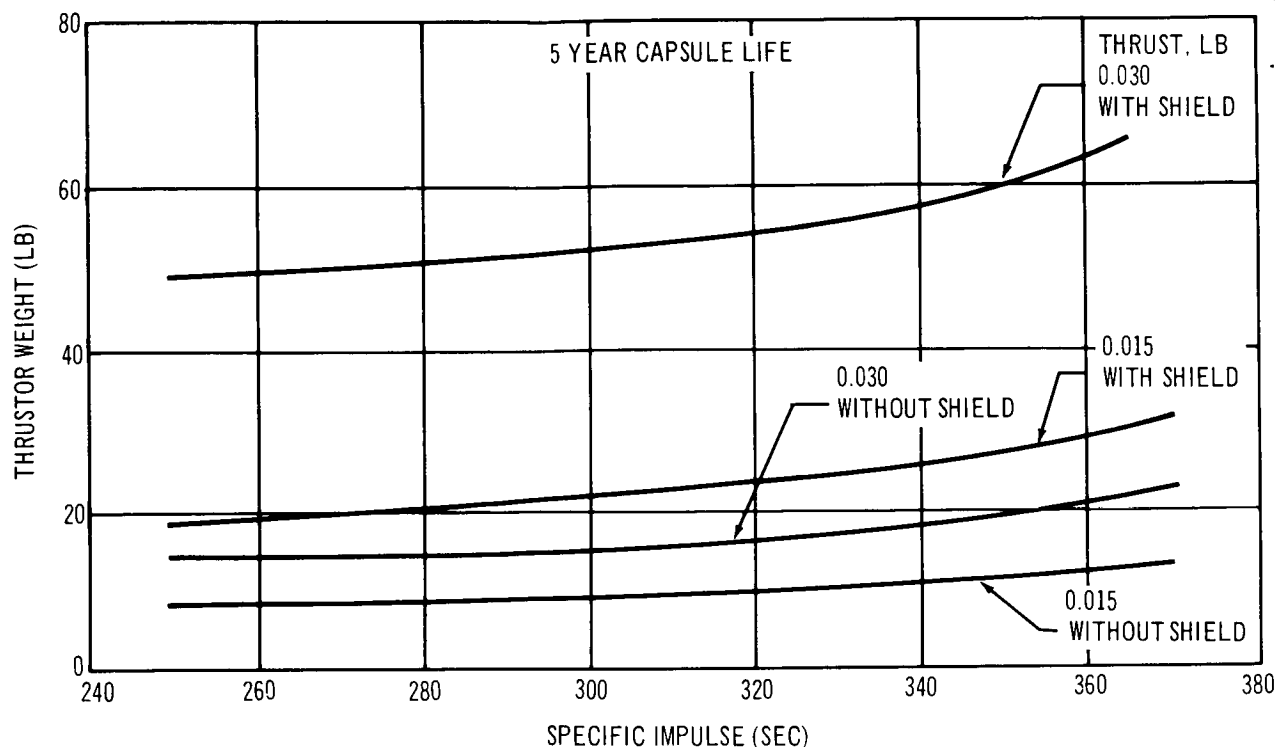


Figure 3-95. Pu-238 Thrustor Weights as a Function of Specific Impulse, RBP Configuration, Ammonia Propellant

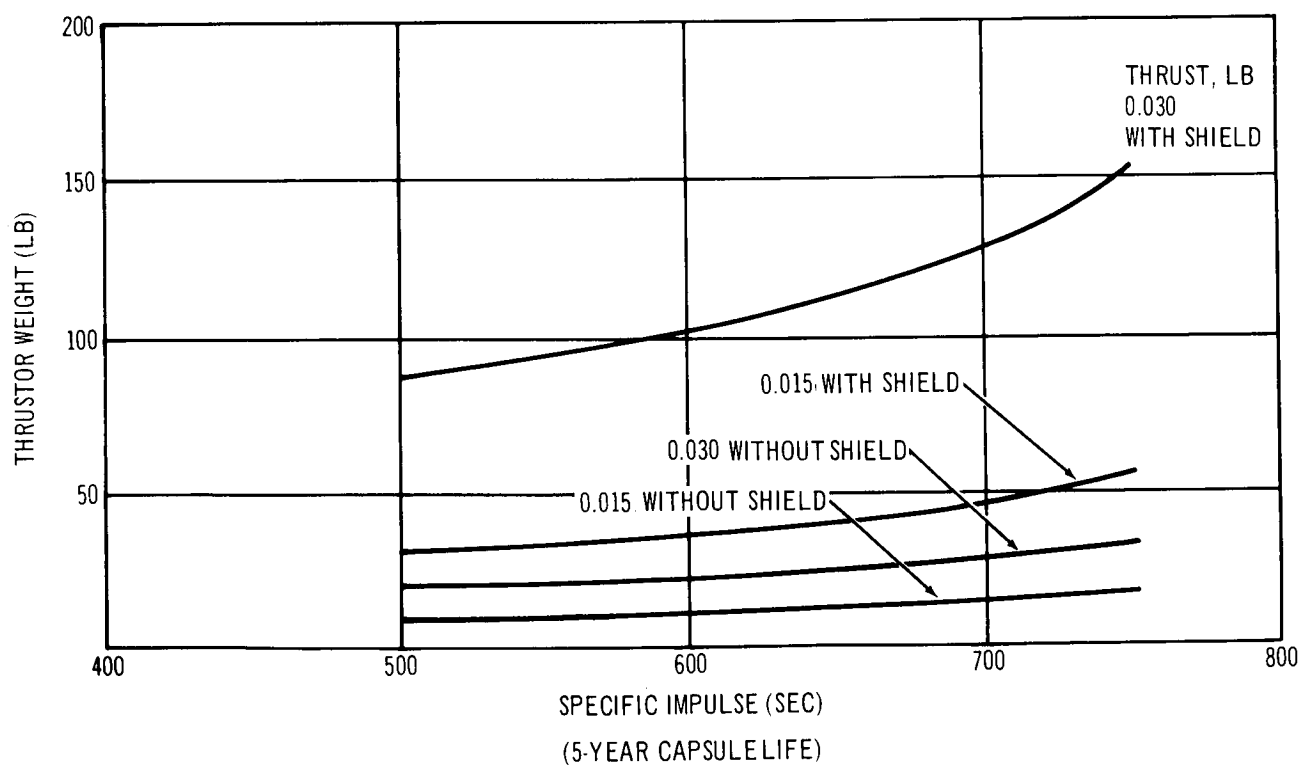


Figure 3-96. Pu-238 Thrustor Weight as a Function of Specific Impulse, RBP Configuration, Hydrogen Propellant

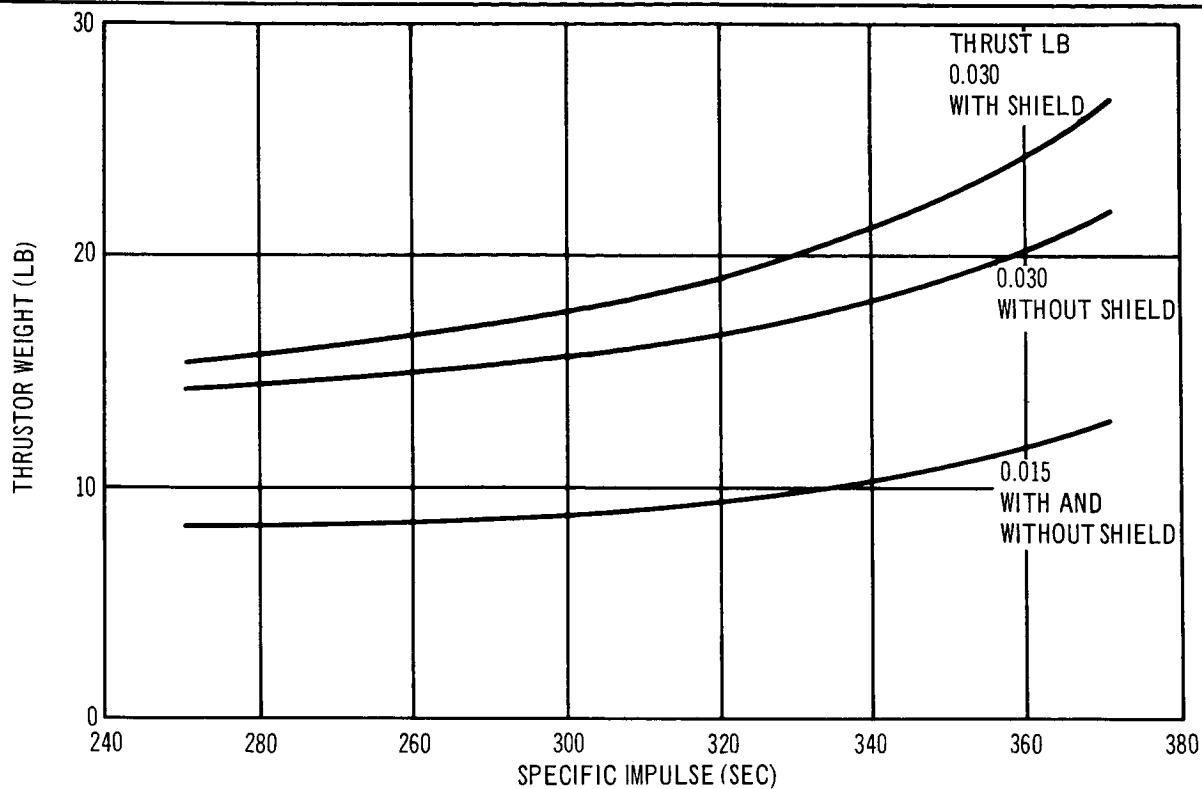


Figure 3-97. Pu-238 Thrustor Weights as a Function of Specific Impulse, Solar Power Configuration, Ammonia Propellant

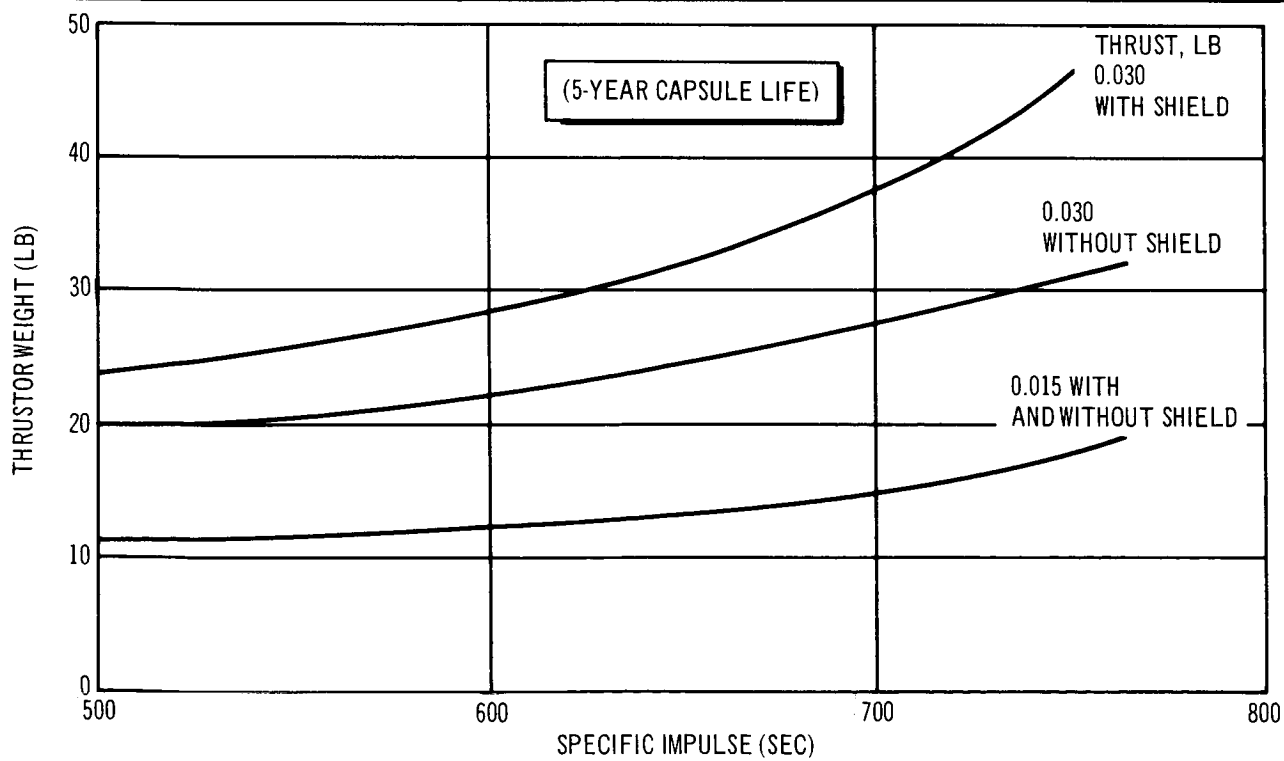


Figure 3-98. Pu-238 Thrustor Weights as a Function of Specific Impulse, Solar Power Configuration, Hydrogen Propellant

3.4.5 Parametric Design Study

The parametric calculations establish the RCS structure factor (dry system weight/dry system weight and propellant weight) for each of the radioisotope fuel candidates for the specific impulse range of interest using ammonia and hydrogen propellants in the zero-g mode for the RBP and solar power configurations. Since one of the primary considerations associated with radioisotope selection is overall system weight, the system structure factors are used as the primary basis for preliminary analysis conclusions.

To establish system structure factors as a function of I_{sp} , propellant tankage and insulation weights were also calculated. In addition, estimates of hardware weights associated with feed system valving and tubing were made. These weights, added to thruster and shield weights established in Section 3.4.4 represent the total system weight.

The tankage weights, calculated for NH_3 and liquid hydrogen, were based on a spherical geometry. The tank material considered was aluminum 2219-T62 having a yield strength of 55,000 psi. The following pressure and temperature criteria were used for stress analysis:

	<u>Hydrogen</u>	<u>Ammonia</u>
1. Operating temperature	45°R	125°F
2. Operating pressure	30 psia	325 psia
3. Design pressure	50 psia	500 psia

Hydrogen tankage insulation requirements were calculated for an ambient thermal environment of 125°F. The permissible heat leak through the insulation was defined by liquid vaporization requirements corresponding to a particular flow rate out of the tank. Thermal conductivity data for superinsulation were obtained from available supplier curves. In addition, a layer of polyurethane insulation was provided adjacent to the cryogenic tank surface to eliminate the possibility of liquifaction during prelaunch operations.

Ammonia tankage design did not call for thermal insulation because tankage operating pressures corresponded to liquid-vapor equilibrium at the ambient temperature of 125°F. However, for meteoroid protection, a polyurethane

foam shield of approximately 5 in. was provided. Tank structural support weights were estimated as 5% of bare tank weight.

Tankage requirements were established for 147-day operation on initial launch and 90-day operation for subsequent resupply launches. The structure factor curves presented in this section are based on per-orbit impulse requirements of 139 lb-sec and 278 lb-sec for the RBP and solar configurations respectively.

System structure factors were calculated for RCS initial launch weights which include a 147-day propellant supply tank filled with a 20-day supply of propellant. Figures 3-99 through 3-102 present structure factor as a function of I_{sp} for the three radioisotope candidates. RCS systems using 2-1/2-year and 5-year Pm-147 fuel loading are also presented.

Resupply structure factors are presented in Figures 3-103 through 3-106. The resupply curve indicated for Pm-147 is applicable for one thruster resupply launch only, with all other 90-day logistic resupplies represented by the propellant resupply only curve. The curve labeled for Po-210 represents all logistic resupply launches since this low half-life radioisotope thruster would need replacement every 90 days. The propellant resupply only curve is applicable to Pu-238 and Pm-147 5-year systems since there is no thruster replacement involved.

Structure factors for the 5-year missions based on initial launch weights with a 20-day supply of propellant and 19 resupply launches are presented in Figures 3-107 through 3-110 for both ammonia and hydrogen propellants in the zero-g mode RBP and solar power configurations.

The parametric design study conclusion indicates that a Pu-238 vented-capsule thruster provides the best relative weight characteristics of all radioisotope candidates considered. In addition, the Pu-238 fuel form also appears most attractive from the standpoint of thruster life since no normal thruster replacement would be required for the 5-year mission period. Further, fuel characteristics permit the attainment of a propellant exhaust temperature of 3,500 °F with both ammonia and hydrogen propellants which will result in a relatively high specific impulse, on the order of 360 and 720 sec, respectively.

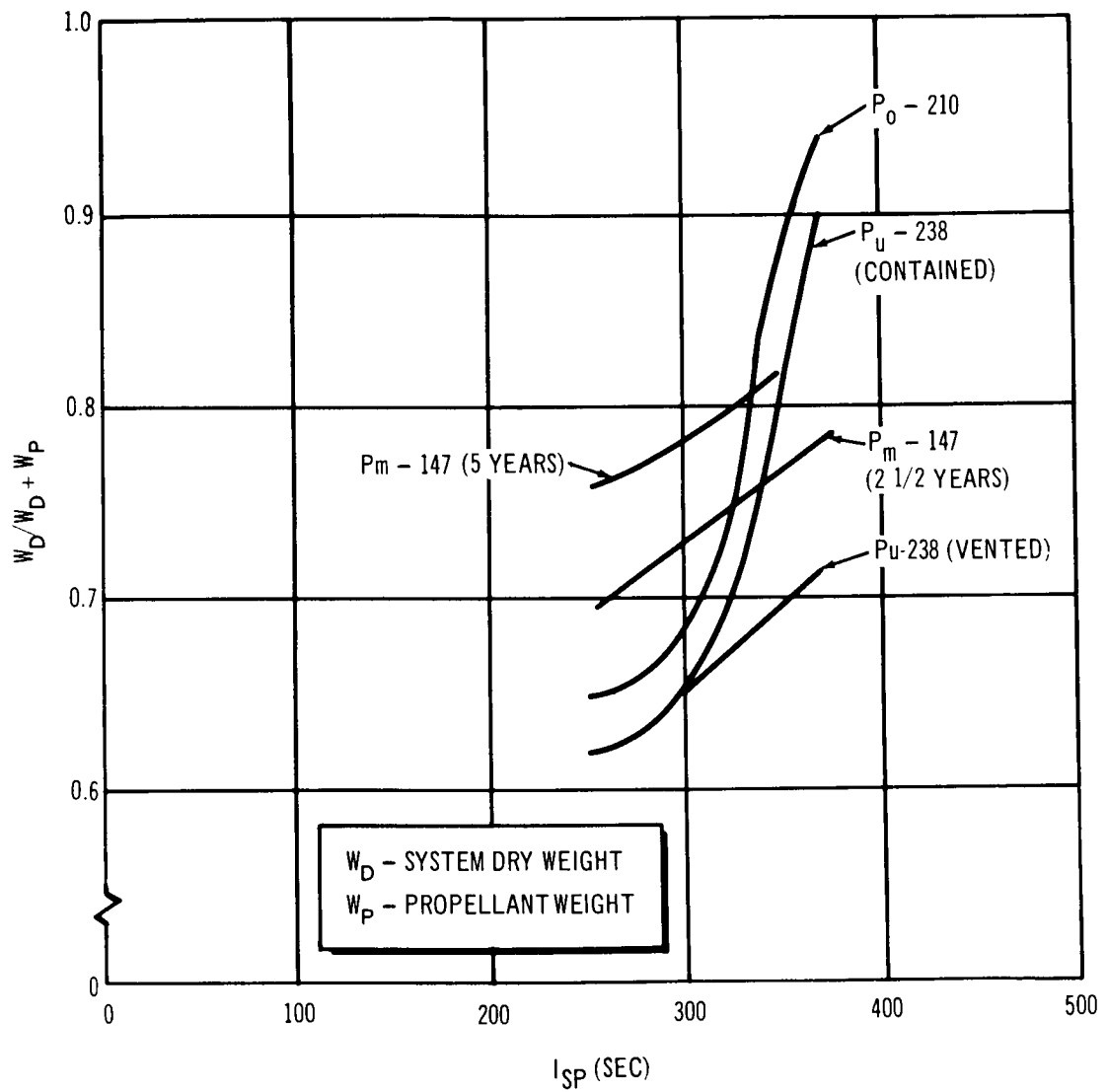


Figure 3-99. Structure Factor, Initial Launch as a Function of I_{SP} Zero G,
RBP Configuration, Ammonia Propellant

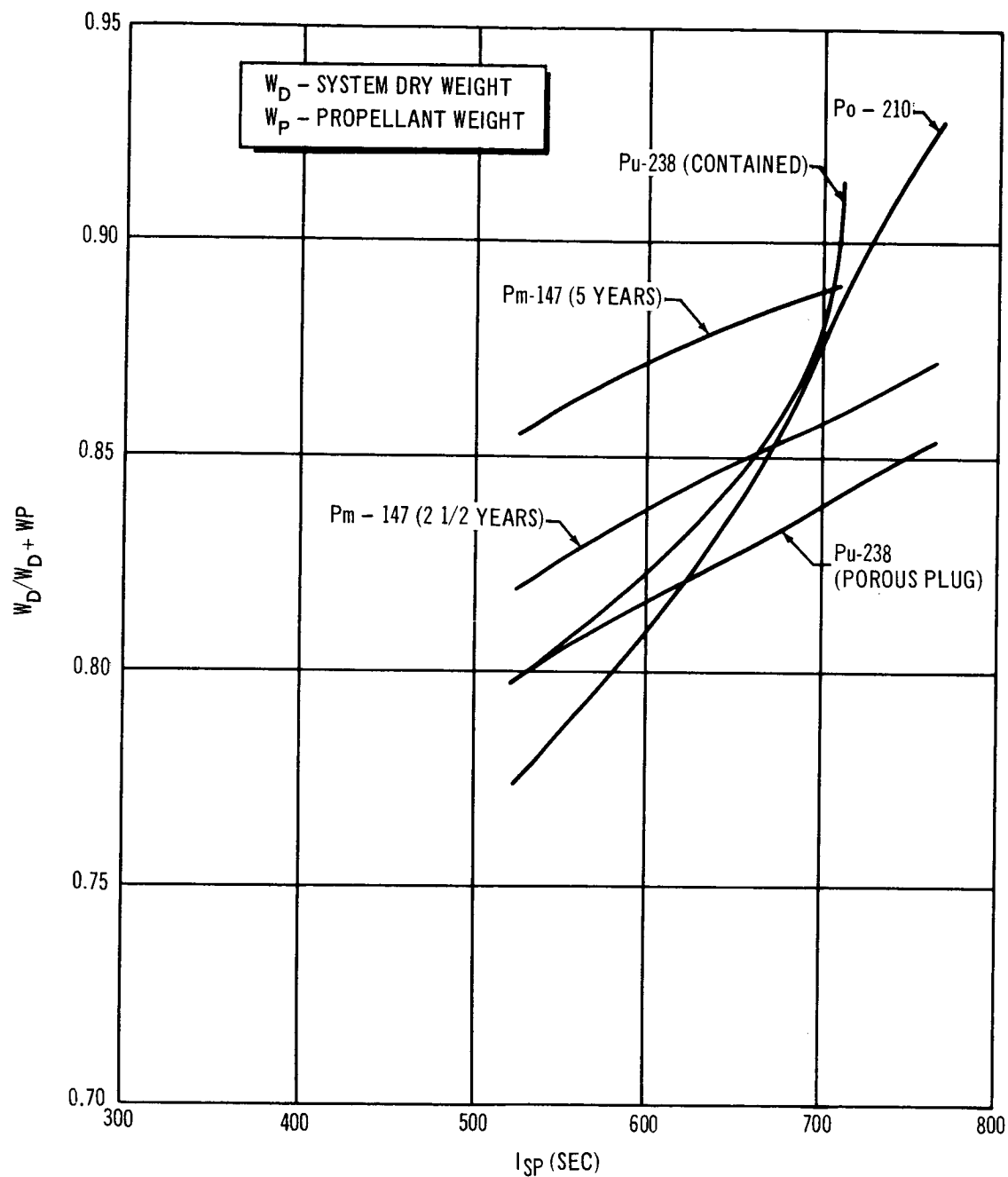


Figure 3-100. Structure Factor of Initial Launch as a Function of I_{SP} Zero G, RBP Configuration, Hydrogen Propellant

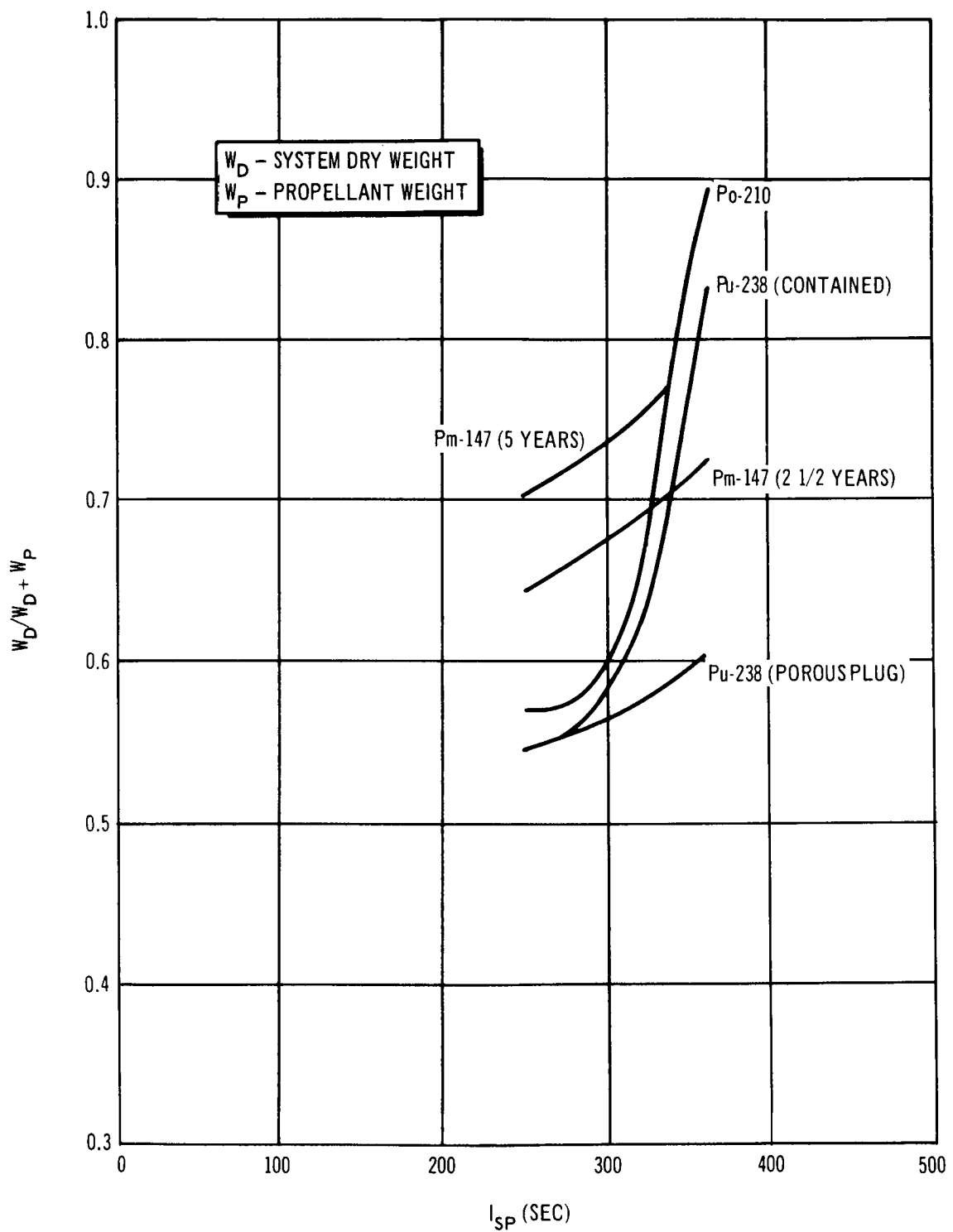


Figure 3-101. Structure Factor of Initial Launch as a Function of I_{SP} Zero G, Solar Power, Ammonia Propellant

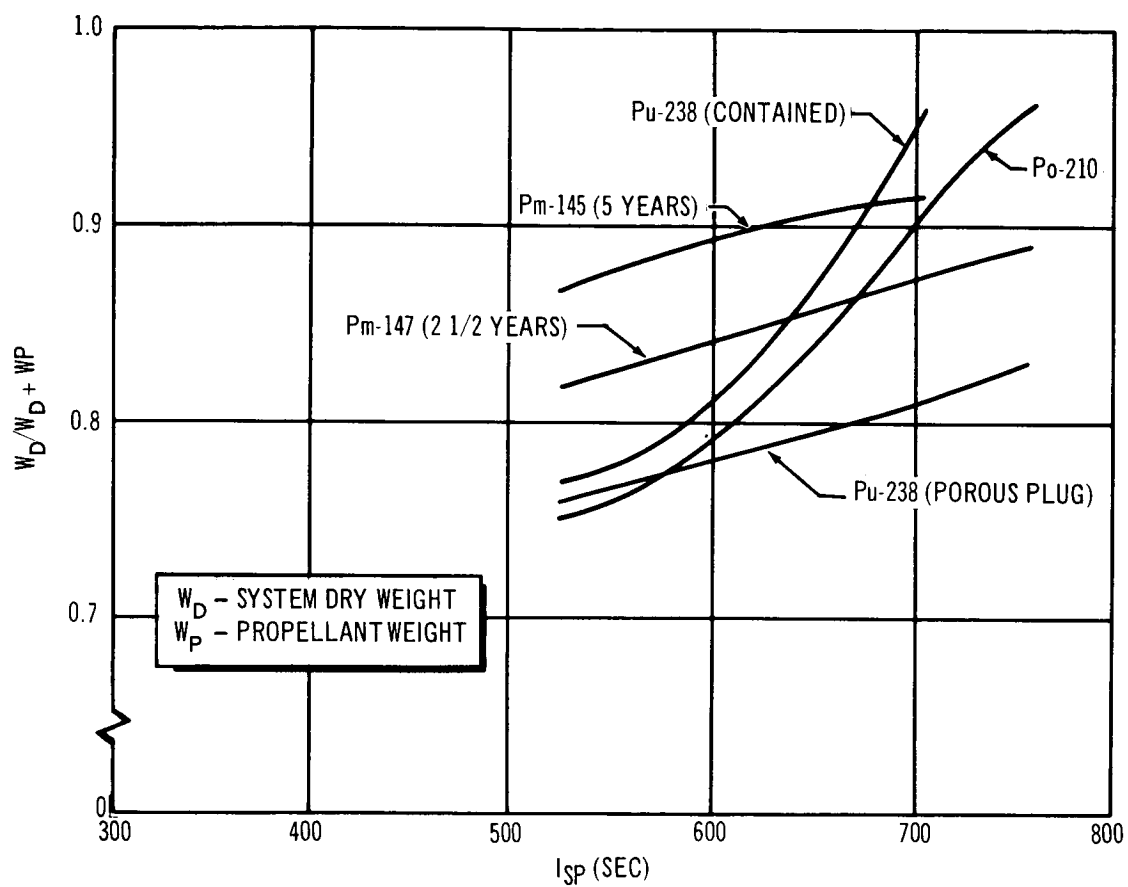


Figure 3-102. Structure Factor of Initial Launch as a Function of I_{sp} Zero G, Solar Power, Hydrogen Propellant

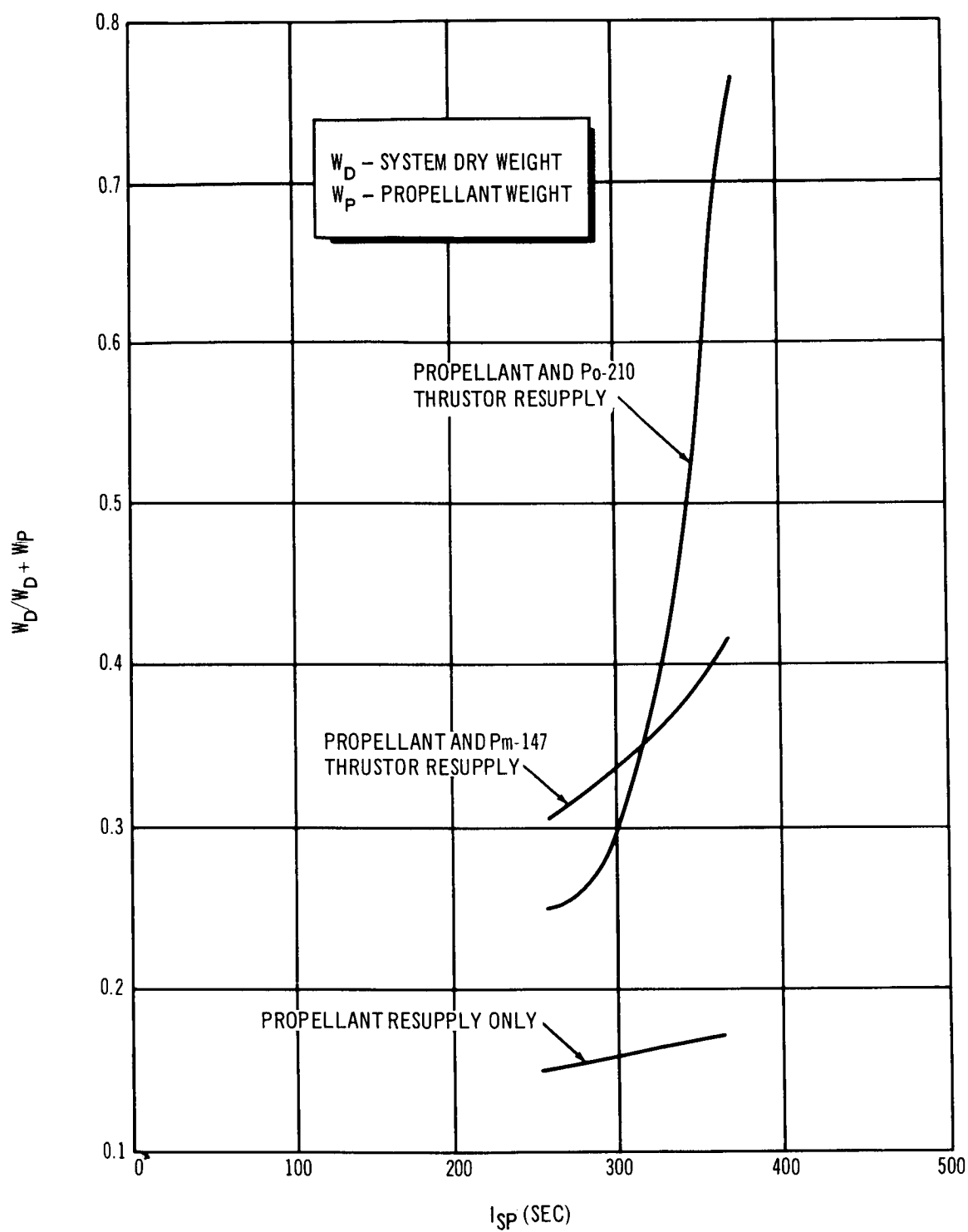


Figure 3-103. Structure Factor, 90-Day Resupply Mission as a Function of I_{SP} Zero G, RBP Configuration, Ammonia Propellant

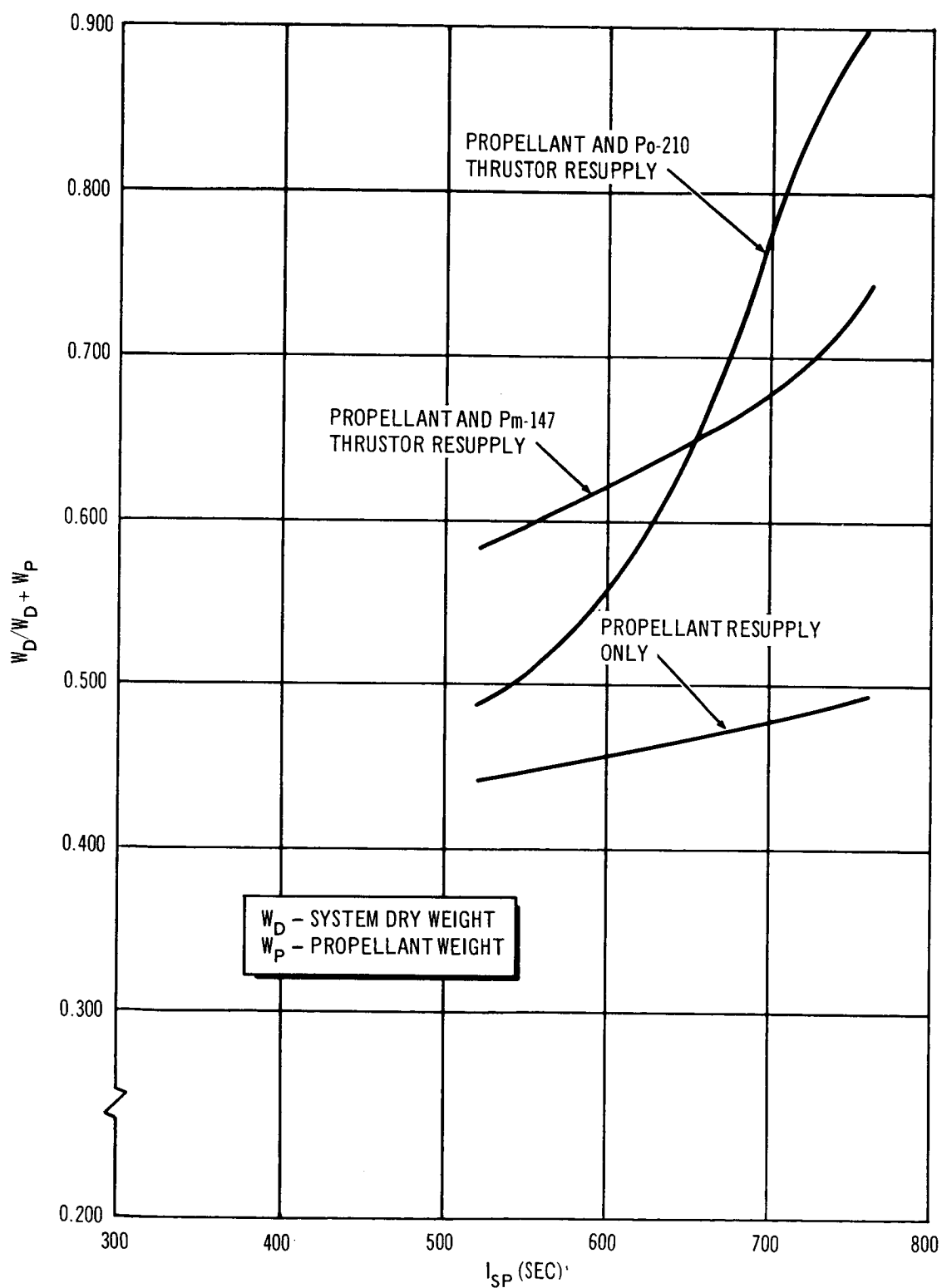


Figure 3-104. Structure Factor, 90- Day Resupply Mission as a Function of I_{SP} Zero G, RBP Configuration, Hydrogen Propellant

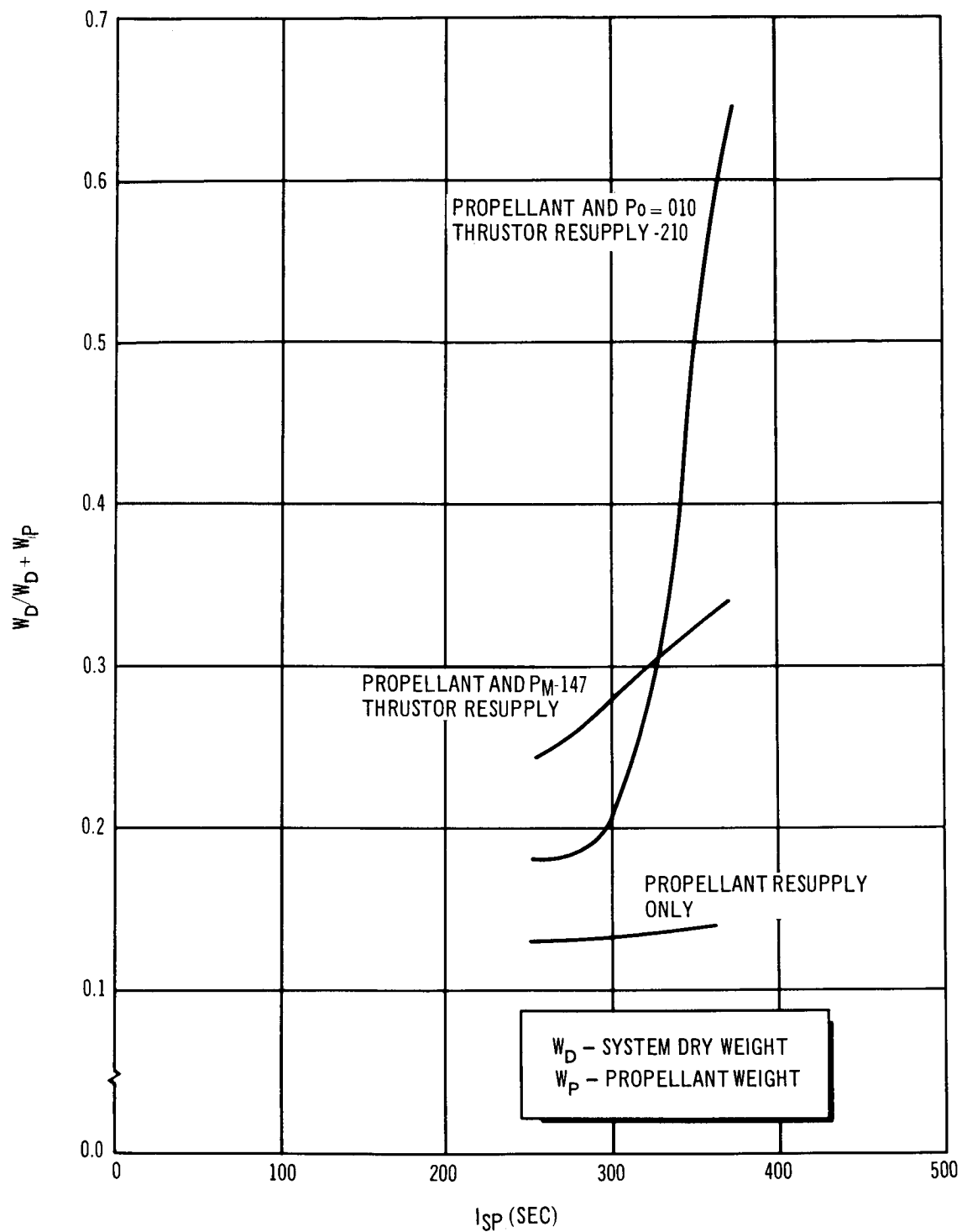


Figure 3-105. Structure Factor, 90-Day Resupply Mission as a Function of I_{SP} Zero G, Solar Power, Ammonia Propellant

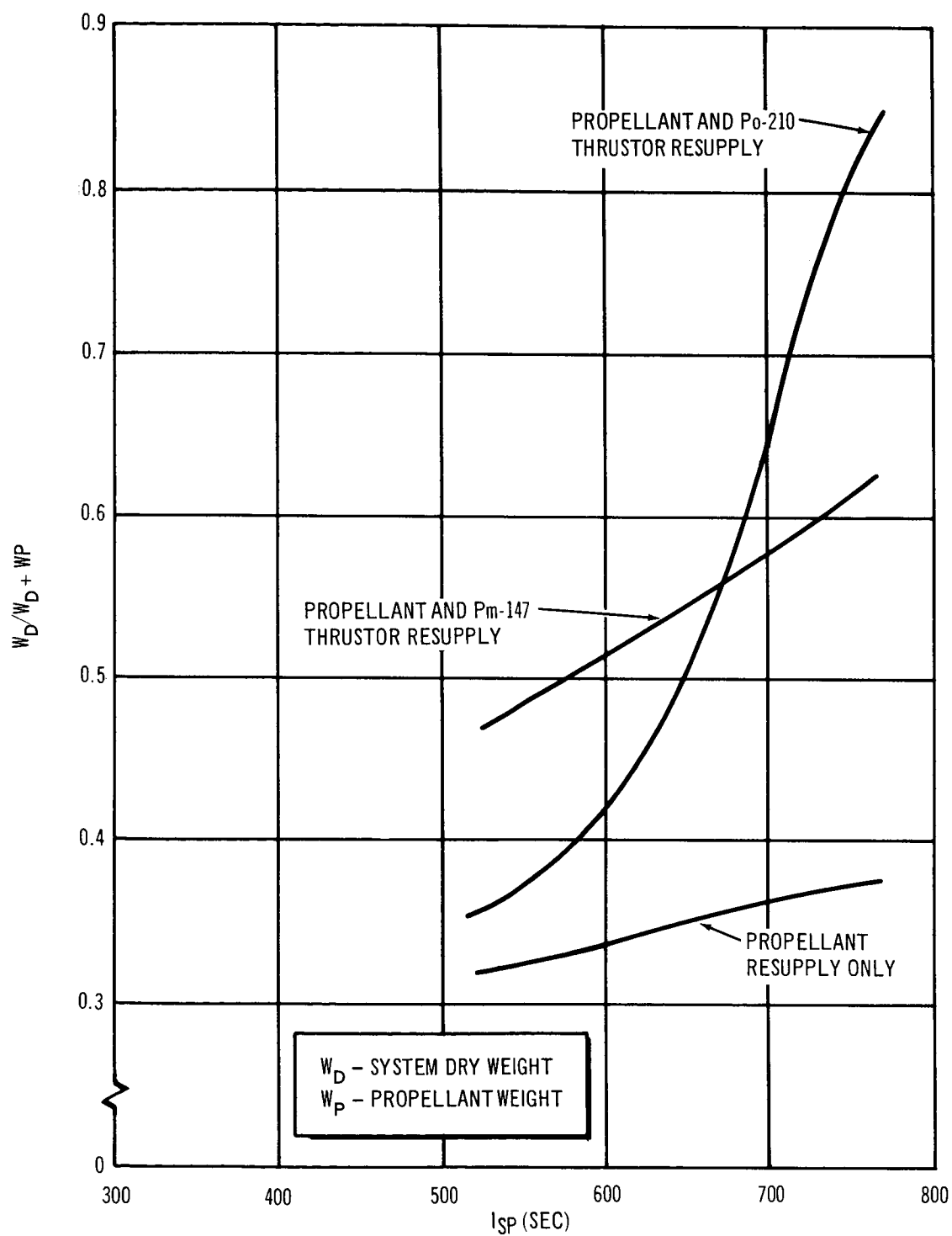


Figure 3-106. Structure Factor, 90 Day-Resupply Mission as a Function of I_{SP} Zero G, Solar Power Hydrogen Propellant

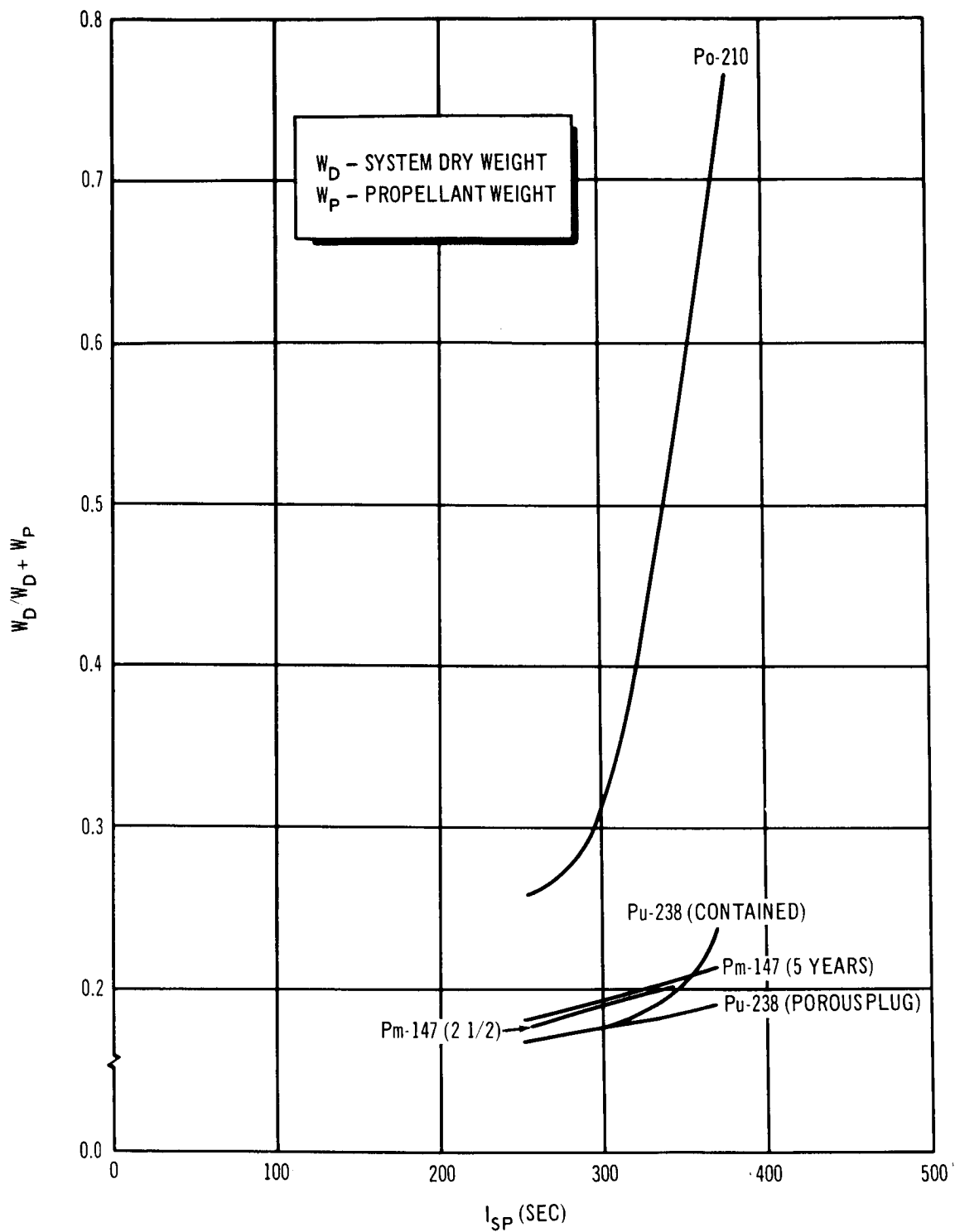


Figure 3-107. Structure Factor, 5-Year Mission as a Function of I_{SP} Zero G, RBP Configuration, Ammonia Propellant

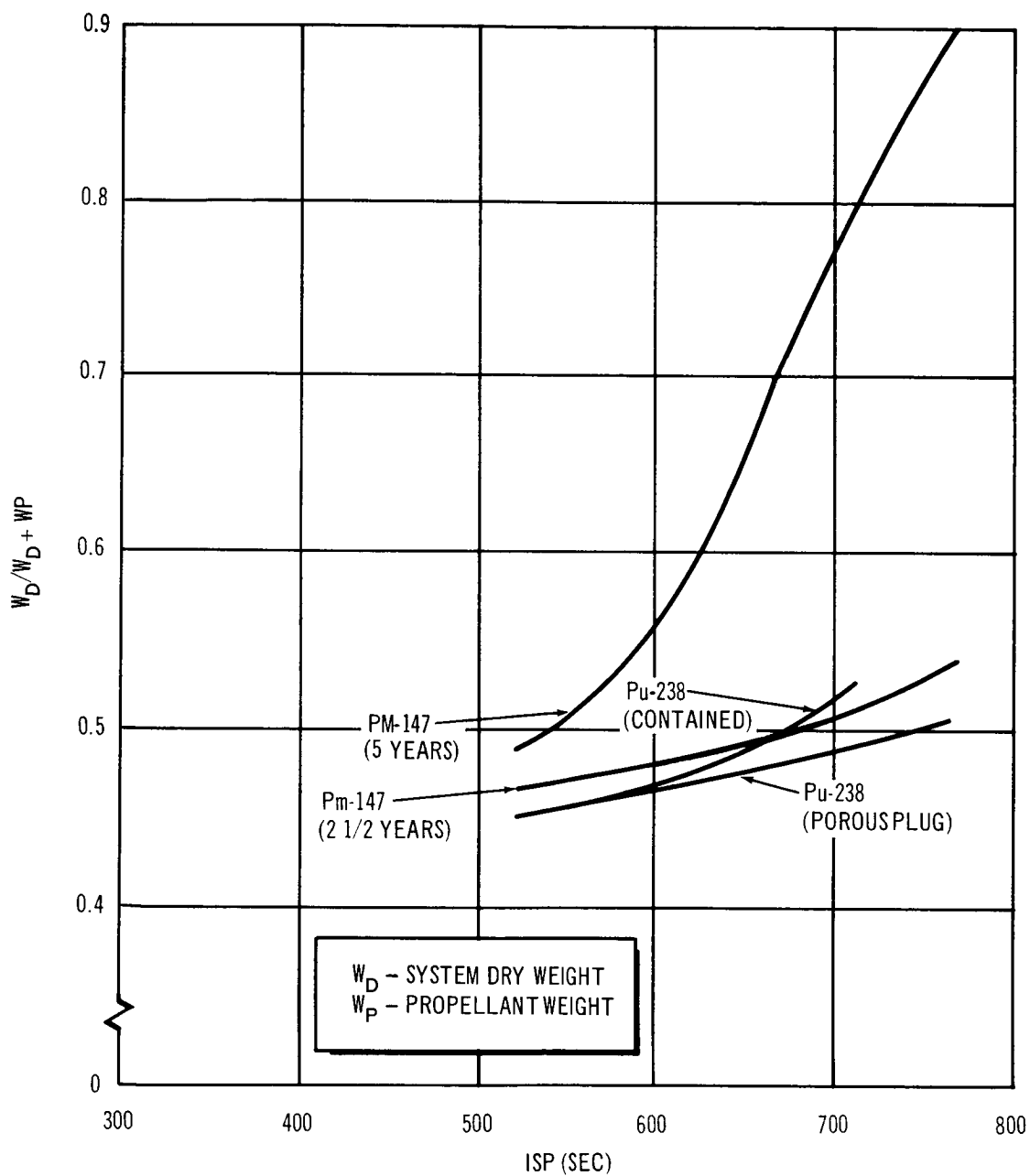


Figure 3-108. Structure Factor, 5-Year Mission as a Function of I_{sp} Zero G, RBP Configuration, Hydrogen Propellant

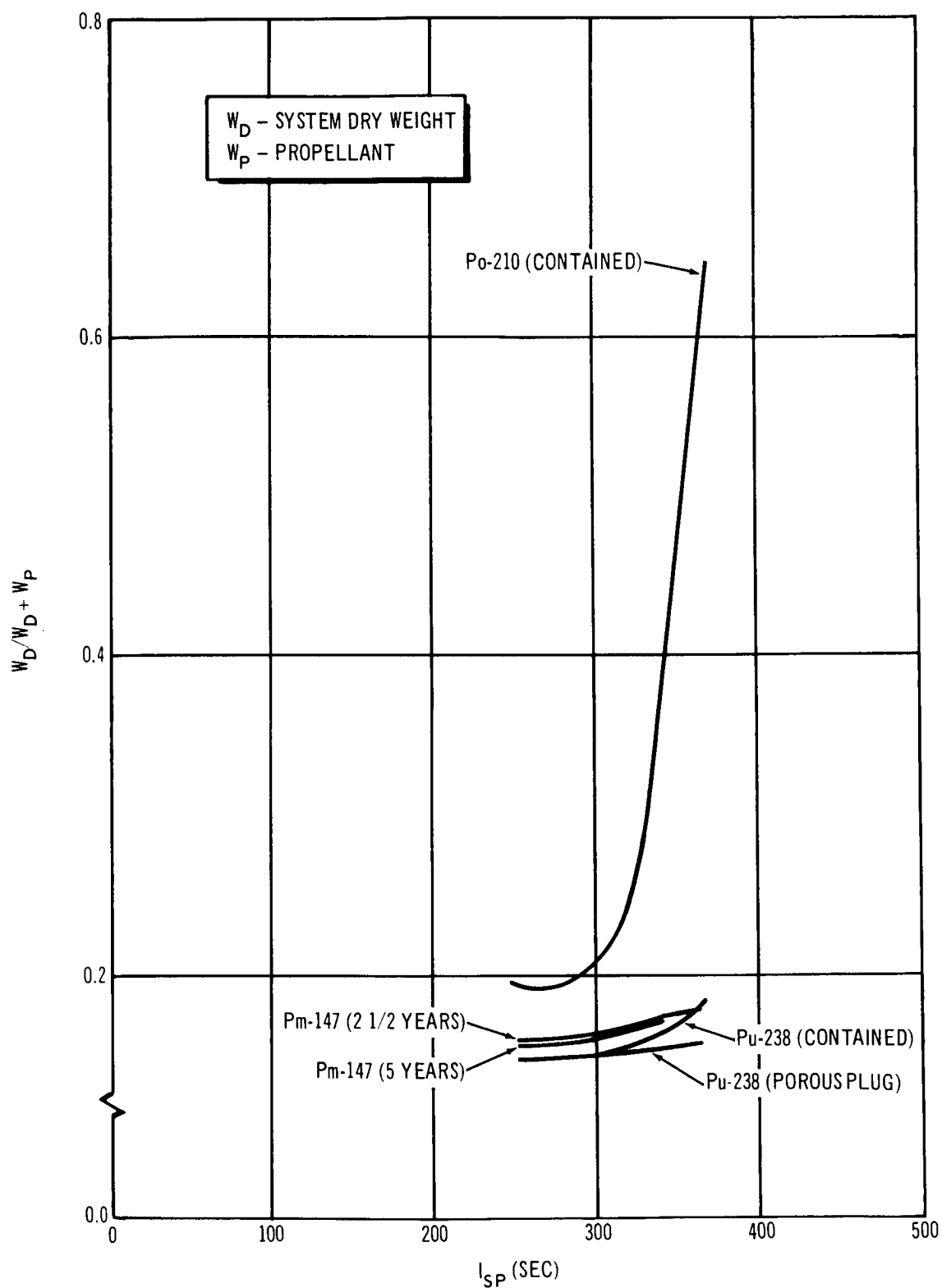


Figure 3-109. Structure Factor, 5-Year Mission as a Function of I_{SP} Zero G, Solar Power, Ammonia Propellant

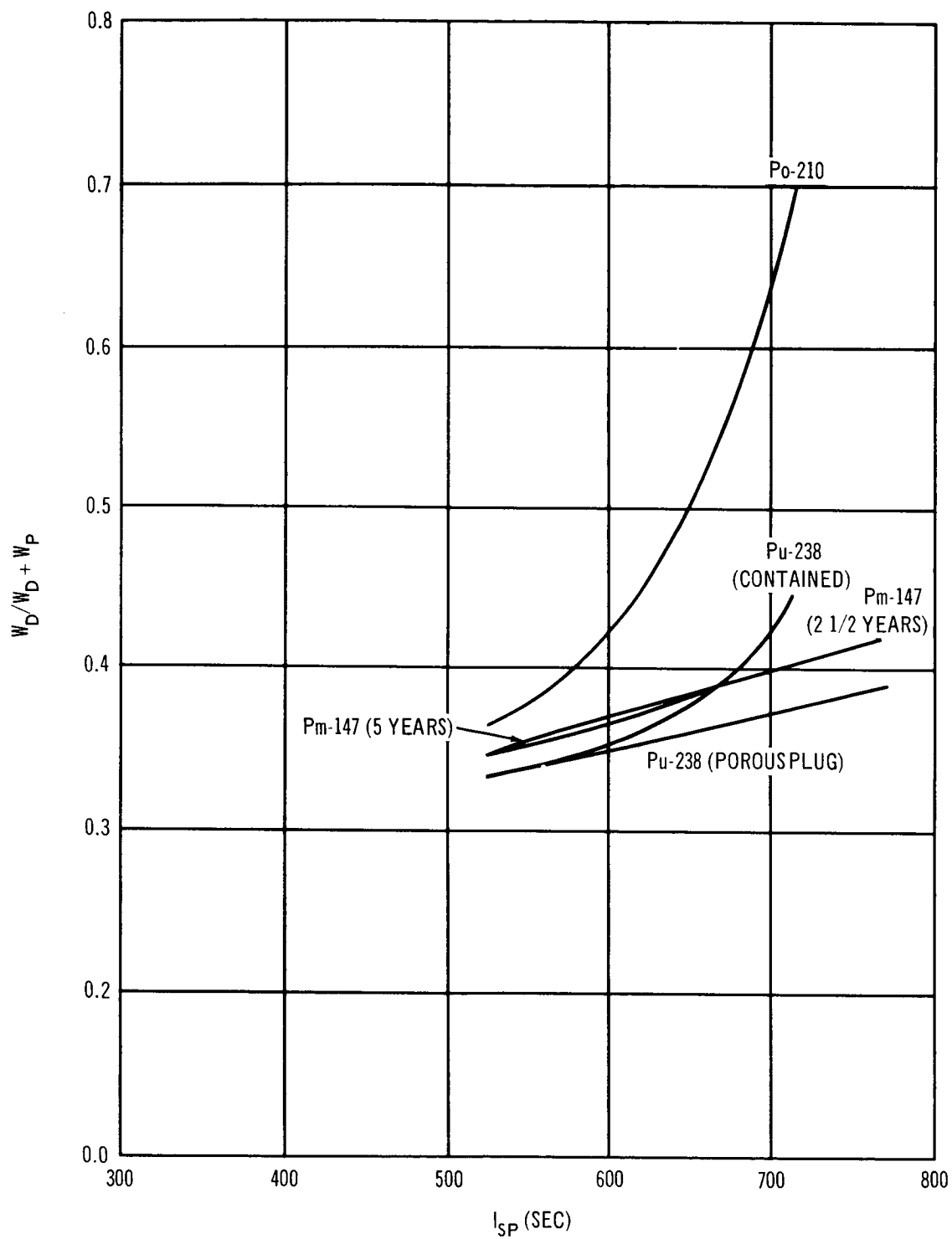


Figure 3-110. Structure Weight Factor, 5-Year Mission as a Function of I_{SP} Zero G, Solar Power, Hydrogen Propellant

3.4.6 Nozzle Efficiency

At the very low flow rates characteristic of the MORL thrusters, the two major contributions affecting nozzle efficiency are those caused by boundary layer buildup in the nozzle and by the nonaxial component of momentum imparted to the expanding fluid as a result of nozzle divergence. The laminar boundary layer formed upstream of the throat grows rapidly in the expansion section of the nozzle and results in a central inviscid isentropic core surrounded by a relatively thick boundary layer. The thick boundary layer decreases the effective area ratio with a portion of the propellant ejected through it at reduced momentum.

The nozzle efficiency, defined as the ratio of the actual delivered specific impulse to the specific impulse of an ideal nozzle with the same area ratio, can be computed by evaluating the mass and momentum flux at the exit. If the standard boundary layer theory is used, and if it is assumed that the flow consists of an isentropic core surrounded by a wall boundary layer, the result can be expressed in the following form:

$$\frac{I_{sp}}{I_{sp_i}} = 1 - \frac{1}{1 + \frac{1}{\gamma M_e^2}} 2 \left(1 + \frac{\delta^*}{2R_i} \right) \frac{\theta}{R_i} - \frac{1}{\gamma M_e^2} \left[2 \frac{\delta^*}{R_i} + \left(\frac{\delta^*}{R_i} \right)^2 \right]$$

where

I_{sp} = specific impulse, predicted

I_{sp_i} = ideal specific impulse

γ = ratio of specific heats

M_e = isentropic core Mach number

δ^* = nozzle exit boundary layer displacement thickness

R_i = exit radius of a frictionless nozzle

θ = boundary layer momentum thickness

The theory assumes that the actual physical nozzle radius $R = R_i + \delta^*$.

The predicted nozzle efficiencies, as a function of nozzle Reynolds number, are presented in Figure 3-111. A nozzle expansion ratio of 50 to 1 was selected to limit nozzle heat losses to reasonably small values.

For the MORL mission, the individual thruster assembly is equipped with a maximum of four nozzles. The flow through each nozzle is independently controlled from a common pressure source. Based on mission requirements, the nozzles delivering the highest total impulse per orbit were designed to provide the highest efficiencies for a given supply pressure. These nozzles are normally associated with the drag, yaw and pitch functions. With the roll total impulse requirements being quite low, the effect of roll nozzle efficiency on overall system performance is small.

For thrust levels of interest a hydrogen supply pressure of 25.0 psia would result in reasonable propellant tank storage pressures and at the same time provide a nozzle efficiency of the order of 90%. This chamber pressure

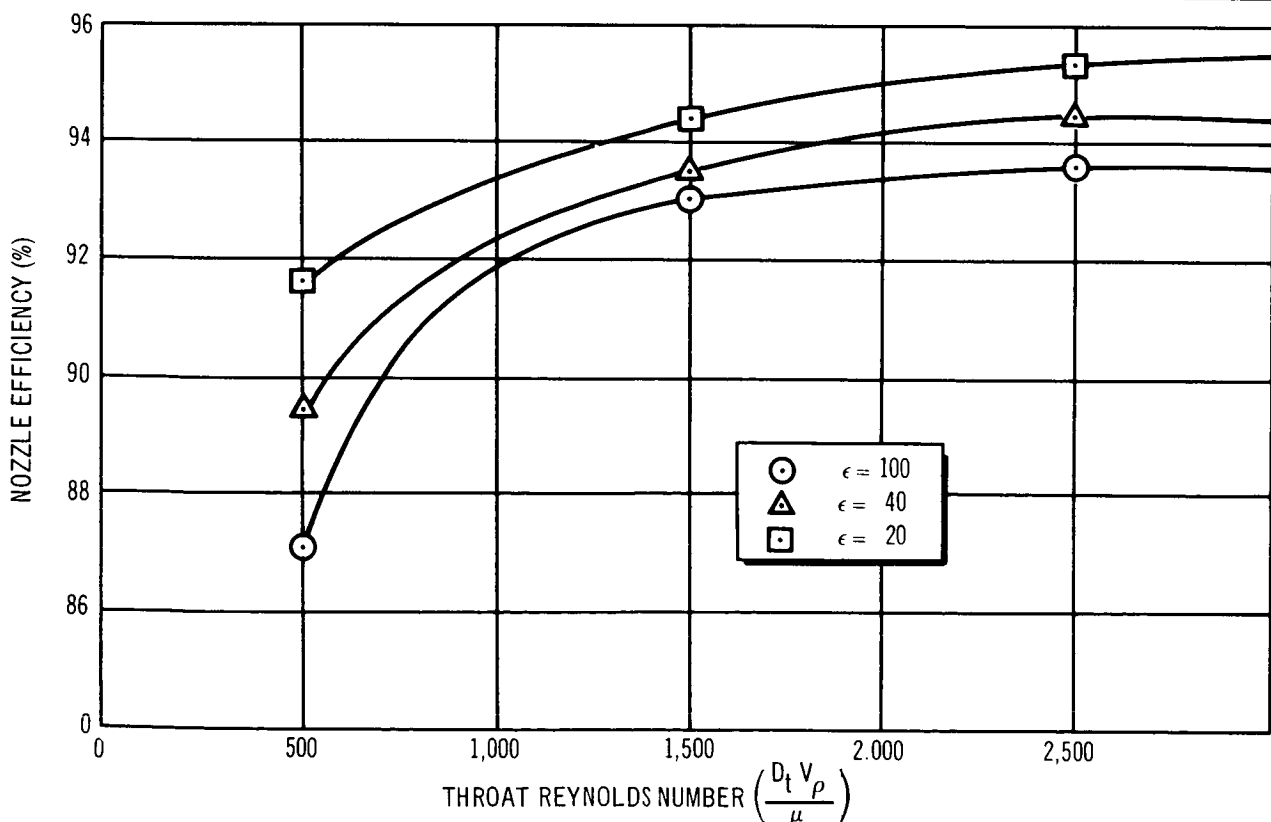


Figure 3-111. Nozzle Efficiency as a Function of Throat Reynolds Number, 20° Half Angle

would also satisfy a nozzle design criterion which sets the minimum nozzle diameter at 0.010 in. for all thrust levels.

Since the ammonia propellant tank was designed to operate at 300 psia, higher thruster supply pressures were feasible. In this case, the nozzle area limitations necessitated a low supply pressure on the order of 25 psia for the low-thrust-level nozzles, whereas the high-thrust-level nozzles could operate in the 50 psia range corresponding to efficiencies of the order of 94%. As a result, it is necessary for the feed system to provide two supply pressures.

Nozzle efficiencies were calculated in the following manner. For a given thrust level, chamber pressure, and 3,500°F gas temperature, the nozzle throat area was obtained from the equation

$$A_t = \frac{F}{P_c C_f}$$

where

- F = thrust, lb
- P_c = chamber pressure, psia
- A_t = throat area in.²
- C_f = thrust coefficient

The calculation of the required flow rate and I_{sp} is then accomplished by a trial and error method by first assuming a nozzle efficiency, η . The mass flow rate was then calculated from the equation

$$F = \dot{m} I_{sp} \eta$$

The Reynolds number ($4\dot{m}/\pi d\mu$) was calculated next and the assumed nozzle efficiency compared with that presented in Figure 3-111. If the two efficiencies were different, a new value of nozzle efficiency was assumed and the procedure repeated until agreement was obtained.

Section 4

BASELINE SYSTEM EVALUATION STUDY

The purpose of this study was to evaluate the components of the Phase IIa baseline Propulsion/Reaction Control system (P/RCS) with respect to recent advancements in technology and revised control requirements and, upon completion of this evaluation, to define an updated system should it be required.

The revised control requirements are based on the MORL Phase IIb baseline configuration which uses a Brayton Cycle power system in place of the Phase IIa solar-panel power system. The P/RCS control logic (that is, combining drag makeup with pitch/yaw control) was established for both the zero-g and artificial-g operational modes.

The Phase IIa baseline (P/RCS) (SM-46087) utilizes storable hypergolic bipropellant fed to radiation cooled engines by a nitrogen gas pressurization system. Metal bellows are employed to provide positive expulsion in the zero-g environment.

The engines deliver a specific impulse of 290 sec (steady state), with an expansion ratio of 100:1 and operate at a chamber pressure of 50 psi. The propellant mixture ratio (O/F) is 1.8:1 giving equal volume tanks. The engine thrust levels are 150 lb for orbit injection, orbit keeping, precession control, and spin/despin. A thrust level of 50 lb provides attitude control. There are sixteen engines on the laboratory: four 150-lb engines and twelve 50-lb engines divided equally into four thrust chamber assemblies.

4.1 PERFORMANCE REQUIREMENTS

Table 4-1 lists the orbit injection, orbit keeping (drag), attitude control (pitch, yaw, roll, precession) and spin-despin impulse requirements for all configurations and modes.

Table 4-1
PROPULSION/RCS ENGINE REQUIREMENTS (TOTAL
IMPULSE/ORBIT* OR EVENT) LB-SEC

Function	Configuration			
	Zero-g		Artificial-g	
	Solar Panel	Isotope Brayton	Solar Panel	Isotope Brayton
Orbit				
Injection	185, 000	185, 000	340, 000	340, 000
Drag	150	90	500	420
Pitch	100	82		
Yaw	113	8		
Roll	8	8		
Precession			500	420
Spin-Despin			300, 000 (one spin and one despin)	300, 000 (one spin and one despin)

*Orbit time: 5, 500 sec

The orbit injection requirements are based on a velocity increase of the vehicle of 214 fps and a vehicle weight of 33, 000 lb for the zero-g configuration and a weight of 58, 000 lb for the artificial-g configuration. This results in a total impulse of 185, 000 and 340, 000 lb-sec for the zero-g and artificial-g configurations, respectively.

The orbit keeping and attitude control are listed separately, defining the requirement for each function to be provided by the thruster system. However, if the pitch/yaw portion of the attitude control requirement is provided with the aft facing engines when in the zero-g configuration, both this requirement and drag makeup are accomplished. This results in an impulse saving for zero-g mode of 150 and 90 lb-sec/orbit for the solar panel and Isotope Brayton Cycle power system configurations, respectively.

A similar accomplishment of two functions can be gained in the artificial-g mode by operating the precession control engines when this thrust vector is parallel to the spin axis. This results in both precession control and drag makeup which gives an impulse saving of 500 and 420 lb-sec/orbit for the solar panel and Isotope Brayton Cycle power system configurations, respectively. To accomplish both attitude control and drag makeup simultaneously, it is necessary to do this on each side of an orbit for maintenance of a circular orbit. This type of control procedure differs from that which was used for the Phase IIa design, in which drag and attitude control were not accomplished simultaneously. The attitude control was accomplished by engines operating in a couple, and the drag makeup was done every fourth day.

The spin-despin requirement for the artificial-g configuration is the same as was established during the Phase IIa study and is performed once every 90 days.

4.2 COMPONENT EVALUATION

Various approaches to component evaluation are discussed in the following subsections.

4.2.1 Engine Concept Selection

The selection of an engine concept requires determination of the cooling method which will best meet MORL system requirements. An optimum system will offer high reliability, long life, high performance (steady-state and pulsed) and minimum system weight.

The Phase IIa study reviewed the applicability of many cooling methods to meet the P/RCS duty requirements. Cooling methods considered by this study were (1) regeneration, (2) open tube, (3) film, (4) transpiration, (5) endothermic heat sink, (6) inert heat sink, (7) ablation, and (8) radiation. The thruster concept selected was the radiation engine.

Because of the subsequent advancements in engine technology since the Phase IIa study (primarily as a result of the recent C-1 competition), it has become necessary to review various cooling methods. The concepts

considered by this restudy were (1) ablation, (2) radiation, (3) radiation/regeneration, and (4) radiation/conduction. These concepts and their applicability to the MORL P/RCS requirements are discussed below.

4.2.1.1 Ablation

This method makes use of a material with a low density and low thermal conductivity to protect the external chamber wall from the high-temperature combustion gas. A problem associated with this type of engine has been an increase in throat area with engine operation. In this concept, a tungsten insert is used to eliminate the problem at the throat. However, this problem still exists in the combustion chamber, where heat flux of $300 \text{ Btu/ft}^2\text{-sec}$ will result in an ablation rate of 7 mils/sec. For the minimum burn time application of 5,000 sec/yr, the pitch/yaw 100-lb engine (zero-g Isotope Brayton configuration) would become excessively heavy, and is not applicable to MORL.

4.2.1.2 Radiation (100%)

This method (Figure 4-1) makes use of a thin-walled combustion chamber (titanium-molybdenum or tantalum-tungsten) maintained at a temperature which ensures structural integrity by radiating heat to the environment. The chamber wall is protected from oxidation by the combustion gas at elevated temperatures by use of a protective coating of either aluminide or molybdenum-disilicide. Because of the high emissivity of these coatings at elevated temperatures, they are also used externally. The life of these coatings, and therefore engine life, is very dependent on coating temperatures reached during thruster operation. For example, a coating temperature of $2,700^\circ\text{F}$ would give a minimum steady-state life of 90 min. and a coating temperature of $3,000^\circ\text{F}$ would reduce the expected life to 4 min. (Marquardt Report No. S-472). Control of this temperature is accomplished by operating these engines at a chamber pressure less than 100 psia.

This concept offers a very light system and has demonstrated efficient operation during both steady-state and pulsed modes of operation. Experimental work has resulted in longer operating times than the other concepts

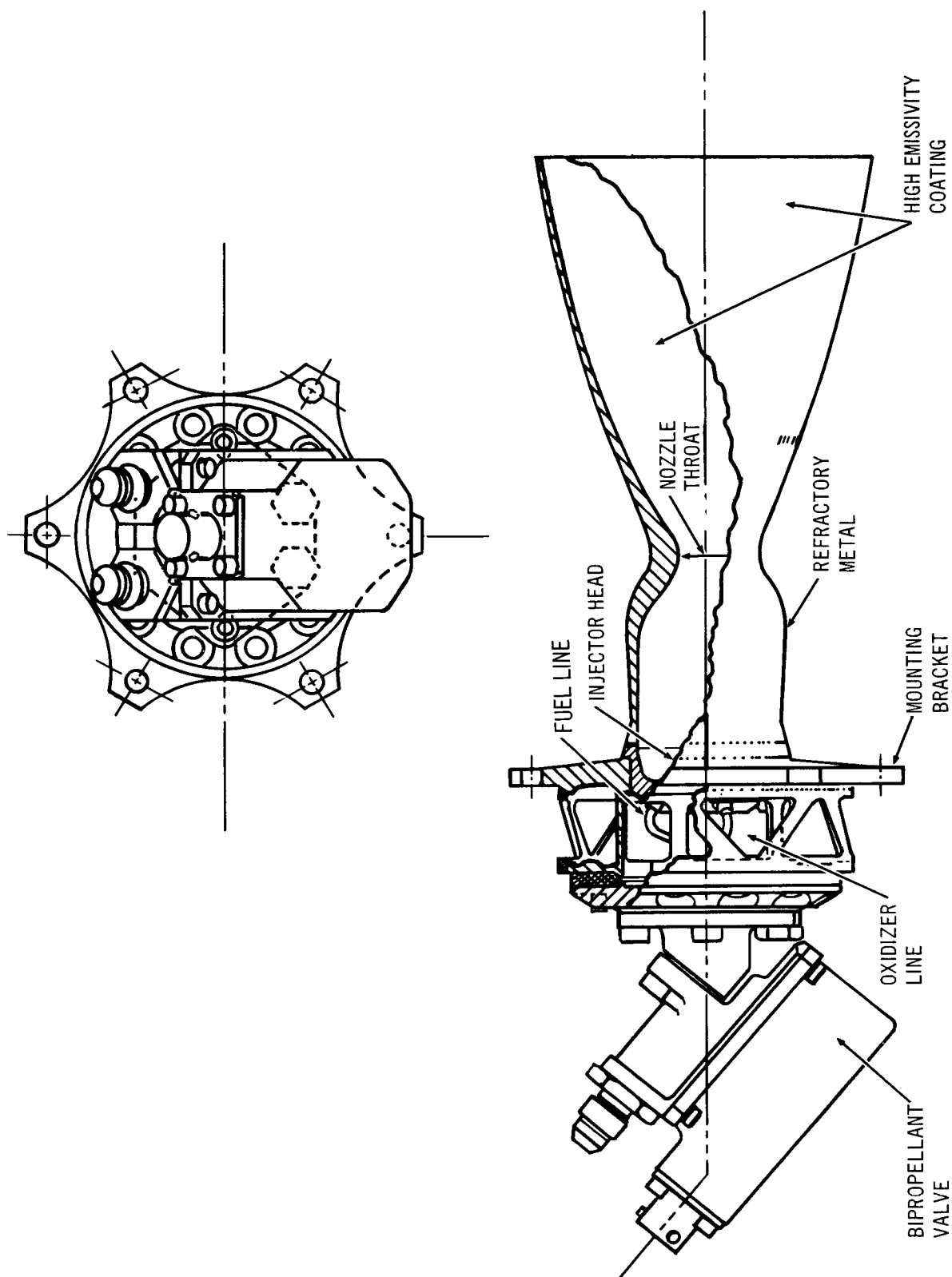


Figure 4-1. Radiation Engine Concept

considered for the MORL application. In addition, this concept inherently imparts more heat to the vehicle than the other concepts considered.

4.2.1.3 Radiation/Regeneration

The pure regeneration concept is hampered by insufficient cooling capability. The small cooling tubes create high pressure drops, resulting in a high tank pressure. This imposes a requirement for a heavier tank, resulting in a high system weight for a pressure-fed system. In addition, there is the constant possibility of thermal decomposition of the coolant and the inability of the injector to operate with the two-phase flow resulting from pulsed operation.

The radiation/regeneration method (Figure 4-2) provides a heat sink for the thin-walled, radiatively cooled combustion chamber (tantulum III) by circulating fuel in a surrounding annulus. The throat is protected from oxidation by a thin coating of hafnium oxide and is cooled directly by conduction through a foamed molybdenum into the heat sink. This concept eliminates many of the problems associated with radiation cooling by transferring the heat, partially by radiation and partially by conduction, to a cold annulus which contains sufficient fluid (sensible heat), thereby ensuring proper cooling and elimination of thermal cracking. This method of cooling is conducive to very long steady-state engine life.

The concept of an engine cooling system constructed of several different metals is more complex than a system using pure radiation and induces additional thermal stress during shutdown period. In addition, a large bulk of propellant could freeze during these shutdown periods; these considerations require a sophisticated active thermal control device, needing a large amount of electrical energy. In addition to supplying sensible heat to the annulus and fuel, this heater must overcome the heat leak where the fuel enters the inner annulus from the nozzle and the nozzle attachment, and still be able to survive the nozzle temperatures.

In summary, integration of this system into MORL would require a heater which has a high energy output and the ability to withstand nozzle temperatures adjacent to the throat.

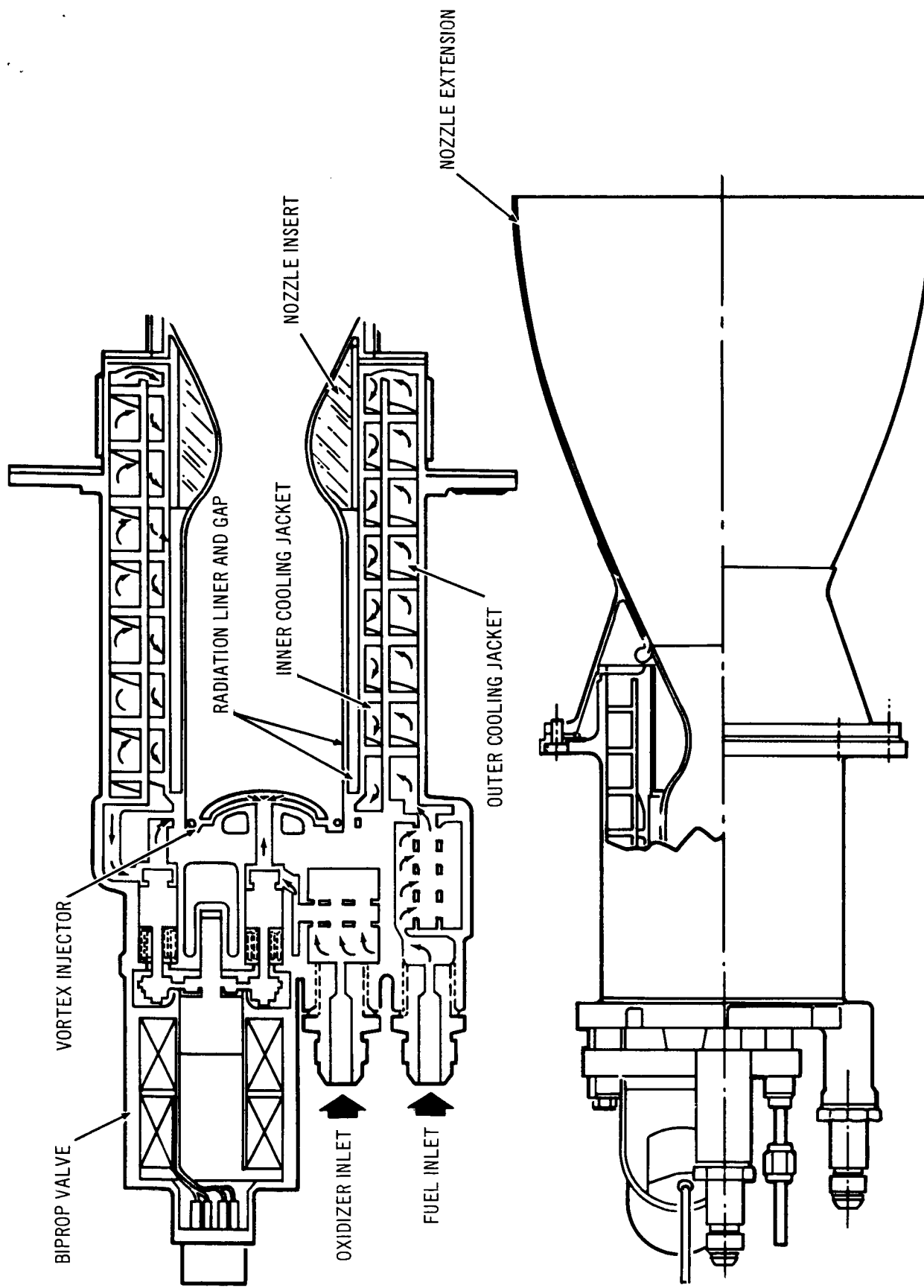


Figure 4-2. Radiation/Regeneration Engine Concept (Radiamic)

4.2.1.4 Radiation Conduction/Film Cooling

This method (Figure 4-3) makes use of a thick-walled beryllium (nonrefractory) chamber. The temperature ensuring structural integrity is maintained by a combination of radiation to the environment and conduction through the chamber wall from the hot throat to the cold injector end, which is maintained cold by film cooling. Beryllium has been chosen for this application because of its low density, high heat capacity, high thermal conductivity, and high melting point. This chamber, utilizing a 40% boundary layer cooling at a chamber pressure of 150 psia, delivers a C^* efficiency of 93.4%, with a maximum steady-state temperature of 1,650°F. The melting point for beryllium is 2,340°F and its useful temperature is 1,840°F. This concept has also demonstrated efficient pulsed operation. However, because of the limited test data to date (2,344 sec obtained during 19,193 cycles), it cannot at the present time be used in the MORL P/RCS.

In summary, the radiation concepts are selected over the ablation concept because of their ability to provide a lightweight system. Three radiation concepts were discussed: (1) 100% radiation cooling, (2) radiation cooling coupled with regeneration cooling, and (3) radiation cooling coupled with conductive cooling. Engine concepts 2 and 3 show great promise, having a potentially higher engine life capability than engine concept 1; however, these new concepts require testing to demonstrate this life capability to meet the MORL system requirements. Therefore, because it has a large backlog of test data which has proven its applicability to MORL system requirements, the 100% radiatively cooled chamber concept remains the baseline choice.

4.2.2 Propellant Selection

The propellant combination used by the P/RCS must have minimum development risk, offer maximum crew safety, provide high reproducible performance, and be thermally compatible with the MORL operational environment.

The propellant bulk-storage temperature on the laboratory for the Brayton Cycle configuration is 125° ±10°F, and for the alternate solar-panel configuration it is 60° ±10°F. The temperature extremes encountered by the propellant are at the engine fuel valve standoff (the hottest temperature) and at the

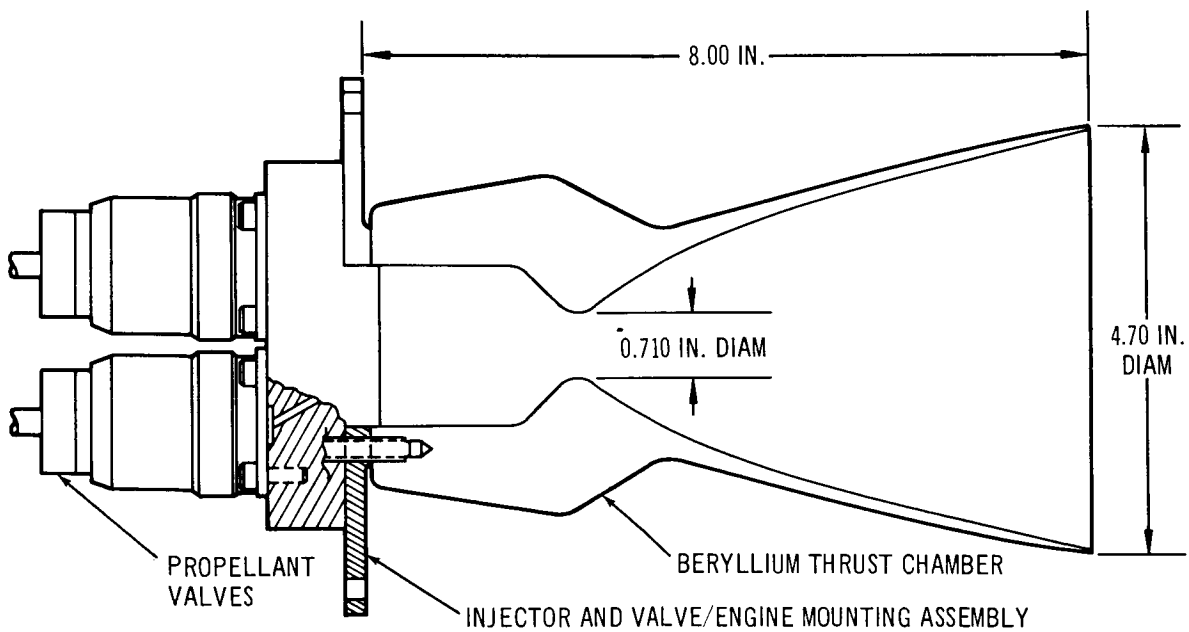
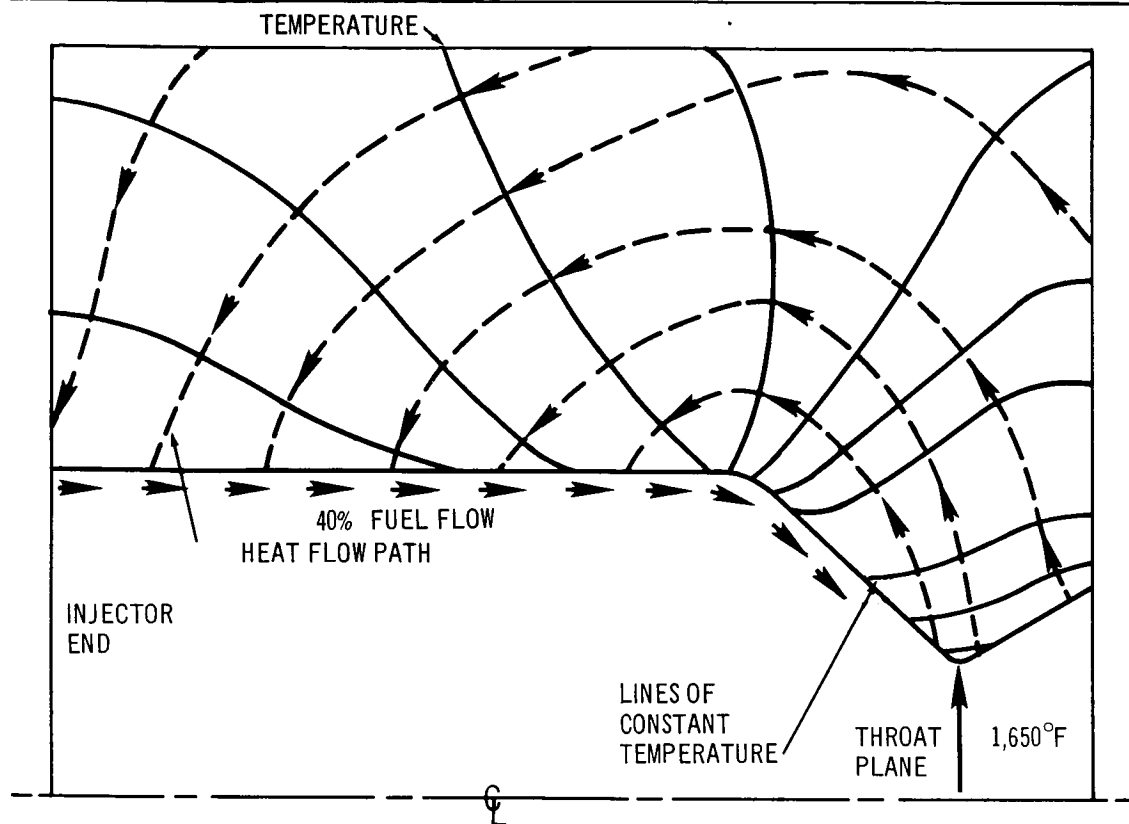


Figure 4-3. Radiation/Conduction Engine Concept

vehicle's skin (the lowest temperature). The temperature obtained at both the fuel and oxidizer valves is shown by Figure 4-4 and Figure 4-5, respectively. These illustrations are the result of a test conducted to establish the fuel and oxidizer valve soakback temperatures for a given engine on time and propellant mixture ratio. These tests were conducted for a radiation-cooled engine which was similar to the one selected in Section 4.2.1 and which used the propellant nitrogen tetroxide/monomethyl hydrazine combination (NTO/MMH), which is a candidate propellant. These figures indicate a maximum temperature of less than 200°F for both the oxidizer and fuel valves for engine on time less than 30 sec, which is in excess of the pulsed requirement established for attitude control. The minimum temperature encountered in the laboratory is on the external surface (vehicle skin) which is maintained at a minimum of 40°F by the Brayton Cycle radiators.

The external temperatures encountered on the Saturn IVB are between -85° and -50°F on the shade side and between +175° and +250°F on the sun side, depending on the surface emissivity. Selecting an emissivity that will maintain the maximum skin temperatures of 200°F (the maximum temperature of the fuel valve) would give a skin temperature on the shade side of -70°F.

Table 4-2 summarizes minimum and maximum temperatures that the propellant will encounter.

Table 4-2
PROPELLANT ENVIRONMENTAL TEMPERATURE

Mode	Configuration	Location (°F)			
		Laboratory		Saturn IVB	
		Min.	Max.	Min.	Max.
Zero-g	Solar Panel	40	200		
	Brayton Cycle	40	200		
Artificial-g	Solar Panel	40	200	-70	200
	Brayton Cycle	40	200	-70	200

The propellants considered during this study were combinations of the oxidizers CLF_3 , IRFNA, and N_2O_4 with the fuels MMH, hydrazine, and a

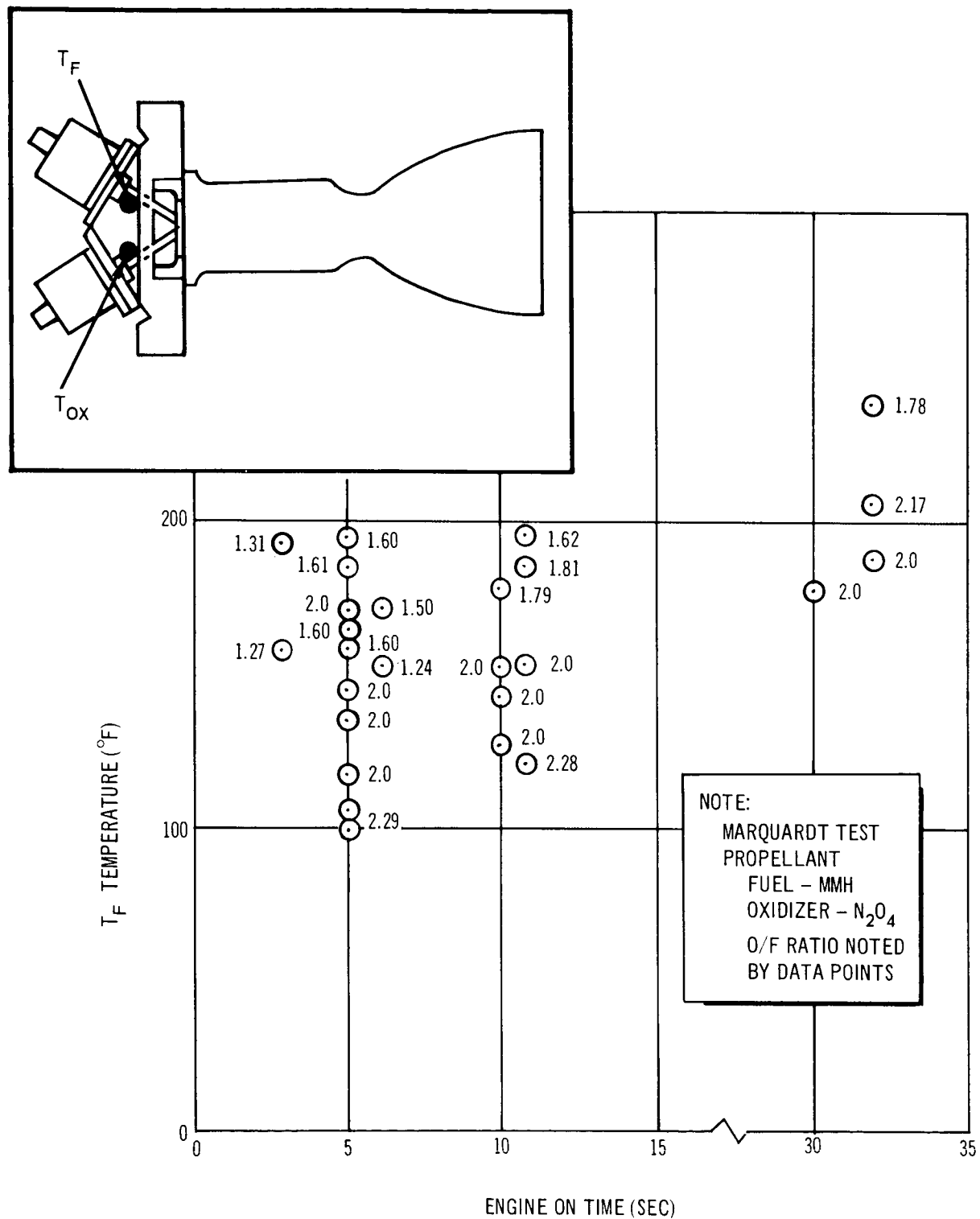


Figure 4-4. Radiation Cooled Engine Maximum Soakback Temperature (Fuel Valve Standoff)

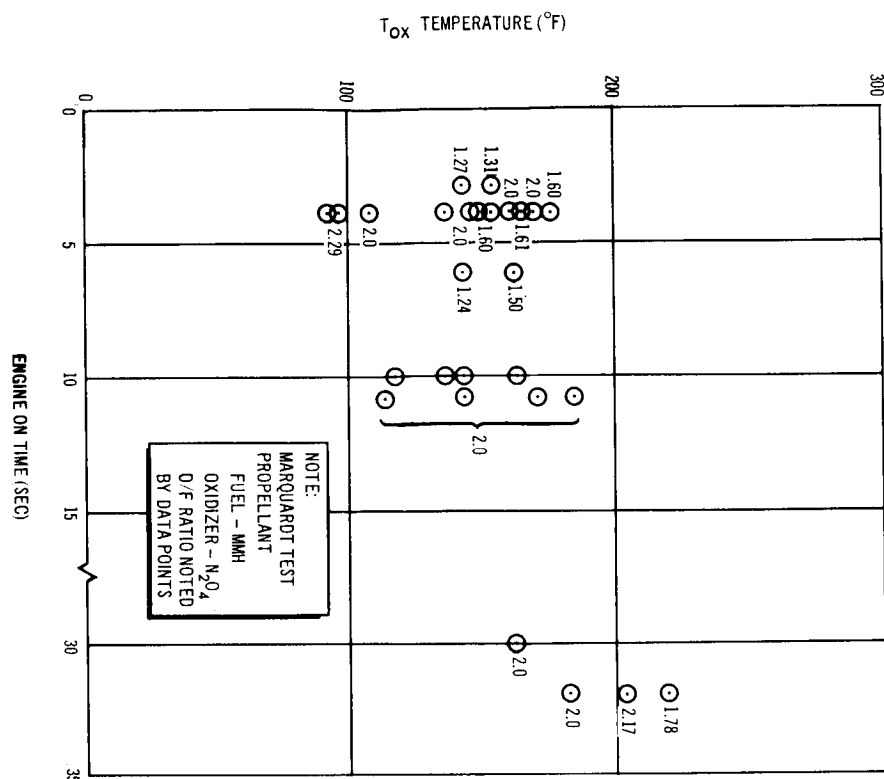


Figure 4-5. Radiation Cooled Engine Maximum Soakback Temperature (Oxidizer Valve Standoff)

50-50 mixture of hydrazine and UDMH. The thermal storage capability of these oxidizers and fuels is shown in Figure 4-6.

Chlorine trifluoride (CTF) offers better thermal characteristics than either IRFNA or NTO. However, the very active chemical nature of CTF (Table 4-3), requires that it be handled with the same care given elemental fluorine; therefore, it does not offer sufficient crew safety to allow its use on MORL. For this reason, IRFNA and NTO would be selected over CTF. IRFNA has been used in various developed systems but has always exhibited erratic ignition; therefore, it requires a more extensive development program than NTO.

The oxidizer that offers the least desirable freezing point is NTO; it has the highest pressure storage requirements of either of the other two oxidizers considered. As in the case of IRFNA, active thermal control is required to prevent freezing aboard the Saturn IVB when a surface emissivity is selected to maintain a maximum temperature of 200°F. This oxidizer offers better crew safety than IRFNA or CTF because it must first undergo a transition to

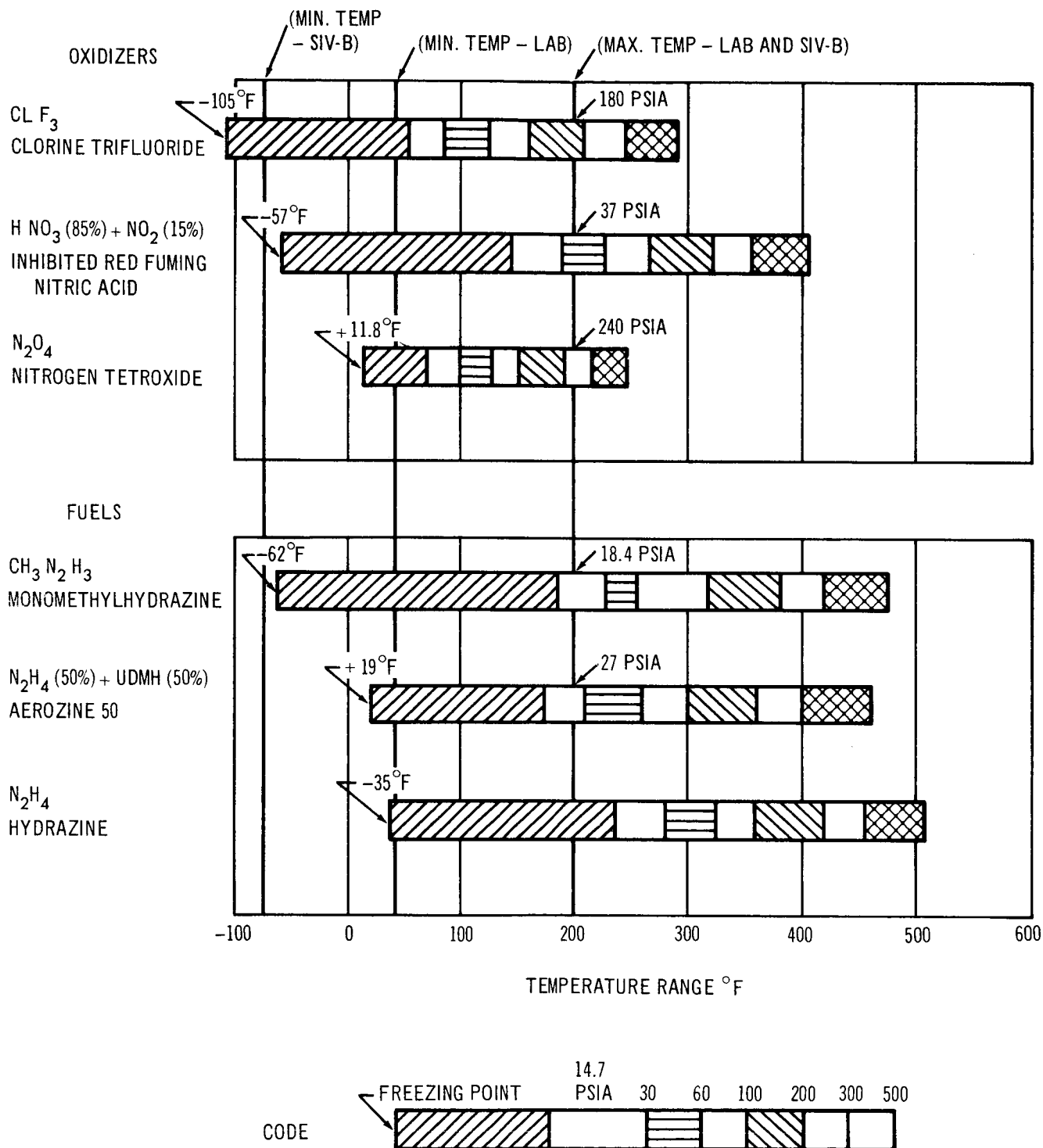


Figure 4-6. Candidate Propellant Storage Requirements

Table 4-3

PROPELLANT PHYSICAL AND CHEMICAL PROPERTIES

Toxicity (Max. Allow. Concentration)		Shock Sensitivity	Materials Compatibility	Remarks
CTF	0.1 ppm	Insensitive to mechanical shock	Compatible--300 series stainless steel, aluminum alloys, Rene-41	1. Handled with precautions similar to those taken with elemental fluorine 2. Nonflammable in air 3. Corrosive resistance depends on the formation of a passive fluoride film
IRFNA	5 ppm	Insensitive to mechanical shock	Compatible--stainless steel (after pickling), aluminum	1. Hygroscopic 2. Erratic combustion behavior
N_2O_4	2.5 ppm	Insensitive to mechanical shock	Compatible--300 series stainless steel, Teflon	1. Hypergolic with many fuels 2. Highly corrosive with the addition of 0.1% of H_2O
MMH	0.1 ppm	Insensitive to mechanical shock	Compatible--Ni, Monel, Ti, Al and Al alloys, stainless steel Marginal--Teflon (considerable losses in tensile strength and elasticity), polyethylene, steels high in carbon at temperatures greater than 165°F	1. More toxic than UDMH or N_2H_4 2. More stable than N_2H_4 , less stable than UDMH
50-50	0.5 ppm	Insensitive to mechanical shock	Compatible--Ni, Ni alloys, Ti alloys, Teflon, Al and Al alloys (with passivation)	1. Nonpyrophoric
N_2H_4	1.0 ppm	Insensitive to mechanical shock	Compatible--Al, Al alloys, stainless steels, inconel, titanium, Kel-F, Teflon, graphite	1. Hygroscopic 2. Has a high freezing point by itself 3. Vapors may be exploded by a spark

nitric and nitrous acid before it will attack metal. The formation of nitrous acid tends to dilute the nitric acid, making it less active and thereby allowing more time for evaporation before it reacts.

Rapid reproducible combustion has been demonstrated by NTO with fuels containing H_2 , thus lending itself as an ideal oxidizer for attitude control system where efficient pulsed operation is required. This oxidizer is being given primary attention by propulsion companies for use in future space systems.

The fuels considered will not offer any danger to the crew, providing a space-suit has been constructed which will protect the crew from the oxidizer. MMH offers the best storage capability of the three fuels considered but, will also require thermal control to prevent freezing aboard the Saturn IVB. This fuel is currently used in developed engines where efficient pulsed and steady-state operation has been demonstrated.

The blend of 50% UDMH and 50% N_2H_4 is at a disadvantage when compared to a fuel composed of a single component; if the blend freezes, separation of the two components will occur and subsequent reheating will not lead to a single phase without the use of a mixing device. However, engines are currently developed which employ this 50-50 mixture as fuel.

Hydrazine is the least toxic of the fuels considered but does not offer maximum crew safety because of its detonation characteristics. It also has the highest freezing point; in addition to requiring active thermal control on the Saturn IVB, this could possibly require active thermal control on the laboratory with the solar panel power system. The other two fuels have been tested extensively for space application, while hydrazine testing has been limited to volume-limited missile systems where the mode of operation is either continuous or, at most, limited to one or two pulses.

The selected oxidizer is NTO because of its superior pulse capability and backlog of test data which was determined to be more important than the elimination of active thermal control aboard the Saturn IVB.

MMH is selected over the 50-50 mixture of hydrazine and UDMH because it offers the same performance with NTO but has better storage characteristics

4.2.3 Engine Performance

The performance of the radiation-cooled engine with propellant combinations of NTO/MMH and NTO/50-50 is shown in Figures 4-7 and 4-8. These figures show the variation of delivered I_{sp} with mixture ratio for various thrust levels at an expansion ratio (ϵ) of 40:1. The delivered I_{sp} curves are based on test data at the given thrust levels furnished by several propulsion contractors. Included is a computed theoretical curve based on frozen equilibrium.

Based on the difference between the plotted delivered and theoretical I_{sp} values, an efficiency of 92% is indicated for the 100-lb thrust level engine and 88% and 85% for the 22-lb and 5-lb thrust level engines, respectively.

A plot of the delivered I_{sp} for the 100-lb thrust engine with both propellant combinations at various mixture ratios and at the expansion ratios of 100:1, 60:1, and 40:1 is shown in Figure 4-9.

Both propellant combinations deliver the same specific impulse at the oxidizer to fuel ratio which gives an equal-volume ratio (equal-volume tanks). At a temperature of 135°F, the equal-volume ratio for NTO/MMH and NTO/50-50 is a weight ratio of 1.6:1 and 1.56:1, respectively, (Figure 4-10) and indicates a specific impulse of 303 sec at an expansion ratio of 100:1.

The steady-state performance of these engines at various thrust levels is shown by Figure 4-11. This figure was constructed using the performance efficiencies indicated by Figure 4-7 and 4-8 for the 22-lb and 5-lb thrust engines, respectively.

The pulsed performance for engines of various thrust level and which employ various fuels with NTO is shown in Figure 4-12. The test data was averaged and is shown in Figure 4-13. The figure shows a plot of pulse width as a function of the ratio of the average specific impulse, for a given pulse width, to the steady-state specific impulse.

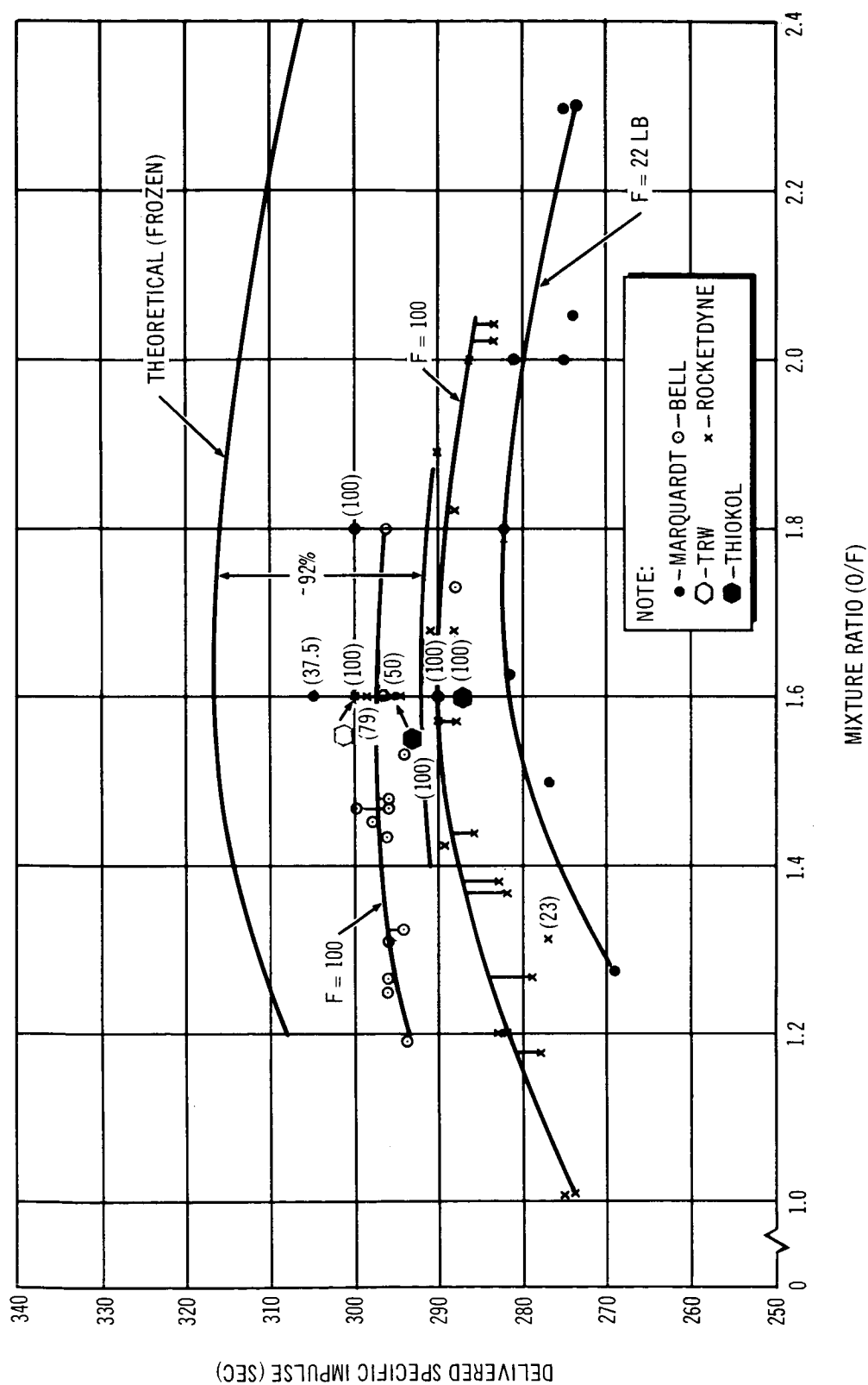


Figure 4-7. P/RCS Engine Performance (N₂O₄/MMH, $\epsilon = 40:1$)

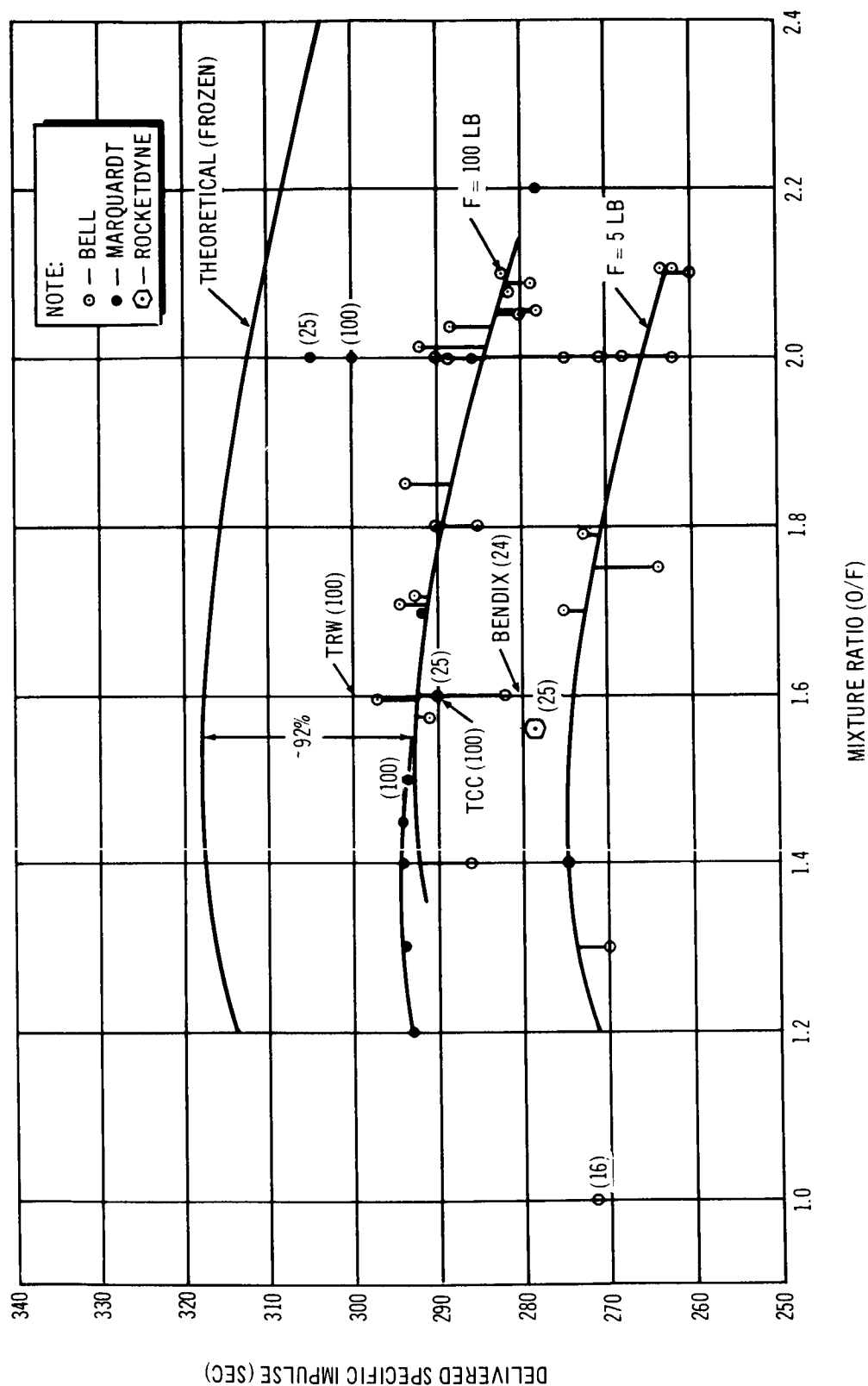


Figure 4-8. P/RCS Engine Performance ($N_2 O_4/50-50 \epsilon = 40:1$)

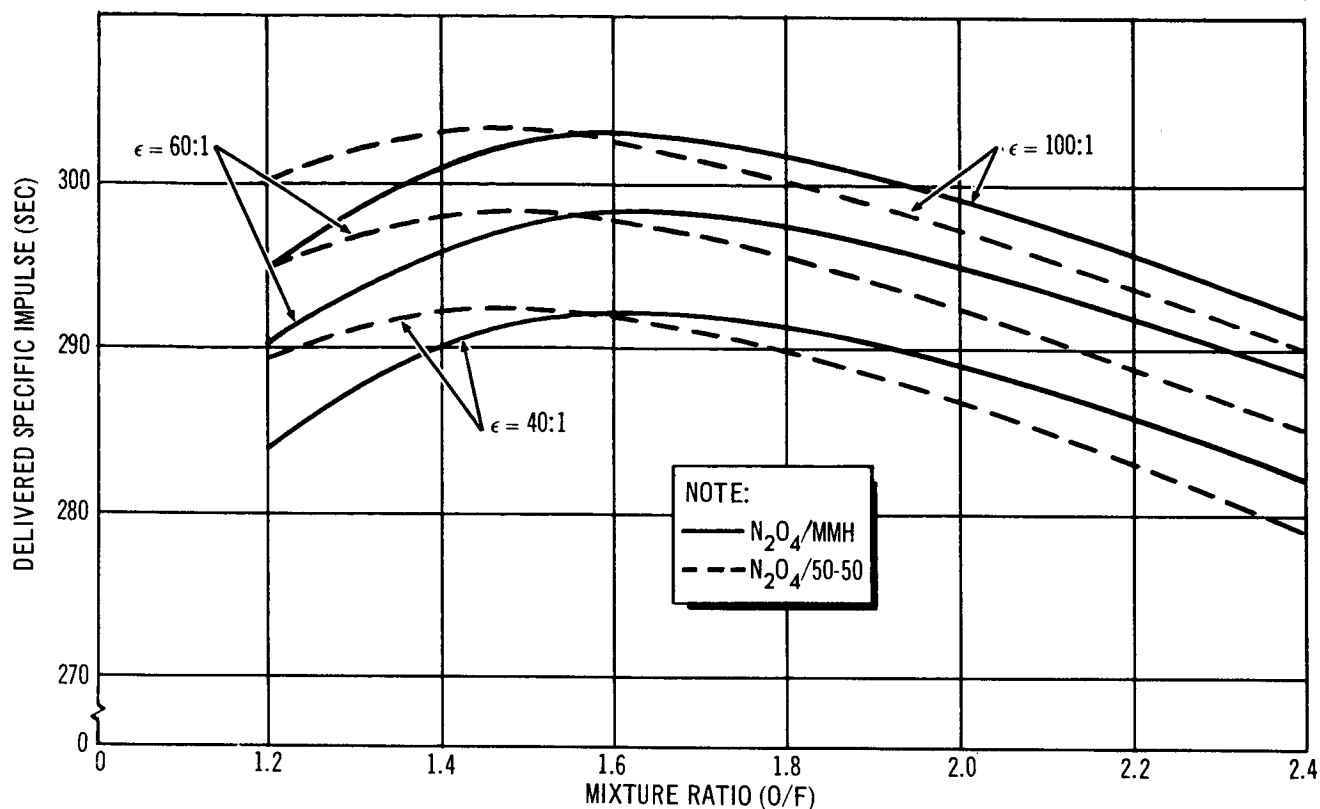


Figure 4-9. P/RCS Engine Performance ($I_{SP\ DEL} = 0.92 I_{SP\ F102}$)

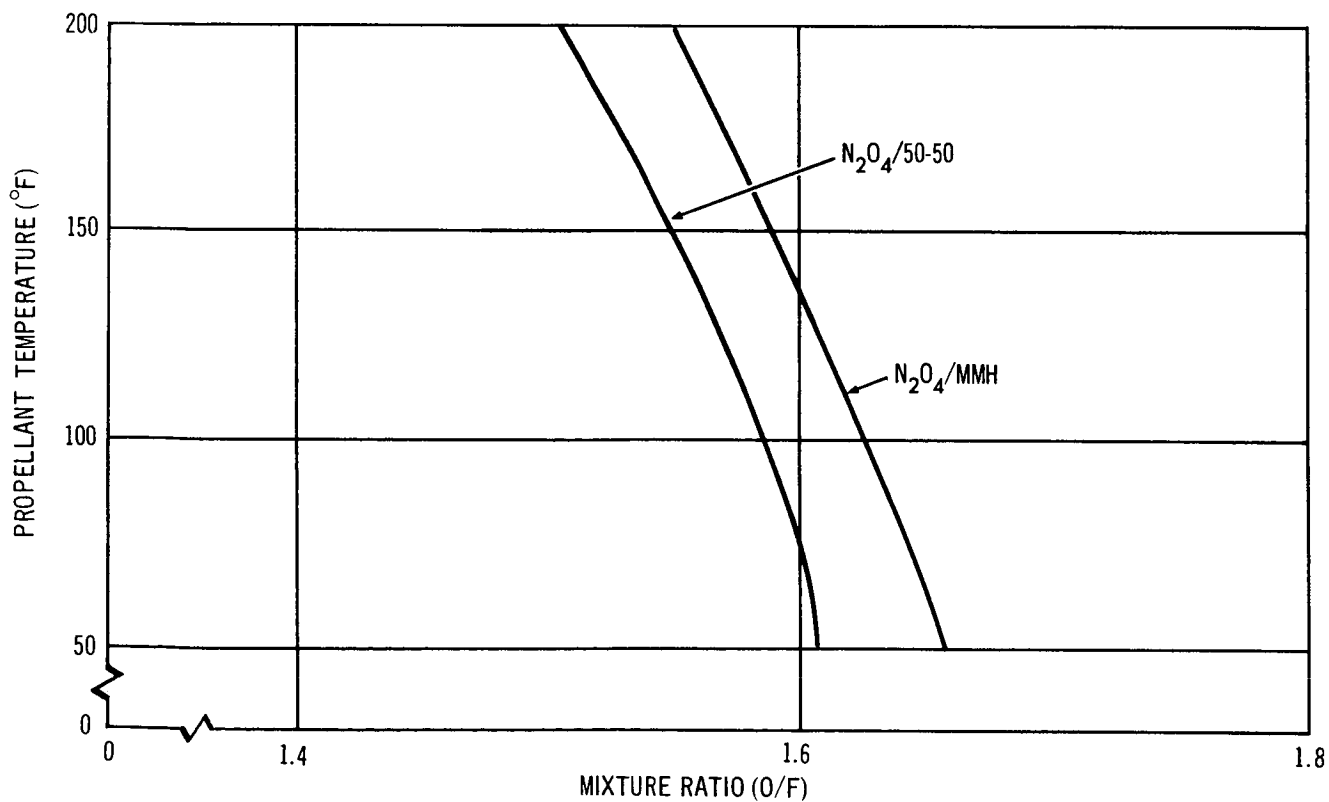


Figure 4-10. Propellant Equal Volume Tank Mixture Ratio

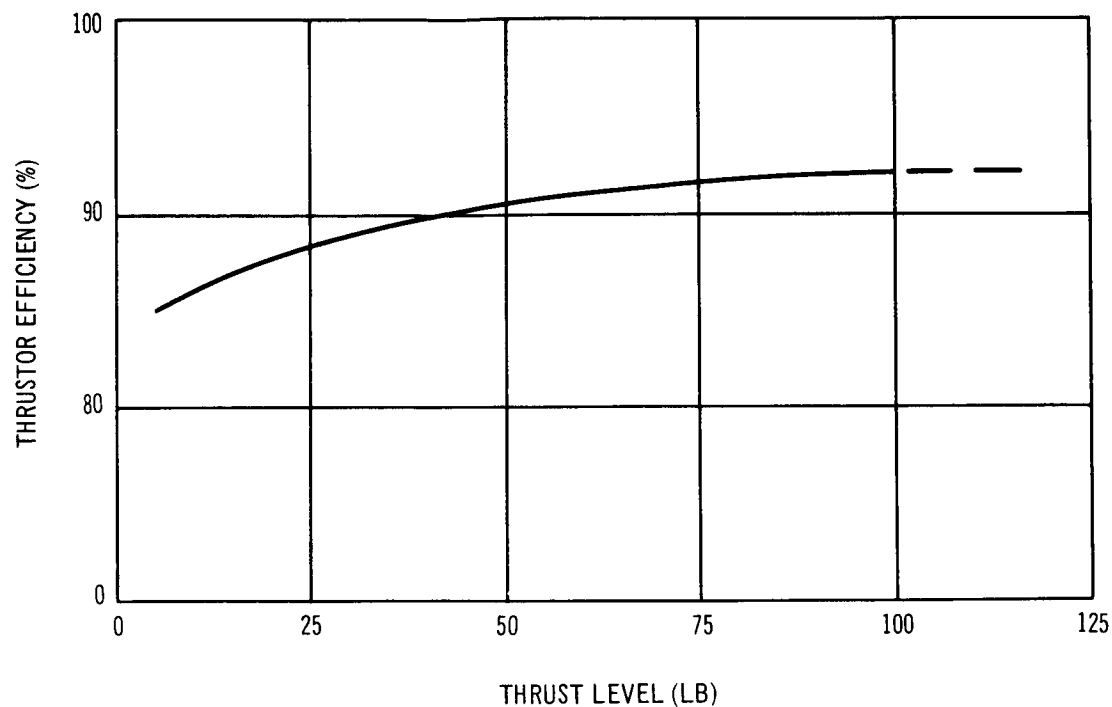


Figure 4-11. P/RCS Bipropellant Engine Thrust Level Efficiency

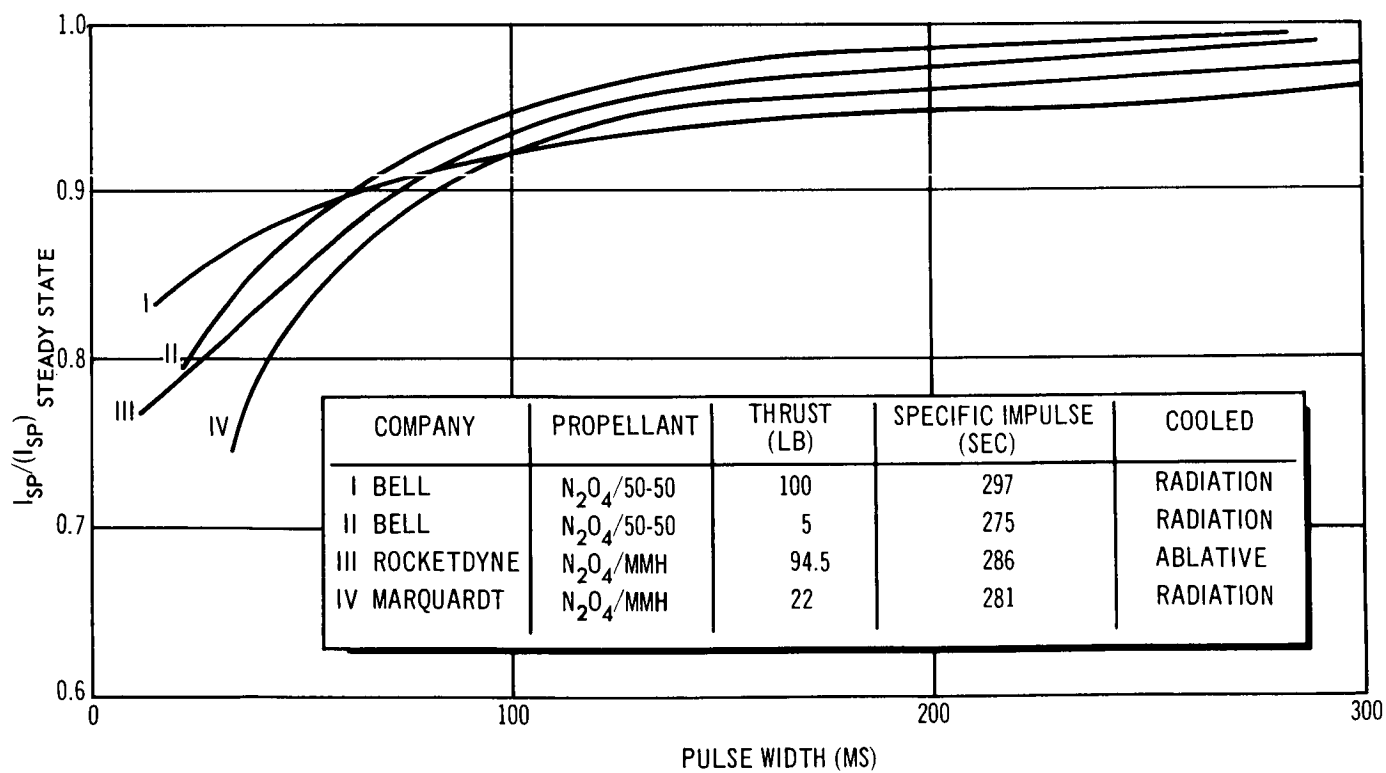


Figure 4-12. P/RCS Engine Performance (Test-Data)

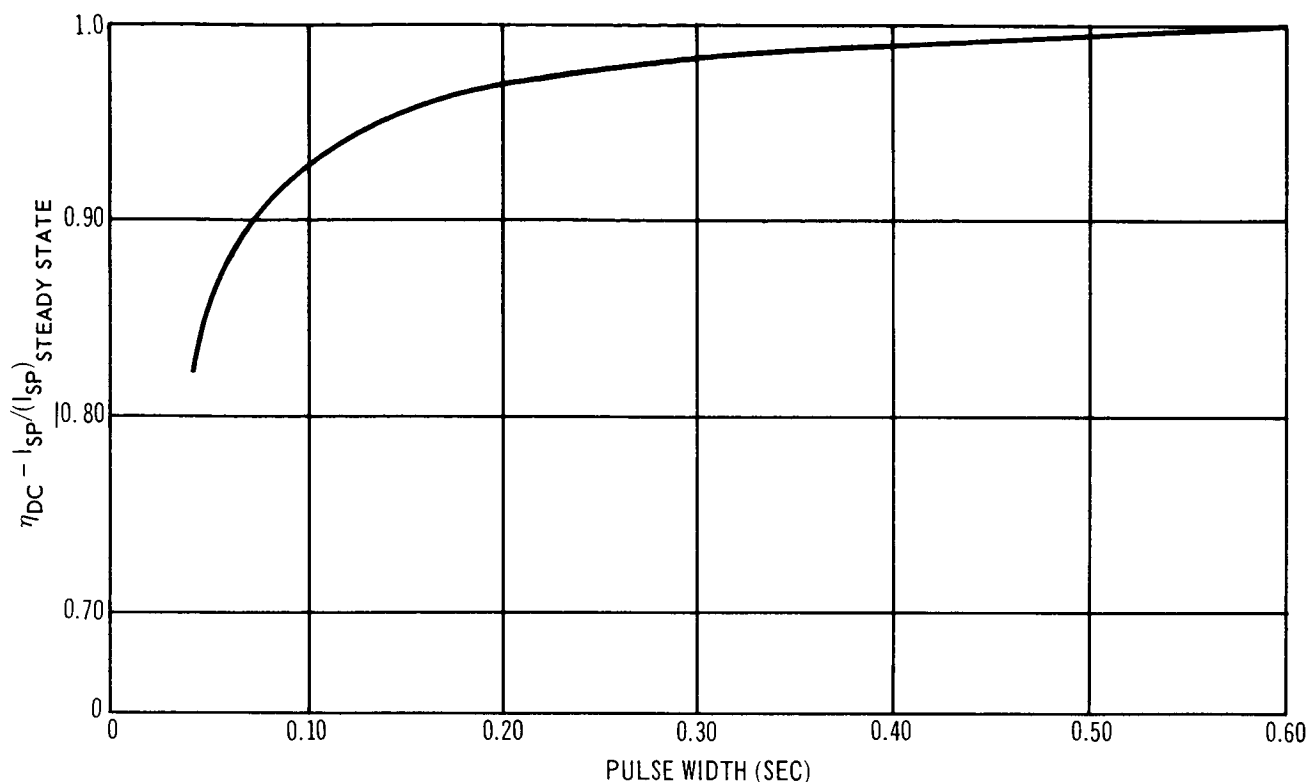


Figure 4-13. P/RCS Bipropellant Engine Duty Cycle Efficiency

4.2.4 Engine Life

The design of a radiatively cooled thruster with a long operating life, when operated in a steady-state mode, is limited to selection of chamber pressure and injectors which provide chamber film cooling. The operating pressures are limited to a range from 25 to 100 psi, which gives a chamber flame temperature of $5,500^{\circ}\text{R}$. Film cooling ranges from a wall flow of 5% to 25% of the main flow stream, the higher value resulting in some performance loss.

Current designs employ either molybdenum or tantalum alloys as combustion chamber and nozzle materials. The tantalum alloys most used contain either 5% molybdenum or 10% tungsten. Both are required to be coated with an oxidation-resistant coating to resist the rapid chemical attack of the oxidizers at elevated chamber temperatures. The coatings in common use are Durak B and Durak MG for the molybdenum chambers and aluminides for the tantalum alloy chambers. Since these materials have a high surface emissivity, they are also used on the external surfaces to further aid in dissipating heat radiatively.

The life of a molybdenum chamber coated with molybdenum-disilicide is discussed herein. The life of this coating, and therefore engine life (primary failure mode), depends on the rate at which it diffuses at the elevated temperatures into the lower silicide compound. This coating degradation for currently developed systems is negligible during pulsed modes of operation in a vacuum. The largest coating loss rate occurs during steady-state operation. For example, the minimum life of this coating is a steady-state mode of operation of 90 min. for a coating temperature of 2,700°F and 4 min. for a temperature of 3,000°F.

The temperature dependency of coating life is shown by Figure 4-14. This figure shows the test results for the Apollo engine in addition to the results of a theoretical study which considered both the internal and external coating losses resulting from diffusion. The thickness of the coating used for this engine and in this analysis was 7.0×10^{-3} in.

Engine life is then obtained from this figure for the MORL thrusters once a coating temperature is established. Figure 4-15 relates coating temperature to engine on time. This figure shows that the coating temperature increases with time to a steady-state value which occurs at approximately

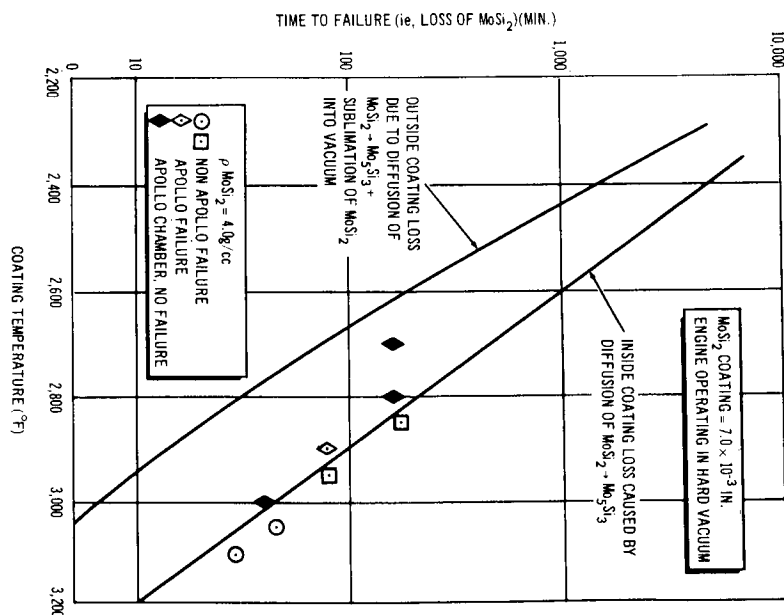


Figure 4-14. Predicted Coating Life as a Function of Maximum Wall Temperature Steady State

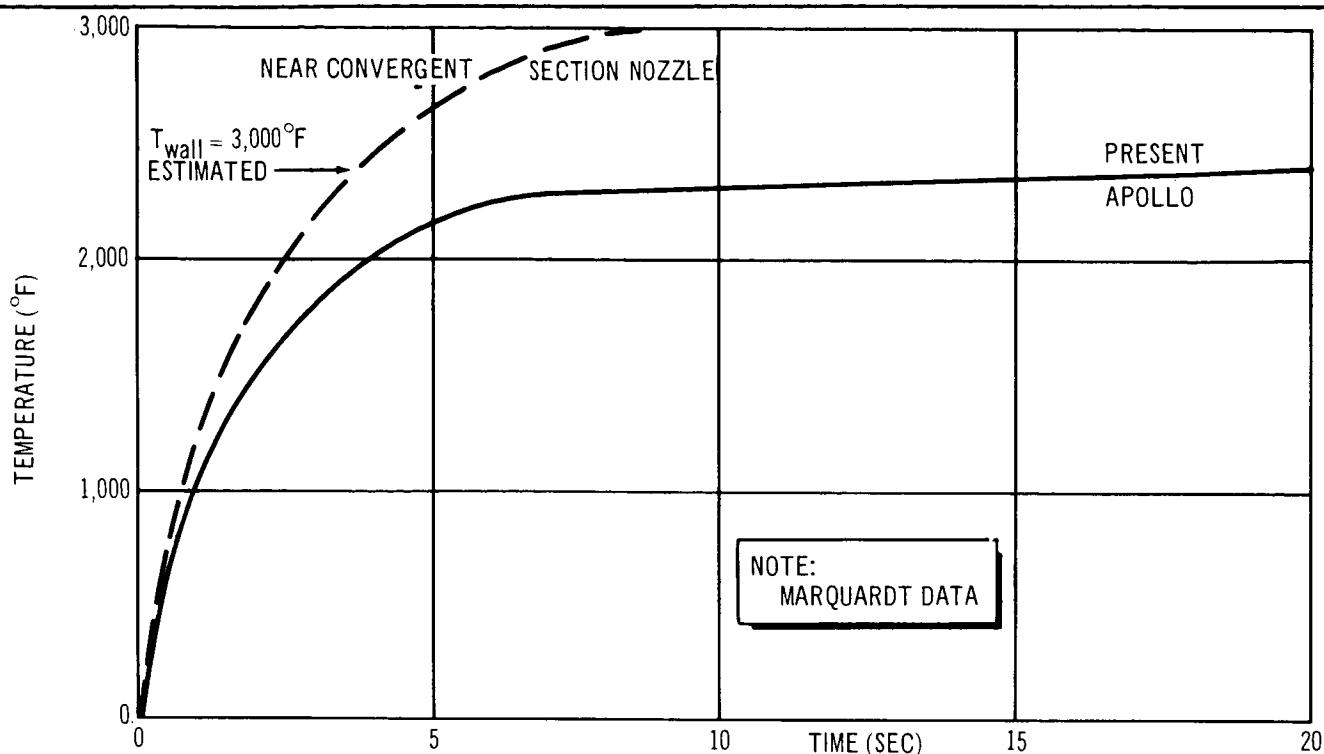


Figure 4-15. P/RCS Engine Maximum Metal Temperature as a Function of Time

12 sec. The temperature of the coating for an initial coating temperature of 100°F for various on times is obtained directly from this figure. The temperature of the coating for initial temperatures exceeding 100°F is determined by subtracting 100°F from the temperature indicated in Figure 4-15 and then adding to this difference the initial coating temperature. Higher initial coating temperatures are a result of the engine's duty cycle or of ambient conditions. The temperature influence of a duty cycle can be estimated by use of Figure 4-16, which shows the temperature drop of the coating as a function of engine off time. This figure indicates that a period of 400 sec is required for the coating temperature to return from the steady-state operational temperature to the initial temperature.

The attitude control engines and precision control engines have an off time between pulses of approximately 2,700 sec ($2.750 t_B$). This guarantees the return of the coating temperature back to the initial temperature. The on time for these engines will not exceed 2 sec. Therefore, the coating temperature should not exceed $1,600^{\circ}\text{F}$ (Figure 4-15) giving a coating life exceeding 1,000 min. (Figure 4-14). The precession control and attitude control engines should not fail because of loss of the protective coating during the 5-year MORL Mission.

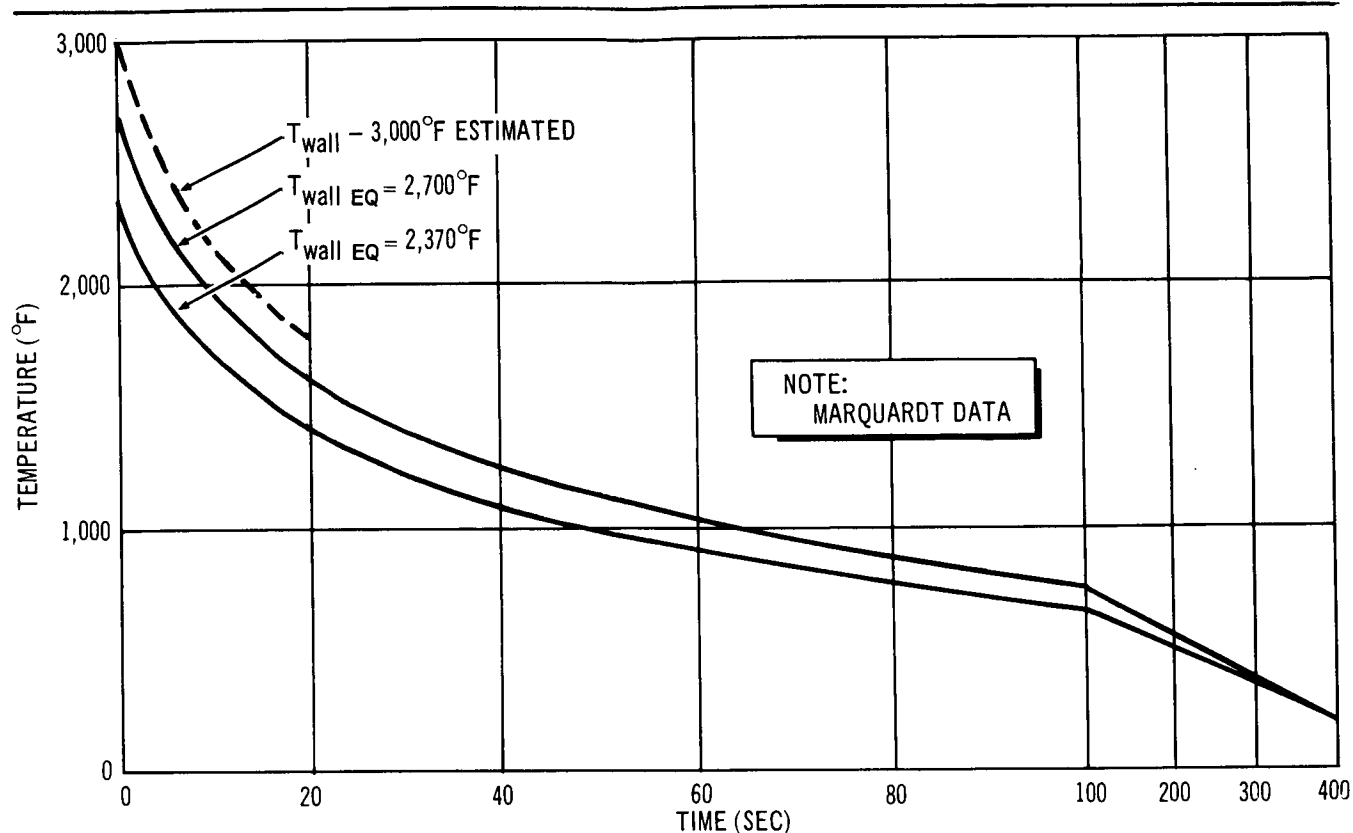


Figure 4-16. P/RCS Engine Cooling Cycle

4.2.5 Pressurant Selection

The two pressurant gases most commonly used throughout industry in various developed systems are helium and nitrogen. The MORL Phase IIa study selected nitrogen over helium because nitrogen offers a much lower leakage rate and gives a lower system weight. This analysis was based on a helium leakage rate of 1 standard cc/hour per flange and for nitrogen a leakage rate of 1 standard cc/day.

The feed system for the update baseline has essentially the same number of connections because it, too, consists of four low-pressure N_2 spheres, four pressure reduction modules, and a high-pressure N_2 sphere. Therefore, on the basis of the results of the previous analysis, nitrogen remains the pressurant gas.

The possibility of a lower-weight system being obtained for the lower-molecular helium is defined by the basic thermodynamic design equations. Because of this potential weight saving, helium should not be eliminated,

but another study should be performed which considers the cost of reducing the helium leakage rate to make it comparable with that of nitrogen. This more effective study based on cost and weight will then determine the pressurant choice more accurately.

4.2.6 Propellant Feed and Transfer Subsystem Selection

The propellants for the laboratory unit are stored in four, equal-volume, stainless steel tanks containing a metal bellows expulsion system. The pressurant storage bottle is an integral part of the propellant tank assembly, forming one enclosure, thereby reducing the tankage weight, and providing a geometry (special convex) which maximizes expulsion efficiency of the bellows. The propellants are contained within the metal bellows. The introduction of the pressurant gas (N_2) into the space between the tank and the bellows causes a controlled bellows collapse which expells the propellants.

The propellant tanks operate at 250 psi, which is sufficient driving pressure to overcome line losses and ensure efficient injector operation during pulsed and steady-state operation.

The propellant feed system is shown schematically in Figure 4-17. The system is equipped with sufficient manifolding so that the tanks can be filled on the ground and refilled in space. For purposes of ground fill, an N_2 purge is included to dry out the tanks and manifolds.

The manifolds, in addition to providing refilling in space, allow transfer of fuel or oxidizer from one tank to the partner tank should the level become low. In like manner, the N_2 system is also manifolded for on-the-ground filling, in-space refilling, and in-space transference of N_2 from one bottle to another.

Each thrust chamber assembly is equipped with a solenoid actuation pre valve coupled with a leak detection device. These valves, with fuel manifold valves, permit the isolation of any thrust chamber, or of a complete thrust chamber cluster, should a malfunction occur.

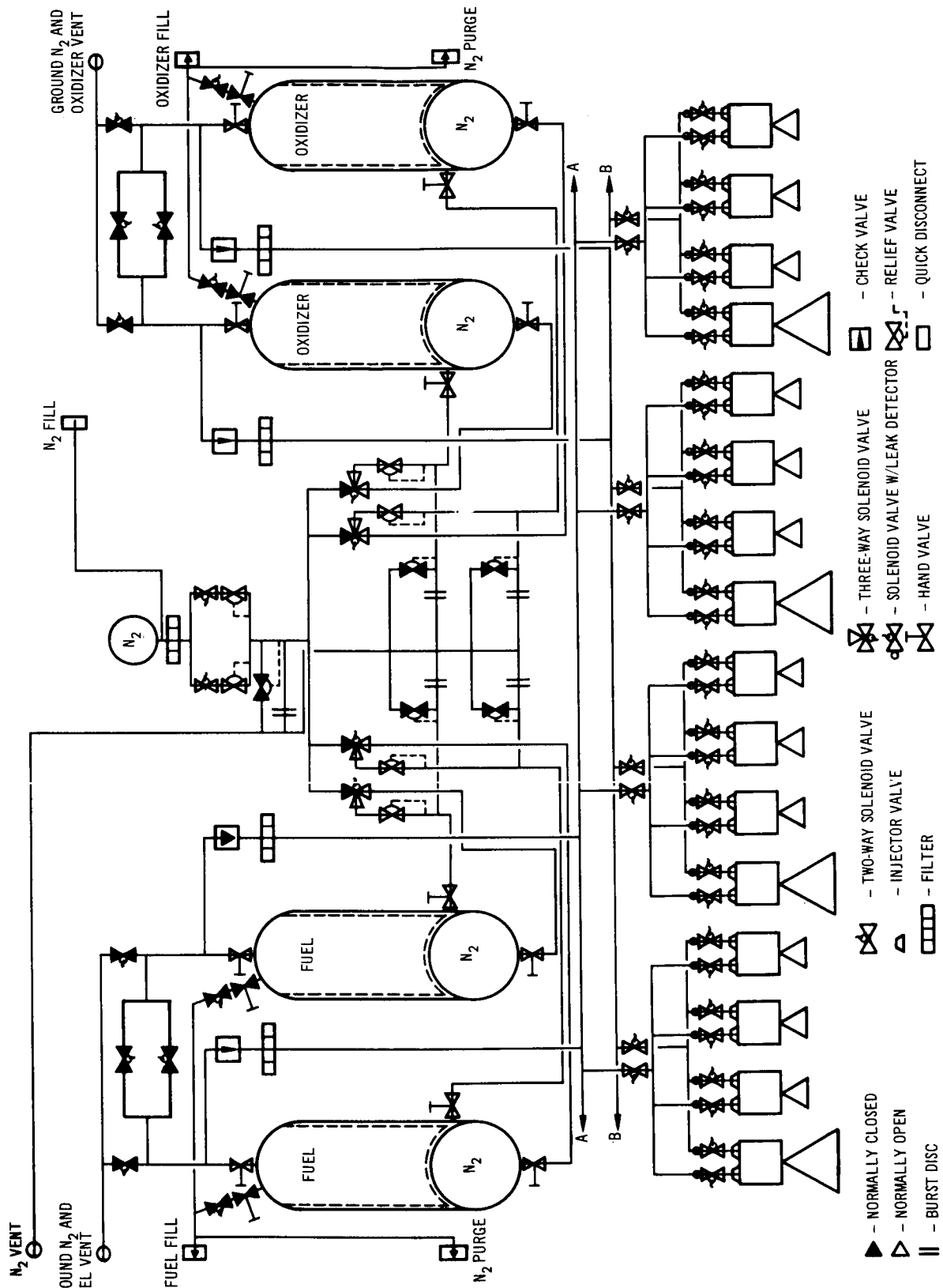


Figure 4-17. P/RCS System Schematic

The fuel manifold completely encircles the periphery of the aft interstage supplying fuel to the thrusters and is provided with sufficient valves to allow isolation of a damaged section and still allow the units to operate normally.

The propellant feed and transfer subsystem on the Saturn IVB is identical to the one that is on the laboratory, except that it has a larger capacity to meet the spin-despin and precession impulse requirements.

4.3 PRELIMINARY DESIGN

The results of the component evaluation study require a preliminary design for further evaluation of system performance with these recent developments. This defined updated system performance can then be further optimized by the system integration portion of this study, which considers in greater depth the system interfaces.

4.3.1 System Performance

The performance of the two configurations (Brayton Cycle and solar-panel power system) and modes (zero-g and artificial-g) will be optimized for minimum propellant consumption by determination of the optimum thrust levels. This analysis is presented below.

4.3.1.1 Zero-g Solar Panel

The optimum thrust level (minimum propellant consumption) was determined for the system requirements listed in Section 4.1. This analysis made use of the resultant propellant savings obtained by implementing pitch/yaw control through a single aft firing thruster which provides translation (orbit keeping). Since the pitch/yaw impulse requirement exceeds the orbit keeping requirement, a portion of this control must be accomplished by operating engines in a couple. This solution was adopted and optimized by use of the engine performance data presented in Figures 4-11 and 4-13.

Figure 4-18 shows the results of this analysis and outlines engine efficiencies, effective specific impulse, and propellant consumption as a function of aft pitch/yaw thrust level for various aft-thrust to forward-thrust ratios.

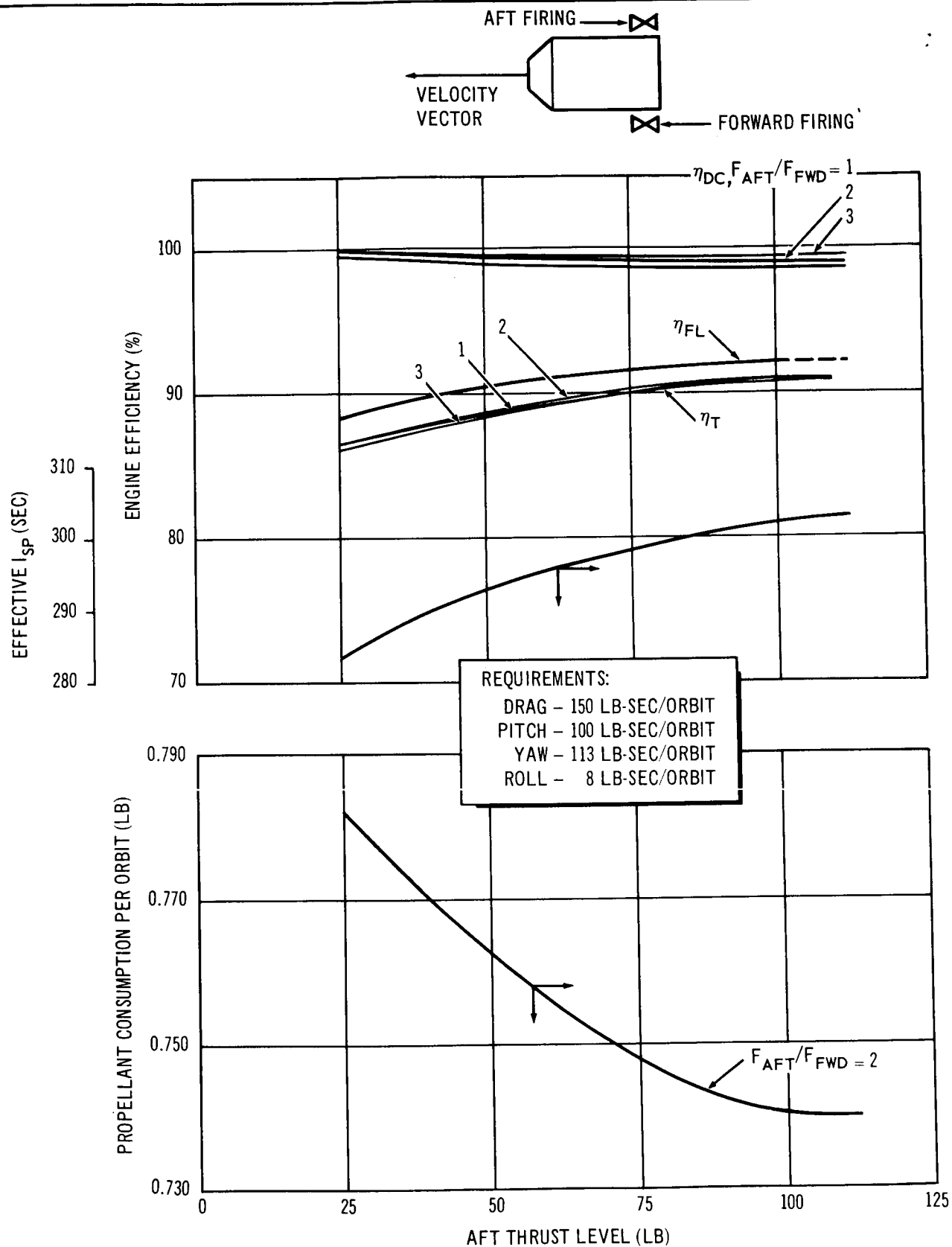


Figure 4-18. P/RCS Bipropellant System Performance, Zero G – Solar Panel

The duty cycle efficiency, $\eta_{D.C.}$, was determined by dividing the impulse requirement for pitch and yaw by the thrust level, which resulted in the required burn time. $\eta_{D.C.}$ is resolved by use of Figure 4-13. This efficiency multiplied by engine efficiency $\eta_{F.L.}$, obtained from Figure 4-11, results in total engine efficiency, (η_T). The effective specific impulse was then determined by multiplying η_T by 329, which is the theoretical frozen specific impulse for the propellant combination NTO/MMH at a mixture ratio of 1.6:1, with a nozzle expansion ratio of 100:1. The impulse requirements, divided by this effective specific impulse, determine the propellant consumption.

The lower curve of Figure 4-18 shows propellant consumption as a function of thrust level for a pitch/yaw aft-thrust to forward-thrust ratio of two. The minimum propellant consumption of 0.740 lb/orbit is obtained at a pitch/yaw aft thrust level of 100 lb. The roll engines are then selected with a thrust level of 50 lb, because 50-lb engines would be developed for the forward facing pitch/yaw engines.

4.3.1.2 Zero-g Brayton Cycle

A similar analysis with a slight modification was implemented for the zero-g laboratory with the Brayton Cycle power system. This modification consisted simply of the assumption that all drag makeup could be accomplished by the aft facing pitch/yaw engines without the need to operate them in a couple at any time. The pitch/yaw impulse requirement is identical to the drag requirement of 90 lb-sec/orbit.

Figure 4-19 shows that the minimum propellant consumption, 0.340 lb/orbit, is obtained at a thrust level of 50 lb, with a roll-engine thrust level of 50 lb. For purposes of redundancy and the availability, the 50-lb engines are selected for the forward facing redundant pitch/yaw engines.

4.3.1.3 Artificial-g Solar Panel

The optimum thrust level was obtained by use of Figures 4-11 and 4-13 modified for cosine losses. The model used to determine this cosine loss, and modified Figure 4-13, are shown in Figure 4-20. This figure is a plot

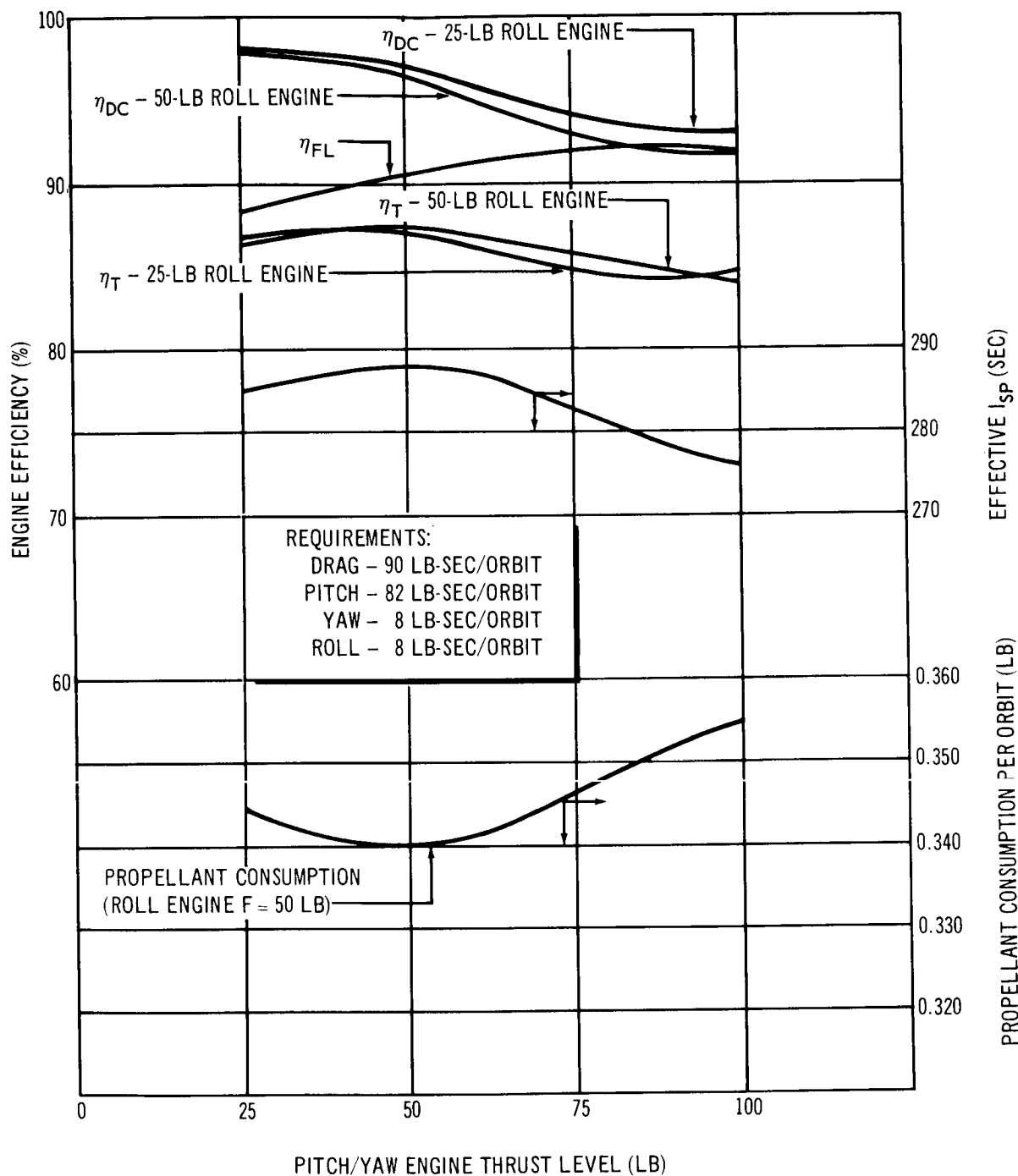


Figure 4-19. P/RCS Bipropellant System Performance, Zero G – Brayton Cycle

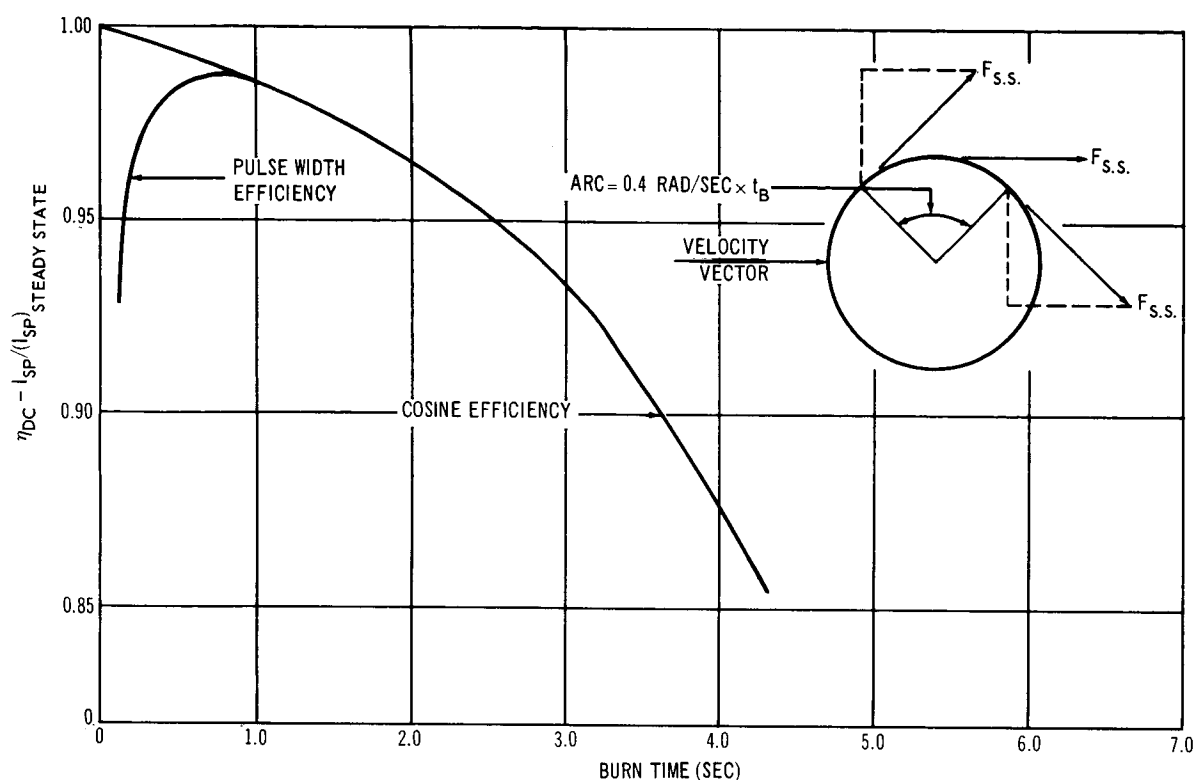


Figure 4-20. P/RCS Bipropellant Artificial G, Engine Efficiency

of D.C. as a function of burn time. It shows that optimum performance is obtained for a burn time of approximately 0.80 sec.

To determine the optimum thrust level for this system, first the impulse requirement was optimized by performing drag makeup at the same time as precession control was performed by the precession control engines by operating the engines when the vehicle's velocity vector was parallel to the spin axis. The resulting total impulse requirement for both precession and drag makeup was 500 lb-sec/orbit. Figure 4-21 shows the results of this analysis giving engine efficiencies, effective specific impulse, and propellant consumption as a function of thrust level.

The duty cycle efficiency was determined from Figure 4-20, by dividing the total impulse by the thrust, resulting in burn time and $\eta_{D.C.}$. The total engine efficiency was then determined by multiplying $\eta_{D.C.}$ by $\eta_{F.L.}$. Engine specific impulse was then determined by multiplying η_T by 329. The lower curve of Figure 4-21 gives the result of dividing the total impulse requirement/orbit by the effective specific impulse.

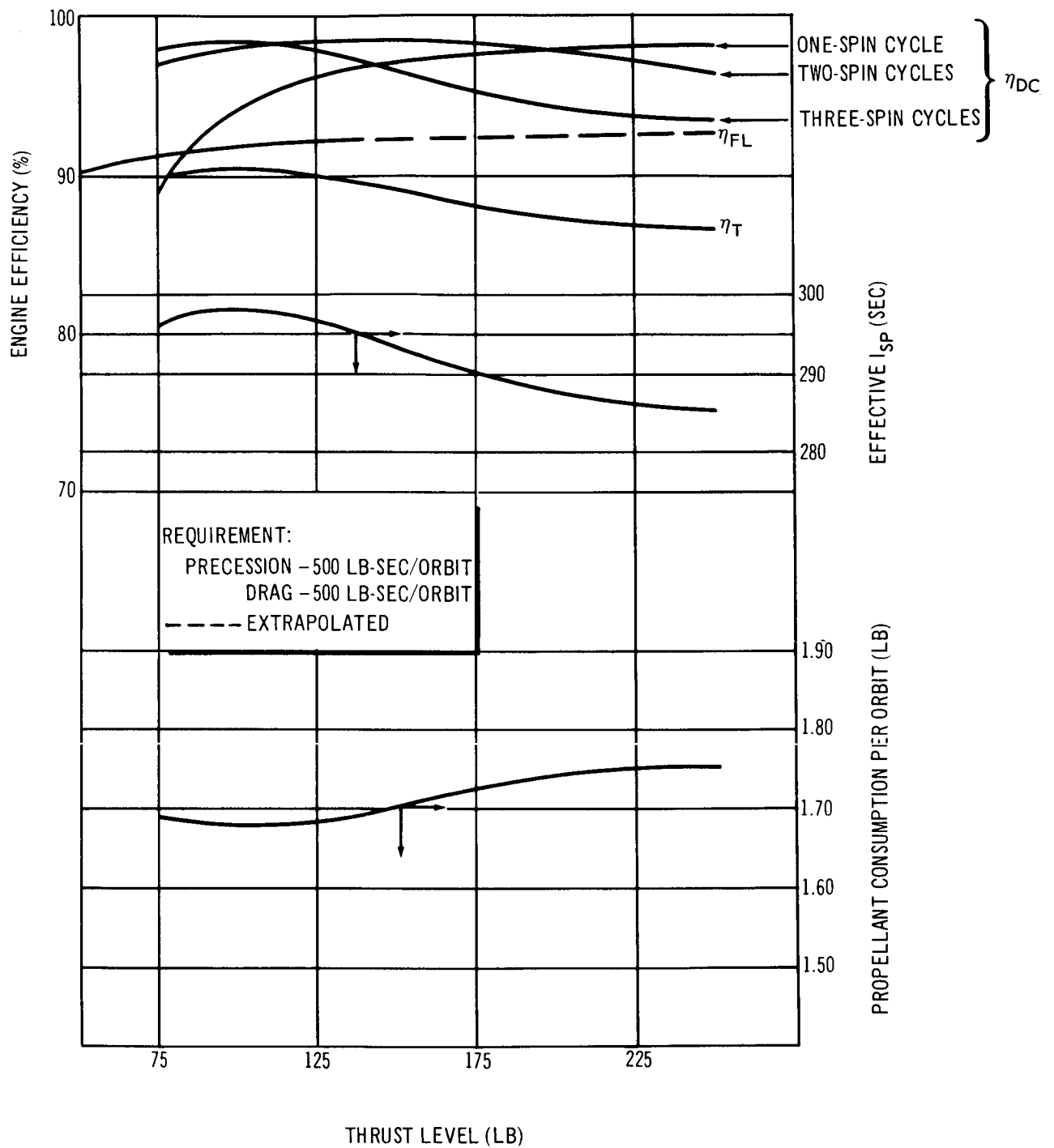


Figure 4-21. P/RCS Bipropellant System Performance, Artificial G, Solar Panel

The minimum propellant consumption of 1.68 lb/orbit is obtained by doing this control during three spin cycles with a thrust level of 100 lb.

The spin-despin engine thrust level is selected at 100 lb because the engines will be available, and fall within the thrust range stated in the MORL Phase IIa study for this function.

4.3.1.4 Artificial-g Isotope Brayton Cycle

This analysis employed the technique described in Section 4.3.1.3, the difference being that the total impulse per orbit was 402 lb-sec as a function of 500 lb-sec. Figure 4-22 shows the results of this analysis.

The minimum propellant consumption of 1.4 lb/orbit is obtained by doing this control during one spin cycle with a thrust level of 100 lb. Again, for the reason previously stated in Section 4.3.1.3, the spin/despin thrust level selected was 100 lb.

4.3.2 System Characteristics

The optimum thrust levels for the configurations and modes considered is shown in Table 4-4. The orbit-injection thrust levels selected for these systems is 400 lb provided by four 100-lb thrust-level engines positioned on the laboratory.

The zero-g, solar-panel laboratory will have 12 engines. Four 100-lb engines, in conjunction with four forward facing pitch/yaw engines with a thrust level of 50 lb, will accomplish orbit injection as well as pitch/yaw control with drag makeup. Roll will be provided by four 50-lb thrust level engines.

The zero-g Brayton Cycle laboratory will have 16 engines; four 100-lb engines for orbit injection, and twelve 50-lb engines for attitude control and drag makeup.

The artificial-g laboratory will have, in addition to these engines positioned on the laboratory, precession and spin-despin engines positioned on the Saturn IVB. The thrust level established for the spin-despin and the

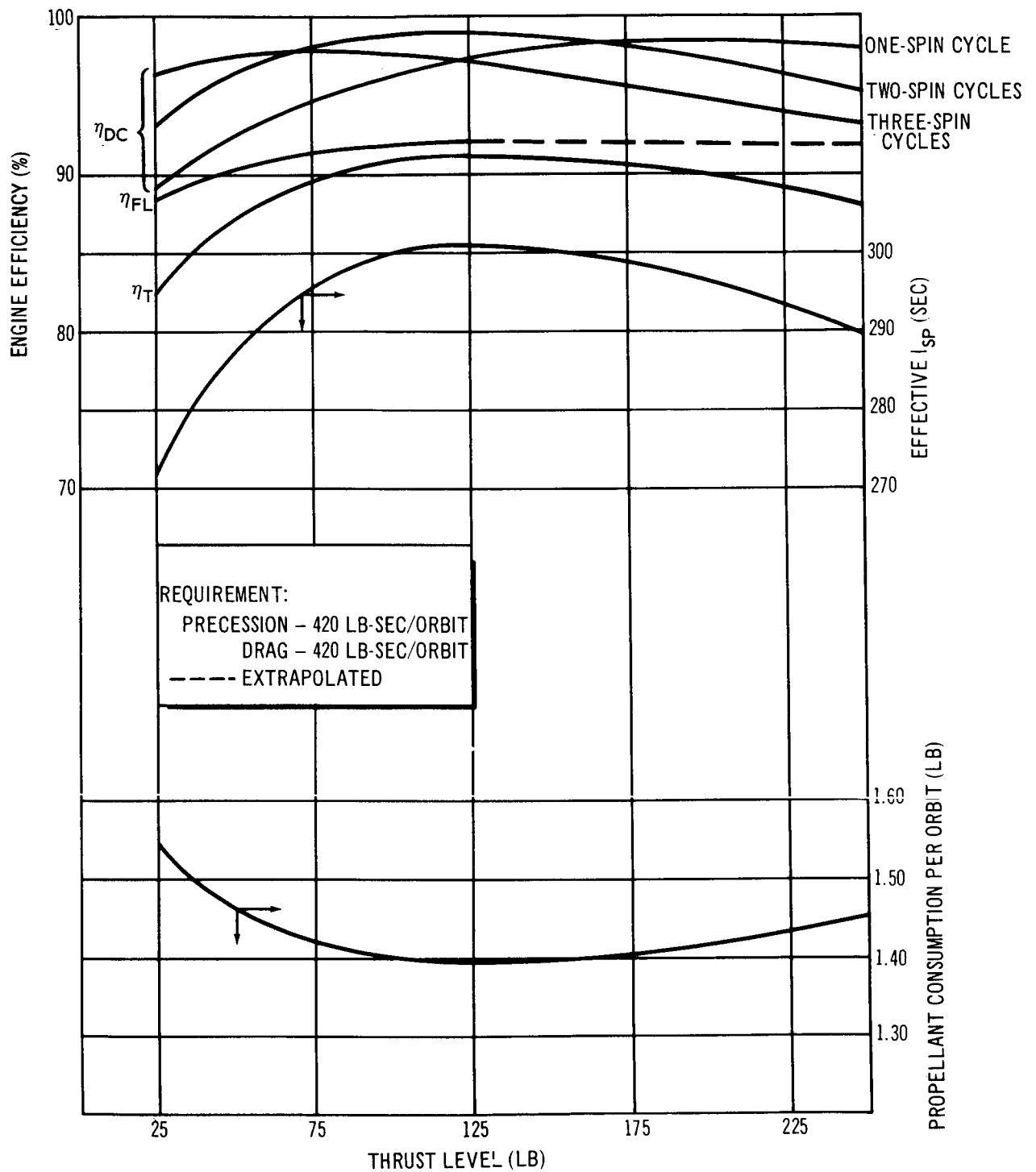


Figure 4-22. P/RCS Bipropellant System Performance, Artificial G-Brayton System

Table 4-4

PROPULSION/REACTION CONTROL SYSTEM THRUST LEVELS

Thruster Function	Zero-g Mode (lb)			Rotating Mode (lb)					
	On Laboratory			Solar Panel			Brayton Cycle		
	Solar Panel	Brayton Cycle	On Laboratory	On Laboratory	Booster	On Laboratory	On Booster	Laboratory	On Booster
Orbit injection	400	400	400	400	---	400	---	---	---
Drag	(100)	(50)			((100))				((100))
Pitch/yaw	100* 50**	50	100* 50**		---	50	---		---
Roll	50	50	50	50	---	50	---		---
Preces- sion	---	---	---	---	100	---	100		100
Spin- despin	---	---	---	---	100	---	100		100

*Aft facing

**Forward facing

() Accomplished by forward facing pitch/yaw engines

(()) Accomplished by precession engines

precession control engines of the solar panel and Isotope Brayton Cycle configurations is 100 lb. Four engines are required: two for spin-despin, and two for precession control.

The propellant requirements on launch (orbit injection plus a 20-day in-orbit supply), the 90-day resupply weight, and the 147-day weights (tank capacity) are shown in Table 4-5. This table shows that the use of the Brayton Cycle results in a propellant saving over the solar-panel configuration. Savings are approximately 1,000 lb for the zero-g mode and approximately 700 lb for the artificial-g mode.

Table 4-5
PROPULSION/REACTION CONTROL SYSTEM
PROPELLANT QUANTITY REQUIREMENTS

Characteristic	MORL		Booster	
	Solar Panel	Brayton Cycle	Solar Panel	Brayton Cycle
Launch weight - 20 day, (lb)	842	716	1,352	1,226
Resupply weight - 90 day, (lb)	1,040	476	2,370	1,970
Tank capacity - 147 day, (lb)	1,710	780	3,880	3,230

4.3.3 Zero-g Brayton-Cycle Laboratory Design

The zero-g mode with Brayton Cycle was selected to be compared with the advance thruster concepts; therefore, it is further defined. The thrust optimization analysis performed used the performance of the engine concept selected in Section 4.2.1 with the propellants selected in Section 4.2.3. Completion of this design was accomplished by use of the information outlined in the component evaluation study.

Table 4-6 lists the propulsion system design parameters. This system has 16 fixed-mounted radiation engines: four 100-lb engines for orbit injection

Table 4-6
ZERO-G, BRAYTON-CYCLE PROPULSION
SYSTEM DESIGN PARAMETERS

System Characteristics	Magnitude or Description
Number of engines	16
Total weight loaded*	967.2 lb
Propellants	
Oxidizer	N_2O_4
Fuel	MMH
Mixture ratio, O/F	1.6:1 (by weight) 1.0:1 (by volume)
Total weight**	783.4 lb
Engines	
Cooling concept	Radiation
Thrust--Attitude control	50 lb
Orbit injection	100 lb
Expansion ratio	100:1
Chamber pressure	90 psi
Vacuum I_{sp} (steady state)	
F = 50 lb	295 sec
F = 100 lb	303 sec
Tankage and Pressurization	
Tank pressure (operating)	250 psi
Tank pressure (maximum)	300 psi
Fuel and oxidizer tank diameter	16.2 in.
Positive expulsion device	Metal bellows
Pressurant	Nitrogen
Pressurant storage pressure	1,500 psi

*147-day propellant supply

**Includes nitrogen

and twelve 50-lb engines for attitude control and drag makeup. The 100-lb engines using the propellant combination NTO/MMH at a mixture ratio of 1.6:1 deliver a specific impulse of 303 sec. The propellant required for the 147-day operational period is 783.4 lb (including weight of N_2 pressurant). The total system weight is 967.2 lb. A schematic of the system is shown in Figure 4-17.

The propellant is stored in a metal bellows contained in four equal-volume tanks. The tank ends are fitted with a low-pressure N_2 bottle that saves weight through the elimination of a bulkhead and, in addition, provides a geometry (spherical convex) which offers optimum bellows expulsion efficiency. For redundancy, the system is also provided with a high-pressure N_2 bottle capable of emptying one tank.

This system, in addition to having the capability of being filled on the ground, has sufficient manifolding to allow refilling in space.

There are four thrust chamber clusters, each consisting of four fixed-mounted, radiation-cooled engines. The manifolds supplying these clusters are fitted with sufficient valves to isolate a single thruster or a complete cluster should a failure occur.

This system, as can be seen from Figure 4-17, offers redundancy by duplication of high-failure components such as the three-way nitrogen valves and the pressure regulators. Adequate screening is provided to remove any entrained particles that could cause injector pre valve or injector valve clogging.

ABBREVIATIONS

C*	--	characteristic velocity
CG	--	center of gravity
CMG	--	control moment gyro
CTF	--	chlorine trifluoride (ClF_3)
EC/LS	--	environmental control and life support system
F_{SS}	--	steady state thrust
HPI	--	high performance insulation
I_{sp}	--	specific impulse
IRFNA	--	inhibited red fuming nitric acid
kWe	--	kilowatts (electrical)
kWt	--	kilowatts (thermal)
MMH	--	monomethyl hydrazine ($\text{CH}_3\text{N}_2\text{H}_3$)
MR	--	mixture ratio
N_2H_4	--	hydrazine (N_2O_4)
NTO	--	nitrogen tetroxide (N_2H_4)
O/F	--	oxidizer/fuel (mixture ratio)
P/RCS	--	propulsion and reaction control systems (includes orbit injection systems)
PBC	--	Plutonium Radioisotope Brayton Cycle (power system)
RIT	--	radioisotope thruster
SCCD	--	standard cubic centimeters per day
SCCH	--	standard cubic centimeters per hour
SCS	--	stabilization and control system
t_b	--	engine burn time
T_F	--	fuel valve temperature
T_{OX}	--	oxidizer valve temperature
UDMH	--	unsymmetrical dimethyl hydrazine

50-50 -- 50% hydrazine + 50% UDMH
 ϵ -- expansion ratio
 η_{DC} -- duty cycle engine efficiency
 η_{FL} -- thrust level engine efficiency
 η_T -- total engine efficiency

NOMENCLATURE

1. Propulsion/Reaction Control System (P/RCS) - Onboard thruster system utilizing propulsion to provide either a velocity increment or attitude control of the vehicle.
2. Thrustor System - Consists of the thruster module, tank and feed subsystem, and associated valves and controls.
3. Thrustor (Thrust chamber assy) - Thrust chamber and nozzle.
4. Phase IIa Propulsion/RCS System - that system defined by DAC Report SM-46087.
5. Updated Liquid Bipropellant System - that system described in DAC SM-48819 resulting from the Baseline Evaluation Study conducted in Phase IIb of the MORL study. Designated Phase IIb baseline.
6. Resistojet Propulsion/RCS System - that system described in DAC Report SM-48819 resulting from the Advanced RCS study conducted in Phase IIb of the MORL study.
7. Radioisotope Thrustor Propulsion/RCS System - that system described in DAC Report SM-48819 resulting from the Advanced RCS study conducted in Phase IIb of the MORL study.
8. Thrustor module - consists of a grouping or cluster of thrusters. Can be one chamber assy with multi nozzle (i. e. Radioisotope thruster module)
9. Orbit Injection System - thruster system used to provide both velocity increment and attitude control for the orbit injection phase of the mission.

PRECEDING PAGE BLANK NOT FILMED.

REFERENCES

1. J. W. Schaefer and J. Ferrante. Analytic Evaluation of Possible Non-cryogenic Propellants for Electrothermal Thrustors. NASA TND-2253, March 1964.
2. R. R. John, J. F. Conners, and S. Bennet. Thirty-Day Endurance Test of a 30 kW Arc Jet Engine. AVCO Research and Advanced Development, Wilmington, Washington, AIAA June 1963, Los Angeles, California.
3. L. E. Wallner and J. Czika, Jr. Arc-Jet Thrustor For Space Propulsion. Lewis Research Center, Cleveland, Ohio, NASA TND-2868, June 1965.
4. E. T. Pitkin. Viscous Laminar Flow in Conical Nozzles. Marquardt Report MR 20, 187, July 1962.
5. B. E. Tinling. Measured Steady State Performance of Water Vapor Jets for Use in Space Vehicle Attitude Control Systems. NASA TN D-1302, May 1962.
6. G. S. Sutherland and M. E. Maes. A Review of Micro-Rocket Technology: 10^{-6} to 1 lb Thrust. AIAA Paper 65-620. Presented at AIAA Propulsion Joint Specialists Conference, 14-18 June 1965.
7. R. P. John and D. Morgan. Resistojet Research and Development - Phase II, 2nd Quarterly Progress Report. NASA CR-54333, AVCO RAD SR65-44, 20 January 1965.
8. R. J. Page and R. A. Short. The Design and Performance of a 3 kW Concentric Tube Resistojet. NASA CR-54410, TMC R-25, 168, September 1965.
9. R. J. Page and C. R. Halbach. Resistojet Engine Performance - A Comparison of Experiment with Theory. Presented at 4th AIAA Electric Propulsion Conference, August 1964.
10. A. D. Jonath. Gasdynamic Problems in Low Pressure Microthrust Engines. AIAA Paper No. 65-616 presented at AIAA Propulsion Joint Specialist Conference, 14-18 June 1965.
11. McAdams. Heat Transmission - 3rd Edition, McGraw-Hill, 1954.

12. M. W. Milligan. Nozzle Characteristics in the Transition Regime Between Continuum and Free Molecular Flow. AIAA Jr. Vol. 2, No. 6, June 1964.
13. G. R. Short and J. M. Howard. Sublimation of Tungsten in Hydrogen. AIAA Paper No. 63024, presented in 1963.
14. C. R. King. Compilation of Thermodynamic Properties, Transport Properties and Theoretical Rocket Performance of Gaseous Hydrogen. NASA TN-275, April 1960.
15. F. W. Spisz. Compilation of Theoretical Rocket Performance for the Chemically Frozen Expansion of Hydrogen. NASA TND-9080, December 1963.
16. E. D. Arnold. Handbook of Shielding Requirements and Radiation Characteristics of Isotopic Power Sources for Terrestrial, Marine and Space Application, ORNL-3576, April 1964.
17. H. H. Van Tuyl, F. P. Roberts, and E. J. Wheelwright. Shielding Requirements for Promethium Sources. HW-77375, April 1963.